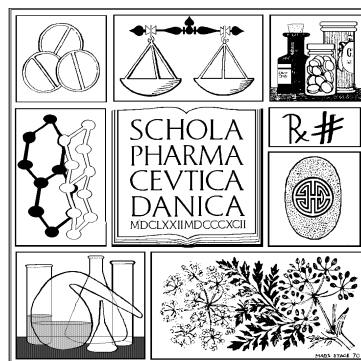


Pharmacophore and receptor models for neurokinin receptors

Anders Poulsen



H. Lundbeck A/S



The Royal Danish
School of Pharmacy

ATV

Danish Academy of
Technical Sciences

Industrial Ph.D. project EF-838

February 2003

Copyright 2003 by Anders Poulsen
Copenhagen - Denmark

ISBN 87-88085-27-9

Preface and Acknowledgements

This thesis, along with the two papers listed below, encompasses a dissertation submitted to the Royal Danish School of Pharmacy with the aim of acquiring a Ph. D. degree. The papers are enclosed in appendix I-II and will be referred to in the text by the Roman numeral of the appendix. This thesis represents the results of my work carried out at the Department of Medicinal Chemistry of the Royal Danish School of Pharmacy, the Department of Computational Chemistry of H. Lundbeck A/S, and during a three-month stay at the College of pharmacy of the University of Michigan. I gratefully acknowledge the Danish Academy of Technical Sciences and H. Lundbeck A/S for their financial support of this Ph. D. Project.

I would like to express my sincere gratitude to my supervisors, Professor Tommy Liljefors (Royal Danish School of Pharmacy), Dr. Berith Bjørnholm (H. Lundbeck), and Klaus Gundertofte (Head of Computational chemistry at H. Lundbeck). Without their support and enthusiasm, this work could never have been realised. I particularly want to thank Tommy and Berith for always being available, and for their guidance on the project.

I am grateful to Professor Henry I. Mosberg of the University of Michigan, for giving me the opportunity to work in his lab. I especially want to thank Dr. Irina D. Pogozheva for teaching me homology modelling of G-protein coupled receptors.

I would like to thank my colleagues of the department of Computational chemistry at H. Lundbeck; Morten Langgård, Jacob Flemming Hansen, Dr. Anne Marie Munk Jørgensen, and Dr. Lena Tagmose, for their help and technical assistance, and for providing me with a perfect place to work. I would also like to thank the chemists working at the NK2 project at H. Lundbeck; Dr. Jan Kehler, Dr. Torre Hansen, Dr. Christian Krog, Dr. Thomas Ruhland, Dr. Friedrich Kroll, and Dr. Gitte Mikkelsen, for an excellent collaboration on the design of new NK2 antagonists. I am grateful to Vibeke Vips Larsen and Annick Somerville for their help with references and for proof reading this thesis.

I want to thank both past and present members of Prof. Liljefors' group for a stimulating and friendly atmosphere. I especially thank my fellow Ph. D. Student Anne Techau Jørgensen for many fruitful discussions on both computational chemistry-related and unrelated subjects.

Finally, I want to thank my wife Violeta Magat Poulsen for supporting me during the writing of this thesis, and my mother Karen Poulsen for taking care of our daughter. I cannot overemphasise how much their help and support have meant to me.

Several compounds have been synthesised, based on ideas arising from the pharmacophore models described in this thesis. Generally, these compounds showed the expected behaviour. Unfortunately, these compounds must be omitted from the thesis, pending patent application.

Copenhagen, 19th December 2002
Anders Poulsen

Abstract

The neurokinin receptors (NKRs) are members of the superfamily of G-protein coupled receptors. It has been demonstrated in clinical trials that selective NKR antagonists show antidepressive and anxiolytic activity. The NKRs have also been linked to other biological effects in the central nervous system, as well as in peripheral tissues. This thesis is devoted to the development of pharmacophore and 7TM receptor models for NKRs with the aim of explaining the structure-activity relationships for ligands that inhibit the NKRs.

Five pharmacophore models have been developed. A pharmacophore model for selective NK1R antagonists. A pharmacophore model for selective NK2R antagonists. Three pharmacophore Models (1-3) for dual NK1R/NK2R antagonists, of which Model 2 is argued to be the one that best represents the binding mode. The NKR antagonists bind to the NK1R and NK2R subtypes in essentially the same conformation, and subtype selectivity is determined by the substitution pattern of mainly three aromatic rings. By using exhaustive conformational analysis and least-squares molecular superimposition studies, a large number of structurally diverse high, moderate and low affinity NKR antagonists have been fitted to the pharmacophore models. Affinities of the NKR antagonists accommodated by the models could be rationalised by the conformational energy penalties for the antagonists to adopt their proposed bioactive conformation. Low or moderate affinity could also be explained by missing pharmacophore elements, solvation energy, or penetration into receptor essential volume.

Using an iterative distance geometry approach, 7TM receptor models for each of the NKR subtypes have been constructed. These models are based on the bovine rhodopsin- X-ray structure. Using published site-directed mutagenesis data, a putative binding site for several NK1R and NK2R antagonists was identified. Selective NK1R antagonists were manually docked into the NK1R model, and found to bind to the receptor in a conformation represented by the NK1 pharmacophore model. Unselective NKR antagonists were docked into all three NKR models. Possible residues responsible for subtype selectivity have been identified. The binding mode at the NK1R, NK2R and NK3R was found to be similar and compatible with pharmacophore Model 2. However, selective NK3R antagonists may have another binding mode.

The pharmacophore models were used as search queries for database search with the program package Catalyst. The search queries were evaluated by searching a drug database with known biological activities. However, the results were not impressive. This was probably due to severe shortcomings in the conformation generation module of Catalyst. Conformational ensembles generated by Catalyst turned out not to be diverse and to show a significant overpopulation of high-energy conformations. The lacking diversity of low energy conformations results in false negatives, and the many high-energy conformations are noise, which results in false positives.

Resumé (Abstract in Danish)

Neurokinin receptorerne (NKR'er) tilhører superfamilien af G-protein koblede receptorer. Kliniske forsøg har vist, at selektive NKR antagonist udviser antidepressiv og angstdæmpende aktivitet. NKR'er er også blevet sat i forbindelse med andre biologiske effekter både i det centrale nervesystem og perifert. Denne afhandling omhandler udviklingen af farmakofor- og 7TM receptor modeller for NKR'er, der kan forklare struktur-aktivitetsforhold for ligander, der hæmmer NKR'er.

Fem farmakoformodeller er blevet udviklet: en farmakoformodel for selektive NK1R antagonist, en farmakoformodel for selektive NK2R antagonist og tre farmakoformodeller (Model 1-3) for NK1R/NK2R antagonist. Om Model 1-3 konkluderes det, at Model 2 bedst repræsenterer den bioaktive konformation. Subtypeselektiviteten er primært bestemt af substitutionsmønsteret i tre aromatiske ringe, og den bioaktive konformation af antagonistene, bundet til NK1R og NK2R subtyperne, er stort set identisk. Ved brug af grundig konformationsanalyse og overlejring af molekyler er et stort antal strukturelt forskellige både høj- medium- og lavaffine antagonist blevet tilpasset farmakoformodellerne. Affiniteten af antagonist med lav- eller medium affinitet kunne forklares med deres høje konformationelle energi, manglende farmakofor elementer eller solvatiserings energi.

Tre 7TM receptor modeller, en for hver af NKR subtyperne, er blevet udviklet ved en iterativ afstandsgeometrisk metode. Disse modeller er baseret på røntgenstrukturen af bovin rhodopsin. Et formodet bindingssted for flere NK1R og NK2R antagonist er blevet identificeret ved hjælp af publiceret mutagenese data. Selektive NK1R antagonist blev manuelt dokket i NK1R modellen. Den receptor-bundne konformation var i overensstemmelse med farmakoformodellen for selektive NK1R antagonist. Uselektive NKR antagonist blev manuelt dokket i alle tre NKR modeller. Aminosyrer, som ser ud til at have indflydelse på subtypeselektivitet, er identificeret. Konformationen af antagonistene bundet til NK1R-, NK2R- og NK3R modellerne var stort set identiske og i overensstemmelse med farmakofor Model 2. Dog kan selektive NK3R antagonist muligvis binde til receptoren på en anden måde.

Farmakofor modellerne blev brugt som hypoteser ved databasesøgning med programpakken Catalyst. Hypoteserne blev evalueret ved at søge i en database med kendte biologiske aktiviteter. Resultaterne var ikke imponerende, hvilket sandsynligvis skyldes konformationsgenereringsmodulet i Catalyst. Det blev vist at konformationelle ensembler genereret af Catalyst ikke er diverse, og at højenergi konformationer er overrepræsenterede. Den manglende diversitet af lavenergi konformationer resulterer i falske negative og de mange højenergikonformationer er støj, der resulterer i falske positive.

Contents

Preface and Acknowledgements	3
Abstract	4
Resumé (Abstract in Danish)	5
1 Introduction	8
1.1 Depression and anxiety disorders	8
1.2 The neurokinin receptors	11
1.3 Structure and ligand based design	13
1.4 The pharmacophore concept and methodology	14
1.5 Aims of the thesis	15
1.6 References	16
2 Pharmacophore models for selective NK1R antagonists	19
2.1 Methods	19
2.1.1 Conformational search, force fields and solvation model	19
2.1.2 Thermodynamics and calculation of the conformational energy penalty	19
2.1.3 Manual superimposition studies	21
2.1.4 Flo99 flexible superimposition search	21
2.1.5 pK _a calculations	22
2.2 SAR of selective NK1R antagonists	22
2.3 Published pharmacophore models for selective NK1R antagonists	28
2.4 Development of a novel pharmacophore model for NK1R antagonists	31
2.4.1 Development	31
2.4.2 Validation	33
2.5 Conclusion	36
2.6 References	36
3 Pharmacophore models for NKR antagonists	41
3.1 SAR of NK1R, NK2R and NK3R antagonists	41
3.2 Previously published pharmacophore models	45
3.3 Development of pharmacophore models for NKR antagonists	47
3.3.1 Pharmacophore models for NKR antagonists	47
3.3.2 Pharmacophore models described in Appendix I	48
3.3.3 Pharmacophore models described in Appendix II	49
3.3.4 Results obtained by an automated fitting method	50
3.3.5 Subtype selectivity	51
3.3.6 A pharmacophore model for selective NK2R antagonists	52
3.4 Conclusion	56
3.5 References	57
4 Database search with Catalyst 4.6	59
4.1 Introduction	59
4.2 The Catalyst program package	59
4.3 Catalyst Hypotheses	60
4.4 The MDDR 3D-database	62
4.5 Statistics for analysing hit lists	63
4.6 Database search using a shape only	65
4.7 Database search using HipHop generated hypotheses	65
4.7.1 Pfizer like compounds	66
4.7.2 Sanofi like compounds	67
4.7.3 Randomly selected compounds	69
4.8 Database search using HypoGen generated hypotheses	71
4.8.1 Pfizer like compounds	72
4.8.2 Sanofi like compounds	72
4.9 Database search using manually generated hypotheses	73
4.9.1 Pfizer like compounds	74
4.9.2 Sanofi like compounds	75
4.10 An evaluation of Catalyst's conformational search algorithm	79
4.10.1 Energy calculations	79
4.10.2 Diverse Sampling	89
4.10.3 Conclusions on Catalyst evaluation	94
4.11 Conclusion	95

4.12 References	96
5 Neurokinin 7TM receptor models	97
5.1 7TM receptor models	97
5.2 Previously published mutagenesis and receptor model studies	98
5.2.1 Selective NK1R antagonists	98
5.2.2 Dual NK1R/NK2R and selective NK2R antagonists	99
5.3 The binding site for NKR antagonists	100
5.4 Development of the neurokinin 7TM receptor models	102
5.4.1 Alignment	103
5.4.2 The program DIANA	105
5.4.3 Construction of an initial receptor model	106
5.4.4 Refinement of the initial model	106
5.4.5 Evaluation of the models	107
5.5 Predictions made from the NKR models	109
5.5.1 Selective NK1R antagonists	109
5.5.2 Selective NK2R and non selective NK1R/NK2R antagonists	110
5.5.3 NK3R antagonists	111
5.6 Conclusion	114
5.7 References	115
List of abbreviations	118
Appendix I	119
Appendix II	134

1 Introduction

1.1 Depression and anxiety disorders

Research into mental disorders goes back to ancient Greece. However, the foundation for modern research in depression was laid by Emil Kraepelin (1856-1926) who suggested that schizophrenia and manic-depressive illness are two separate disorders. Today, two lines of depression are recognised; bipolar (manic-depression) and unipolar (major depressive disorder) depression. They are both further divided into subtypes of bipolar or unipolar depression. The main symptoms of depression are depressed mood and negative thoughts, apathy, loss of energy, fatigue, sleep difficulties, irritability, changes in appetite and weight. The bipolar depression is characterised by interchanging periods of depression and mania. In unipolar depression, the manic symptoms are absent, but sometimes psychotic symptoms are present [1]. Depression is a recurring illness. More than 65% of the people that develop a depression will have one or more relapses later in life. The number of relapses is generally larger for bipolar depression. A depression typically lasts for 3-12 months, but could be longer or even chronic. Both types of depression can be successfully treated with cognitive therapy and antidepressant drugs. In addition, severe depression can be treated with the controversial electro shock therapy. It is estimated that depression costs the Danish society approximately eight billion DKK per year. Of these, 30% is direct expenses for the treatment and 70% is indirect in the form of lost production [2].

The neurobiology of depression remains poorly understood. The amine hypothesis states: "There is a decreased availability of the neurotransmitters norepinephrine (NE) and serotonin (5-HT) in the brains of people suffering from depression". This hypothesis has successfully been employed in the development of new antidepressants, but it fails to explain how and why this unbalance arises. It is clear that both genetic and social factors are involved. About 10% of children with a depressed parent develop depression. In monozygotic twins the concordance is above 50%, whereas the concordance is 15% for dizygotic twins. These numbers should be compared with the prevalence of depression in the population. It is estimated that 2-4% of Danish men and 5-9% of women will develop a depression at some stage during their life [2]. Depression occurs in all races, and the prevalence is believed to

be fairly constant. Some factors increase the risk of developing depression. Among these are: Traumatic experiences, age, change of lifestyle, hormonal changes, alcohol and drug abuse as well as certain types of medicine and other illnesses, both physical and mental [3].

Anxiety disorders have received much less attention than depressive disorders. Currently five major anxiety disorders are recognised: General anxiety disorder, panic disorder, social anxiety disorder, post-traumatic stress disorder, obsessive-compulsive disorder, specific phobia and acute stress disorder. Diagnosing anxiety disorders may be difficult because of the high degree of comorbidity they share with each other and with mood disorders, especially unipolar depression. Symptoms of anxiety disorders include feelings of impending doom, worries, irrational fear of a situation, an activity or object. The symptoms manifest themselves in different ways in each anxiety disorder. Both genetic and social factors are involved in the cause of anxiety disorders. Few hereditary studies have been published. In monozygotic twins the concordance is significantly higher than for dizygotic twins. Rates of panic disorders in relatives of panic probands were 2-21% compared to 2-4% in relatives of controls [3].

Discovery of the first drugs that have been effective in the treatment of depression happened by chance in the 1950's. The drug Iproniazid was used for the treatment of tuberculosis. Structural modifications of the antipsychotic drug Chlorpromazine resulted in Imipramine and later in other tricyclic drugs. It was found that these drugs had an antidepressant effect, but they also had serious side effects. Iproniazid could induce a hypertensive crisis because of an interaction with diets containing tyramine. The tricyclic drugs are sedative, fattening and are deadly toxic in high doses, which is a very unfortunate property for an antidepressant. Iproniazid is a monoamine oxidase inhibitor (MAOI). The monoamine oxidase (MAO) enzyme degrades the monoamines NE, dopamine (DA) and 5-HT. Imipramine was found to have another mechanism of action, namely the blockade of the NE and 5-HT transporters. However, both mechanisms lead to the same net result, an increase of the NE and 5-HT concentration in the synapse [4].

These observations led to the formulation of the amine hypothesis discussed above. Later, Arvid Carlsson further developed this theory and postulated that increasing the NE levels in depressed people would give them back their drive, whereas increasing 5-HT levels would elevate their mood. To increase the drive in

people suffering from depression without elevating their mood could initiate suicide. However, if the mood of the depressed was increased, the increase in drive would follow automatically [4]. Carlson's hypothesis set the stage for the selective serotonin reuptake inhibitors (SSRIs), the first of which was introduced in the 1980's. These are the major antidepressant drugs of today [2]. Compared to the tricyclic antidepressants they have very few side effects. However, the SSRIs do not work for approximately 30% of the patients. This group is treated with the old tricyclic antidepressants or electro shock therapy. SSRIs have a slow onset of action, and some patients experience sexual dysfunction when taking SSRIs. This has led to a renewed interest in the research for novel antidepressants with a novel mechanism of action.

Several types of drugs have been demonstrated to be effective in the treatment of anxiety disorders. They belong to the same classes as antidepressants, i.e. tricyclics, benzodiazepines, MAOIs and SSRIs. However, the neurobiology of anxiety disorders remains poorly understood and the ultimate mechanism of action of these drugs remains undetermined [3].

Recently, it has been demonstrated that selective neurokinin receptor (NKR) antagonists show antidepressive and anxiolytic activity. In a clinical study by Kramer et al. [5], the selective neurokinin 1 receptor (NK1R) antagonist MK869 (compound **39**, Table 2.4 [6]) was compared to the SSRI Paroxetine. MK869 appears to be effective as an antidepressant with efficacy matching that of Paroxetine. The anxiolytic effects may be slightly greater than those of the SSRI, and MK869 has fewer side effects than Paroxetine. A few neurological studies have shed light on how the antidepressant effect of NKR antagonists is elicited. Repeated administration with antidepressant compounds causes a reduction of substance P (SP, the endogenous ligand of the NK1R, see Section 1.2) biosynthesis in discrete brain regions in rats [7]. Therefore, alterations in neurokinin systems may contribute to their antidepressant activity. Acute stress has been demonstrated to result in an increase in SP content in certain brain areas of rats [8]. The mechanism of action of NK1R and NK2R antagonists in reducing responses to stress is believed to be preventing the stress-induced increase in SP and neurokinin A (NKA) levels. Several studies have indicated a link between SP levels and anxiety. The selective NK1 antagonist CGP49823 (compound **124**, Figure 4.3 [9]) is reported to show anxiolytic effect in rats [10]. Fehder et al. [11] have shown that the SP levels in peripheral blood in humans correlates with the anxiety level measured on the multiple affect adjective checklist

and they conclude that SP may serve as a mediator in stress induced immune reactions.

The reader is referred to the books "Comprehensive textbook of psychiatry" [3] and "Handbook of Depression and Anxiety" [1] for more information on depression and anxiety disorders. The books "The Psychopharmacologists" [12] and "Antidepressants – New Pharmacological Strategies" [13] describe the history and strategy for the development of antidepressants. Stout et al. [14] is a review of NK1R antagonists as potential antidepressants.

1.2 The neurokinin receptors

Research into the NKRs dates back to 1931 when Euler and Gaddum extracted a substance from horse brain and intestine that caused vasodilation in rabbit peripheral tissues. In 1934, this agent was named substance P, but it was not until 1971 that its structure was identified to be an undecapeptide (Table 1.1). The same year, SP was synthesised. It was established that SP is the mammalian analogue of the tachykinins found in amphibians and it was therefore included in this family of signalling peptides. Since its discovery, SP has been found in numerous tissues and has been shown to affect several different types of cells. It has also been established that SP is a neurotransmitter that is involved in signalling painful or noxious stimuli.

Three NKR subtypes, NK1, NK2 and NK3, have been identified by molecular cloning and sequence analysis [15-17]. They are classified according to their endogenous ligands. The NK1R has the highest affinity for SP, the NK2R has the highest affinity for NKA (also named substance K, neurokinin α and neuromedin L), and the NK3R has the highest affinity for neurokinin B (NKB, also named neurokinin β and neuromedin K). However, the ligands act as full agonists on all three receptors [18]. See Table 1.1 for the structure of the endogenous ligands. The NKRs have been linked to such biological effects as decrease of blood pressure, plasma extravasation, smooth muscle contractions and release of secretory products, neurotransmitters, histamine and prostaglandins [18]. Recently, it has been demonstrated that selective NKR antagonists show antidepressive [19], antipsychotic [20], and anxiolytic effects [10] (Section 1.1). NKRs could also be involved in neurodegenerative diseases [20]. Selective binding and efficacy assays have been developed for each of the NKR subtypes. This has led to the identification of large amounts of both peptide and non-

peptide antagonists. Some of these are now in development for the treatment of emesis, depression, anxiety, psychosis, colitis, pain, asthma, migraine, inflammation, bronchitis and incontinence [21].

Table 1.1: Structure of the endogenous ligands of the NKRs.

Receptor	Ligand	Structure
NK1	SP	H-Arg-Pro-Lys-Pro-Gln-Gln-Phe-Phe-Gly-Leu-Met-NH ₂
NK2	NKA	H-His-Lys-Thr-Asp-Ser-Phe-Val-Gly-Leu-Met-NH ₂
NK3	NKB	H-Asp-Met-His-Asp-Phe-Phe-Val-Gly-Leu-Met-NH ₂

The NKRs are proteins composed of 350 to 500 amino acids. They belong to the superfamily of G-protein coupled receptors (GPCRs) [18]. GPCRs are transmembrane proteins that transfer signals across the cell membrane. That is, GPCRs transmit intercellular signals by coupling to an intracellular G-protein as a response to a specific binding of a transmitter molecule. GPCRs are classified by their endogenous ligands. The NKRs belong to the largest group of GPCRs, the rhodopsin-like GPCRs. This group includes most of the other well-studied, neurotransmitter receptors like the monoaminergic and opioid receptors.

As is the case for most other GPCRs, NKRs have not yet been crystallised, so no experimental structures are available. However, the X-ray structure of the GPCR bovine rhodopsin [22] has recently been published (PDB file 1F88). The GPCRs contain seven transmembrane α -helices (7TM) of approximately 25 residues length. The helices are connected by intra- and extracellular loops. The *N*-terminal is located on the extracellular side whereas the *C*-terminal extends into the cytoplasm. The loop regions and the *N*- and *C*-terminals are surrounded by an aqueous environment and consist primarily of hydrophilic amino acids. The 7TM region is in a lipid environment and consists of amphiphilic helices. The sequence identity between bovine rhodopsin and the NKRs is 20-25%. The transmembrane part of the receptors where the non-peptide antagonists bind shows even higher sequence identity. Figure 1.1 show a schematic view of a NK2R model based on the structure of bovine rhodopsin. This model will be further discussed in Chapter 5.

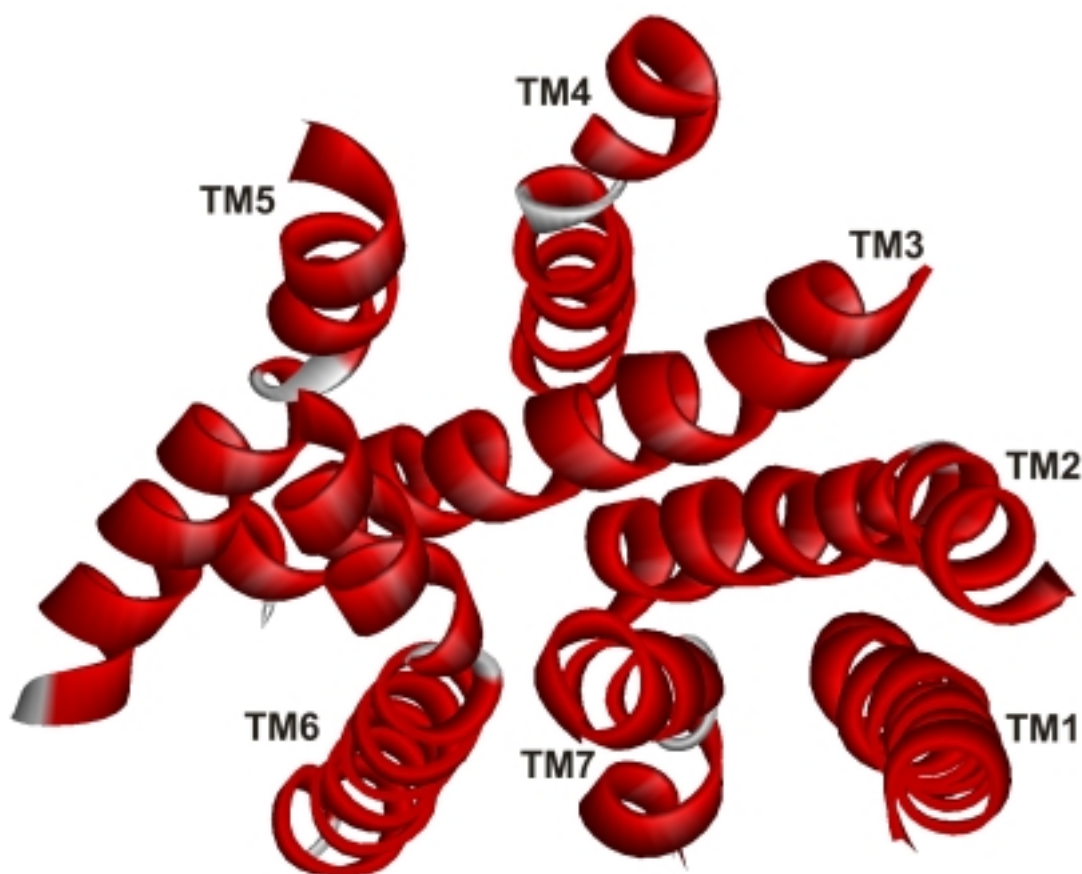


Figure 1.1: A schematic view of the NK2R model seen from the extracellular side. Only the 7TM part of the receptor are shown. The areas where the helices bend are coloured grey.

The reader is referred to the reviews by Regioli et al. [18], Aamir et al. [23] and Maggi [24] for more information on NKRs. Raffa [20] describes the possible role of NKRs in CNS disorders. The publications by Schwartz and Holst [25], Bikker et al. [26] and Chollet and Turcatti [27] provide information on the pharmacology, structure and modelling of GPCRs.

1.3 Structure and ligand based design

The three-dimensional structure(s) of a molecule provide important information about the properties of the molecule and help in understanding the biological activity of the molecule. This is true for both large molecules like receptors or enzymes (drug targets) and smaller drug like molecules. The ligand needs to be both sterically and electronically complementary to the receptor-binding cavity in order to attain activity. This is sometimes described by the key-in-a-lock metaphor. If a 3D structure of the drug target can be obtained by X-ray crystallography, preferably with a co-crystallized ligand, then the ligand-receptor interaction can be studied directly.

Potential ligands may be docked into the binding site, and the knowledge obtained from the docking may be used in the design of new ligands with optimal ligand-receptor interaction. This approach is called structure-based ligand design.

If the structure of the drug target is unknown, as is the case with most GPCRs, information about the binding site and the ligand-receptor interaction can be obtained by studying the ligands and their binding data. This indirect approach is called ligand-based design and includes the qualitative method pharmacophore modelling and the QSAR (Quantitative Structure-Activity Relationship) methods. If the X-ray structure of a protein related to the target protein exists, a homology model of the target can be constructed. The quality of a homology model may not be sufficient for structure-based design, but the model can serve as a help in the development or validation of a pharmacophore model.

The reader is referred to the reviews by Taylor and Jewsbury [28], Flower [29], Greer et al. [30], and the book “3D QSAR in Drug Design: Ligand-Protein Interactions and Molecular Similarity” [31] for more information on structure- and ligand-based design.

1.4 The pharmacophore concept and methodology

A pharmacophore model describes the nature of and the spatial relationships between structural features recognized at a receptor site and responsible for the affinity of ligands at that site. The first step in the construction of the pharmacophore model is the selection of a set of high affinity ligands with the same binding mode. The set should be selected from the criteria of structural diversity and low flexibility. Next, functional groups considered essential for biological activity (the pharmacophore elements) are identified. The most important step is identification of the putative receptor-bound conformation. This is done by superimposing low energy conformations of the most rigid ligands. The ligands are superimposed so that the pharmacophore elements overlap and a common template, i.e. a pharmacophore model can be identified [32]. It is important to use less flexible ligands for the construction of the pharmacophore model since this reduces the number of possible models. Structure-Activity Relationship (SAR) data and the calculation of conformational energies are used to evaluate the pharmacophore models. The pharmacophore model can be used as a search query for database search, as a starting

point for 3D-QSAR, as a tool for designing new high affinity ligands and to rationalise SAR data.

To explore the conformational space of a ligand, a conformational analysis is performed. This is done by utilising a molecular modelling program package containing a search algorithm and a force field. Since the biological environment of a drug molecule is mostly aqueous, calculations should be made using a solvation model [32]. The protonation state of the ligands in the biological environment also has to be considered. This is necessary since the protonation of a molecule will alter both its sterical and electronic properties.

RMS values are used as a measure of how well the proposed bioactive conformations fit the pharmacophore model. For certain pharmacophore elements, site-points should be used instead of superimposing the ligand atoms [32]. For hydrogen bond donors or acceptors, a dummy atom 2.8 Å from the heteroatom of the ligand will emphasize the directional aspect of the ligand-receptor interaction. Each pharmacophore element should be weighed equally in the RMS, otherwise the value is misleading.

Information about the receptor cavity can be obtained by analysing the ligands in their putative bioactive conformation. Low affinity ligands might intrude into regions that are occupied by the receptor resulting in unfavourable ligand-receptor interactions. The space occupied by the receptor is referred to as the receptor-essential volume. If such areas can be identified, they can be included in the pharmacophore model. Receptor-essential volumes are often necessary pharmacophore elements in models discriminating between different receptor subtypes [32].

The reader is referred to the book "Pharmacophore Perception, Development, and Use in Drug Design" [33] for more information on pharmacophore modelling.

1.5 Aims of the thesis

The development of a drug is a costly and time-consuming process. It is therefore of great importance to have satisfactory tools and models as a basis for drug design and development. The present work is directed towards increasing our knowledge about ligands that inhibit the NKRs. Structure-activity relationships (SAR) is a major component in the drug development process. The aim of the project is to analyse SAR for antagonists of, primarily, the NK1R and NK2R subtypes. The identification of the

bioactive conformation and its interactions with the target receptor provides essential knowledge for the design of new drugs. State-of-the-art programs like Molecular Mechanics, Quantum Mechanics and Molecular Graphics programs will be used in the development of 3D-pharmacophore models and receptor models for the NK1R and NK2R.

The developed 3D-pharmacophore and receptor models will be used as tools for the rational design of new active and selective compounds with increased affinity for the target receptors. A comparative analysis of the 3D-pharmacophore and receptor models will make it possible to design drugs which are selective for one or more subtypes of the receptors. The pharmacophore models will also be used as search queries for database search. In this way, new leads can be identified and the time-consuming drug design process may be shortened.

1.6 References

1. Boer, J. A. den, and Sitsen, J. M., (Eds.), Handbook of depression and anxiety: A biological approach, Marcel Dekker Inc., New York, **1994**.
2. Bech, P., (Ed.), Depressionssygdommen og dens behandling. Depressionssygdommen set med lægernes øjne, Psykiatri Fondens Forlag, Copenhagen, Denmark, **2001**.
3. Kaplan, H. I. and Sadock, B. J., (Eds.), Comprehensive Textbook of Psychiatry/VI, Williams & Wilkins, Baltimore, Maryland, USA, **1995**.
4. Bøgesø, K. P. and Bang-Andersen, B. In Krogsgaard-Larsen, P., Liljefors, T., and Madsen, U., (Eds.), Textbook of drug design and discovery, Taylor & Francis, London and New York, **2002**: 299-327.
5. Kramer, M. S., Cutler, N., Feighner, J., Shrivastava, R., Carman, J., Sramek, J. J., Reines, S. A., Liu, G., Snavely, D., Wyatt-Knowles, E., Hale, J. J., Mills, S. G., MacCoss, M., Swain, C. J., Harrison, T., Hill, R. G., Hefti, F., Scolnick, E. M., Cascieri, M. A., Chicchi, G. G., Sadowski, S., Williams, A. R., Hewson, L., Smith, D. and Rupniak, N. M., Distinct mechanism for antidepressant activity by blockade of central substance P receptors. *Science*. **1998**, 281: 1640-1645.
6. Hale, J. J., Mills, S. G., MacCoss, M., Finke, P. E., Cascieri, M. A., Sadowski, S., Ber, E., Chicchi, G. G., Kurtz, M., Metzger, J., Eiermann, G., Tsou, N. N., Tattersall, F. D., Rupniak, N. M., Williams, A. R., Rycroft, W., Hargreaves, R. and MacIntyre, D. E., Structural optimization affording 2-(R)-(1-(R)-3, 5-bis(trifluoromethyl)phenoxy)-3-(S)-(4-fluoro)phenyl-4-(3-oxo-1,2,4-triazol-5-yl)methylmorpholine, a potent, orally active, long-acting morpholine acetal human NK-1 receptor antagonist. *J. Med. Chem.* **1998**, 41: 4607-4614.
7. Brodin, E., Ögren, S. O. and Theodorsson-Norheim, E., Effects of subchronic treatment with imipramine, zimelidine and alaproclate on regional tissue levels of substance P- and neurokinin A/neurokinin B-like immunoreactivity in the brain and spinal cord of the rat. *Neuropharmacology*. **1987**, 26: 581-590.

8. Rosen, A., Brodin, K., Eneroth, P. and Brodin, E., Short-term restraint stress and s.c. saline injection alter the tissue levels of substance P and cholecystokinin in the peri-aqueductal grey and limbic regions of rat brain. *Acta Physiol. Scand.* **1992**, 146: 341-348.
9. Ofner, S., Hauser, K., Schilling, W., Vassout, A. and Veenstra, S. J., SAR of 2-benzyl-4-aminopiperidines: CGP 49823, an orally and centrally active non-peptide NK1 antagonist. *Bioorg. Med. Chem. Lett.* **1996**, 6: 1623-1628.
10. File, S. E., Anxiolytic action of a neurokinin1 receptor antagonist in the social interaction test. *Pharmacol. Biochem. Behav.* **1997**, 58: 747-752.
11. Fehder, W. P., Sachs, J., Uvaydova, M. and Douglas, S. D., Substance P as an immune modulator of anxiety. *Neuroimmunomodulation.* **1997**, 4: 42-48.
12. Healy, D., *The psychopharmacologists*, Chapman & Hall, London, UK, **1996**.
13. Skolnick, P. (Ed.), *Antidepressants: New pharmacological strategies*, Humana Press, Totowa, New Jersey, USA, **1997**.
14. Stout, S. C., Owens, M. J. and Nemeroff, C. B., Neurokinin (1) receptor antagonists as potential antidepressants. *Annu. Rev. Pharmacol. Toxicol.* **2001**, 41: 877-906.
15. Gerard, N. P., Eddy, R. L., Jr., Shows, T. B. and Gerard, C., The human neurokinin A (substance K) receptor. Molecular cloning of the gene, chromosome localization, and isolation of cDNA from tracheal and gastric tissues. *J. Biol. Chem.* **1990**, 265: 20455-20462.
16. Takahashi, K., Tanaka, A., Hara, M. and Nakanishi, S., The primary structure and gene organization of human substance P and neuromedin K receptors. *Eur. J. Biochem.* **1992**, 204: 1025-1033.
17. Takeda, Y., Chou, K. B., Takeda, J., Sachais, B. S. and Krause, J. E., Molecular cloning, structural characterization and functional expression of the human substance P receptor. *Biochem. Biophys. Res Commun.* **1991**, 179: 1232-1240.
18. Regoli, D., Boudon, A. and Fauchere, J. L., Receptors and antagonists for substance P and related peptides. *Pharmacol. Rev.* **1994**, 46: 551-599.
19. Nutt, D., Substance-P antagonists: a new treatment for depression? *Lancet* **1998**, 352: 1644-1646.
20. Raffa, R. B., Possible role(s) of neurokinins in CNS development and neurodegenerative or other disorders. *Neurosci. Biobehav. Rev.* **1998**, 22: 789-813.
21. von Sprecher, A., Gerspacher, M. and Anderson, G. P., Neurokinin antagonists as potential therapies for inflammation and rheumatoid arthritis. *IDrugs* **1998**, 1: 73-91.
22. Palczewski, K., Kumasaka, T., Hori, T., Behnke, C. A., Motoshima, H., Fox, B. A., Le, T., I, Teller, D. C., Okada, T., Stenkamp, R. E., Yamamoto, M. and Miyano, M., Crystal structure of rhodopsin: A G protein-coupled receptor. *Science* **2000**, 289: 739-745.
23. Khawaja, A. M. and Rogers, D. F., Tachykinins: receptor to effector. *Int. J. Biochem. Cell. Biol.* **1996**, 28: 721-738.
24. Maggi, C. A., The mammalian tachykinin receptors. *Gen. Pharmacol.* **1995**, 26: 911-944.
25. Schwartz, T. W. and Holst, B. In Foreman, J. C. and Johansen, T., (Eds.), *Textbook of receptor pharmacology*, CRC press, Boca Raton, **2002**: 81-109.

26. Bikker, J. A., Trumpp-Kallmeyer, S. and Humblet, C., G-Protein coupled receptors: models, mutagenesis, and drug design. *J. Med. Chem.* **1998**, 41: 2911-2927.
27. Chollet, A. and Turcatti, G., Biophysical approaches to G protein-coupled receptors: structure, function and dynamics. *J. Comput.-Aided. Mol. Des.* **1999**, 13: 209-219.
28. Taylor, R. D., Jewsbury, P. J. and Essex, J. W., A review of protein-small molecule docking methods. *J. Comput.-Aided. Mol. Des.* **2002**, 16: 151-166.
29. Flower, D. R., Modelling G-protein-coupled receptors for drug design. *Biochim. Biophys. Acta* **1999**, 1422: 207-234.
30. Greer, J., Erickson, J. W., Baldwin, J. J. and Varney, M. D., Application of the three-dimensional structures of protein target molecules in structure-based drug design. *J. Med. Chem.* **1994**, 37: 1035-1054.
31. Kubinyi, H., Folkers, G. and Martin, Y. C., (Eds.), 3D QSAR in Drug Design: Ligand-Protein Interactions and Molecular Similarity, Kluwer Academic Publishers, Dordrecht, **1998**.
32. Liljefors, T. and Pettersson, I., In Krogsgaard-Larsen, P., Liljefors, T., and Madsen, U., (Eds.), Textbook of drug design and discovery, Taylor & Francis, London and New York, **2002**: 86-116.
33. Güner, O. F., (Ed.), Pharmacophore perception, development, and use in drug design, International University Line, La Jolla, CA, USA, **2000**.

2 Pharmacophore models for selective NK1R antagonists

2.1 Methods

The methods outlined in this section were applied in the development of the pharmacophore models described in this and in the following chapter.

2.1.1 Conformational search, force fields and solvation model

The molecules were built using the program package MacroModel version 7.0 and 7.1 [1;2]. The molecules were protonated as they were expected to be found in an aqueous solution at physiological pH (see section 2.1.5). The conformational space was then searched using the Monte Carlo Multiple Minimum (MCMM) method [3]. All heavy atoms and hydrogens on heteroatoms were superimposed in the test for duplicate conformations. All rotatable single bonds were included in the conformational search. All flexible rings were ring-opened and the rings were allowed to invert. However, known chiral centers were not allowed to invert. The search was continued until the lowest energy conformations were found at least five times. The energy minimisation was carried out with the truncated Newton conjugate gradient (TNCG) algorithm and the MMFF94s [4] force field as implemented in MacroModel. This force field has proven to be one of the best methods for reproducing experimental conformational energies [5;6]. Default parameters were used, except for van der Waals and electrostatic cut-offs which were set to 100 Å. This means effectively no cut-offs on van der Waals and electrostatic forces. The conformational searches were done for aqueous solution with the Generalised Born/Solvent Accessible surface (GB/SA) continuum solvation model [7;8] as implemented in MacroModel. For compounds for which no low energy conformation that fitted the pharmacophore model could be found, further conformational searches by this standard procedure using the AMBER*, MM3* and MM2* force fields as implemented in MacroModel were performed.

2.1.2 Thermodynamics and calculation of the conformational energy penalty

The change in free energy (ΔG) for the binding of the ligand to the receptor to form the ligand-receptor complex is related to the equilibrium constant (K) as described by Equation 2.1, where R is the gas constant and T is the absolute temperature. A

thermodynamic cycle is displayed in Figure 2.1 [9]. The only terms that we are able to calculate with reasonable accuracy are $\Delta G_{\text{conf}}(\text{Ligand})$ and $\Delta G_{\text{solv}}(\text{Ligand})$. From Equation 2.2 we see that $\Delta G_{\text{conf}}(\text{Ligand})$ contributes directly to ΔG . By combining Equation 2.1 and 2.2, we can calculate that each 5.6 kJ/mol of $\Delta G_{\text{conf}}(\text{Ligand})$ lowers the K_i by a factor of ten. Because of the rapid decline of K_i with increasing $\Delta G_{\text{conf}}(\text{Ligand})$, only low energy conformations are of biological interest.

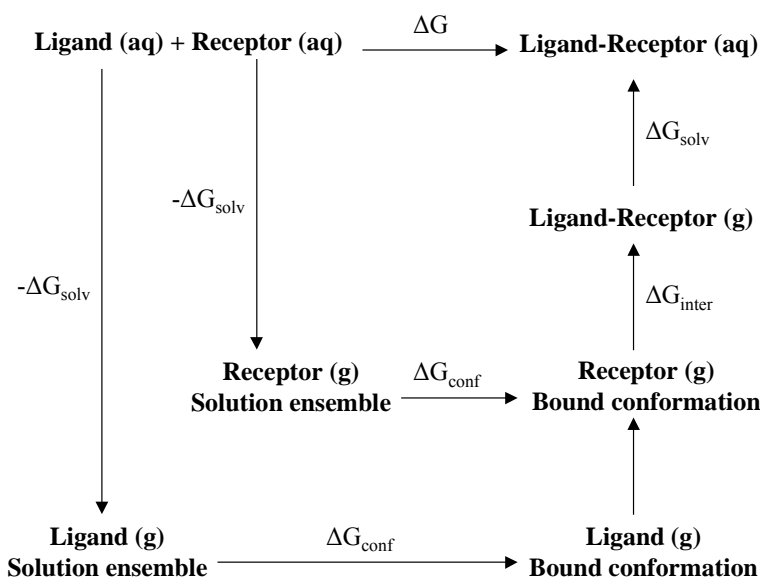


Figure 2.1: A thermodynamic cycle for the binding of the ligand to the receptor to form the ligand-receptor complex. ΔG_{solv} are the change in free energy of solvation. ΔG_{conf} is the change in conformational free energy. ΔG_{inter} is the change in free energy of interaction between the ligand and receptor.

The conformational energy penalty for the putative bioactive conformation of the ligand was calculated by subtracting the internal (steric) energy of the preferred conformation in aqueous solution ($\Delta H_{\text{conf}}(\text{GlobalMinimum})$, the energy of the global energy minimum in solution excluding the hydration energy) from the calculated energy of the putative bioactive conformation ($\Delta H_{\text{conf}}(\text{LigandBound})$) [9]. This is equivalent to making the approximation in Equation 2.3. Since the conformational ensemble was represented by only the global minimum, entropy effects have not been taken into account. For flexible molecules, this leads to an underestimation of the energy penalty. A limit of 12.6 kJ/mol (3 kcal/mol) for acceptable energy penalties was imposed as recommended by Boström et al. [9].

$$\Delta G = RT \ln K_i, K_i = I / K \Leftrightarrow \Delta G = -RT \ln K \quad (\text{Equation 2.1})$$

$$\Delta G = \Delta G_{solv}(LigandReceptorComplex) - \Delta G_{solv}(Ligand) - \Delta G_{solv}(Receptor) + \Delta G_{conf}(Ligand) + \Delta G_{conf}(Receptor) + \Delta G_{inter} \quad \text{(Equation 2.2)}$$

$$\Delta G_{conf}(Ligand) \approx \Delta H_{conf}(LigandBoundConf - GlobalMinimum) \quad \text{(Equation 2.3)}$$

2.1.3 Manual superimposition studies

Aromatic rings, hydrogen bond donors (in most cases the protonated nitrogen atom of an amine) and hydrogen bond acceptors were chosen as pharmacophore elements. For each of the aromatic rings, centroids were constructed. A putative hydrogen bonding site point was represented by a dummy atom 2.8 Å from the heteroatom of the ligand in the direction of the hydrogen bond. The dummy atom was used to evaluate the direction of the hydrogen bond donor-acceptor interactions. The dummy atoms together with the centroids were used as fitting points for superimposing the ligands, except when noted. In that case, the heteroatoms of the ligand and centroids were used as fitting points. The fitting method employed was least-squares rigid body molecular superimposition using the MacroModel program. The superimposition was evaluated in terms of RMS values of the fitting points. A RMS value of 0.6 Å has been used as a soft indicator to determine whether a fit is acceptable or not. The aromatic pharmacophore elements were fitted in a coplanar orientation if energetically possible. The RMS values do not give any measure of this coplanarity since only the centroids are superimposed.

2.1.4 Flo99 flexible superimposition search

The automatic fitting algorithm QXP is part of the program package Flo99 [10;11]. QXP is a flexible fitting algorithm that assigns an attractive force between similar atoms in different molecules. Structures were built and imported from MacroModel. QXP works best when only two or three structures are fitted at a time. Either one structure was used as a template, or all structures were kept flexible. Default parameters were used, except when noted. The force field implemented in Flo is an all atoms force field without electrostatics. This is not state-of-the-art for calculating conformational energy penalties. Therefore, the output conformations from Flo99 was exported to MacroModel where each structure was relaxed by using flat bottomed

Cartesian constraints with a half width of 0.2 Å and the default restraining force constant of 500 kJ/mol*Å². The conformational energy was calculated using the MMFF94s force field as previously described [9].

2.1.5 pK_a calculations

In order to identify the protonation state of the ligands at physiological pH, the pK_a values of the basic nitrogens were calculated by use of the program MolSurf 99/1 [12]. Some compounds contain more than one basic nitrogen but only the pK_a for the most basic nitrogen is calculated by MolSurf. MolSurf is parameterised so that it requires a Spartan [13] archive file with the neutral compound as input. Each of the putative bioactive conformations were imported into Spartan for a full AM1 geometry optimisation followed by a single point HF calculation with the 3-21G* basis set. Default settings were used for both programs.

2.2 SAR of selective NK1R antagonists

Compound **1** (Table 2.1) was the first non-peptide NK1R antagonist to be published. A derivative, compound **2**, without the methoxy group, was discovered by random screening, and the subsequent optimisation yielded compound **1**. This is a selective and potent NK1R antagonist with a K_i of 0.8 nM. Systematic modification of the functional groups (compounds **3-6**) have identified the essential pharmacophore elements. Compound **3** proves that one of the phenyls of the benzhydryl group is essential for high NK1 affinity. The secondary nitrogen and oxygen in the benzylamine and benzylether group respectively, are probably hydrogen bond acceptors. NMR measurements confirm that only one nitrogen is protonated at physiological pH, and that is the quinuclidine nitrogen. Therefore, both the benzylamine nitrogen in **1** and the benzylether oxygen atom in **8** can be hydrogen bond acceptors, whereas only the benzylamine nitrogen in **1** can act as a donor. If the hydrogen bonding group is blocked as in compound **4**, the affinity decreases by a factor of 150. For compound **13**, the effect of removing the oxygen atom (X in compound **15**) is even more pronounced.

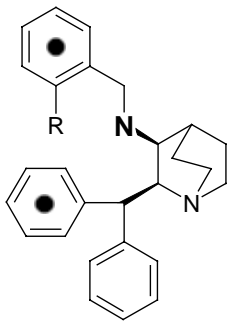
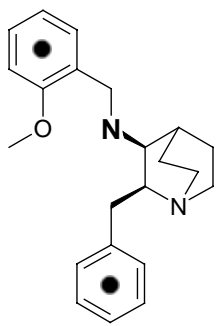
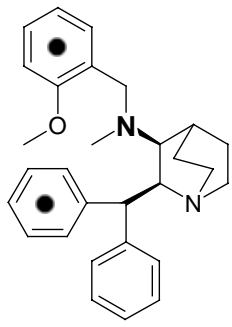
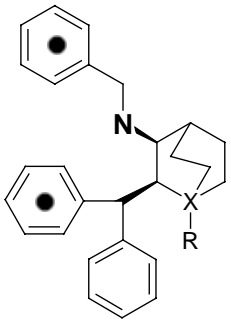
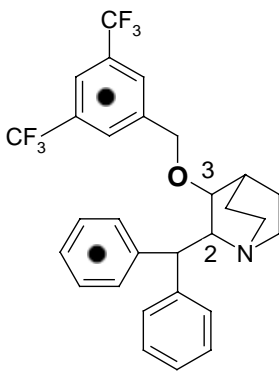
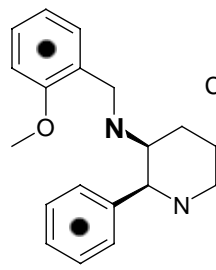
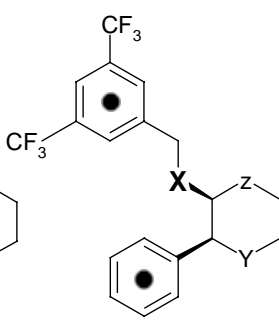
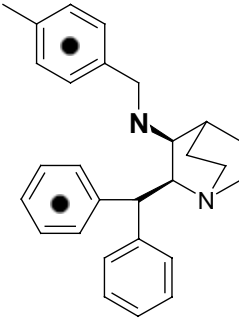
Compounds **5-7** demonstrate that the quinuclidine nitrogen is not essential for high NK1 affinity. However by comparing compounds **5** and **7** it is evident that a hydrogen bonding group in this area increases NK1 affinity. The effect of removing

the piperidine nitrogen (Y in compound **12**) from compound **12** is even more pronounced than removing the quinuclidine nitrogen from compound **1**. Compound **14** has a very low affinity.

The stereochemistry is important for NK1 affinity with one diastereomeric pair (compounds **8** and **9**) being high affinity antagonists while the other pair (compounds **10** and **11**) show more than a 100 fold lower affinity.

Compounds **12** and **13** are very minimalistic in the sense that they show high affinity and contain nothing but the essential pharmacophore elements. A large number of analogues of compounds **1**, **8**, **12** and **13** with substituents in the phenyl and quinuclidine ring have been synthesised. The SAR of these compounds is summarised in Figure 2.2. The NK1 affinity decreases when the benzhydryl phenyl or the equivalent phenyl in compounds **12-13** are substituted, except for the 4-F analogue that is equally potent as the unsubstituted analogue [14]. Small aliphatic substituents are tolerated in the quinuclidine ring, but this decreases the NK1 affinity slightly [15;16]. The quinuclidine or piperidine nitrogen can be substituted with relatively large groups containing hydrogen bonding atoms [14;17]. The benzyl group tolerates relatively large substituents in the 3-position, like pyridine and other heteroaromatics. 3,5-disubstitution or 2-methoxy-5-disubstitution is better than mono substitution [18]. Substitution in the 4-position decreases affinity (compound **16**), and only methoxy is tolerated in the 2-position [19]. Several linkers (C in Figure 2.2) between the quinuclidine ring and the benzyl group have been tested, but the optimal for NK1 affinity is just an oxygen or nitrogen atom [19].

Table 2.1: SAR of the first non-peptide NK1R antagonists. Centroids and atoms in bold mark the selected pharmacophore elements.

			
1 R=OMe (CP96345)	3	4	5 R=H, X=C 6 R=CH ₃ , X=N ⁺ 7 R=CH ₂ CONH ₂ , R=N ⁺
			
8 2S,3S 9 2R,3S 10 2S,3R 11 2R,3R	12 (CP99994)	13 X=O, Y=NH, Z=CH ₂ 14 X=O, Y=Z=CH ₂ 15 X=CH ₂ , Y=NH, Z=O	16

Compound	NK1 IC ₅₀ /nM	Reference	Compound	NK1 IC ₅₀ /nM	Reference
1	2.1, 0.8, 0.5	[20], [19]	9	0.7	[21]
2	16, 85	[20], [19]	10	270	[21]
3	487	[20]	11	570	[21]
4	383	[20]	12	0.8, K _i = 0.17	[22], [23]
5	22	[24]	13	1.4	[25]
6	12.2	[17]	14	2632	[26]
7	1.3	[17]	15	1530	[27]
8	1.3	[21]	16	246	[19]

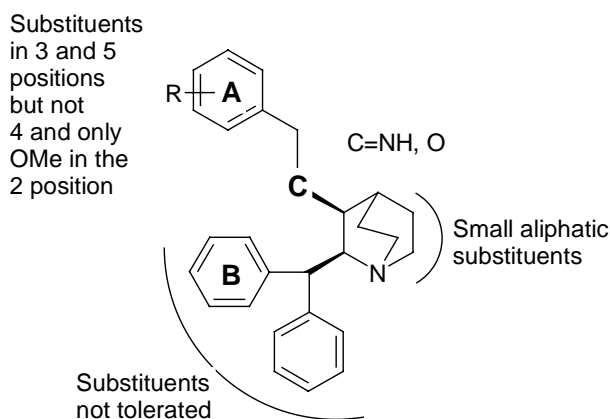
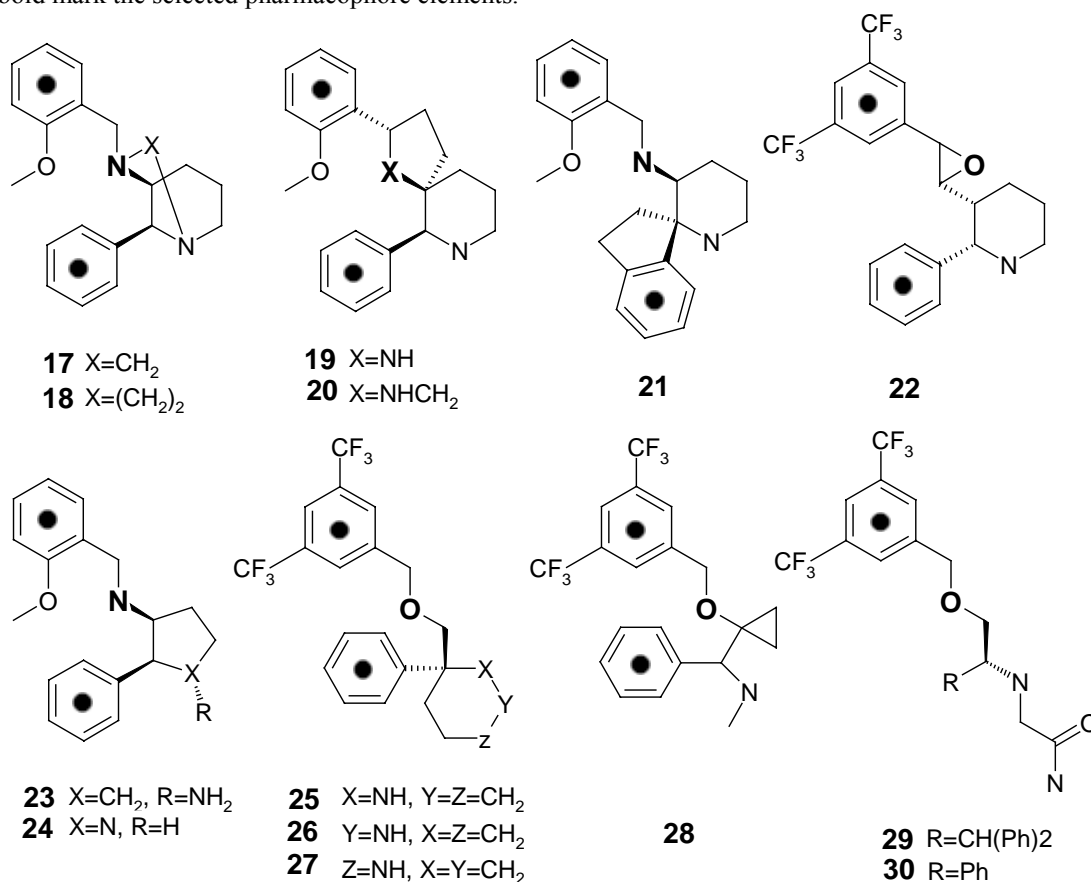


Figure 2.2: A summary of the SAR of selective NK1R antagonists. The letters in bold marks the three pharmacophore elements. A and B are aromatic rings and C is a hydrogen bond acceptor.

The scaffolds of **1** and **12** have been modified in numerous ways (Table 2.2). A number of constrained analogues of **12** have been synthesised (compounds **17-21**). In compounds **17-18**, the two nitrogen atoms have been incorporated in a ring, and in compounds **19-20**, the piperidine ring and the linker are converted to a spirocycle. In compound **21**, the phenyl group is connected to the piperidine ring in a spirocycle, and in compound **22**, the linker is constrained by an epoxy ring. In compounds **23-24**, the piperidine ring has been replaced by five-membered rings, and in compounds **25-27**, the substituents on the piperidine ring are on a quaternary carbon. Compounds **29-30** are ring-opened analogues of **8** and **13**, respectively, whereas compound **28** is a constrained analogue of **30**.

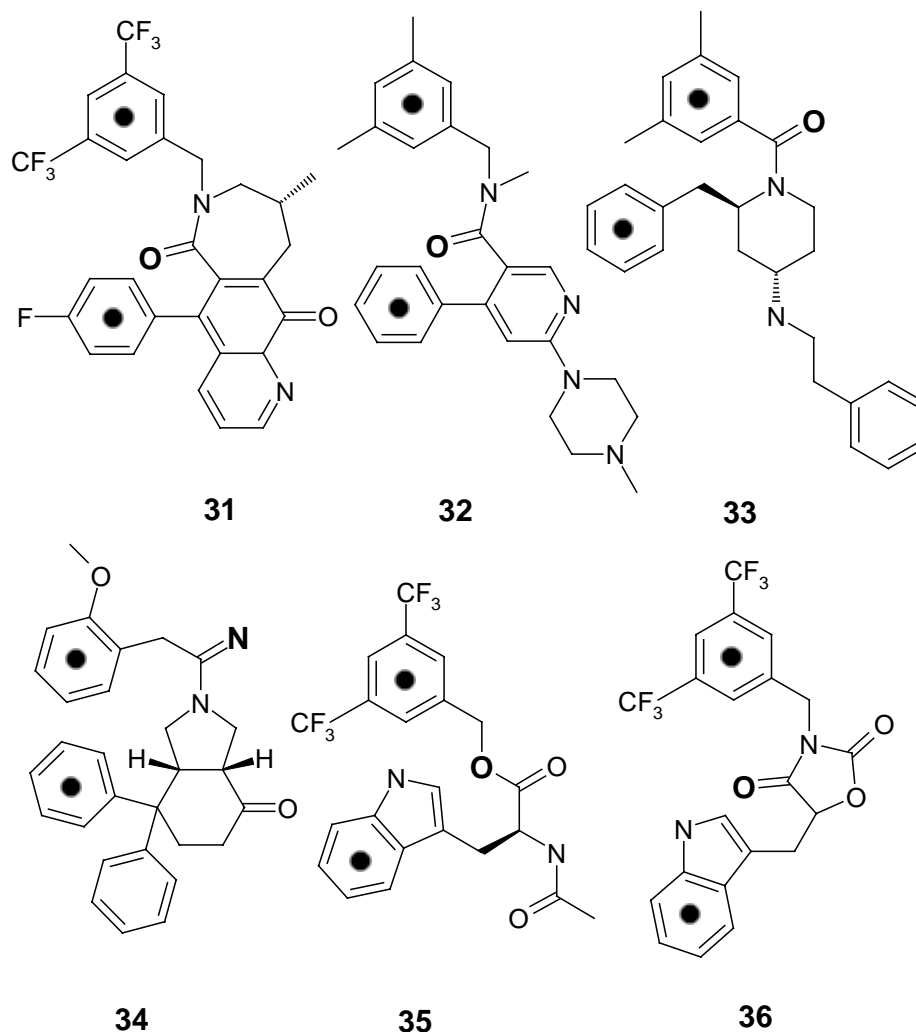
Table 2.2: Selective NK1R antagonists derived from the compounds **1** and **12**. Centroids and atoms in bold mark the selected pharmacophore elements.



Compound	NK1 IC ₅₀ / nM	Reference	Compound	NK1 IC ₅₀ / nM	Reference
17	0.61	[28]	24	7	[25]
18	0.36	[28]	25	1.0	[29]
19	K _i > 10000	[30]	26	20	[29]
20	K _i = 2	[30]	27	0.95	[29]
21	40	[22]	28	K _i = 150	[31]
22	87	[27]	29	0.53	[32]
23	12	[33]	30	8, 8	[34], [35]

A number of selective NK1R antagonists that are not derived from compounds **1** or **12** are believed to share the binding mode of **1** and **12** (Table 2.3). Compounds **31-32** are derived from benzodiazepine gastrin/cholecystokinin antagonists. A number of similar scaffolds has been reported [36;37]. Several analogues of the 4-amino-piperidin-amide compound **33** with different substituents on the 4-amine have been reported. The perhydroisoindole compound **34** was the second non-peptide NK1R antagonist described. It is six times more potent at the rat NK1R than at the human NK1R. However, compounds in this series with higher selectivity for the human NK1R have been described [36;38]. Compound **35** is a L-tryptophan ester derivative, while compound **36** has the ester linkage replaced by a conformationally constrained heterocycle.

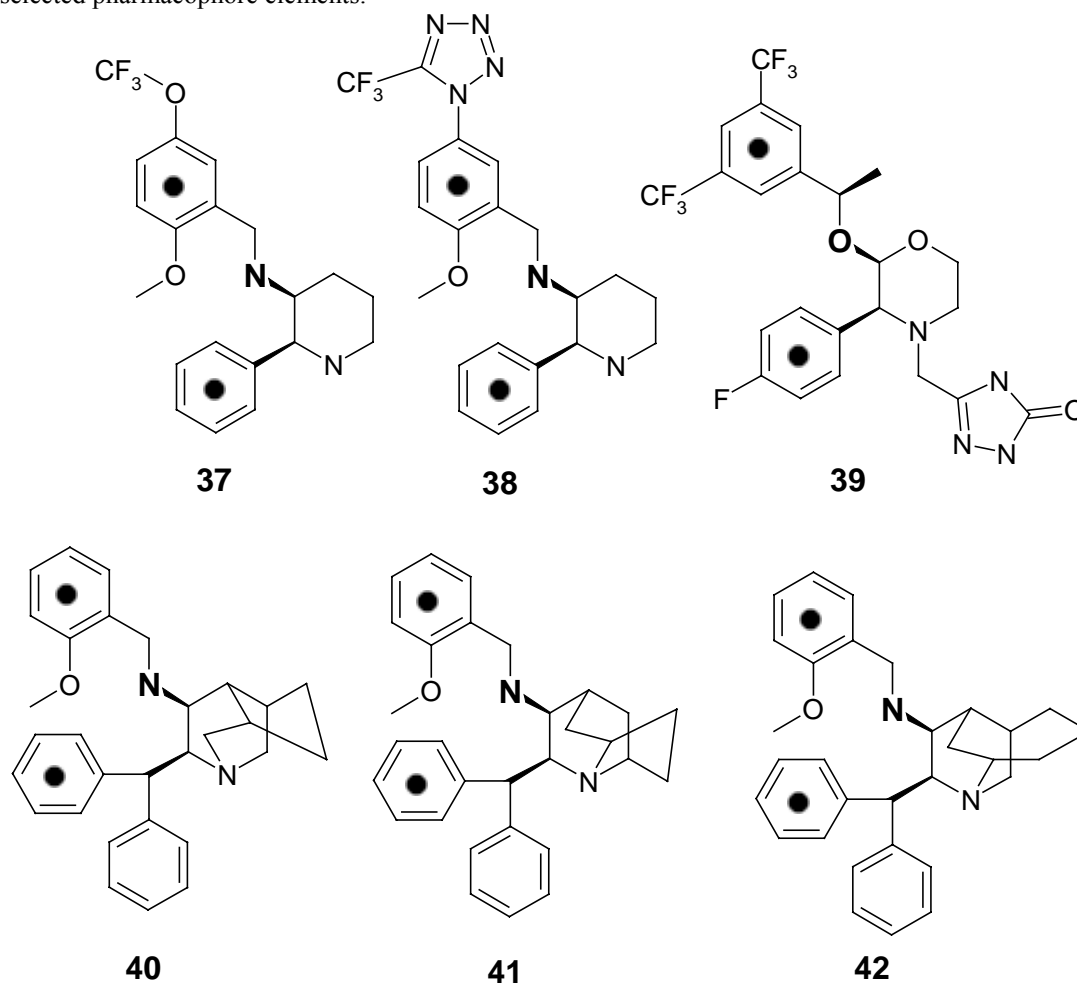
Table 2.3: Selective NK1R antagonists that share the binding mode of compounds **1** and **12**. Centroids and atoms in bold mark the selected pharmacophore elements.



Compound	NK1 IC ₅₀ / nM	Reference	Compound	NK1 IC ₅₀ / nM	Reference
31	0.45	[39]	34	49	[40]
32	K _i = 1.4	[41]	35	1.6	[42]
33	12	[43], [44]	36	22	[45]

Compounds **37-42** were used to explore the receptor dimensions (Table 2.4). Compounds **37-39** are second generation NK1R antagonists with improved ADME profiles due to the substitution of the benzylic position and the piperidine nitrogen (compound **39**) or the benzyl phenyl ring (compounds **37** and **38**). They have been in phase II clinical trials for the treatment of emesis [46]. Compound **39** has a methyl in the benzylic position and a large substituent on the morpholine nitrogen. Compounds **40-42** include a tricyclic moiety.

Table 2.4: NK1R antagonists fitted to the pharmacophore model. Centroids and atoms in bold mark the selected pharmacophore elements.



Compound	NK1 IC ₅₀ / nM	Reference	Compound	NK1 IC ₅₀ / nM	Reference
37	0.16	[47]	40	2.4	[16]
38	K _i = 0.2	[18]	41	0.92	[16]
39	0.09	[14]	42	1.9	[16]

2.3 Published pharmacophore models for selective NK1R antagonists

A number of pharmacophore models have been published for selective NK1R antagonists. Goldstein et al. [49] have used DISCO, the automated pharmacophore generation module from the SYBYL program package. As input structures they use a surprisingly diverse set consisting of both peptides, peptidomimetics and small non-peptides like compounds **8**, **9**, **12** and **33** are used. The descriptions of the obtained models are vague and little structural similarity is found in the figures with superimposition of compounds.

Jacoby et al [50] derive a pharmacophore model for chemically modified dipeptide selective NK1R antagonists and two non-peptide antagonists (Compounds **1** and **35**). In this model, the antagonists bind with two aromatic rings in a parallel

displaced conformation. The pharmacophore model is combined with a receptor model study, where it is shown that a hydrogen bond acceptor in the antagonists interacts with a donor in the receptor (Gln165). All pharmacophore elements are found to interact with residues which have been identified to be important for binding by site directed mutagenesis. However, the pharmacophore model is not evaluated by calculating conformational energy penalties or RMS values.

Takeuchi et al. [51] have developed a pharmacophore model comprising compounds from several structurally diverse classes, all of which are discussed in Section 2.2. The model only contains two pharmacophore elements, two aromatic rings. A constrained conformational search procedure are used, where the constraints derived from the conformational search of the first compound are used to constrain the conformational search for the next, and so on. The authors end up with a set of intramolecular distances (an Imap), containing 188 common alignments. In four of these the two aromatic rings form a T shape and an L shape in the rest (Figure 2.3). It is concluded that a conformation in which the aromatic rings are stacked cannot represent a common binding mode. Argumentation of whether the L or T shape represents the protein bound conformation are not given, but the T shape is chosen for a CoMFA analysis. This seems surprising, considering the overweight of alignments in which the two aromatic rings form an L shape. In the T conformation, there is a favourable interaction between the rings, whereas the opposite is true for the L shape. However, this argument is not given and conformational energies are not considered at all. Furthermore, the authors presume that only the L, T and parallel arrangement of the aromatic rings are possible and do not consider the parallel displaced and tilted arrangement.

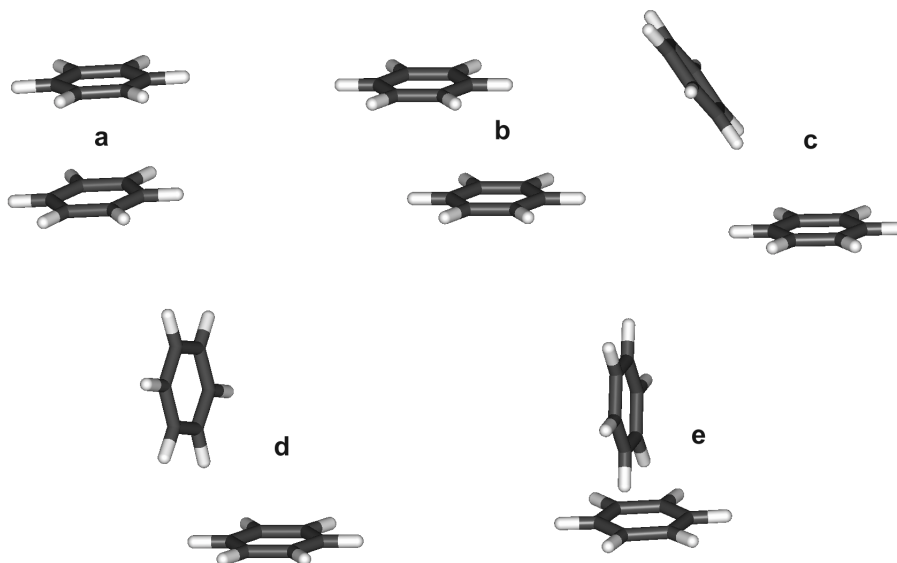


Figure 2.3: Illustrations of the arrangement of two phenyl rings. a: Stacked or parallel. b: Parallel displaced. c: Parallel displaced and tilted. d: L shape. e: T shape or edge to ring face.

Swain et al. [19] have conducted a modelling and mutagenesis study of compounds **1** and **8**. It is suggested that compound **1** has the two aromatic rings in an parallel conformation and that there is an intramolecular hydrogen bond between the methoxy group and the secondary amine. However, believe compound **8** is suggested to have the aromatic rings in an edge to ring face arrangement. Three amino acids residues are identified as important for the binding of compound **8** to the NK1R and they are proposed to interact with specific groups in compound **8**. This is discussed in detail in Section 5.2. The quinuclidine nitrogen is proposed to be protonated and interact with the receptor, but specific interactions are not identified.

Armour et al. [37] have modelled analogues of compound **31**. Veenstra et al. [44] have studied compounds **12** and analogues of compound **33**. McLeod et al. [42] have studied compounds **8** and **35**. These papers suggest that the NK1R antagonists bind in a conformation with parallel displaced and tilted aromatic rings. Lewis et al. [45] have studied compound **36** and derivatives. Several conformations are identified with the aromatic rings in either a parallel or tilted orientation. Lowe et al. [20] was the first to suggest a binding model for **1**, however no bioactive conformation is reported.

Desai et al. [23;30] have conducted a modelling study of compounds **1**, **12**, **19** and **20**. The authors conclude that the two aromatic rings are parallel and are hydrophobically collapsed. In their stereo illustrations, the rings appear stacked.

However, a stacked conformation is energetically unfavourable whereas a parallel displaced conformation is energetically favourable.

Caliendo et al. [52] have studied three tripeptide NK1 antagonists by nuclear magnetic resonance (NMR). The low energy solution conformations of the peptides have two aromatic rings in a stacked, parallel displaced or parallel displaced and tilted arrangement. These arrangements are superimposed on compounds **1**, **35** and **36**, and the authors conclude that the putative bioactive conformation of NK1 antagonists have two aromatic rings in a U-shape (In their illustrations the aromatic rings appear stacked). Another NMR study of compound **12** [22] and several X-ray structures of selective NK1 antagonists have been reported [15;17;19;20;28;36;37;42;44;45]. However it should be noted that X-ray or NMR conformations may be different from the bioactive conformation.

2.4 Development of a novel pharmacophore model for NK1R antagonists

2.4.1 Development

The two aromatic rings (A and B) and the hydrogen bond acceptor (C) were chosen as pharmacophore elements (Figure 2.2). Compounds **1**, **12**, **18**, **20** and **24** were used to derive the pharmacophore model. These compounds were chosen for their varying degree of flexibility. The following criteria must be fulfilled in the pharmacophore model: The aromatic rings are fitted in an approximately coplanar orientation, the hydrogen bond acceptor is accessible and the acceptor-donor vectors are pointing in the same direction, and the conformational energies are low. Only one superimposition was found for which these criteria are fulfilled. In this pharmacophore element, A and B are in a parallel, displaced and tilted orientation. The superimposition is shown in Figure 2.4 together with the pharmacophore model. The pharmacophore model was defined as the pharmacophore elements in the conformation of compound **12** from the superimposition in Figure 2.4 top.

No model could be obtained by Flo99 when the more rigid compounds **18** and **20** were included in the flexible superimpositioning search. However, a search with the compounds **1**, **12** and **24** yielded one solution in which the criteria for the pharmacophore model were fulfilled. This is shown in Figure 2.5, where the hydrogen bond acceptors are represented as vectors. In this solution, there is no hydrogen bond between the methoxy oxygen and the benzylamine. When calculated by MMFFs, the

conformational energies are quite high (7.0, 11.5 and 15.1 kJ/mol for compounds **1**, **12** and **24**, respectively). However, when the bonds in the benzylamine group are rotated about to form the intramolecular hydrogen bond (as shown in Figure 2.5), the solution found by Flo99 is transformed into the manually generated pharmacophore model.

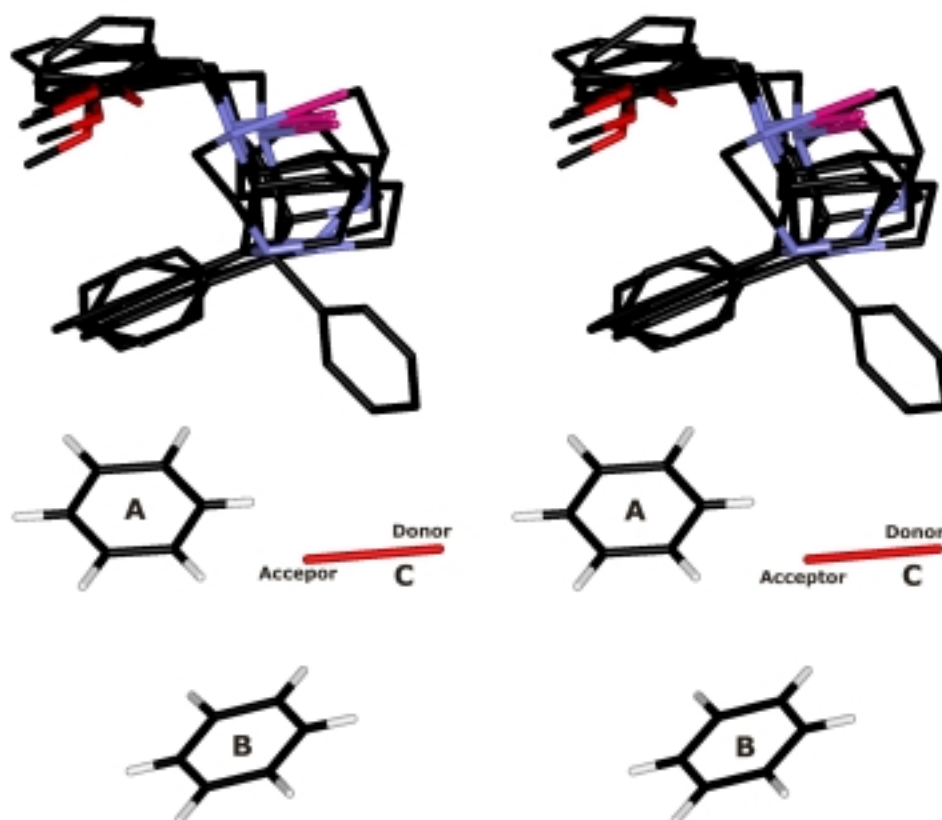


Figure 2.4: Top: Superimposition of compounds **1**, **12**, **18**, **20** and **24**. Stereo image, hydrogen atoms are removed for clarity. Bottom: The pharmacophore model. Stereo image.

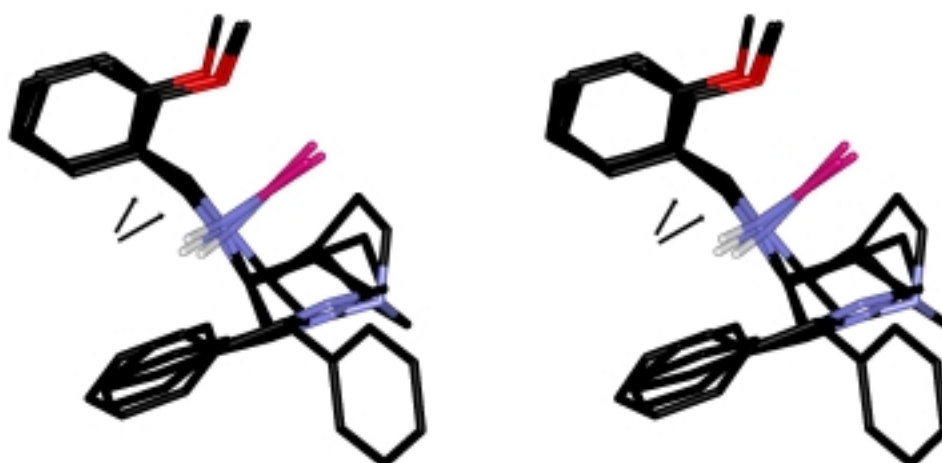


Figure 2.5: The superimposition found by Flo99. Stereo image, hydrogens are removed for clarity. The hydrogen bond acceptors are represented as vectors. The arrows indicate bonds, which by changes of dihedral angles will transform these conformations to make them fit the pharmacophore model in Figure 2.4.

2.4.2 Validation

Compounds **1-11** and **13-42** (Tables 2.1-2.4) were used to evaluate the pharmacophore model. The conformational energy and RMS value of the fits are shown in Table 2.5. Figure 2.6 shows a superimposition of compounds **1-10** and **12-42** (Compound **11** has another stereochemistry than **1**). All compounds could be fitted to the model with a low conformational energy and a low RMS value, except compounds **3, 4, 17-19, 28, 31, 32** and **34**. Compounds **3, 18, 19** and **28** could be fitted to the model with a low RMS value but a higher conformational energy. Compounds **3** and **28** have moderate affinity for the NK1R and conformational energies of 17.7 and 15.5 kJ/mol, respectively, while compound **19** is inactive and has a conformational energy of 34.0 kJ/mol. The conformational energy penalties for these compounds provide a good explanation for the observed low affinities. If the conformational energy of compound **18** is calculated by AMBER* or MM3*, it is within the accepted limit. The conformational energy of compound **17** is also lower when calculated by AMBER* and MM3*. The high energy calculated by MMFFs could be an artefact of the force field. It is reasonable to assume that the uncertainty of the energy is higher for the constrained bicyclic systems of **17** and **18** since these ring systems have probably not been used for the parameterisation of the force field.

Compounds **4** and **15** could be fitted to the model with a low conformational energy. However, compound **4** has a methyl group that points in the direction of the hydrogen bond acceptor vector, and compound **15** has the acceptor atom replaced by a carbon atom. This explains their reduced NK1 affinity. Compounds **17, 31, 32** and **34** could be fitted to the model with a low conformational energy and a low RMS value only when the hydrogen bond acceptor atom was used as a fitting point instead of the dummy atom. This is because there is a significant angle between the direction of the lone pair on the hydrogen bond acceptor atom (of pharmacophore element C) and the hydrogen bond acceptor vector. However, it is not unreasonable to assume that they fit the pharmacophore model as argued in Appendix II (A small deviation from the ideal angle of the hydrogen bond results in a small decrease in hydrogen bond energy, while the change in RMS value is large). Compounds **10** and **11** could also be fitted to the model with a low conformational energy and a low RMS value only when the hydrogen bond acceptor atom was used as a fitting point. However, for these compounds, the lone pair on the hydrogen bond acceptor atom (of pharmacophore element C) is pointing in the wrong direction. Compounds **10** and **11** are the

enantiomers of the high affinity compounds **9** and **8**, respectively. The moderate NK1R affinity of these compounds can be explained by the missing hydrogen bond interaction.

All high affinity compounds could be fitted to the model with low RMS value and a low conformational energy penalty. A number of weak or inactive close analogues of high affinity compounds were fitted to the model. These are missing a pharmacophore element (compounds **4**, **10**, **11** and **14-15**), have a high conformational energy penalty (compounds **3**, **19** and **28**), or occupy a receptor essential volume (compound **16**). The model can also distinguish between the high affinity (compounds **8** and **9**) and weak (compounds **10** and **11**) stereoisomers of compound **8**.

The pharmacophore model is consistent with the modelling studies by Armour et al. [37], Veenstra et al. [44] and McLeod et al. [42]. The pharmacophore model differs from that of Takeuchi et al. [51] and Swain et al. [19] and the modelling study by Desai et al. [30]. In these models, pharmacophore elements A and B are edge-to-ring face or stacked, respectively. Figure 2.7 shows a superimposition of three conformations of compound **8** with pharmacophore elements A and B parallel, displaced and tilted, stacked and edge-to-ring face, respectively. The difference between the three conformations lies mostly in the orientation of pharmacophore element A.

Table 2.5: Conformational energy penalties (E_{conf}) and RMS values of compounds fitted to the model. The energies are calculated by MMFFs, except when noted. Centroids and dummy atoms are used as fitting points, except numbers in parenthesis where centroids and the hydrogen bond acceptor atom are used.

Compound	$E_{\text{conf.}} / \text{kJ/mol}$	RMS / Å	Compound	$E_{\text{conf.}} / \text{kJ/mol}$	RMS / Å
1	-2.3	0.27	20	3.6	0.34
2	-6.5	0.27	21	-1.4	0.34
3	17.7	0.11	22	-5.6	0.53 (0.49)
4	-4.8	(0.25)	23	-1.0	0.10
5	5.1	0.15	24	-3.7	0.08
6	-0.8	0.36	25	-1.9	0.28
7	-6.9	0.36	26	6.8	0.28
8	5.4	0.05	27	0.3	0.26
9	0.4	0.21	28	15.5	0.70
10	9.4	(0.65)	29	-1.1	0.52
11	0.3	(0.12)	30	3.7	0.12
12	-8.1	Template	31	-5.5	1.13 (0.29)
13	4.6	0.18	32	-3.3	0.65 (0.27)
14	5.6	0.18	33	3.3	0.29
15	-5.1	0.40	34	0.0	1.25 (0.57)
16	-2.5	0.34	35	-5.4	0.16
17	10.7	(0.35)	36	6.4	0.62
17 ^a	9.7	(0.42)	37	-6.0	0.14
17 ^b	7.0	(0.34)	38	-0.3	0.26
18	15.7	0.50 (0.23)	39	4.4	0.31
18 ^a	10.5	0.49 (0.25)	40	-3.6	0.06
18 ^b	3.4	0.52 (0.29)	41	-2.9	0.05
19	34.0	0.11	42	-0.3	0.18

^aAMBER* ^bMM3*

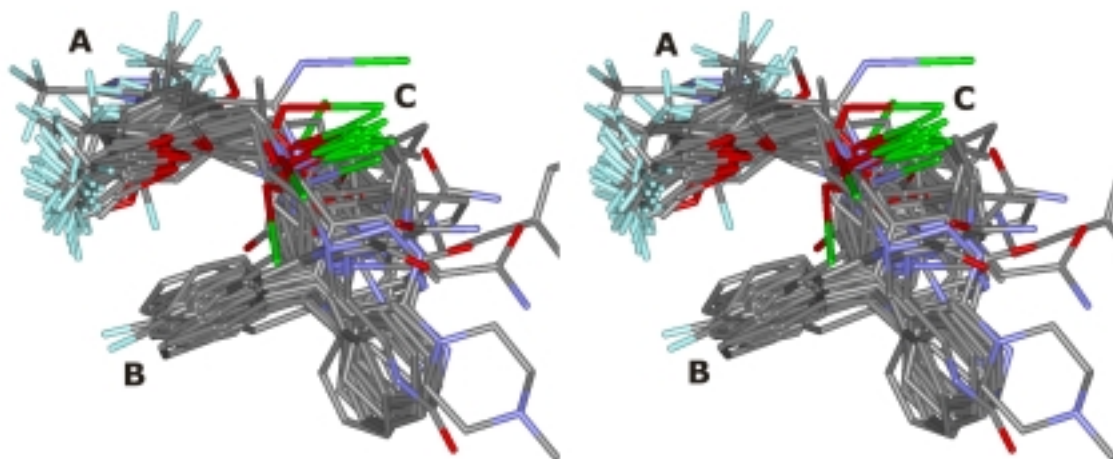


Figure 2.6: A superimposition of compounds 1-10 and 12-42. Compound 11 are the enantiomer of 8. Stereo image. Hydrogen atoms are removed for clarity.

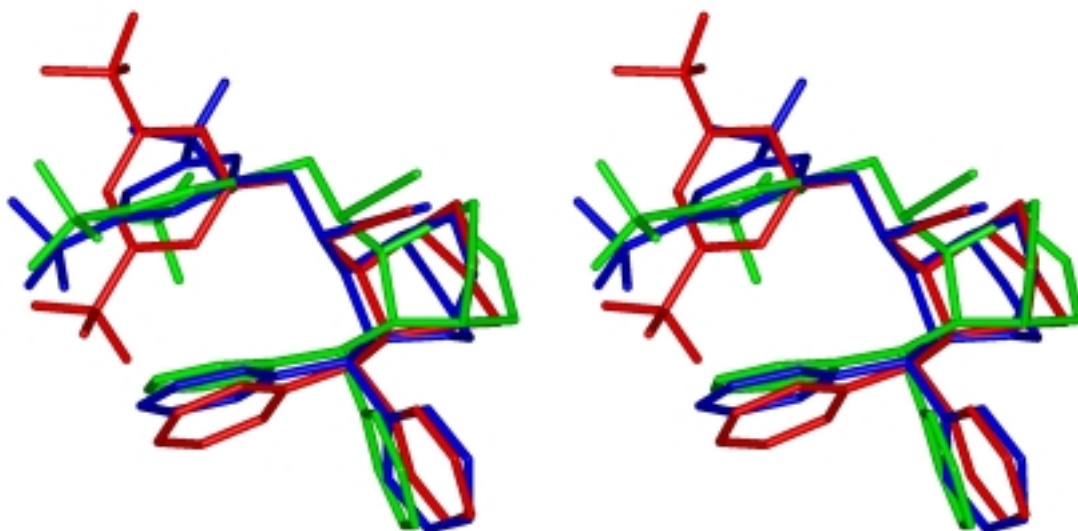


Figure 2.7: A superimposition of compound **8** with pharmacophore elements A and B parallel, displaced and tilted (blue), stacked (green) and edge-to-ring face (red). Stereo image. Hydrogen atoms are removed for clarity.

2.5 Conclusion

A pharmacophore model for selective NK1R antagonists has been developed. The model consists of two aromatic rings and a hydrogen bond acceptor. The aromatic rings are in a parallel, displaced and tilted conformation. The hydrogen bond acceptor is represented as a vector to emphasize the directionality of the hydrogen bond. The pharmacophore model is consistent with the modelling studies by Armour et al. [37], Veenstra et al. [44] and McLeod et al. [42]. The model differs from the pharmacophore model published by Takeuchi et al. [51] and Swain et al. [19] and the modelling study by Desai et al. [30] by the arrangement of pharmacophore element A.

The model was evaluated against 42 structurally diverse and selective NK1R antagonists with affinities ranging from sub-nanomolar to inactive. The model could successfully explain the NK1 affinities of all compounds fitted to the model. All high affinity compounds could be fitted to the model with low RMS values and a low conformational energy penalty. All weak or inactive compounds fitted to the model are missing a pharmacophore element, have a high conformational energy penalty, or occupy receptor essential volume. The model can also distinguish between the affinities for the four stereoisomers of compound **8**.

2.6 References

1. Macromodel 7.1. Schrödinger Inc., 1500 SW First Avenue, Suite 1180, Portland, Oregon 97201.

2. Mohamadi, F., Richards, N. G. J., Guida, W. C., Liskamp, R., Lipton, M., Caufield, C., Chang, G., Hendrickson, T. and Still, W. C., MacroModel - An Integrated Software System for Modelling Organic and Bioorganic Molecules Using Molecular Mechanics. *J. Comput. Chem.* **1990**, 11: 440-467.
3. Chang, G., Guida, W. C. and Still, W. C., An Internal Coordinate Monte Carlo Method for Searching Conformational Space. *J. Am. Chem. Soc.* **1989**, 111: 4379-4386.
4. Halgren, T. A., MMFF VI. MMFF94s option for energy minimization studies. *J. Comput. Chem.* **1999**, 20: 720-729.
5. Halgren, T. A., MMFF VII. Characterization of MMFF94, MMFF94s, and other widely available force fields for conformational energies and for intermolecular-interaction energies and geometries. *J. Comput. Chem.* **1999**, 20: 730-748.
6. Gundertofte, K., Liljefors, T., Norrby, P. O. and Pettersson, I., A comparison of conformational energies calculated by several molecular mechanics methods. *J. Comput. Chem.* **1996**, 17: 429-449.
7. Hasel, T. F., Hendrickson, T. F. and Still, W. C., A Rapid Approximation to the Solvent Accessible Surface Areas of Atoms, *Tetrahedron Comput. Methods* **1988**, 1: 103-116
8. Still, W. C., Tempczyk, A., Hawley, R. C. and Hendrickson, T., Semianalytical Treatment of Solvation for Molecular Mechanics and Dynamics. *J. Am. Chem. Soc.* **1990**, 112: 6127-6129.
9. Boström, J., Norrby, P.-O. and Liljefors, T., Conformational energy penalties of protein-bound ligands. *J. Comput.-Aided Mol. Des.* **1998**, 12: 383-396.
10. McMartin, C. and Bohacek, R. S., Flexible matching of test ligands to a 3D pharmacophore using a molecular superposition force field: comparison of predicted and experimental conformations of inhibitors of three enzymes. *J. Comput.-Aided Mol. Des.* **1995**, 9: 237-250.
11. McMartin, C. and Bohacek, R. S., QXP: powerful, rapid computer algorithms for structure-based drug design. *J. Comput.-Aided Mol. Des.* **1997**, 11: 333-344.
12. Sjöberg, P. In Waterbeemd, H. v. d., Testa, B. and Folkers, G., (Eds.), Computer-Assisted Lead Finding and Optimization, Verlag Helvetica Chimica Acta, Basel, **1997**: 83-93.
13. Spartan 5.0. Wavefunction Inc., 18401 Von Karman Ave., Suite 370, Irvine, CA 92612. **1997**.
14. Hale, J. J., Mills, S. G., MacCoss, M., Finke, P. E., Cascieri, M. A., Sadowski, S., Ber, E., Chicchi, G. G., Kurtz, M., Metzger, J., Eiermann, G., Tsou, N. N., Tattersall, F. D., Rupniak, N. M., Williams, A. R., Rycroft, W., Hargreaves, R. and MacIntyre, D. E., Structural optimization affording 2-(R)-(1-(R)-3, 5-bis(trifluoromethyl)phenoxy)-3-(S)-(4-fluoro)phenyl-4- (3-oxo-1,2,4-triazol-5-yl)methylmorpholine, a potent, orally active, long-acting morpholine acetal human NK-1 receptor antagonist. *J. Med. Chem.* **1998**, 41: 4607-4614.
15. Lowe, J. A. I., Drozda, S. E., Snider, M., Longo, K. P. and Rizzi, J. P., Nuclear variations of quinuclidine substance P antagonists: 2-Diphenylmethyl-1-azabicyclo(3.2.2)nonan-3-amines. *Bioorg. Med. Chem. Lett.* **1993**, 3: 921-924.
16. Lowe, J. A., Drozda, S. E., McLean, S., Bryce, D. K., Crawford, R. T., Snider, R. M., Longo, K. P., Nagahisa, A. and Tsuchiya, M., Aza-tricyclic substance P antagonists. *J. Med. Chem.* **1994**, 37: 2831-2840.
17. Lowe, J. A. I., Drozda, S. E., McLean, S., Crawford, R. T., Bryce, D. K. and Bordner, J., N-alkyl quinuclidinium substance P antagonists. *Bioorg. Med. Chem. Lett.* **1994**, 4: 1153-1156.

18. Ward, P., Armour, D. R., Bays, D. E., Evans, B., Giblin, G. M. P., Heron, N., Hubbard, T., Liang, K., Middlemiss, D., Mordaunt, J., Naylor, A., Pegg, N. A., Vinader, M. V., Watson, S. P., Bountra, C. and Evans, D.C., Discovery of an orally bioavailable NK1 receptor antagonist, (2S,3S)-(2-methoxy-5-tetrazol-1-ylbenzyl)(2-phenylpiperidin-3-yl)amine (GR203040), with potent antiemetic activity. *J. Med. Chem.* **1995**, 38: 4985-4992.
19. Swain, C. J., Seward, E. M., Cascieri, M. A., Fong, T. M., Herbert, R., MacIntyre, D. E., Merchant, K. J., Owen, S. N., Owens, A. P. and Sabin, V., Identification of a series of 3-(benzyloxy)-1-azabicyclo[2.2.2]octane human NK1 antagonists. *J. Med. Chem.* **1995**, 38: 4793-4805.
20. Lowe, J. A., Drozda, S. E., Snider, R. M., Longo, K. P., Zorn, S. H., Morrone, J., Jackson, E. R., McLean, S., Bryce, D. K. and Bordner, J., The discovery of (2S,3S)-cis-2-(diphenylmethyl)-N-[(2-methoxyphenyl)methyl]-1-azabicyclo[2.2.2]-octan-3-amine as a novel, nonpeptide substance P antagonists. *J. Med. Chem.* **1992**, 35: 2591-2600.
21. Swain, C. J., Seward, E. M., Sabin, V., Owen, S., Baker, R., Cascieri, M. A., Sadowski, S., Strader, C. and Ball, R. G., Quinuclidine based NK-1 antagonists 2: Determination of the absolute stereochemical requirements. *Bioorg. Med. Chem. Lett.* **1993**, 3: 1703-1706.
22. Armour, D. R., Watson, S. P., Pegg, N. A., Heron, N. M., Middlemiss, D., Chan, C., Cholerton, T. J., Hubbard, T., Vinader, M. V., Davies, H. G., Cocker, J. D., Bays, D. E. and Ward, P., Spiro-piperidine non-peptide neurokinin-1 receptor antagonists. *Bioorg. Med. Chem. Lett.* **1995**, 5: 2671-2676.
23. Desai, M. C., Lefkowitz, S. L., Thadeio, P. F., Longo, K. P. and Snider, R. M., Discovery of a potent substance P antagonist: recognition of the key molecular determinant. *J. Med. Chem.* **1992**, 35: 4911-4913.
24. Fong, T. M., Yu, H., Cascieri, M. A., Underwood, D., Swain, C. J. and Strader, C. D., The role of histidine 265 in antagonist binding to the neurokinin-1 receptor. *J. Biol. Chem.* **1994**, 269: 2728-2732.
25. Harrison, T., Williams, B. J., Swain, C. J. and Ball, R. G., Piperidine-ether based hNK1 antagonists 1: Determination of the relative and absolute stereochemical requirements. *Bioorg. Med. Chem. Lett.* **1994**, 4: 2545-2550.
26. Mills, S. G., MacCoss, M., Underwood, D., Shah, S. K., Finke, P. E., Miller, D. J., Budhu, R. J., Cascieri, M. A., Sadowski, S. and Strader, C. D., 1,2,3-trisubstituted cyclohexyl substance P antagonists: Significance of the ring nitrogen in piperidine-based NK-1 receptor antagonists. *Bioorg. Med. Chem. Lett.* **1995**, 5: 1345-1350.
27. Ladduwahetty, T., Keown, L., Cascieri, M. A. and Sadowski, S., Morpholine-based substance P antagonists: Assessment of the 3-point binding model. *Bioorg. Med. Chem. Lett.* **1994**, 4: 1917-1920.
28. Howard, H. R., Shenk, K. D. and Coffman, K. C., Synthesis of conformationally restricted substance P antagonists. *Bioorg. Med. Chem. Lett.* **1995**, 5: 111-114.
29. Stevenson, G. I., MacLeod, A. M., Huscroft, I., Cascieri, M. A., Sadowski, S. and Baker, R., 4,4-Disubstituted piperidines: a new class of NK1 antagonist. *J. Med. Chem.* **1995**, 38: 1264-1266.
30. Desai, M. C., Vincent, L. A. and Rizzi, J. P., Importance of parallel vectors and "hydrophobic collapse" of the aligned aromatic rings: discovery of a potent substance P antagonist. *J. Med. Chem.* **1994**, 37: 4263-4266.
31. Aitken, D. J., Onger, S., Vallee-Goyet, D., Gramain, J. C. and Husson, H. P., Synthesis, modelling and NK1 antagonist evaluation of a non-rigid cyclopropane-containing analogue of CP-99,994. *Bioorg. Med. Chem. Lett.* **2001**, 11: 659-661.

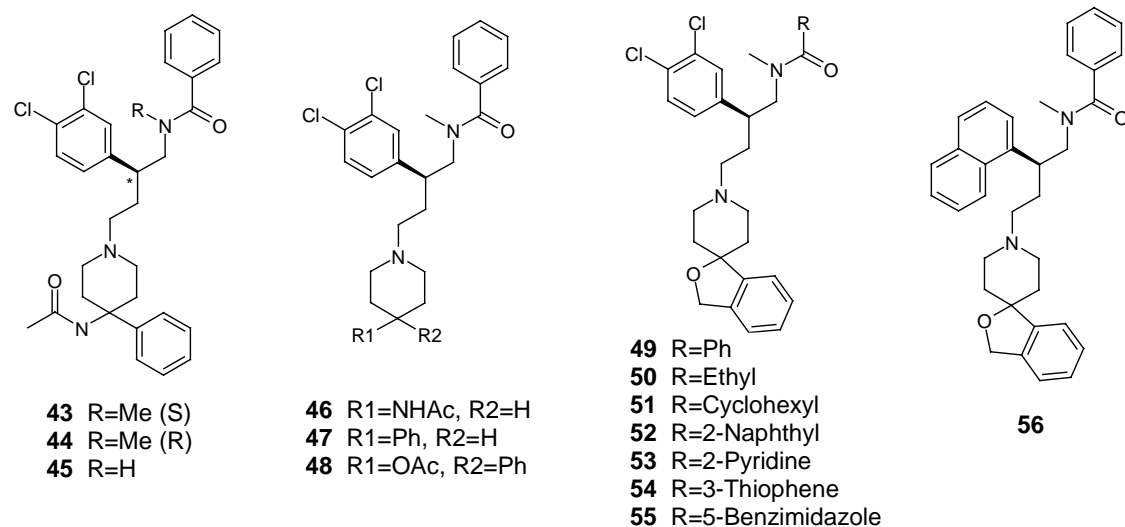
32. Williams, B.J., Teall, M., Mc Kenna, J., Harrison, T., Swain, C.J., Cascieri, M.A., Sadowski, S., Strader, C. and Baker, R., Acyclic NK-1 antagonists: 2-Benzhydryl-2-aminoethyl ethers. *Bioorg. Med. Chem. Lett.* **1994**, 4, 1903-1908.
33. Finke, P. E., Meurer, L., MacCoss, M., Mills, S. G., Sadowski, S., Cascieri, M. A., Metzger, J., Eiermann, G. and MacIntyre, D. E., Discovery of potent human NK1 antagonists having a cyclopentane based core structure. Proceedings from the 219th ACS National Meeting, San Francisco, CA, March 26-30, **2000**.
34. Owens, A. P., Harrison, T., Moseley, J. D., Swain, C. J., Sadowski, S. and Cascieri, M. A., High affinity phenylglycinol-based NK1 receptor antagonists. *Bioorg. Med. Chem. Lett.* **1998**, 8: 51-56.
35. Owens, A. P., Williams, B. J., Harrison, T., Swain, C. J., Baker, R., Sadowski, S. and Cascieri, M. A., Phenyl-glycinol based NK1 receptor antagonists - towards the minimum pharmacophore. *Bioorg. Med. Chem. Lett.* **1995**, 5, 2761-2766.
36. Natsugari, H., Ikeura, Y., Kiyota, Y., Ishichi, Y., Ishimaru, T., Saga, O., Shirafuji, H., Tanaka, T., Kamo, I. and Doi, T., Novel, potent, and orally active substance P antagonists: synthesis and antagonist activity of N-benzylcarboxamide derivatives of pyrido[3,4-b]pyridine. *J. Med. Chem.* **1995**, 38: 3106-3120.
37. Armour, D. R., Aston, N. M., Morriss, K. M. L., Congreve, M. S., Hawcock, A. B., Marquess, D., Mordaunt, J. E., Richards, S. A. and Ward, P., 1,4-Benzodiazepin-2-one derived neurokinin-1 receptor antagonists. *Bioorg. Med. Chem. Lett.* **1997**, 7: 2037-2042.
38. Grisoni, S., Huon, C. and Peyronel, J.-F., 4,4-Diphenyl-7-perhydrothiapyrano(3,4-c)pyrrolone, a new series of substance P receptors antagonists. *Bioorg. Med. Chem. Lett.* **1995**, 5: 1591-1594.
39. Natsugari, H., Ishimaru, T., Doi, T., Ikeura, Y. and Kimura, C., Benzylbenzadiazopine and benzodiazocine derivatives useful as neurokinin antagonists. EP733632. **1996**.
40. Garret, C., Carruette, A., Fardin, V., Moussaoui, S., Peyronel, J. F., Blanchard, J. C. and Laduron, P. M., Pharmacological properties of a potent and selective nonpeptide substance P antagonist. *Proc. Natl. Acad. Sci U S A.* **1991**, 88: 10208-10212.
41. Boes, M., Galley, G., Godel, T., Hoffman, T., Hunkeler, W., Schnider, P. and Stadler, H., Biphenyl derivatives useful as antagonists of the NK1 receptor. WO-00053572. **2000**.
42. MacLeod, A. M., Merchant, K. J., Brookfield, F., Kelleher, F., Stevenson, G., Owens, A. P., Swain, C. J., Cascieri, M. A., Sadowski, S. and Ber, E., Identification of L-tryptophan derivatives with potent and selective antagonist activity at the NK1 receptor. *J. Med. Chem.* **1994**, 37: 1269-1274.
43. Veenstra, S. J., Hauser, K., Schilling, W., Betschart, C. and Ofner, S., SAR of 2-benzyl-4-aminopiperidines NK1 antagonists. Part 2. Synthesis of CGP 49823. *Bioorg. Med. Chem. Lett.* **1996**, 6: 3029-3034.
44. Veenstra, S. J., Hauser, K. and Felber, P., Studies on the active conformation of the NK1 antagonist CGP 49823. Part 2. Fluoro-olefin analogs of tertiary amide rotamers. *Bioorg. Med. Chem. Lett.* **1997**, 7: 351-354.
45. Lewis, R. T., MacLeod, A. M., Merchant, K. J., Kelleher, F., Sanderson, I., Herbert, R. H., Cascieri, M. A., Sadowski, S., Ball, R. G. and Hoogsteen, K., Tryptophan-derived NK1 antagonists: conformationally constrained heterocyclic bioisosteres of the ester linkage. *J. Med. Chem.* **1995**, 38: 923-933.
46. von Sprecher, A., Gerspacher, M. and Anderson, G. P., Neurokinin antagonists as potential therapies for inflammation and rheumatoid arthritis. *IDrugs* **1998**, 1: 73-91.

47. McLean, S., Ganong, A., Seymour, P. A., Bryce, D. K., Crawford, R. T., Morrone, J., Reynolds, L. S., Schmidt, A. W., Zorn, S., Watson, J., Fossa, A., DePasquale, M., Rosen, T., Nagahisa, A., Tsuchiya, M. and Heym, J., Characterization of CP-122,721; a nonpeptide antagonist of the neurokinin NK1 receptor. *J. Pharmacol. Exp. Ther.* **1996**, 277: 900-908.
48. Gitter, B. D. and Iyengar, S., Methods of treating or preventing sleep apnea. WO-09731635. **1997**.
49. Goldstein, S., Neuwels, M., Moureau, F., Berckmans, D., Lassoie, M.-A., Differding, E., Houssin, R. and Hénichart, J.-P., Bioactive conformations of peptides and mimetics as milestones in drug design: Investigation of NK₁ receptor antagonists. *Lett. Pept. Sci.* **1995**, 2: 125-134.
50. Jacoby, E., Boudon, A., Kucharczyk, N., Michel, A. and Fauchere, J. L., A structural rationale for the design of water soluble peptide-derived neurokinin-1 antagonists. *J. Recept. Signal Transduct. Res.* **1997**, 17: 855-873.
51. Takeuchi, Y., Shands, E. F., Beusen, D. D. and Marshall, G. R., Derivation of a three-dimensional pharmacophore model of substance P antagonists bound to the neurokinin-1 receptor. *J. Med. Chem.* **1998**, 41: 3609-3623.
52. Caliendo, G., Grieco, P., Perissutti, E., Santagada, V., Saviano, G., Tancredi, T. and Temussi, P. A., Conformational analysis of three NK1 tripeptide antagonists: a proton nuclear magnetic resonance study. *J. Med. Chem.* **1997**, 40: 594-601.

3 Pharmacophore models for NKR antagonists

3.1 SAR of NK1R, NK2R and NK3R antagonists

Compound **43** is the first selective non-peptide NK2R antagonist published (Table 3.1). Like the selective NK1R antagonists (Section 2.2), compound **43** has two aromatic rings connected by a linker holding a hydrogen bond acceptor. The chirality has a large impact on the NK2 affinity, as the enantiomer **44** is almost inactive. The de-methyl analogue compound **45** is much less active. This could be due to the conformational properties of the amide. The methyl group makes the cis conformation energetically accessible, whereas in the de-methyl analogue, only the trans conformation is energetically accessible, as discussed in Appendix II. Unlike the selective NK1R antagonists, a complete systematic modification of pharmacophore elements has not been published for this type of NKR antagonists. However, the phenyl and the hydrogen bonding substituents on the piperidine ring, which are missing in compounds **46** and **47** respectively, are essential for high affinity. In compound **48**, the hydrogen bonding group can only function as an acceptor. In compounds **50-55**, the phenyl on the amide group has been exchanged with other groups. Small aromatic rings are preferred in this position. Few antagonists have been published with other groups in place of the di-Cl-phenyl group. However, it seems like a 3,4-substituted phenyl group is the optimal moiety.

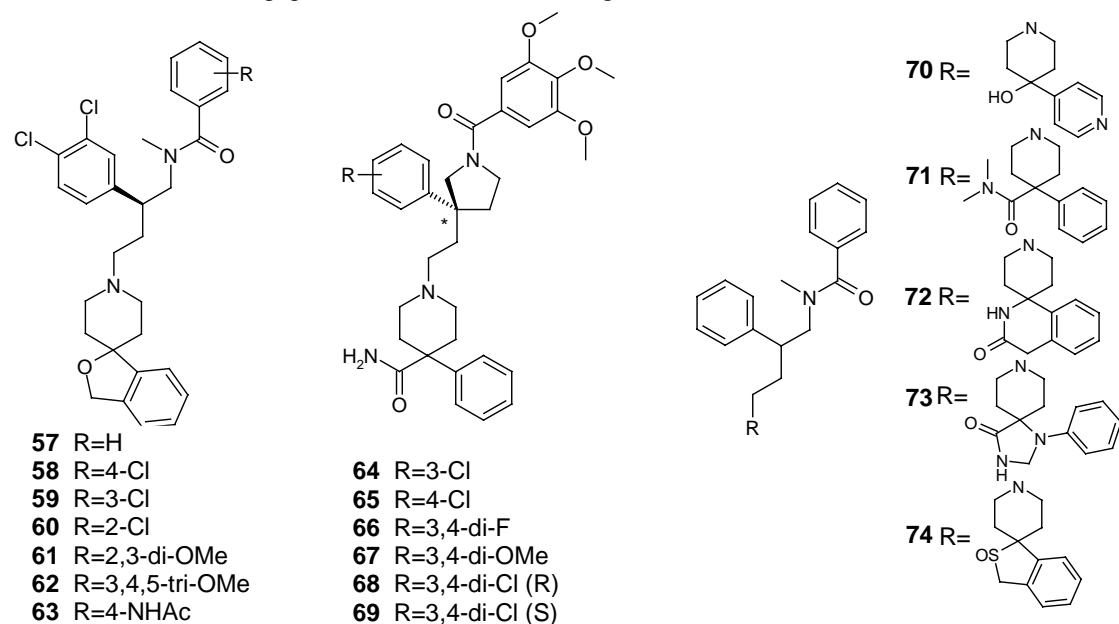
Table 3.1: SAR of the first selective non-peptide NK2R antagonists.

Compound	NK2 IC ₅₀ /nM	Reference	Compound	NK2 IC ₅₀ /nM	Reference
43 ^a	K _i =0.5, 0.44	[1], [2]	50	670	[3]
44	K _i =945	[1]	51	280	[3]
45	K _i >100	[1]	52	57	[3]
46	>1000	[4]	53	38	[3]
47	180	[4]	54	46	[3]
48	K _i =0.3	[1]	55	17	[3]
49	84	[3]	56	500	[3]

^a NK1 IC₅₀=593nM, NK3 IC₅₀=208nM [2].

Selective NK1R, NK2R, NK3R, dual NK1R/NK2R, dual NK2R/NK3R and nonselective NKR antagonists with a binding mode similar to **43** have been published. Table 3.2 describes the SAR of dual NK1R/NK2R antagonists. Compounds **58-63** comprise a series with substituents in the benzamide moiety. No substituents, or a polar substituent in the 4-position, is optimal for selective NK2R antagonism, whereas 3,4,5-trimethoxy substitution is optimal for NK1 affinity. In the ring-closed analogues of **43**, compounds **64-69**, the phenyl group on the chiral carbon is substituted. Small halides in the 3 and 4 positions are essential for NK2 affinity, whereas the NK1 affinity is largely unaffected, except by larger substituents, as in **67**. The piperidine tail also influences the subtype selectivity, as exemplified by compounds **70-74**. The position of the aromatic ring is important for NK2 affinity, where the tolerance is greater for NK1R antagonists, as in compound **73**. The basic aromatic ring of compound **70** reduces NK2 affinity, whereas it is of minor importance for the NK1 affinity.

Table 3.2: SAR of non-peptide dual NK1R/NK2R antagonists.

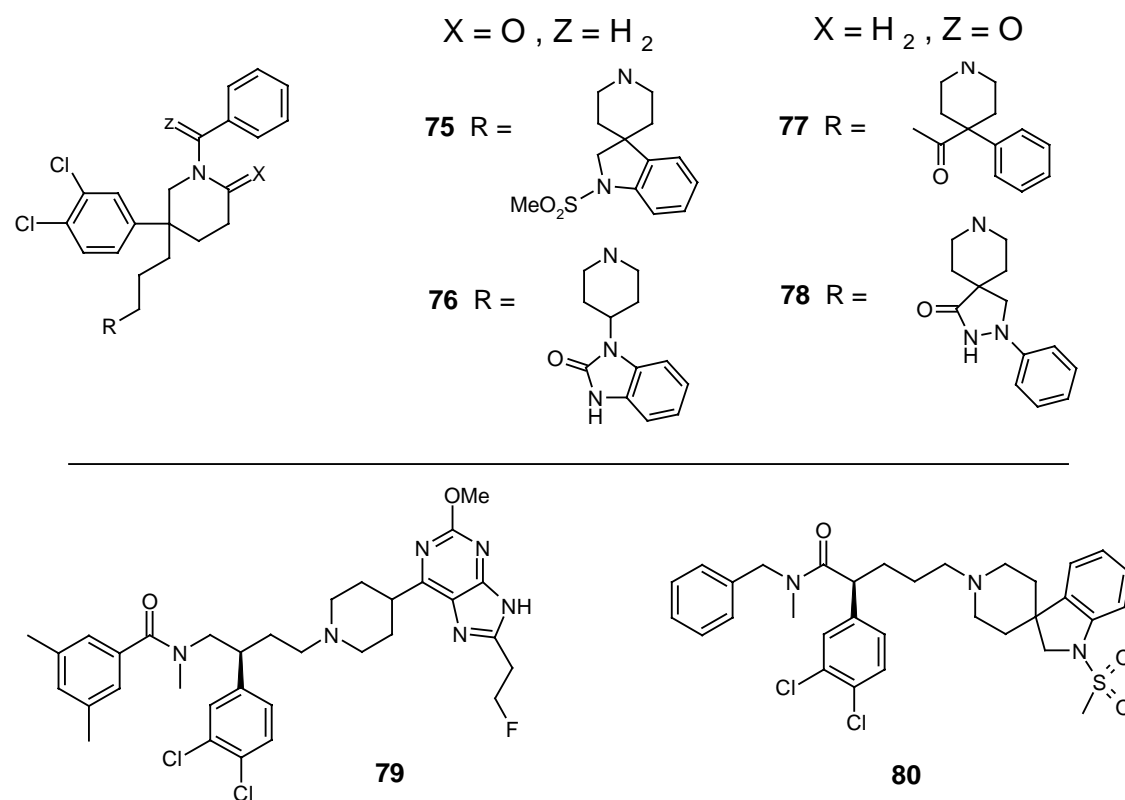


Compound	NK1 IC ₅₀ /nM	NK2 IC ₅₀ /nM	Reference	Compound	NK1 IC ₅₀ /nM	NK2 IC ₅₀ /nM	Reference
57	710	84	[5]	66	9.76	74.5	[6]
58	610	120	[5]	67	36.7	2770	[6]
59	310	260	[5]	68 ^a	3.11	8.4	[2]
60	640	150	[5]	69 ^b	160	760	[2]
61	73	95	[5]	70	1.9	89	[7]
62	33	180	[5]	71	17	5.5	[7]
63	2100	24	[5]	72	12	3.0	[7]
64	10.7	190	[6]	73	5.0	160	[7]
65	8.62	57.9	[6]	74	6.7	7.5	[7]

^aNK3 IC₅₀=21.0nM, ^bNK3 IC₅₀=2307nM.

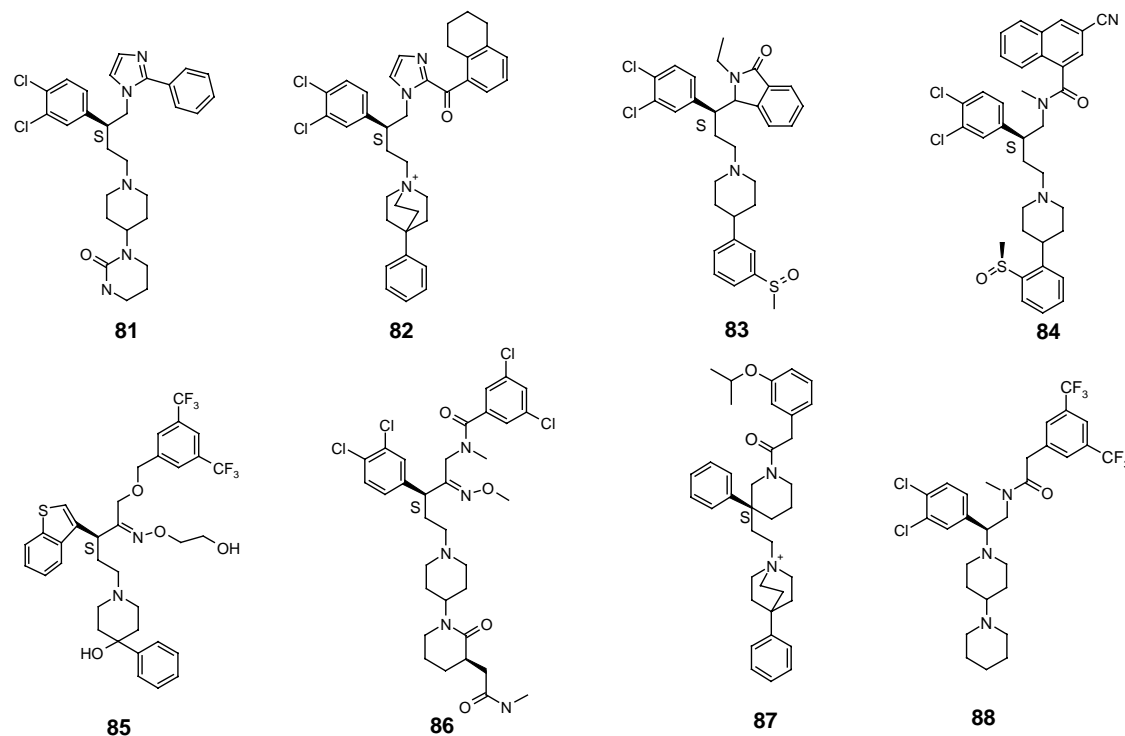
Table 3.3 describes the SAR of dual NK2R/NK3R and nonselective NKR antagonists. In most NK3R antagonists, the linker connecting the piperidine ring to the chiral carbon is three atoms long, whereas it is two atoms in most published NK1R and NK2R antagonists. The nonselective NKR antagonists **68** and **79** have a two-atom linker, but the selective NK3R antagonists all have 3-atom linkers. The position of the hydrogen bond acceptor is responsible for subtype selectivity. If the carbonyl is in the ring (X=O and Z=H₂ as in compounds **75** and **76**), the NK3 affinity is reduced, whereas the benzylic carbonyl (X=H₂ and Z=O as in compounds **77** and **78**) reduces NK2 affinity. Substitution of the aromatic rings is probably also responsible for NK3 selectivity. However, few NK3R antagonists in these series have been published.

Table 3.3: SAR of non-peptide dual NK2R/NK3R and unselective NKR antagonists.



Compound	NK1 IC ₅₀ /nM	NK2 IC ₅₀ /nM	NK3 IC ₅₀ /nM	Reference
75	763	2.2	25	[8]
76	743	6.4	539	[8]
77	460	389	1.5	[8]
78	108	50	6.8	[8]
79	0.45	9	25	[9]
80	100-500	30	0.6	[10]

A wide variety of scaffolds for NKR antagonists related to compound **43** have been described. In compounds **81** and **82**, there is an imidazole ring in the linker holding the two aromatic rings. The extra carbonyl group in compound **82** is important for NK1 affinity, whereas **81** is a selective NK2R antagonist. In compound **83**, the linker is ring closed to form a 2,3-dihydro-isindol-1-one group. The dual NK1R/NK2R antagonist **84** is a close analogue of **43**. In compounds **83** and **84**, the hydrogen bond acceptor is moved from the piperidine ring to the phenyl ring. Compounds **85** and **86** have an oxime group in the linker connecting the two aromatic rings. These types of compounds are nonselective or dual NK1R/NK2R antagonists. A number of different linkers holding the two aromatic rings have been described [11]. The selective NK1R antagonist compounds **87** and **88** are analogues to compounds **77** and **43** respectively. In **87** and **88**, the benzamide has been exchanged for a benzylamide.

Table 3.4: SAR of NK1R antagonists with different scaffolds. n.a.: Not available.

Compound	NK1 IC ₅₀ /nM	NK2 IC ₅₀ /nM	NK3 IC ₅₀ /nM	Reference
81	inactive	K _i = 23	inactive	[12]
82	2	24	n.a.	[13]
83	n.a.	8.9	n.a.	[14]
84	0.12	0.64	74	[15]
85	K _i = 1.8	K _i = 23	n.a.	[16]
86	1.3	0.4	0.3	[17]
87	K _i = 0.27	K _i = >1000	K _i = >1000	[18]
88	0.75	n.a.	n.a.	[19]

3.2 Previously published pharmacophore models

Elliot et al. [20] have published a pharmacophore model for a series of serine derived NK1R antagonists (Figure 3.1). However, the model only describes the tail part of the antagonists and consists of an aromatic ring and a hydrogen bond acceptor. The authors argue that the phenyl ring is equatorial to the piperidine ring. In compound **90**, the ring opened analogue of **89**, there is an intramolecular hydrogen bond, and the difference between the axial and equatorial conformation is 11 kJ/mol (as calculated by MMFFs + GB/SA¹). It is therefore unlikely that the axial conformation is the bioactive conformation. They also note that compounds with a flexible side chain,

¹ The author's unpublished results

which are unable to lock the conformation via the intramolecular hydrogen bond, have much lower NK1 affinity.

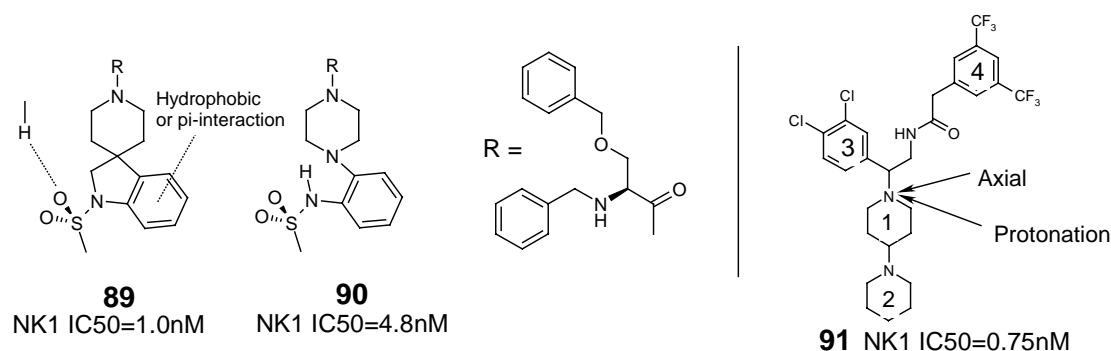


Figure 3.1: Left: The pharmacophore model published by Elliot et al. [20]. Right: Typical compound in the series studied by Verdani et al. [19].

Verdani et al. [19] have conducted a 4D-QSAR study on a series of NK1R antagonists (Figure 3.1 right). In the alignment, the two aromatic rings (3 and 4 in Figure 3.1) are in a stacked conformation. They conclude that polar substituents in ring 4 reduce the affinity due to higher desolvation energy and that the 3,5-di-CF₃ substitution in ring 4 contributes to high NK1 affinity. The majority of ligands in the study contain two piperidine rings (numbered 1 and 2 in Figure 3.1) that are connected by a single bond. Verdani et al. conclude that the ligands are mono protonated, and it is the nitrogen in ring 1 that is protonated. Since this nitrogen has an amide in the β -position, it is the least basic one [21]. If compounds **91** and **43** are superimposed, it is the nitrogen in ring 2 that overlays with the basic nitrogen in compound **43**. It is therefore more likely that it is the nitrogen in ring 2 that is protonated. It is claimed that the conformational energy penalties of the conformations in the alignment are between 0 and 20.5 kJ/mol (calculated by AMBER as implemented in MacroModel). However, it appears that the piperidine rings were not ring-opened during the conformational search, and only conformations where the N-substituent on piperidine ring 1 is in an axial position (as indicated in Figure 3.1) were considered. The conformational energy of the lowest energy conformation of compound **91** with piperidine ring 1 axial is more than 20 kJ/mol above the global energy minima, no matter which piperidine ring is protonated². Therefore the conformational energies are probably much higher than reported by

² The author's unpublished results

Verdani et al. [19]. The conformation of the aromatic rings and the linker that connects them are low in energy, but the conformation of the piperidine rings are not. In Verdani et al. [22] the same NK1R antagonists have been investigated by a 5D-QSAR approach. In this study, the substituents on the nitrogen of ring 1 are also axial.

3.3 Development of pharmacophore models for NK1R antagonists

3.3.1 Pharmacophore models for NK1R antagonists

Three pharmacophore models, Models 1-3, have been derived for NK1R antagonists for which SAR is discussed in Section 3.1. These models are described in two papers (Appendices I and II). The NK1R antagonists described in Section 3.1 are composed of two fragments defined as the head and tail, respectively in Figure 3.2. The head of most NK1R antagonists consists of two aromatic rings (pharmacophore elements A and B) connected by a linker holding a hydrogen bond acceptor (pharmacophore elements E and F). The tail of most NK1R antagonists consists of a 4-substituted piperidine ring holding an aromatic ring (pharmacophore elements C) and a group incorporating a hydrogen bond acceptor (pharmacophore elements G). The basic nitrogen is calculated to be protonated at physiological pH and will therefore function as a hydrogen bond donor (pharmacophore elements D). Because of the fragment based approach used to derive the pharmacophore models in Appendix I the number of fragments and pharmacophore elements differ between Appendix I and II. (Figure 3.2)

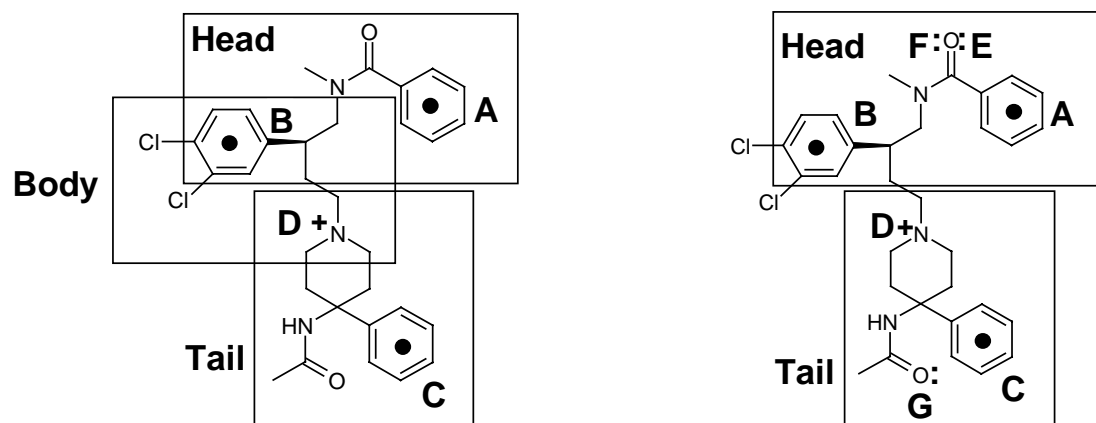


Figure 3.2: Definition of fragments and the pharmacophore elements that constitutes the pharmacophore models described in Appendix I (left) and Appendix II (right).

3.3.2 Pharmacophore models described in Appendix I

The compounds used to derive and evaluate the pharmacophore models are shown in Figure 3 in Appendix I. Each compound was divided into three fragments as defined in Figure 3.2 left. A sub-pharmacophore was derived for each of the three fragments. In each compound the partition into fragments was chosen so that part of the fragments superimposed. This ensured that the sub-pharmacophores could be assembled in an unique way. Two pharmacophore models were derived (Figure 3.3), one in which pharmacophore element C is axial relative to the piperidine of compound **43**, and one in which it is equatorial. The equatorial orientation is generally the one of lowest conformational energy. In these models the NK2R antagonists bind in an extended conformation with two aromatic rings (pharmacophore elements A and B) in a parallel displaced and tilted orientation. Pharmacophore element D is represented as a vector to emphasise the directionality of the hydrogen bond donor-acceptor interaction. These models were evaluated against 25 structurally diverse NK2R antagonists. 23 of the antagonists could be fitted to the pharmacophore models with a low conformational energy penalty and a low RMS value. Furthermore, the models were able to explain the enantioselectivity of the compounds **43** and **44** (Table 3.1).

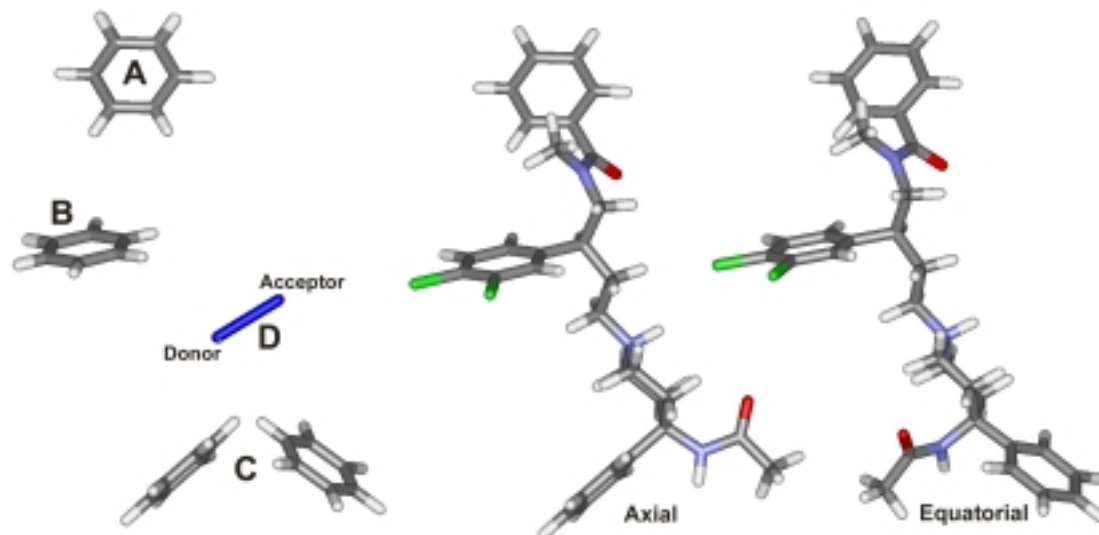


Figure 3.3: Left: The pharmacophore models described in Appendix I. The pharmacophore element C can be axial or equatorial relative to the piperidine ring of compound **43**. Center and right: The putative bioactive conformation of compound **43** with pharmacophore element C axial respectively equatorial to the piperidine ring.

3.3.3 Pharmacophore models described in Appendix II

The pharmacophore model described in Section 3.3.2 does not explain the importance of the hydrogen bond acceptors in the tail and head fragments of NKR antagonists (Pharmacophore elements E, F and G in Figure 3.2). By using a new procedure for superimposition it was possible to add one hydrogen bond acceptor to the tail part of the previous model, resulting in pharmacophore Model 1. Instead of representing the hydrogen bond acceptor as a vector in the direction of the lone pair on the hydrogen bond acceptor atom, the direction was allowed to deviate somewhat from the ideal hydrogen bond geometry (Figure 3 in Appendix II). By altering the position of pharmacophore element A, two more hydrogen bond acceptor vectors could be incorporated resulting in Models 2 and 3. Both Models 2 and 3 are described by seven pharmacophore elements: Three hydrophobic groups, three hydrogen bond acceptors and a hydrogen bond donor (Figure 3.4). Model 1 contains the same hydrophobic groups and hydrogen bond donor as Models 2 and 3, but only one hydrogen bond acceptor. In Model 1 the antagonists bind in an extended conformation with two aromatic rings in a parallel displaced and tilted conformation. Model 2 has the same two aromatic rings in a parallel displaced conformation where as Model 3 has the rings in an edge to ring face conformation. A superimposition of pharmacophore Models 1-3 is shown in Figure 3.4.

The pharmacophore models were evaluated against 21 structurally diverse non peptide NKR antagonists (Figure 4 in Appendix II). 16 of the 21 NKR antagonists could be fitted to both Model 2 and 3 with a low conformational energy penalty and a low RMS value. Two of the remaining five antagonists could be fitted to Model 2 with a low conformational energy penalty. The remaining three antagonists (compounds **102**, **104**, and **111**, Figure 3.7) were concluded to have another binding mode. The pharmacophore models were also evaluated against the 7TM NKR models described in Section 5.5. It was found that only pharmacophore Model 2 is compatible with the 7TM receptor models. Therefore it is concluded that pharmacophore Model 2 is the model that best describes the actual binding mode of the NKR antagonists.

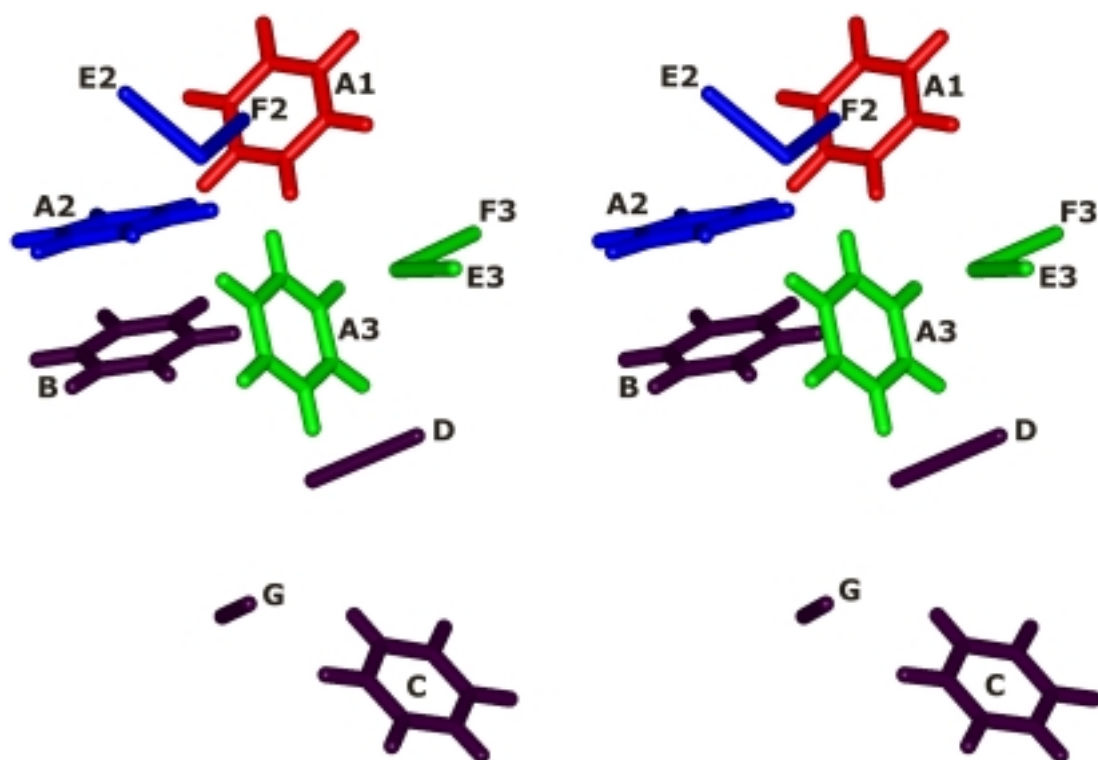


Figure 3.4: A superimposition of the pharmacophore Models 1-3 described in Appendix II. Stereo image. Black: The pharmacophore element B, C, D and G are identical in all three models. Red: Pharmacophore Model 1. Blue: Pharmacophore model 2. Green: Pharmacophore Model 3.

3.3.4 Results obtained by an automated fitting method

The flexible fitting algorithm QXP in the program Flo99 (Section 2.1.4) was used to investigate if the pharmacophore models obtained by rigid-body least-squares superimposition could be supported. Superimpositions leading to pharmacophore Model 1 were obtained as described in Appendix I. Compounds **43** and **92-93** (Figure 3.5) were chosen, since they were used to derive pharmacophore Models 2 and 3. All compounds were kept flexible during the fitting procedure. Using the global energy minima conformations found by MMFFs + GB/SA as input and the default settings in Flo99, pharmacophore Model 2 was found, but not Model 3. The fit resembling pharmacophore Model 2 is shown in Figure 3.6, left. This is the superimposition with the highest score. Increasing the number of steps to 1000, the similarity distance to 1 Å, or the energy window to 100 kJ/mol did not change the result. However, by using the conformations fitted to pharmacophore Model 3 as input, Model 3 could be obtained. The substituents that are axial in Model 2 are equatorial in Model 3. The reason why we could find either Models 2 or Model 3 is that Flo99 was unable to generate a conformation with an axial substituent from an input structure where the same substituent is equatorial. This substituent is indicated in Figure 3.5 by an arrow.

Both pharmacophore Models 2 and 3 were supported by Flo99, and in each case the superimposition of compounds leading to the pharmacophore models were the highest scoring solutions found.

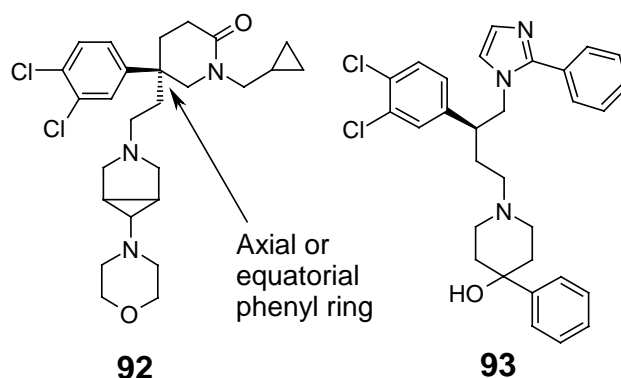


Figure 3.5: Compounds **92-93**, as well as **43**, were used as input for Flo99. Data and references are given in Table 3.1, 3.2 and in Appendix II.

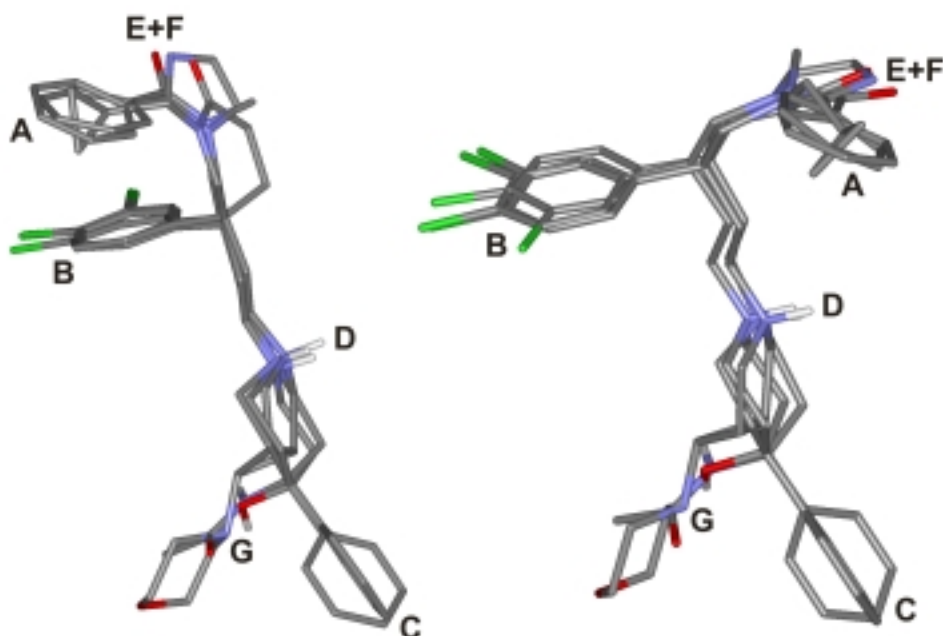


Figure 3.6: The superimpositions supporting the pharmacophore models. Left: Superimposition found by Flo99 leading to Model 2. Right: Superimposition found by Flo99 leading to Model 3.

3.3.5 Subtype selectivity

In the papers in Appendix I and II, the focus has been on NK2R antagonists. However, dual NK1R/NK2R and NK2R/NK3R antagonists are included in the work. The conclusion is that pharmacophore Model 2 represents the binding mode at the NK1R and NK2R subtypes. Subtype selectivity is determined by the substitution pattern of pharmacophore elements A and B and the nature of the group holding pharmacophore element G. Nonselective (compounds **68**, **75** and **79**, Table 3.2 and 3.3) and some selective NK3R antagonists (compounds **77** and **78**, Table 3.3) can also

be fitted to the pharmacophore model with low RMS deviations and low conformational energies. The selective NK3R antagonist compound **80** may also be fitted to pharmacophore Model 2 in a low energy conformation, but the hydrogen bond acceptor (pharmacophore element F) cannot be addressed. However, **80** may be docked into the 7TM NK3R model (Section 5.5) in this conformation, and the hydrogen bond acceptor is found to interact with another residue. It is likely that the pharmacophore model also describes antagonist binding to the NK3R subtype, but if the model is to describe the ligand receptor interactions of compound **80**, an alternative hydrogen bond acceptor site must be defined. However, the limited structural information available for NK3R antagonists in the literature does not allow the definition of this alternative hydrogen bond acceptor.

3.3.6 A pharmacophore model for selective NK2R antagonists

In Appendix II, it was concluded that the selective NK2R antagonists **102**, **104** and **111** (Figure 3.7) have another binding mode than the rest of the compounds described in Appendix I and II and Section 3.1. It was therefore decided to develop a pharmacophore model for this type of compounds. In Smith et al. [23], SAR around the benzyl group of compound **104** is described. A benzyl or 4-methyl-benzyl (compound **114**) is optimal for NK2 affinity. The two aromatic rings (A and B), the basic nitrogen (C) and a hydrogen bond acceptor (D) were chosen as pharmacophore elements. These are marked with centroids, lone pairs and "+" in Figure 3.7. Compounds **102**, **104**, and **111** were used to construct the model. They were chosen for their high NK2 affinity and structural diverse head fragments (see compound **111** for definition of head and tail fragments). However, since the tails of all compounds are identical and flexible, there is not enough information to derive a model for this part of the molecules. Ali et al. [24] have used a receptor model for the design of a ligand with a constrained tail (compound **112**). However, this compound does not have its tail in an extended conformation and have reduced NK2 affinity. Since large surface area, few intramolecular interactions, and high radius of gyration are descriptors that characterise bioactive conformations of ligands [25], the tail was modelled in an extended low energy conformation. The basic nitrogen is calculated to be protonated at physiological pH (Appendix I). The hydrogen bond donor (the protonated nitrogen) and the hydrogen bond acceptor (in most cases an oxygen atom) were represented as vectors. The approach for construction of the model is described

in Appendix II. Only one superimposition was found, for which the aromatic rings superimpose, and the hydrogen bond donor and acceptor vectors point in the same direction. The pharmacophore model was defined as the average position of the pharmacophore elements for the three compounds **102**, **104**, and **111** (Figure 3.8).

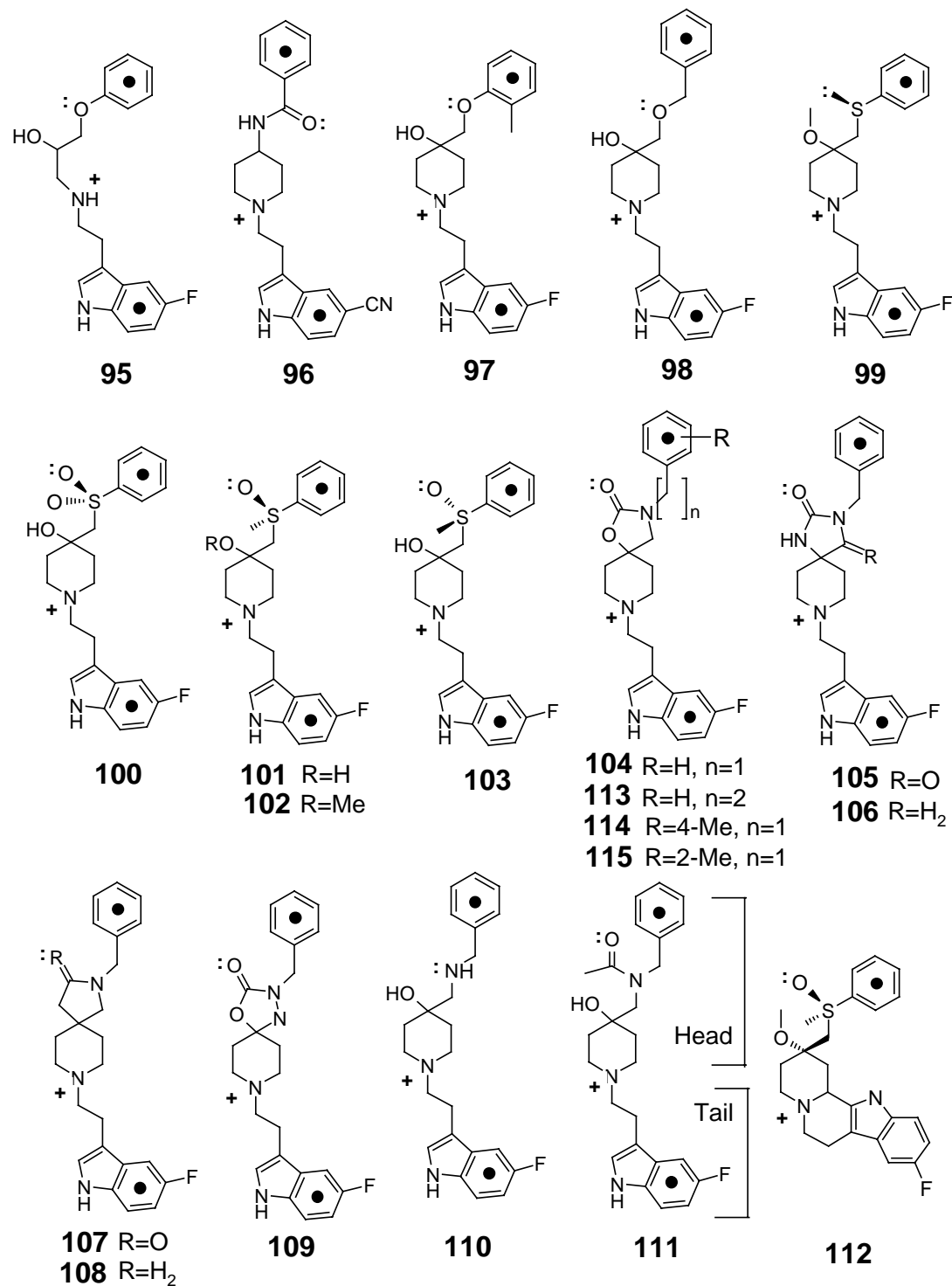


Figure 3.7: Compounds fitted to the pharmacophore model. The pharmacophore elements are marked by centroids, +, and lone pairs.

Table 3.5: Data of compounds fitted to the pharmacophore model. Deviation from ideal hydrogen bonds. (Ideal Angle = 0° and Length = 2.8 Å). IC₅₀ affinity of racemate. K_i affinity of pure enantiomer. For RMS values in parenthesis, the RMS is calculated by using the hydrogen bond acceptor atom instead of the dummy atom. Energies in parentheses are calculated from a global energy minimum chosen as the first conformation without electrostatic collapse.

Compound	Activity Rat colon K _i / nM	Pharm. Element C Angle / °	Pharm. Element D Angle / °	RMS / Å	Energy kJ/mol	Reference
95	1000	39.1	58.9	0.76	27.1 (15.1)	[26]
96	1600	10.2	26.5	0.34	5.7	[26]
97	32	34.2	32.7	0.85 (0.16)	8.0	[26]
98	32	15.1	58.5	0.52 (0.07)	7.6	[26]
99	4	10.5	39.0	0.55 (0.02)	3.2	[26]
100	32	6.8	24.0	0.24	-0.9	[26]
101	0.3	6.2	12.9	0.24	0.2	[26]
102	0.1	0.0	24.0	0.14	1.9	[26]
103	8	9.7	66.9	0.64 (0.19)	17.9	[26]
104	1.3	20.9	31.8	0.15	1.2	[23]
105	130	31.3	52.6	0.21	21.5 (18.6)	[26]
106	1.3	11.7	36.1	0.11	8.7	[26]
107	1.3	9.2	38.5	0.16	8.3	[26]
108	6.3	26.1	-	0.06	21.0 (5.6)	[26]
109	10	11.5	36.6	0.16	4.0	[26]
110	100	23.8	51.5	0.50	18.7 (7.2)	[26]
111	1.6	14.2	35.9	0.26	-5.7	[26]
112	IC ₅₀ =25μM	Does not fit the pharmacophore model				[24]

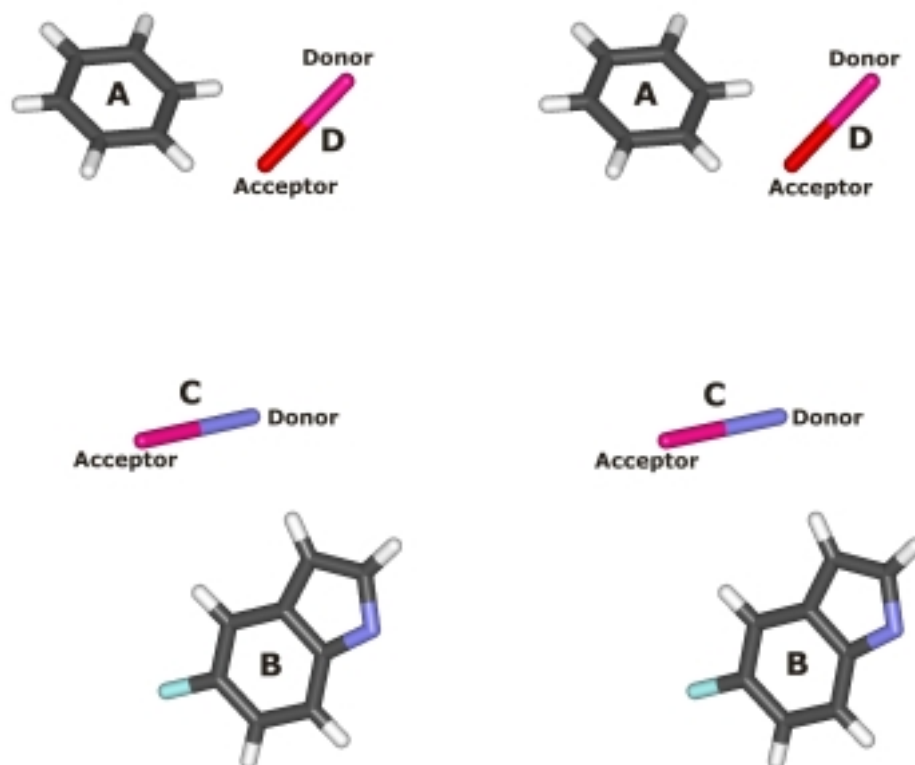


Figure 3.8: The pharmacophore model. Stereo image. The indole ring (pharmacophore element B) is included in the model, but its position in relation to the other pharmacophore elements is uncertain.

The pharmacophore model was evaluated against 14 selective NK2R antagonists. The conformational energy and RMS of the fits are shown in Table 3.5. Figure 3.9 shows a superimposition of compounds **95-111**. All compounds could be fitted to the model with a low conformational energy and a low RMS value, except compounds **95, 97, 103, 105, 108, and 110**. In compounds **95, 105, 108, and 110**, there is an electrostatic collapse in the global energy minimum. An electrostatic interaction is observed between the hydrogen of the protonated nitrogen and the ring face of the indole. This is probably an artefact of the force field. If the global energy minimum is taken as the first conformation without the electrostatic collapse, the conformational energies are lower. It is still high for compounds **95** and **105**, but these compounds have low NK2 activities. The conformational energy is also high for compound **103**. In the global energy minima of **103** and the putative bioactive conformation of its enantiomer (compound **101**), there is an intramolecular hydrogen bond between the hydroxy group and the sulfonyl oxygen. This is not found in the putative bioactive conformation of **103**. However, **103** is a factor of 27 less active than its enantiomer, and the high conformational energy could explain this. Compound **97** was fitted to the model with a low conformational energy but a high RMS. If the hydrogen bond acceptor is used as a fitting point instead of the dummy atom, the fit is much better in terms of RMS.

The almost inactive compound **96** fits the model with a low conformational energy. The reduced affinity could be caused by the cyano group penetrating into receptor essential volume. The reduced affinity of compounds **97** and **98** can be explained by the 2-methyl group in **97** and the longer linker in **98**. The 2-Me and phenethyl analogues of compound **104** (compound **115** and **113**) have a ten- and eight-fold lower NK2 affinity respectively. Compound **100** has an extra highly polar oxygen atom compared to compound **101**. If this atom is not engaged in an interaction with the receptor, the extra energy penalty for desolvation will reduce its affinity. The difference in solvation energy between compounds **100** and **101** is calculated to be 19 kJ/mol by using MMFFs + GB/SA. The benzylic nitrogen in compound **110** has a lone pair, but this is probably forming an intramolecular hydrogen bond to the hydroxy group. Therefore **110** does not have a hydrogen bond acceptor that can participate in an interaction with the receptor, which explains the poor affinity of the compound.

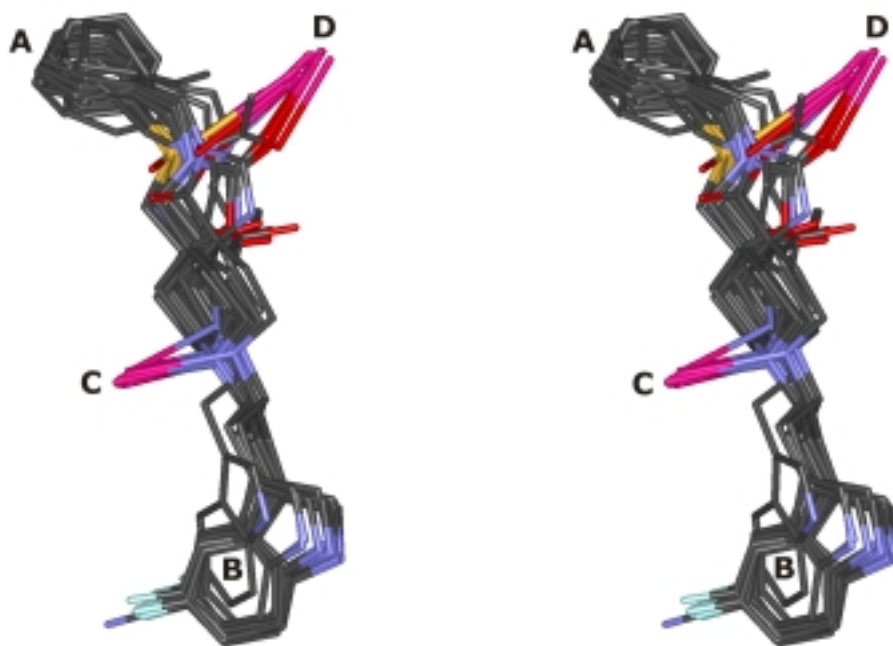


Figure 3.9: Superimposition of compounds **95-111**. Stereo image, hydrogens are removed for clarity.

3.4 Conclusion

Three pharmacophore models embracing selective NK1R, NK2R, NK3R, dual NK1R/NK2R, dual NK2R/NK3R, and nonselective NK1R/NK2R/NK3R antagonists have been developed. They are described in Appendices I and II.

A pharmacophore model for the selective NK2R antagonists **95-111** has been derived. The model consists of two aromatic rings, a protonated nitrogen that functions as a hydrogen bond donor and a hydrogen bond acceptor. The hydrogen bonding interactions are represented as vectors. The ligands bind in an extended conformation. However, all published NK2R antagonists with this binding mode contain the same flexible tail fragment. A unique position for pharmacophore element B could therefore not be identified. All high affinity antagonists could be fitted to the model with a low conformational energy. Compounds with reduced affinity could also be fitted to the model. However, the reduced affinity could be explained by a high conformational energy penalty, higher desolvation energy, unfavourable substituents, or missing pharmacophore elements.

3.5 References

1. Edmonds-Alt, X., Proietto, V., Broeck, D. V., Vilain, P., Advenier, C., Neliat, G., Fur, G. L. and Brelière, J.-C., Pharmacological Profile and Chemical Synthesis of SR48968, a Non-Peptide Antagonist of the Neurokinin A (NK₂) Receptor. *Bioorg. Med. Chem. Lett.* **1993**, 3: 925-930.
2. Burkholder, T. P., Kudlacz, E. M., Le, T.-B., Knippenberg, R. W., Shatzer, S. A., Maynard, G. D., Webster, M. E. and Horgan, S. W., Identification and chemical synthesis of MDL 105,212, a non-peptide tachykinin antagonist with high affinity for NK1 and NK2 receptors. *Bioorg. Med. Chem. Lett.* **1996**, 6: 951-956.
3. Kubota, H., Kakefuda, A., Nagaoka, H., Yamamoto, O., Ikeda, K., Takeuchi, M., Shibamura, T. and Isomura, Y., Spiro-substituted piperidines as neurokinin receptor antagonists. II. Syntheses and NK2 receptor-antagonistic activities of N-[2-aryl-4-(spiro-substituted piperidin-1'-yl)butyl]carboxamides. *Chem. Pharm. Bull. (Tokyo)* **1998**, 46: 242-254.
4. Kubota, H., Fujii, M., Ikeda, K., Takeuchi, M., Shibamura, T. and Isomura, Y., Spiro-substituted piperidines as neurokinin receptor antagonists. I. Design and synthesis of (+/-)-N-[2-(3,4-dichlorophenyl)-4-(spiro [isobenzofuran-1(3H),4'piperidin]-1'-yl)butyl]-N-methylbenzamide, YM-35375, as a new lead compound for novel neurokinin receptor antagonists. *Chem. Pharm. Bull. (Tokyo)* **1998**, 46: 351-354.
5. Kubota, H., Kakefuda, A., Okamoto, Y., Fujii, M., Yamamoto, O., Yamagiwa, Y., Orita, M., Ikeda, K., Takeuchi, M., Shibamura, T. and Isomura, Y., Spiro-substituted piperidines as neurokinin receptor antagonists. III. Synthesis of (+/-)-N-[2-(3,4-dichlorophenyl)-4-(spiro-substituted piperidin-1'-yl)butyl]-N-methylbenzamides and evaluation of NK1-NK2 dual antagonistic activities. *Chem. Pharm. Bull. (Tokyo)* **1998**, 46: 1538-1544.
6. Burkholder, T. P., Kudlacz, E. M., Maynard, G. D., Liu, X. G., Le, T.-B., Webster, M. E., Horgan, S. W., Wenstrup, D. L., Freund, D. W., Boyer, F., Bratton, L., Gross, S., Knippenberg, R. W., Logan, D. E., Jones, B. K. and Chen, T.-M., Synthesis and structure-activity relationships for a series of substituted pyrrolidine NK1/NK2 receptor antagonists. *Bioorg. Med. Chem. Lett.* **1997**, 7: 2531-2536.
7. Nishi, T., Fukazawa, T., Ishibashi, K., Nakajima, K., Sugioka, Y., Iio, Y., Kurata, H., Itoh, K., Mukaiyama, O., Satoh, Y. and Yamaguchi, T., Combined NK1 and NK2 tachykinin receptor antagonists: synthesis and structure-activity relationships of novel oxazolidine analogues. *Bioorg. Med. Chem. Lett.* **1999**, 9: 875-880.
8. Harrison, T., Korsgaard, M. P., Swain, C. J., Cascieri, M. A., Sadowski, S. and Seabrook, G. R., High affinity, selective neurokinin 2 and neurokinin 3 receptor antagonists from a common structural template. *Bioorg. Med. Chem. Lett.* **1998**, 8: 1343-1348.
9. Gerspacher, M. and von Sprecher, A., Dual neurokinin NK₁/NK₂ receptor antagonists. *Drugs of the Future* **1999**, 24: 883-892.
10. Shah, S. K., Spiro-substituted azacycles as neurokinin-3 antagonists. US5434158. **1995**.
11. Shih, N. Y., Albanese, M., Anthes, J. C., Carruthers, N. I., Grice, C. A., Lin, L., Mangiaracina, P., Reichard, G. A., Schwerdt, J., Seidl, V., Wong, S. C. and Piwinski, J. J., Synthesis and structure-activity relationships of oxime neurokinin antagonists: discovery of potent arylamides. *Bioorg. Med. Chem. Lett.* **2002**, 12: 141-145.
12. Miller, S. C., Jacobs, R. T. and Shenvi, A. B., N-[4-piperidino-2-phenyl]butylazole derivatives useful as NK-2 antagonists. EP-739891. **1996**.
13. Monaghan, S. M., Alker, D. and Burns, C. J., Quaternary ammonium compounds as tachykinin antagonists. WO9857972. **1998**.

14. Shenvi, A. B., Jacobs, R. T., Miller, S. C., Macht, C. J. and Veale, C. A., Cyclic amide derivatives as neurokinin A antagonists. WO-09516682. **1995**.
15. Albert, J. S., Aharony, D., Andisik, D., Barthlow, H., Bernstein, P. R., Bialecki, R. A., Dedinas, R., Dembofsky, B. T., Hill, D., Kirkland, K., Koether, G. M., Kosmider, B. J., Ohnmacht, C., Palmer, W., Potts, W., Rumsey, W., Shen, L., Shenvi, A., Sherwood, S., Warwick, P. J. and Russell, K., Design, synthesis, and SAR of tachykinin antagonists: modulation of balance in NK(1)/NK(2) receptor antagonist activity. *J. Med. Chem.* **2002**, 45: 3972-3983.
16. Shankar, B. B., Substituted oximes derivatives usefull as neurkinin antagonists. WO-09818785. **1998**.
17. Anthes, J., Chapman, R., Richard, C., Eckel, S., Corboz, M., Hey, J., Fernandez, X., Greenfeder, S., McLeod, R., Sehring, S., Rizzo, C., Crawley, Y., Shih, N., Piwinski, J., Reichard, G., Ting, P., Carruthers, N., Cuss, F., Billah, M., Kreutner, W. and Egan, R., SCH 206272: a potent, orally active tachykinin NK(1), NK(2), and NK(3) receptor antagonist. *Eur. J. Pharmacol.* **2002**, 450: 191-202.
18. Emonds-Alt, X., Doutremepuich, J. D., Heaulme, M., Neliat, G., Santucci, V., Steinberg, R., Vilain, P., Bichon, D., Ducoux, J. P. and Proietto, V., In vitro and in vivo biological activities of SR140333, a novel potent non-peptide tachykinin NK1 receptor antagonist. *Eur. J. Pharmacol.* **1993**, 250: 403-413.
19. Vedani, A., Briem, H., Dobler, M., Dollinger, H. and McMasters, D. R. Multiple-conformation and protonation-state representation in 4D-QSAR: The neurokinin-1 receptor system. *J. Med. Chem.* **2000**, 43: 4416-4427.
20. Elliott, J. M., Broughton, H., Cascieri, M. A., Chicchi, G., Huscroft, I. T., Kurtz, M., MacLeod, A. M., Sadowski, S. and Stevenson, G. I., Serine derived NK1 antagonists. 2: A pharmacophore model for arylsulfonamide binding. *Bioorg. Med. Chem. Lett.* **1998**, 8: 1851-1856.
21. Anker, L., Testa, B., Waterbeemd, H.v.de. and Bornand-Crausaz, A., Basicity, Lipophilicity, and Lack of Receptor Interaction of *N*-Aminoalkylbenzamides and *N*-Aminoalkyl-*o*-anisamides as Model Compounds of Dopamine Antagonists. *Helv. Chim. Acta* **2002**, 66: 542-556.
22. Vedani, A. and Dobler, M., 5D-QSAR: The key for simulating induced fit? *J. Med. Chem.* **2002**, 45: 2139-2149.
23. Smith, P. W., Cooper, A. W., Bell, R., Beresford, I. J., Gore, P. M., McElroy, A. B., Pritchard, J. M., Saez, V., Taylor, N. R. and Sheldrick, R. L., New spiropiperidines as potent and selective non-peptide tachykinin NK2 receptor antagonists. *J. Med. Chem.* **1995**, 38: 3772-3779.
24. Ali, M. A., Bhogal, N., Fishwick, C. W. and Findlay J. B., Spatial requirements of the antagonist binding site of the NK2 receptor. *Bioorg. Med. Chem. Lett.* **2001**, 11: 819-822.
25. Diller, D. J. and Merz, K. M., Can we separate active from inactive conformations? *J. Comput.-Aided. Mol. Des.* **2002**, 16: 105-112.
26. Cooper, A. W. J., Adams, H. S., Bell, R., Gore, P. M., McElroy, A. B., Pritchard, J. M., Smith, P. W. and Ward, P., GR159897 and Related Analogues as Highly Potent, Orally Active Non-Peptide Neurokinin NK₂ Receptor Antagonists. *Bioorg. Med. Chem. Lett.* **1994**, 4: 1951-1956.

4 Database search with Catalyst 4.6

4.1 Introduction

When a 3D pharmacophore model has been developed, the next step would be to use it in the search for new ligands. Searching commercially available or in-house databases is a way to obtain ready-made ligands that can serve as lead structures. This procedure could reduce the expenditure on the synthesis of new chemical entities and high throughput screening. To perform these tasks, one needs a program that can convert the 3D pharmacophore model into a search query, represent each structure in the database as a conformational model, and search the 3D database with the query.

4.2 The Catalyst program package

Catalyst [1] is a program package from Accelrys (former Molecular Simulations Inc.). The program provides a modelling environment and consists of several modules, which can be bought independently. Below is a description of the modules important for database search and hypothesis generation [2]. In Catalyst, 3D-pharmacophore models and queries for searching 3D databases are called hypotheses. Pharmacophore elements and functional groups are termed features.

VISUALIZER: Together with Compare, this module is the core requirement of Catalyst. It is an environment for modelling, database search and QSAR. The module allows structure editing and manual generation of hypotheses.

COMPARE: Provides the ability to fit compounds and hypotheses, and determine their degree of similarity, both geometrically and functionally. In a database search, COMPARE fits the original hypothesis onto the hit molecules obtained from the search and a score are calculated according to the geometrical fit.

INFO and database Server: This is Catalyst's information management software, which builds and administers databases. The information stored in the database is both 1D, 2D, 3D and 4D with each molecule being described by a conformational model, its features and shape descriptors generated by the SHAPE module.

HipHop and HypoGen: These modules allow the user to automatically generate hypothesis from a set of ligands and their activities (activities are only required by HypoGen) [3;4]. The module HipHop analyses the ligands for common features in

3D-space, while HypoGen utilises SAR information. HypoGen requires an input with affinities spanning several orders of magnitude.

SHAPE: The philosophy of SHAPE is that drug molecules must fit into a receptor cavity with a specific shape before they can bind. The module allows a compound, an alignment of several compounds or a binding cavity to be converted into a shape hypothesis. The conformers of 3D databases can be described in terms of shape indices that can be searched with a shape hypothesis. Shape hypotheses can be combined with feature based hypotheses.

ConFirm: The primary aim of ConFirm's approach to conformation generation is to explore compounds in terms of all the energetically accessible conformations available under physiological conditions [5-7]. ConFirm uses a semi systematic search algorithm and a fragment library for flexible rings. When the conformation of a molecule is found with its features in one arrangement, poles are added to the force field, so the features will not be found in that arrangement again [4;5]. There are two methods for conformational analysis. Fast conformation generation uses a heuristic method that quickly builds a geometrically diverse conformational model. Best conformational analysis allows all internal coordinates to vary [2].

4.3 Catalyst Hypotheses

In Catalyst, a hypothesis can be constructed from four different kinds of objects [2;8]:

Function: This is a pharmacophore element. Catalyst comes with 11 predefined functions; HB ACCEPTOR (vector), HB ACCEPTOR lipid (vector), HB DONOR (vector), HYDROPHOBIC (point), HYDROPHOBIC aliphatic (point), HYDROPHOBIC aromatic (point), NEG CHARGE (atom), NEG IONIZABLE (point), POS CHARGE (atom), POS IONIZABLE (point), RING AROMATIC (vector). They can be classified according to which receptor-ligand interaction they represent, namely hydrophobic, hydrogen bond donor, hydrogen bond acceptor, *pi*-stacking and salt-bridge. It is possible to modify a predefined function or make new functions.

Fragment: A fragment is a substructure made up of specifications for atoms and bonds. Each atom in the fragment may be specified to be a particular element, or it may be any of several elements. Similarly, each bond may be specified to be a particular bond type, or it may be any of several types. Catalyst comes with 117

predefined fragments. These can be modified, or the user may create their own fragments.

Exclusion volume: An excluded volume can be added to a hypothesis (or to a template molecule) to specify one or more spherical spaces that must not contain any atoms or bonds. An exclusion volume can represent a region in space that might impinge sterically on a receptor. An exclusion volume can be interpreted as a geometrical constraint, and this is how it is treated in Catalyst.

Shape: A Catalyst shape is defined by a set of three-dimensional coordinates, each with a corresponding radius. These points can be the centres of atoms in a molecule and the radius associated with each atom. Shapes can be constructed automatically from a single conformer of a molecule or from a set of aligned molecules. If the hypothesis is build from functions only, one would expect to find all compounds fitting the pharmacophore model. If a Shape is included in the hypothesis, one would expect to find only compounds that are geometrically similar to the compound from which the Shape was constructed. Using a Shape limits therefore the possibilities of finding new leads. However, if only functions are used to build the hypothesis, one can not avoid "wrong" mappings. I.e. when a compound maps the hypothesis but does so in a wrong conformation or orientation, so that there is a reduced molecular overlap with other compounds that map the hypothesis (Figure 4.1). To avoid this, one must include exclusion volumes or a shape in the hypothesis. Exclusion volumes is the best option since no shape is favoured and the possibility of finding new leads is therefore not compromised. However, deducing the exclusion volumes requires an extensive SAR knowledge.

Each object is associated with a set of geometric constraints. These can be constraints on location, distance, angle, and torsion. Property constraint can also be associated with a hypothesis. These are 1D specifications such as an allowable range for molecular weight. Each type of constraint can be used in a hypothesis to specify physical limitations on the characteristics of target molecules.

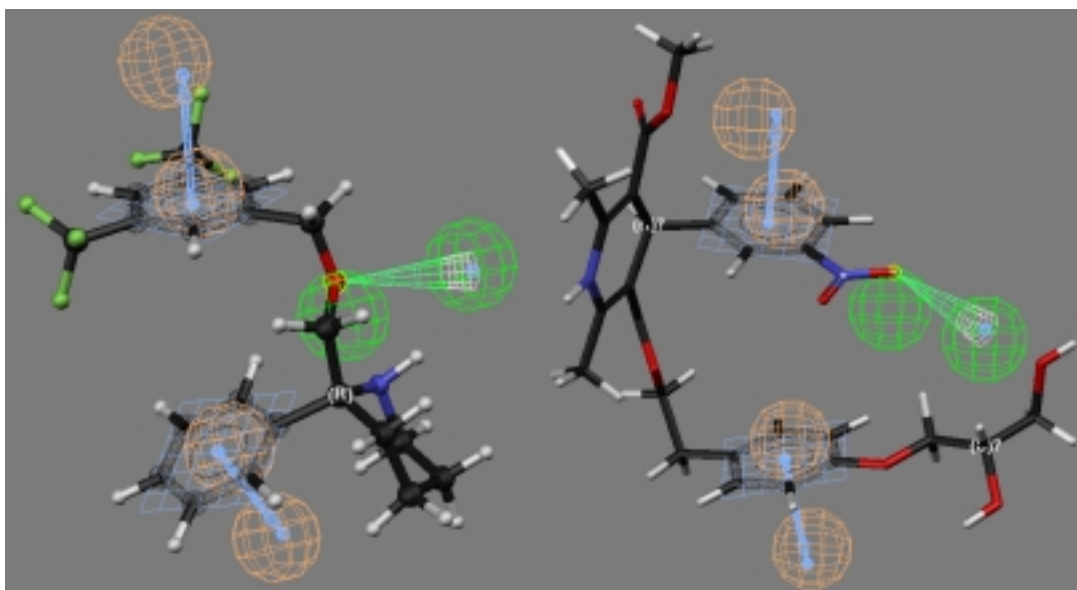


Figure 4.1: Example of "correct" mapping (left) and "wrong" mapping (right) to the NK1 hypothesis 1a (Section 4.9.1). Left: The NK1R antagonist occupies an area where there is a molecular overlap with other NK1R antagonists. Right: The pyridine ring occupies an area where there is no molecular overlap with NK1R antagonists.

4.4 The MDDR 3D-database

MDL's Drug Data Report (MDDR) [9] is a database of compounds with known biological activities. In the MDDR database, the compounds are classified according to their mode of action. The NK1R antagonists are classified as Regulatory Peptides and divided into four groups: Substance P antagonists, NK1R antagonists, NK2R antagonists and NK3R antagonists (Table 4.1). The Substance P group contains both NK1R antagonists, NK2R antagonists, dual NK1R/NK2R antagonists and probably NK3R antagonists.

The 3D database was constructed from the 2D ISIS database. This database contains a large amount of fragmented structures (structures that are stored as two molecules in the same entry e.g. salts) that Catalyst is unable to handle. These were removed. The database also contains some structures that are not drug-like and therefore of no interest for virtual screening. In order to reduce the number of non-drug like compounds, carbohydrates, DNA, RNA and compounds with a molar weight above 800 g/mole were removed. Also compounds containing metal atoms and saturated carbon chains of more than eight atoms were removed. Altogether 44% of the compounds in the 2D database were removed. A 3D catalyst database was created from the remaining structures with the fast conformation generation algorithm.

The database contains different classes of NKR antagonists, which do not share the same binding mode. Since the compounds are classified according to biological activity and not binding mode, two artificial categories were created. The 3D database was analysed for compounds which share binding mode with compounds **1** and **12** (Table 2.1). The SAR of these compounds is described in Section 2.2. There are 295 compounds in the 3D database, which are believed to share this binding mode, and they are referred to as Pfizer-like. All of these are classified as SP antagonists. The 3D database was also analysed for compounds which share binding mode with compound **43** (Table 3.1). The SAR of this type of NKR antagonists is discussed in Section 3.1. There are 95 compounds in the 3D database which are believed to share this binding and they are referred to as Sanofi-like. Among these, 53, 41, and 1 compounds are classified as NK1R, NK2R and NK3R antagonists, respectively. In the analysis of the search results, focus will be on the Pfizer- and Sanofi like compounds. However, since they are not native categories in the MDDR database, the search results will also be analysed for the native categories of SP, NK2 and NKR antagonists.

Table 4.1: Compounds in the MDDR database. n.a.: Number not available (\geq number in 3D database).

MDDR Database	2D	3D	% in 3D
Total	121788	67889	100
Substance P antagonists	1394	780	1.15
NK1R antagonists	255	103	0.15
NK2R antagonists	288	82	0.12
NK3R antagonists	37	5	0.01
Pfizer-like antagonists	n.a.	295	0.43
Sanofi-like antagonists	n.a.	95	0.06
Total NKR antagonists	1974	970	1.43

4.5 Statistics for analysing hit lists

To analyse the hit list obtained from a database search, one needs a goodness of hit (GH) metric. It is common to describe the hit list in terms of enrichment (E). This is defined in Equation 4.1 as the fraction of actives in the hit list divided by the fraction of actives in the database. H_a is the number of actives in the hit list, H_t is the number of compounds in the hit list, A is the number of actives in the database and D is the number of compounds in the database. However, the enrichment is not a good GH metric because it carries no information about the number of false negatives. The

enrichment will be approximately the same number if $H_a \approx H_t$, no matter the size of the hit list.

$$E = \frac{H_a / H_t}{A / D} = \frac{H_a D}{H_t A} \quad \text{Equation 4.1}$$

A GH metric should contain information about the two parameters' yield of actives (%Y) and percentage of actives (%A) defined in Equation 4.2. Maximising %Y and %A is equivalent to minimising the amount of false negatives and false positives, respectively (Equation 4.3). The higher the %Y and %A values, the higher the GH score. However, the two parameters are not independent. While maximising one parameter, the other is usually sacrificed. Güner and Henry [10] have proposed the GH score in Equation 4.3. The first bracket is a linear combination of %Y and %A assigned weights of 3 and 1 respectively. The second bracket is a function that penalises for large hit lists; i.e. if we retrieve the entire database the %Y is high but the result is useless.

$$\%Y = \frac{H_a}{H_t} \times 100 \quad , \quad \%A = \frac{H_a}{A} \times 100 \quad \text{Equation 4.2}$$

$$\text{FalseNegatives} = A - H_a \quad , \quad \text{FalsePositives} = H_t - H_a \quad \text{Equation 4.3}$$

$$GH = \left[\frac{H_a (3A + H_t)}{4H_t A} \right] \times \left[1 - \frac{H_t - H_a}{D - A} \right] \quad \text{Equation 4.4}$$

The theoretical best case where a database search returns 100% of the active compounds and nothing else corresponds to a GH of 1.00. The theoretical worst case where the whole database with the exception of the active compounds is retrieved corresponds to a GH of zero. Güner and Henry [10] analyses a number of database searches. A typical good result is described as retrieving 200 hits with 80 actives from a 50,000 compound database with 100 actives. This corresponds to a GH of 0.5. A typical bad result is described as retrieving 1000 hits with 50 actives from a 50,000 compound database with 200 actives. This corresponds to a GH of 0.16.

The GH calculated in the following sections are not exact GH but the theoretical lowest GH value. In this case, some of the false positives might be NK active, even though they are not registered as such in the database.

4.6 Database search using a shape only

In Table 4.2, the results of searches with queries consisting of a NKR antagonist shape only, are displayed. The GH is between 0.06 and 0.13. Using the shape of the global minima (found by Catalyst best search) of **1** returns most of the database. The shape of the putative bioactive conformation of **1** (Section 2.4) gives a GH of 0.11 and an enrichment of 3.4 for Pfizer like compounds. The shape of the putative bioactive conformation of **43** (pharmacophore Model 1-3 described in Appendix II) gives a GH of 0.09-0.13 and an enrichment of 6.5-11 for Sanofi like compounds. Searching with a shape only gives a poor result in terms of GH. The maximal %A are 49% for the Pfizer like compounds and 53% for the Sanofi like compounds. By adding a shape to a hypothesis, one can therefore only expect to find around 50% of these types of compounds.

Interestingly, the shape of the conformation fitted to pharmacophore Model 1 gives the best result, and the shape of the conformation fitted to pharmacophore Model 2 gives the second best result. In the ensembles of Sanofi like compounds generated by Catalyst, a conformation fitting pharmacophore Model 1 is therefore more often present than conformations fitting pharmacophore Model 2 and 3.

Table 4.2: Search results for the shape only hypotheses. Pfizer: Pfizer like compounds. Sanofi: Sanofi like compounds. Glob. Min. is the global minima found by Catalyst Best search. Pharm shape is derived from a conformation of compound **1** or **43** fitted to the pharmacophore models described in Section 2.4 and Appendix II, respectively.

Hypothesis	Hits	NK	GH	SP	GH	Pfizer	GH
Glob. Min. Shape 1	20,000	-	-	-	-	-	-
Pharm Shape 1	9638	253	0.07	243	0.08	144	0.11
Hypothesis	Hits	NK	GH	SP	GH	Sanofi	GH
Glob. Min. Shape 43	2661	120	0.06	20	0.06	24	0.07
Pharm1 Shape 43	3797	135	0.06	34	0.10	50	0.13
Pharm2 Shape 43	4063	137	0.06	36	0.11	37	0.10
Pharm3 Shape 43	1892	113	0.07	27	0.09	29	0.09

4.7 Database search using HipHop generated hypotheses

The automatic hypothesis generation with HipHop was done by the following procedure:

- For each compound a best quality conformational model was generated with default parameters; Max number of conformers = 250 and energy range = 20 kcal/mol.

- An automatic hypothesis generation was run. The hypotheses was allowed to contain the features: 0-5 “hydrophobic”, 0-5 “HB Acceptor features” (default), 0-5 “HB donor”, 0-5 “Pos. Ionizable”, and 0-5 “Ring Aromatic”.
- All other parameters were set to default. Therefore the program will stop after 10 hypotheses are generated.

4.7.1 Pfizer like compounds

The NK1R antagonists selected for the automatic hypothesis generation are shown in Figure 4.2. For each hypothesis, a best fit best conformation compare fit with compound **1** was done, and compound **1** was converted to a shape, and merged with the hypothesis. The results from the database search are shown in Table 4.3. All searches for hypotheses without shape were stopped when 20.000 hits (30% of the database) were obtained. Searches with shape returned between 0.9% (Hypothesis 9) and 8.8% (Hypothesis5) of the database. Hypothesis 9 gave the highest enrichment of Pfizer like compounds (6.1) and GH score (0.15) while Hypothesis 5 gave the highest %A (29%) with a GH of 0.08. This is somewhat better than search with a shape only (Section 4.6). A good enrichment factor are obtained, but the %A are disappointing. This is reflected in the poor GH scores. The GH for SP antagonists was marginally higher (0.18) than for Pfizer like compounds for hypothesis 9. This hypothesis can distinguish between SP antagonists and inactive but not between Pfizer like compounds and SP antagonists. This was unexpected considering the input structures to HipHop.

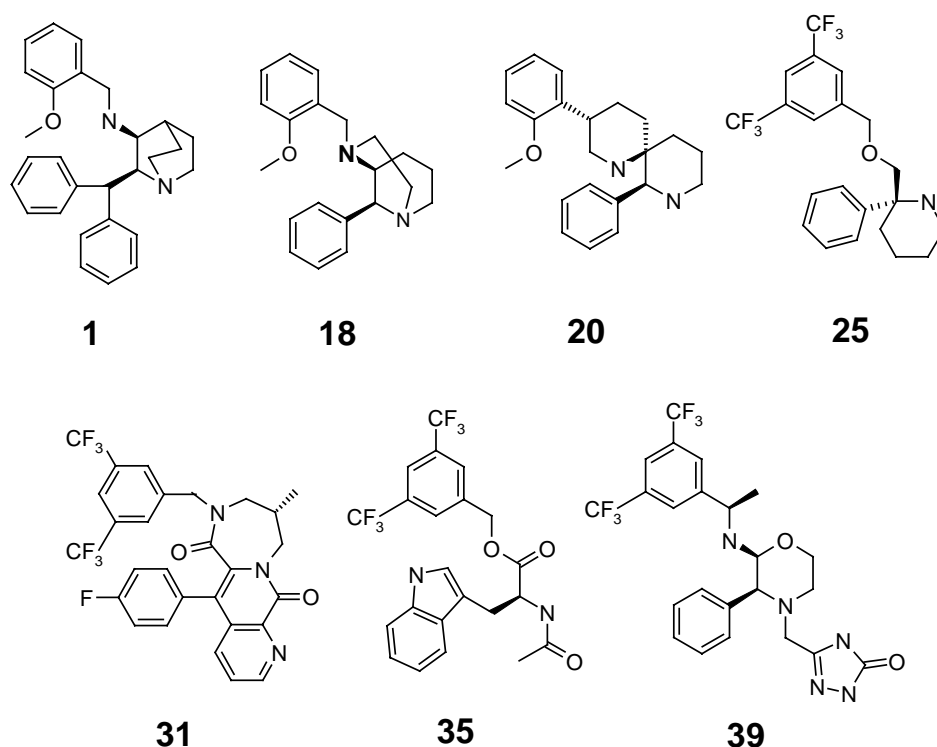


Figure 4.2: NK1R antagonists used for the automatic hypothesis generation with HipHop. The compounds are described in Section 2.2.

Table 4.3: Search results for the NK1 hypotheses generated by HipHop. Hyp.: Hypothesis number. Av.: Average. Pfizer: Pfizer like compounds.

Hyp.	No Shape			With Shape of compound 1			Pfizer	GH
	Hits	Hits	NK	GH	SP	GH		
1	20,000	2438	138	0.08	132	0.08	57	0.06
2	20,000	750	109	0.14	103	0.13	60	0.11
3	20,000	1806	168	0.11	162	0.12	82	0.10
4	20,000	2931	160	0.08	152	0.08	62	0.07
5	20,000	5990	228	0.08	215	0.09	86	0.08
6	20,000	3710	148	0.06	138	0.07	43	0.04
7	20,000	856	85	0.10	84	0.10	39	0.07
8	20,000	1037	76	0.07	71	0.07	39	0.06
9	20,000	618	122	0.18	119	0.18	72	0.15
10	20,000	1998	183	0.11	173	0.12	84	0.10
Av.	20,000	2213.4	141.7	0.10	134.9	0.10	62.4	0.08

4.7.2 Sanofi like compounds

The compounds used to generate the hypotheses are shown in Figure 4.3. For each hypothesis, a best fit best conformation compare fit with compound **43** was done, and **43** was converted to a shape, and merged with the hypothesis. The search results are shown in Table 4.4. Hypothesis 5 with a shape gives the best GH (0.15) and the highest enrichment (113), but only 11% of the Sanofi like compounds are returned. Hypothesis 6 without shape returns 54% of the Sanofi like compounds and 10% of the database. These results are marginally better than search with a shape only (Section

4.6). Both a good enrichment factor and %A are obtained, but not both for a search with the same hypothesis, resulting in a low GH.

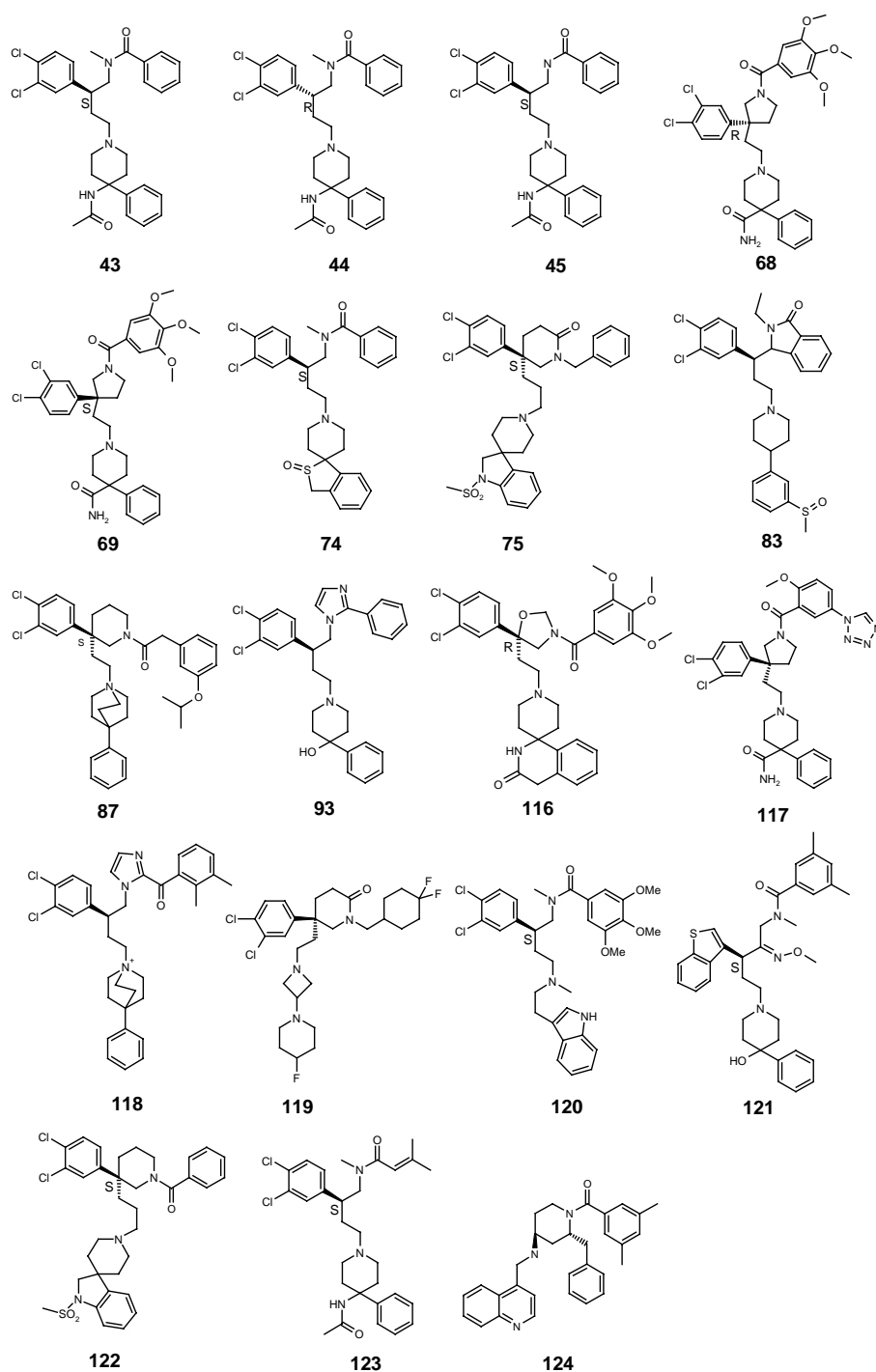


Figure 4.3: The NK2R antagonists used for automatic hypothesis generation. Compounds **43**, **68**, **74**, **75** and **116-119** were used as input for HipHop, while all compounds were used as input for HypoGen. Compounds **43-45**, **68**, **69**, **74**, **75**, **83** and **87** are described in Section 3.1, while compounds **93** and **116-123** are described in Appendices I and II. Compound **124** (NK1 IC_{50} =13 nM, NK2 IC_{50} =2790 nM and NK3 IC_{50} =2650 nM) [11] is an analogue of compound **22**.

Table 4.4: Search results for the NK2 hypotheses generated by HipHop. Sanofi: Sanofi-like. Hyp.: Hypothesis number. Av.: Average.

Hyp	Hits	No Shape					
		NK	GH	NK2	GH	Sanofi	GH
1	4800	83	0.03	32	0.10	36	0.09
2	5889	104	0.04	39	0.11	40	0.10
3	5075	72	0.03	32	0.09	33	0.08
4	4734	78	0.03	31	0.09	32	0.08
5	6595	115	0.04	43	0.12	46	0.11
6	6492	130	0.04	47	0.13	51	0.13
7	4151	111	0.05	26	0.08	39	0.10
8	4356	124	0.05	29	0.09	43	0.11
9	3798	112	0.05	40	0.12	46	0.12
10	6881	114	0.04	44	0.12	52	0.13
Av.	5277.1	104.3	0.04	36.3	0.11	41.8	0.11
Hyp	Hits	With Shape of compound 43					
		NK	GH	NK2	GH	Sanofi	GH
1	138	6	0.03	3	0.03	5	0.04
2	103	13	0.10	7	0.07	10	0.10
3	2	0	0.00	0	0.00	0	0.00
4	68	8	0.09	5	0.07	7	0.10
5	63	12	0.15	6	0.09	10	0.15
6	285	21	0.06	15	0.08	17	0.09
7	17	3	0.13	3	0.14	3	0.14
8	18	3	0.13	3	0.13	3	0.13
9	134	10	0.06	4	0.03	6	0.05
10	161	17	0.08	13	0.10	16	0.12
Av.	98.9	9.3	0.08	5.9	0.09	7.7	0.09

4.7.3 Randomly selected compounds

The poor results obtained by search with HipHop generated hypotheses inspired a comparison with random. Ten compounds from the 3D database were randomly selected and an automatic hypothesis generation was run (Figure 4.4). For each hypothesis a “best fit best conformation compare fit” with compound **1** or **43** was done. The conformation returned by Compare was converted to a shape and merged with the hypothesis. This way, the selected shape is not biased by any foreknowledge of the conformations of NKR antagonists, only by the fit to the randomly generated hypothesis. The 3D-MDDR database was searched with each of the 30 hypotheses (10+10 with and 10 without a shape). The results are shown in Table 4.4. All searches by hypotheses without shape was stopped when it reached the maximum allowed 20,000 hits. A randomly generated hypothesis returns almost the entire database. This corresponds to a GH score of zero. However, when a shape of a NK1R antagonist is added to the hypothesis the number of hits is dramatically decreased, and the GH increases to between 0.03 and 0.10. The average enrichment of NKR antagonists is a factor of 3. In most cases, the addition of the shape of NK2R antagonist **43** results in a wrong mapping (Figure 4.1), and the database search returns no hits. The hypotheses

generated by HipHop for the selective NK1R antagonists (Section 4.7.1) performed poorly but somewhat better than random. The hypotheses generated by HipHop for the Sanofi like antagonists (Section 4.7.2) performed poorly but significantly better than random.

Table 4.5: Search results for the hypotheses generated by HipHop from the randomly selected compounds in Figure 4.2. Hyp.: Hypothesis number. Av.: Average. Pfizer: Pfizer like compounds. Sanofi: Sanofi like compounds.

Hyp.	No Shape			With Shape of compound 1				
	Hits	Hits	NK	GH	SP	GH	Pfizer	GH
1	20,000	731	74	0.09	73	0.10	27	0.05
2	20,000	2917	136	0.07	129	0.07	49	0.05
3	20,000	771	52	0.06	52	0.07	4	0.01
4	20,000	5519	135	0.05	127	0.05	46	0.04
5	20,000	1701	121	0.08	116	0.09	41	0.05
6	20,000	557	17	0.03	16	0.03	5	0.01
7	20,000	1682	91	0.06	87	0.07	43	0.05
8	20,000	1848	63	0.04	61	0.04	28	0.03
9	20,000	2497	71	0.04	69	0.04	25	0.03
10	20,000	3399	108	0.05	104	0.05	58	0.06
Av.	20,000	2162.2	86.8	0.06	72.4	0.06	32.6	0.04
Hyp.	No Shape			With Shape of compound 43				
	Hits	Hits	NK	GH	NK2	GH	Sanofi	GH
1	20,000	591	21	0.03	2	0.01	1	0.00
2	20,000	475	20	0.04	3	0.01	3	0.01
3	20,000	91	3	0.03	0	0.00	0	0.00
4	20,000	552	38	0.06	9	0.04	8	0.03
5	20,000	59	2	0.03	0	0.00	0	0.00
6	20,000	53	1	0.01	0	0.00	0	0.00
7	20,000	696	19	0.03	9	0.04	10	0.04
8	20,000	79	10	0.10	0	0.00	0	0.00
9	20,000	51	0	0.00	0	0.00	0	0.00
10	20,000	45	3	0.05	2	0.04	3	0.06
Av.	20,000	269.2	11.7	0.04	2.5	0.01	2.5	0.01

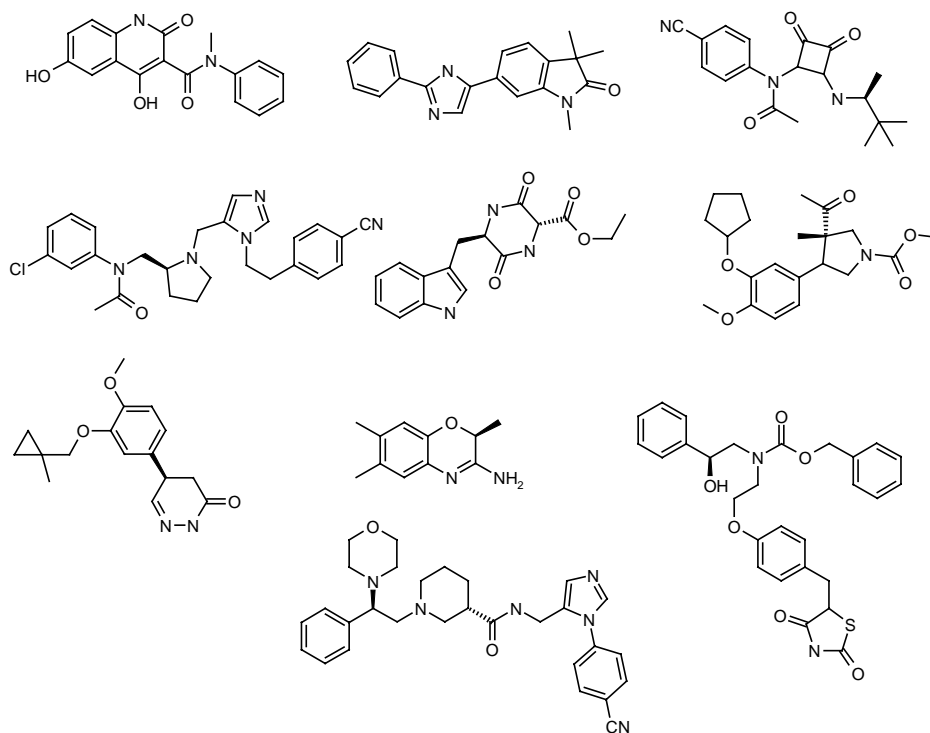


Figure 4.4: 10 randomly selected compounds from the 3D-MDDR database.

4.8 Database search using HypoGen generated hypotheses

The automatic hypothesis generation with HypoGen was done by the following procedure:

- Input structures were selected from the criteria that they should share the same binding mode, be structurally diverse, and the affinity data should cover several orders of magnitude.
- For each compound, a best quality conformational model was generated with default parameters; Max number of conformers = 250 and energy range = 20 kcal/mol.
- The compounds were associated with an uncertainty of 3.
- An automatic hypothesis generation was run. The hypotheses was allowed to contain the features: 0-5 “hydrophobic”, 0-5 “HB Acceptor features” (default), 0-5 “HB acceptor lipid”, 0-5 “Hydrophobic aromatic”, and 0-5 “Ring Aromatic”.

All other parameters were set to default. The program would therefore stop after 10 hypotheses were generated.

4.8.1 Pfizer like compounds

Compounds **1-11**, **14-16**, **18**, **20**, **23**, **25**, **26**, and **29-36** (Table 2.1-2.3) were used as input to HypoGen. Hypogen returned only three hypotheses. For each hypothesis, a best fit best conformation compare fit with compound **1** was done, and **1** was converted to a shape and merged with the hypothesis. However, compound **1** failed to map one of the features in all three hypotheses. This was unexpected, since compound **1** and a number of derivatives thereof were included in the input to HypoGen. The search results are shown in Table 4.6. Between 19% and 27% of the database are returned in searches without shape. When a shape is added the number of hits decreases to a few hundreds, but the numbers of actives returned are close to zero. In terms of GH, the search results without shape are marginally better than search with a shape only (Section 4.6), but the enrichment is slightly lower.

Table 4.6: Search results for the NK1 hypotheses generated by HypoGen. Hyp.: Hypothesis number. Av.: Average. Pfizer: Pfizer like hits.

Hyp	Hits	NK	GH	No Shape			
				SP	GH	Pfizer	GH
1	18493	511	0.11	454	0.12	167	0.11
2	12753	367	0.09	298	0.09	70	0.05
3	14203	472	0.12	403	0.12	143	0.10
Av.	15149.7	450.0	0.11	385.0	0.11	126.7	0.09
Hyp	Hits	NK	GH	With Shape			
				SP	GH	Pfizer	GH
1	103	5	0.04	5	0.04	0	0.00
2	449	10	0.02	10	0.02	1	0.00
3	23	1	0.03	1	0.03	0	0.00
Av.	191.7	5.3	0.03	5.3	0.03	0.3	0.00

4.8.2 Sanofi like compounds

The compounds used as input to HypoGen are shown in Figure 4.4. For each hypothesis, a best fit best conformation compare fit with compound **43** was done, and **43** was converted to a shape and merged with the hypothesis. The search results are shown in Table 4.7. Although compound **43** mapped all of the features in all ten hypotheses, virtually no hits were obtained by hypotheses including a shape. For hypotheses without a shape, the GH is between 0.02 and 0.09. Except for hypothesis 7 (which was stopped at 20,000 hits), the searches returned between 1.9% and 5.8% of the database. Hypothesis 10 gives the largest enrichment of Sanofi like compounds (9.4) with a GH of 0.08, whereas hypothesis 8 gives the best GH with an enrichment of 8.8. This is comparable to search with a shape only (Section 4.6).

Table 4.7: Search results for the NK2 hypotheses generated by HypoGen. Hyp.: Hypothesis number. Av.: Average.

Hyp	Hits	No Shape					
		NK	GH	NK2	GH	Sanofi	GH
1	2510	95	0.05	22	0.07	24	0.07
2	1659	81	0.06	19	0.06	20	0.06
3	1836	28	0.02	12	0.04	15	0.04
4	1287	27	0.02	12	0.04	14	0.04
5	2022	29	0.02	12	0.04	13	0.04
6	2995	36	0.02	14	0.04	16	0.04
7	20000	344	0.07	26	0.06	19	0.04
8	2175	43	0.03	15	0.05	20	0.06
9	2675	123	0.06	26	0.08	33	0.09
10	2051	104	0.06	24	0.08	27	0.08
Av.	3921	91	0.04	18.2	0.06	20.1	0.06
Hyp	Hits	With Shape					
		NK	GH	NK2	GH	Sanofi	GH
1	3	1	0.25	0	0	0	0
2	2	1	0.38	0	0	0	0
3	6	0	0.00	0	0	0	0
4	7	0	0.00	0	0	0	0
5	4	0	0.00	0	0	0	0
6	14	0	0.00	0	0	0	0
7	27	2	0.06	0	0	0	0
8	6	0	0.00	0	0	0	0
9	7	1	0.11	0	0	0	0
10	2	1	0.38	0	0	0	0
Av.	7.8	0.6	0.12	0	0	0	0

4.9 Database search using manually generated hypotheses

The pharmacophore models described in Section 2.4 and Appendix II were converted into hypotheses by the following procedure:

- The putative bioactive conformation of the template molecule was imported from MacroModel 7.0.
- The pharmacophore elements were mapped with appropriate functions.
- All functions were fixed by the default location constrains (except hypotheses described in Table 4.11) and merged into the final hypothesis.
- For each hypothesis, a rigid fit with the template was done and the template was converted to a shape and merged with the hypothesis. Default parameters were used except for the hypotheses described in Table 4.11.
- The MDDR database was searched using both the hypotheses with and without a shape.

4.9.1 Pfizer like compounds

The putative bioactive conformation (Section 2.4) of the selective NK1R antagonists **1** and **12** (Table 2.1) was used to build the search queries. The two aromatic ring pharmacophore elements (A and B in Figure 2.2) were mapped as ring aromatic. The hydrogen bond acceptor pharmacophore element C was mapped as hydrogen bond donor lipid. However, a part of the molecules penetrated the tolerance sphere of the putative hydrogen bond donor atom in the search query, and the hydrogen bond donor was therefore seen as inaccessible by Catalyst. These parts of the molecules (coloured green in Figure 4.5) had to be deleted before the hydrogen bond acceptor function could be added to the hypothesis. These hypotheses are named 1a (Figure 4.5 right) and 12a. In the hypotheses b, c, and d the basic ring nitrogen of **1** and **12** was mapped by a hydrogen bond acceptor lipid, a hydrogen bond donor, and a positive ionisable, respectively.

The MDDR database was searched with each of the hypotheses, and the results are shown in Table 4.8. The GH varies between 0.03 and 0.39. Both high yield and high enrichment were obtained, but not with the same hypotheses. The search with hypothesis 1a without shape found 70% of all Pfizer like compounds, but 25% of the database was retrieved, corresponding to a GH of 0.14. Adding a shape to the hypotheses reduces both the total number of hits and %A significantly. The search with hypothesis 1d with a shape gave an enrichment factor of 87, but only 18% of the Pfizer like compounds were retrieved, corresponding to a GH of 0.33. Hypothesis 1d with a shape, and 12d without shape give the best search results. Considerably better than any of hypotheses generated by the automated methods. However, since they contain a positively ionisable function, the hypotheses cannot retrieve NK1R antagonists without a basic nitrogen in the area corresponding to the ring nitrogen in compounds **1** and **12**. Since the template molecules failed to map the hydrogen bond acceptor before part of the molecules was deleted, it is reasonable to assume that the same is true for some of the NK1R antagonists in the database. These shortcomings severely limits %A.

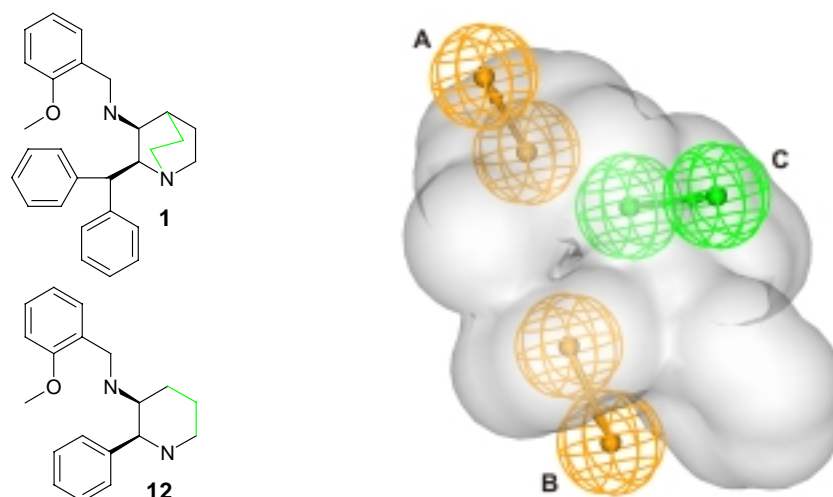


Figure 4.5: Left: The derivatives of **1** and **12** used to build the hypotheses. In these compounds, the part of the molecule coloured in green was deleted. Right: The NK1 hypothesis 1a with a shape. Solid grey: The shape hypothesis. Orange: The ring aromatic functions. Green: The hydrogen bond acceptor lipid function.

Table 4.8: The results from searching the MDDR database with the NK1 hypotheses a-d.

Hyp ^a	Hits	NK	GH	No Shape			
				SP	GH	Pfizer	GH
1a	17196	589	0.13	527	0.14	206	0.14
1b	1424	68	0.05	64	0.05	21	0.03
1c	477	49	0.09	48	0.09	15	0.04
1d	679	130	0.18	123	0.17	83	0.16
12a	16494	572	0.13	520	0.15	199	0.13
12b	2277	59	0.03	57	0.04	29	0.03
12c	543	41	0.07	40	0.07	23	0.05
12d	616	134	0.20	129	0.20	94	0.19
Hyp	Hits	NK	GH	With Shape			
				SP	GH	Pfizer	GH
1a	665	91	0.13	89	0.13	53	0.10
1b	277	25	0.07	24	0.07	15	0.05
1c	131	16	0.10	15	0.09	12	0.08
1d	143	71	0.39	71	0.39	54	0.33
12a	1688	59	0.04	59	0.04	36	0.05
12b	350	25	0.06	25	0.06	17	0.05
12c	122	22	0.14	22	0.14	15	0.10
12d	129	42	0.25	42	0.26	30	0.20

^aNumbers 1 and 12 refer to the template molecule that were used to construct the hypotheses.

4.9.2 Sanofi like compounds

The three putative bioactive conformations of the NK2R antagonist **43** (one for each of the pharmacophore Models 1-3, Appendix I and II) were used to build the search queries. The pharmacophore element A (Figure 1 in Appendix II) was mapped as hydrophobic. The aromatic pharmacophore element B was mapped as ring aromatic. The aromatic pharmacophore element C was mapped as hydrophobic aromatic, since it could not always be fitted in a coplanar orientation. The basic nitrogen pharmacophore element D was mapped as hydrogen bond donor lipid or positively

ionisable. In some hypotheses, the pharmacophore elements E, F and G were also included as hydrogen bond acceptors. Table 4.9 lists the functions that constitute each hypothesis.

Table 4.10 lists the results of the database search. The GH is between 0 and 0.76. Hypothesis 1b without shape gave the highest %A of Sanofi like compounds (53%) with 1.2% of the database retrieved and a GH of 0.17. Hypothesis 3l gave the highest enrichment factor of 715, but only 3.2% of the Sanofi like compounds were retrieved, resulting in a GH of 0.76. The addition of a hydrogen bond acceptor representing pharmacophore element E, F or G increases %Y and GH, but reduces %A. Hypotheses constructed from pharmacophore Model 1 give the best results, followed by hypotheses constructed from pharmacophore Model 3. The results are significantly better than search with a shape only, or search with a hypotheses generated by one of the automated methods.

To improve the search results, the tolerance spheres in hypotheses 1a and 1b were varied between 1 Å and 2.5 Å (1.5 Å being default), and the shape were similarity varied between 30% and 55% (50% being default). The search results are shown in Table 4.11. Reducing the tolerance spheres and increasing the shape similarity increases the GH and %Y but reduces %A. Increasing the tolerance spheres and reducing the shape similarity increases the %A somewhat but it also results in an exponential increase of false positives. Hypothesis 1a with 55% shape similarity gave the highest %Y (81%) of Sanofi like compounds with a %A of 18%, which is half the %A obtained by 1a with the default shape similarity of 50%.

Although high Y% were obtained, this could only be combined with a moderate %A. In terms of GH, good search results were obtained (e.g. hypothesis 3l), but these were extreme situations where the number of false positives was very low and the number of false negatives very high. There is a large difference in the %A obtained with search hypotheses derived from the different pharmacophore models. Unexpectedly, hypotheses derived from pharmacophore Model 2 give the lowest %A. The low %A obtained, especially from searches with hypotheses derived from pharmacophore Model 2, is probably due to the conformational properties of the molecules in the database. The putative bioactive conformation may not be present in the ensemble generated by Catalyst.

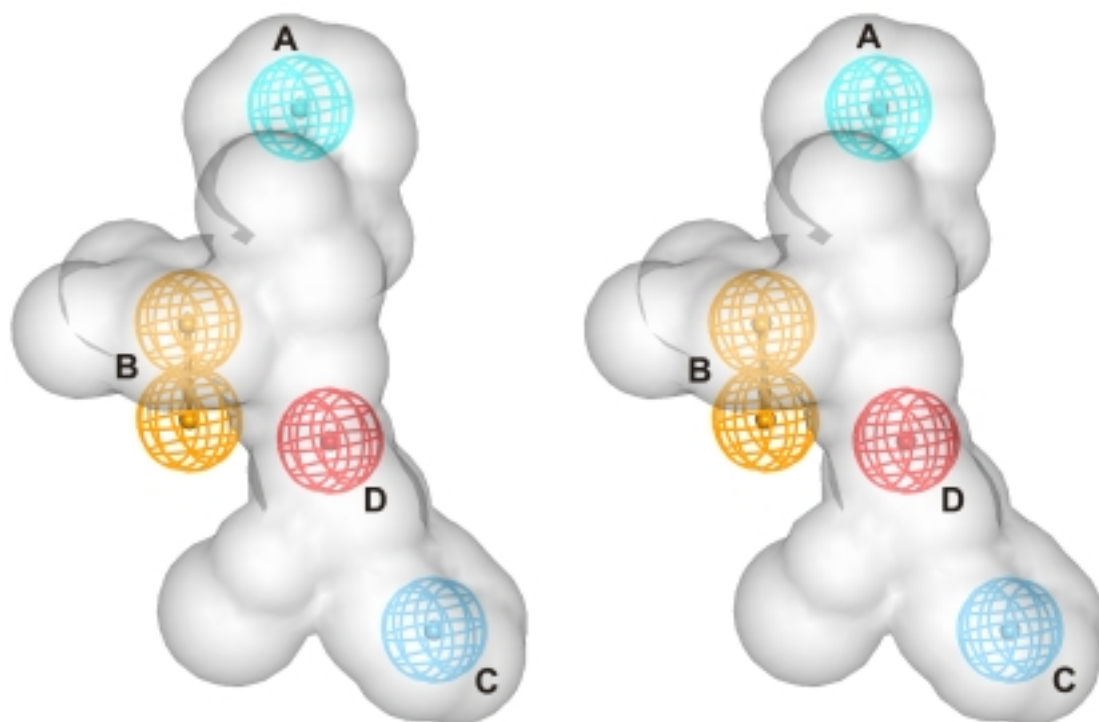


Figure 4.6: The hypothesis 1b with shape. Stereo image. Solid grey: The shape hypothesis. Orange: The ring aromatic function. Cyan: The hydrophobic function. Red: The positive ionisable function. Blue: The hydrophobic aromatic function.

Table 4.9: Composition of the manually constructed search queries. Abbreviations: Ar.: Aromatic, HBA: Hydrogen bond acceptor. Pos: Positively. The pharmacophore elements refer to the pharmacophore models described in Appendix II

Model	Pharmacophore element						
	A	B	C	D	E	F	G
a	Hydrophobe	Ring Ar.	Hydrophobe Ar.	HBA Lipid	-	-	-
b	Hydrophobe	Ring Ar.	Hydrophobe Ar.	Pos. Ionizable	-	-	-
c	Hydrophobe	Ring Ar.	Hydrophobe Ar.	HBA Lipid	HBA	-	-
d	Hydrophobe	Ring Ar.	Hydrophobe Ar.	Pos. Ionizable	HBA	-	-
e	Hydrophobe	Ring Ar.	Hydrophobe Ar.	HBA Lipid	-	HBA	-
f	Hydrophobe	Ring Ar.	Hydrophobe Ar.	Pos. Ionizable	-	HBA	-
g	Hydrophobe	Ring Ar.	Hydrophobe Ar.	HBA Lipid	HBA	-	-
h	Hydrophobe	Ring Ar.	Hydrophobe Ar.	Pos. Ionizable	HBA	-	-
i	Hydrophobe	Ring Ar.	Hydrophobe Ar.	HBA Lipid	-	-	HBA
j	Hydrophobe	Ring Ar.	Hydrophobe Ar.	Pos. Ionizable	-	-	HBA
k	Hydrophobe	Ring Ar.	Hydrophobe Ar.	HBA Lipid	HBA	-	HBA
l	Hydrophobe	Ring Ar.	Hydrophobe Ar.	Pos. Ionizable	HBA	-	HBA

Table 4.10: The results from searching the MDDR database with the NK2 hypotheses. The composition of hypotheses a-l is described in Table 4.9. The numbers 1-3 refer to the pharmacophore models described in Appendix II.

Hyp	Hits	NK	GH	No Shape		Sanofi	GH
				NK2	GH		
1a	889	65	0.07	37	0.14	41	0.14
2a	2165	66	0.04	26	0.09	33	0.10
3a	2664	154	0.08	35	0.11	40	0.11
1b	842	79	0.09	39	0.15	50	0.17
2b	1747	109	0.07	36	0.12	46	0.14
3b	1635	178	0.12	38	0.13	49	0.15
2c	48	8	0.13	3	0.06	6	0.11
3c	32	9	0.21	3	0.08	8	0.21
2d	91	18	0.15	8	0.09	14	0.15
3d	73	24	0.25	12	0.16	20	0.26
2e	72	5	0.05	3	0.04	5	0.07
3e	49	8	0.12	4	0.07	7	0.13
2f	129	17	0.10	7	0.06	11	0.09
3f	106	27	0.20	12	0.12	21	0.20
2g	60	8	0.10	5	0.08	8	0.12
3g	43	12	0.21	5	0.10	10	0.20
2h	103	20	0.15	9	0.09	15	0.15
3h	83	25	0.23	12	0.14	21	0.24
1i	60	23	0.29	20	0.31	23	0.35
2i	115	9	0.06	8	0.08	9	0.08
3i	144	21	0.11	14	0.12	15	0.12
1j	69	33	0.37	25	0.35	29	0.39
2j	112	15	0.10	13	0.13	14	0.13
3j	122	28	0.18	18	0.17	21	0.18
2k	4	2	0.38	0	0.00	0	0.00
3k	1	0	0.00	0	0.00	0	0.00
2l	3	2	0.50	1	0.25	2	0.51
3l	3	3	0.75	1	0.25	3	0.76

Hyp	Hits	NK	GH	With Shape		Sanofi	GH
				NK2	GH		
1a	59	38	0.49	25	0.39	34	0.52
2a	44	16	0.28	11	0.22	15	0.30
3a	25	14	0.42	7	0.23	11	0.36
1b	116	48	0.32	28	0.27	40	0.36
2b	115	23	0.16	14	0.13	20	0.18
3b	59	27	0.35	15	0.24	19	0.29
2c	6	3	0.38	1	0.13	3	0.38
3c	6	6	0.75	1	0.13	5	0.64
2d	16	6	0.28	2	0.10	5	0.25
3d	13	12	0.70	6	0.36	10	0.60
2e	5	2	0.30	1	0.15	2	0.31
3e	3	3	0.75	0	0.00	3	0.76
2f	19	4	0.16	2	0.09	4	0.17
3f	5	5	0.75	1	0.15	4	0.61
2g	6	3	0.38	1	0.13	3	0.38
3g	6	6	0.75	1	0.13	5	0.64
2h	21	6	0.22	2	0.08	5	0.19
3h	12	12	0.75	6	0.39	10	0.65
1i	20	16	0.60	13	0.53	16	0.64
2i	2	1	0.38	1	0.38	1	0.38
3i	3	2	0.50	1	0.25	2	0.51
1j	28	22	0.59	17	0.51	20	0.59
2j	7	2	0.21	2	0.22	2	0.22
3j	9	8	0.67	6	0.52	7	0.60
2k	0	0	0	0	0	0	0
3k	0	0	0	0	0	0	0
2l	0	0	0	0	0	0	0
3l	0	0	0	0	0	0	0

Table 4.11: The results from searching the MDDR database with the NK2 hypotheses 1a and 1b with modified constraints. Radius of tolerance spheres in Å and shape similarity in %.

Hyp	Hits	NK	GH	No Shape			
				NK2	GH	Sanofi	GH
1a-1.0Å	61	28	0.35	20	0.31	25	0.37
1b-1.0Å	131	55	0.33	32	0.28	40	0.33
1a-1.3Å	309	52	0.14	32	0.17	38	0.19
1b-1.3Å	454	68	0.13	36	0.17	47	0.20
1a-1.4Å	523	58	0.10	35	0.16	41	0.17
1b-1.4Å	612	73	0.11	38	0.16	49	0.19
1a-1.5Å	889	65	0.07	37	0.14	41	0.14
1b-1.5Å	842	79	0.09	39	0.15	50	0.17
1a-1.7Å	2233	103	0.06	42	0.14	46	0.13
1b-1.7Å	1338	94	0.08	39	0.14	51	0.16
1a-2.0Å	5127	172	0.06	51	0.15	54	0.14
1b-2.0Å	2079	119	0.07	39	0.13	51	0.15
1a-2.5Å	12264	430	0.11	64	0.16	63	0.14
1b-2.5Å	4047	285	0.12	42	0.13	55	0.15
Hyp	Hits	NK	GH	With shape			
				NK2	GH	Sanofi	GH
1a-1.0Å	24	20	0.63	14	0.48	19	0.64
1b-1.0Å	51	34	0.51	20	0.35	30	0.52
1a-1.3Å	42	35	0.63	23	0.48	31	0.64
1b-1.3Å	95	47	0.38	28	0.31	39	0.41
1a-1.4Å	55	38	0.53	25	0.42	34	0.55
1b-1.4Å	102	46	0.35	28	0.29	39	0.39
1a-1.5Å	59	38	0.49	25	0.39	34	0.52
1b-1.5Å	116	48	0.32	28	0.27	40	0.36
1a-1.7Å	78	39	0.38	25	0.32	34	0.42
1b-1.7Å	136	49	0.28	28	0.24	41	0.33
1a-2.0Å	108	42	0.30	26	0.26	36	0.34
1b-2.0Å	149	50	0.26	28	0.23	41	0.31
1a-2.5Å	144	44	0.24	27	0.22	37	0.29
1b-2.5Å	157	50	0.25	28	0.22	41	0.30
1a-30%	831	64	0.07	37	0.14	41	0.14
1b-30%	808	78	0.09	39	0.15	49	0.17
1a-35%	771	61	0.07	37	0.15	41	0.15
1b-35%	780	78	0.09	39	0.15	49	0.17
1a-40%	504	55	0.10	34	0.15	41	0.17
1b-40%	641	74	0.10	38	0.16	49	0.18
1a-45%	188	48	0.20	30	0.21	38	0.25
1b-45%	318	65	0.17	35	0.19	47	0.23
1a-50%	59	38	0.49	25	0.39	34	0.52
1b-50%	116	48	0.32	28	0.27	40	0.36
1a-51%	53	37	0.53	25	0.43	33	0.55
1b-51%	94	46	0.38	27	0.30	38	0.40
1a-52%	38	29	0.58	18	0.41	26	0.58
1b-52%	73	38	0.40	22	0.29	32	0.41
1a-55%	21	18	0.65	11	0.43	17	0.65
1b-55%	29	19	0.50	12	0.35	18	0.51

4.10 An evaluation of Catalyst's conformational search algorithm

4.10.1 Energy calculations

To investigate the quality of the force field and conformational search algorithm used by Catalyst [5], eight NKR antagonists representing different degrees of flexibility

were selected (Figure 4.7). These were subjected to a conformational search using both Catalyst's Fast and Best conformational search algorithm. The conformational ensemble generated by Catalyst was exported to MacroModel, where each conformation was minimised using the MMFFs, MMFFs+GB/SA, MM3* and MM3*+GB/SA force fields. The conformational space was also searched using MacroModel and the above mentioned force fields. The global energy minima were exported to Catalyst where the conformational energy was calculated. An overview of these calculations is shown in Figure 4.8. Since the philosophy of Catalyst conformational search algorithm is to sample feature space and not local minima space [5], it was expected that some conformations were far from a local minimum. Minimising a Catalyst conformation to the nearest local minimum may result in an energy that does not reflect the actual energy of the original conformation. After the minimisation, the conformation may be significantly different from that obtained by Catalyst. The conformational ensemble was therefore also minimised by MMFFs, MMFFs+GB/SA, MM3* and MM3*+GB/SA with flat bottomed Cartesian constraints of 0.2Å. A rigorous conformational search was done for each compound, using the MCMM method with each of the above mentioned force fields, and the conformational energy was calculated in relation to the global energy minima.

This evaluation is only meaningful if Catalyst is compared to a high quality force field. MM3* and MMFFs were selected since they are widely used and have proved to be among the best force fields to reproduce experimental conformational energies [12].

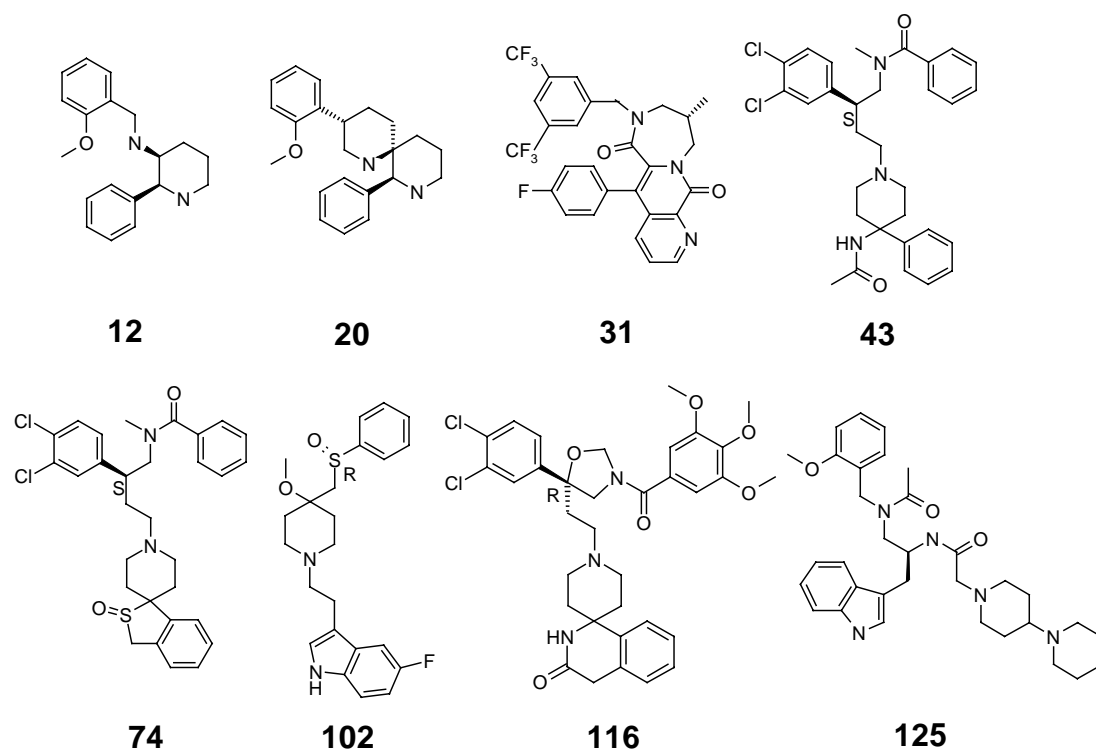


Figure 4.7: Structures of the compounds used for the evaluation of Catalyst force field and conformational search algorithm. Compounds **12**, **20** and **31** are selective NK1R antagonists described in Section 2.2. Compounds **43** and **74** are selective NK2R antagonists described in Section 3.1. Compound **102** are a selective NK2R antagonists described in Section 3.3.6. Compound **116** are described in Appendix I. Compound **125** is a selective NK1R antagonist with NK1 IC₅₀=0.15 nM, NK2 pA₂=4.7, NK3 pA₂=4.7 [11].

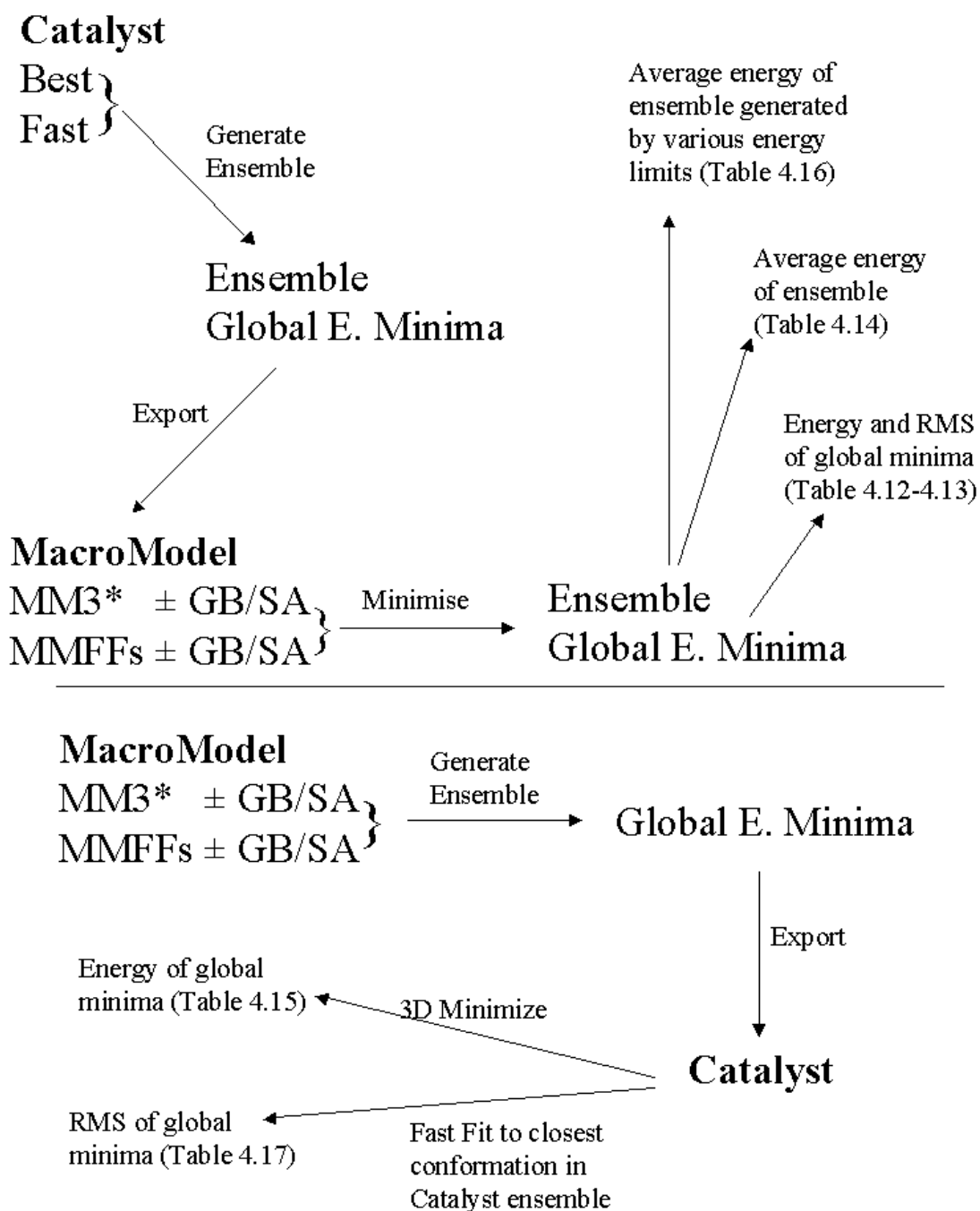


Figure 4.8: An overview of the calculations performed to evaluate Catalyst's conformation generation module.

Table 4.12 displays the conformational energy penalties of the global energy minima found by Catalyst calculated by the various force fields. In most cases, the energy is calculated to be higher than the guideline for acceptable conformational energy penalties of 12.5 kJ/mol [13]. Especially when flat bottomed Cartesian constraints are used. When using a solvation model, the strength of the electrostatic interactions are reduced, and one could expect the conformations to resemble more those obtained by a force field without electrostatic interactions. The Catalyst force

field does not contain any electrostatic terms. For conformations fully minimised by MM3*+GB/SA and MMFFs+GB/SA, just over half of the global energy minima are calculated to have a conformational energy penalty below the threshold, while most of the conformations fully minimised by MM3* and MMFFs are high in energy.

The energy of the global energy minima obtained by the Best conformational search is generally lower than the global energy minima as found by the Fast conformational search (5.9 kJ/mol on average).

Table 4.12: Conformational energy penalties (kJ/mol) of Catalyst global energy minima, calculated by various methods. Cpd.: Compound. Av.: Average. Colour codes: Red: conformational energy below 4.2 kJ/mol. Green: conformational energy below 8.4 kJ/mol. Cyan: conformational energy below 12.5 kJ/mol.

Cpd.	Catalyst Method	MM3*	MM3* GB/SA	MMFFs	MMFFs GB/SA	MM3* Constr.	MM3* GB/SA Constr.	MMFFs Constr.	MMFFs GB/SA Constr.
43	BEST	37.5	24.7	39.1	20.2	41.0	33.0	50.6	39.0
43	FAST	26.3	9.6	37.6	4.8	29.9	16.8	39.7	14.6
74	BEST	13.6	8.2	22.3	10.0	14.1	10.5	22.6	17.9
74	FAST	28.6	13.4	37.9	4.5	30.6	16.8	40.5	8.8
116	BEST	16.7	6.1	15.1	3.2	28.4	18.4	44.8	33.4
116	FAST	34.3	24.8	57.6	24.6	61.9	60.5	70.0	55.4
102	BEST	11.4	4.5	33.5	14.7	12.3	6.3	39.4	18.1
102	FAST	18.1	10.7	21.3	5.6	32.5	18.0	51.2	21.9
12	BEST	28.5	23.0	13.7	1.5	30.8	25.0	16.0	3.2
12	FAST	28.2	20.6	24.2	6.7	33.5	25.8	31.9	14.5
20	BEST	4.9	9.0	17.1	10.3	8.6	13.8	27.6	22.8
20	FAST	24.6	37.4	61.4	63.0	71.1	81.3	86.7	90.3
31	BEST	0.3	1.0	0.1	0.3	48.0	34.2	24.4	4.9
31	FAST	0.1	1.0	4.5	0.3	26.9	18.9	17.1	6.6
125	BEST	46.0	33.0	49.0	32.5	40.0	32.9	103.9	81.1
125	FAST	31.7	14.8	28.6	10.1	18.9	13.2	33.2	20.6
Av.	BEST	19.9	13.7	23.7	11.6	27.9	21.8	41.2	27.6
Av.	FAST	24.0	16.5	34.1	15.0	38.2	31.4	46.3	29.1

Table 4.13 displays the RMS between Catalyst global energy minima and the same structure minimised by the MMFFs, MMFFs+GB/SA, MM3* and MM3*+GB/SA force fields. When the structures are minimised with flat bottomed constraints of 0.2Å, they are almost identical with the global energy minima as found by Catalyst (RMS=0.123-0.155Å). When minimised to the nearest local minima, large conformational changes (>0.5 Å) are seen for most of the compounds. Table 4.12 and 4.13 show that the global energy minima obtained by Catalyst are generally both far from a minimum and high in energy.

Table 4.13: RMS (Å) between Catalyst global energy minima and the minimised structure. Cpd.: Compound. Av.: Average. Cyan fields: RMS below 0.5 Å.

Cpd.	Catalyst Method	MM3*	MM3* GB/SA	MMFFs	MMFFs GB/SA	MM3* Constr.	MM3* GB/SA Constr.	MMFFs Constr.	MMFFs GB/SA Constr.
43	BEST	1.26	1.02	0.90	0.75	0.14	0.14	0.14	0.14
43	FAST	0.54	0.51	0.47	0.41	0.12	0.12	0.13	0.13
74	BEST	0.36	0.40	0.41	0.42	0.13	0.13	0.13	0.13
74	FAST	0.37	0.34	0.48	0.37	0.13	0.13	0.13	0.13
116	BEST	0.80	0.89	1.08	1.09	0.15	0.15	0.14	0.14
116	FAST	1.37	1.11	0.58	1.02	0.13	0.13	0.15	0.15
102	BEST	0.41	0.41	0.59	0.48	0.13	0.14	0.14	0.14
102	FAST	0.65	0.70	0.60	0.56	0.14	0.14	0.14	0.14
12	BEST	0.58	0.52	0.58	0.47	0.13	0.13	0.13	0.12
12	FAST	0.74	0.66	0.36	0.34	0.14	0.14	0.13	0.13
20	BEST	0.40	0.45	0.54	0.57	0.13	0.13	0.14	0.14
20	FAST	1.80	1.80	0.68	0.72	0.14	0.14	0.15	0.15
31	BEST	0.91	0.88	0.92	0.77	0.10	0.11	0.12	0.13
31	FAST	0.61	0.57	0.61	0.50	0.12	0.12	0.12	0.12
125	BEST	0.52	0.58	2.60	2.55	0.15	0.15	0.16	0.16
125	FAST	0.53	0.84	0.65	0.72	0.13	0.13	0.15	0.15
Av.	BEST	0.65	0.64	0.95	0.89	0.13	0.13	0.14	0.14
Av.	FAST	0.82	0.81	0.56	0.58	0.13	0.13	0.14	0.14

Table 4.14 displays the average energy of the conformational ensemble generated by Catalyst Best and Fast search, calculated by the various force fields. Generally, the Best conformational search methods gives the lowest average energies when the ensemble is minimised to the nearest local minima. However, when minimised with flat bottomed Cartesian constraints, it is generally the Fast conformation generation algorithm that gives the lowest average energies. This reflects the fact that the Best conformation generation algorithm finds more conformations than the Fast conformation generation algorithm. But these extra conformations are merely distortions of low energy conformations. In some cases, the global energy minima are calculated to have a higher conformational energy penalty than the average conformational energy penalty. These are coloured red in Table 4.14. The average energy is generally within the default 84 kJ/mol (20 kcal/mol) energy limit set by Catalyst. However, for the ensembles minimised with flat bottomed Cartesian constraints, most of the average energies are approaching this limit, indicating that many conformations have significantly higher conformational energies.

Table 4.14: Average conformational energy penalty (kJ/mol) of Catalyst conformational ensemble, calculated by various methods. Cpd.: Compound. Av.: Average. Colour codes: Red: Below energy of global energy minima found by Catalyst. Green: Within 4.2 kJ/mol of global energy minima found by Catalyst. Cyan: Within 8.4 kJ/mol of global energy minima found by Catalyst.

Cpd.	Catalyst Method	MM3*	MM3* GB/SA	MMFFs	MMFFs GB/SA	MM3* Constr.	MM3* GB/SA Constr.	MMFFs Constr.	MMFFs GB/SA Constr.	Catalyst	Number of Conf.
43	BEST	40.4	35.2	39.0	28.9	66.8	62.1	77.9	68.8	47.8	192
43	FAST	37.2	29.2	40.7	24.8	53.7	45.5	66.3	51.1	48.3	199
74	BEST	27.7	25.0	33.5	20.4	53.1	50.0	73.7	62.3	45.3	183
74	FAST	33.8	29.0	42.0	24.8	49.7	45.1	65.0	49.1	55.3	100
116	BEST	39.1	35.0	39.6	25.6	56.4	52.1	74.7	65.7	44.5	107
116	FAST	45.3	38.3	54.0	32.3	78.1	71.6	89.8	70.4	49.8	225
102	BEST	25.7	22.5	41.9	33.9	49.0	45.3	81.6	70.7	43.7	230
102	FAST	36.1	32.0	44.3	36.7	55.4	51.8	77.0	65.0	41.6	225
12	BEST	31.5	26.7	27.5	15.2	54.9	48.8	60.7	46.8	49.7	71
12	FAST	27.6	22.7	15.8	7.0	40.4	35.4	38.9	29.3	25.3	10
20	BEST	30.5	38.4	45.1	44.4	59.3	66.6	79.0	75.4	54.2	56
20	FAST	24.7	35.8	52.6	58.1	71.1	81.3	93.0	97.4	44.2	5
31	BEST	10.8	3.3	9.7	2.8	41.9	33.1	47.1	27.7	32.8	140
31	FAST	11.5	4.7	15.2	3.6	42.3	36.2	40.7	25.3	29.7	67
125	BEST	54.0	41.7	66.2	47.3	76.9	66.2	125.6	96.6	41.1	202
125	FAST	55.8	42.4	72.6	46.7	65.3	53.8	110.8	77.0	47.2	216
Av.	BEST	32.5	28.5	37.8	27.3	57.3	53.0	77.5	64.3	44.9	147.6
Av.	FAST	34.0	29.3	42.2	29.2	57.0	52.6	72.7	58.1	42.7	130.9

Table 4.14 reveals that the energy, for many of the global energy minima, is comparable to the average energy of the conformational ensemble. This reflects that Catalyst's energy rank ordering of conformations is more or less arbitrary. Figure 4.9 is a plot of the conformational energy calculated by the various force fields versus conformation number (as ranked by Catalyst). When minimised with constraints, the trend is that the conformational energy rises with increasing conformation number. This trend is absent when full minimisation to the nearest energy minima is used, only the variation in energy increases with increasing conformation number. Figure 4.9 clearly reveals that many of the conformations found by Catalyst are just distortions of low energy conformations, and that the energy rank ordering is more or less arbitrary. This is typical for all the compounds examined.

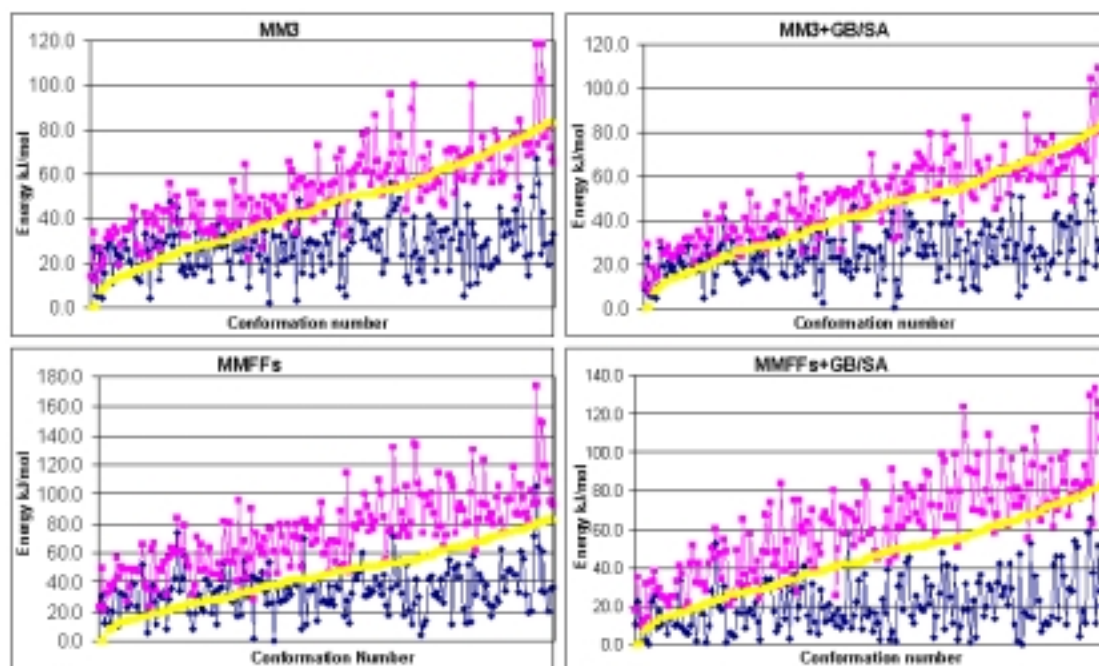


Figure 4.9: Conformational energy penalties for compound **74** calculated by various methods, plotted versus the conformation number (ranked by Catalyst). Yellow: Energy calculated by Catalyst. Pink: Energy calculated in MacroModel on conformation minimised using flat bottomed Cartesian constraints. Blue: Energy calculated in MacroModel on fully minimised conformation.

The global energy minima found by MMFFs, MMFFs+GB/SA, MM3* and MM3*+GB/SA were imported into Catalyst, where they were subjected to a minimisation (Called a 3D minimisation in Catalyst). This is the only way to relax a conformation, so the energy can be meaningfully calculated in Catalyst. When Catalyst reports the energies from a conformational search, it is the conformational energy penalty relative to the global energy minima. The global energy minima found by Catalyst were therefore also subjected to a minimisation to calculate the absolute energy in Catalyst's force field. This changed the conformations slightly, except for compound 125, for which a large change was observed. Table 4.15 displays the conformational energy penalties of the global energy minima found by MMFFs, MMFFs+GB/SA, MM3*, MM3*+GB/SA, and Fast conformational search, relative to the global energy minima as found by Catalyst's best conformational search. Half of the global energy minima found by MM3* and MMFFs are found to be low energy conformations in Catalyst's force field. MM3*+GB/SA and MMFFs+GB/SA global energy minima are generally lower in energy. When electrostatic interactions of MMFFs and MM3* are reduced by the solvation model, the conformational energies are closer to those obtained by a force field without electrostatic interactions. When using Catalyst's Fast conformation generation algorithm, only half the global energy

minima obtained are low energy conformations in Catalyst's own force field. Especially for MM3*+GB/SA, some energies are calculated to be negative. This means that Catalyst does not find the global energy minima in its own force field when generating an ensemble.

Table 4.15: Conformational energy penalties for global energy minima obtained from the various force fields, calculated by Catalyst. The energies are relative to the global energy minima as found by the Best conformational search. Colour codes: Cyan: Negative energies. Red: High conformational energy.

Compound	Catalyst Fast	MM3*	MM3* GB/SA	MMFFs	MMFFs GB/SA
43	13.7	4.2	-2.6	14.6	9.9
74	16.4	18.4	1.8	25.7	12.8
116	56.6	18.1	-0.5	65.4	37.4
102	9.5	6.2	2.0	5.5	7.5
12	7.6	-2.3	-2.3	-0.4	0.1
20	63.4	16.9	-5.7	0.4	1.0
31	2.6	2.5	2.5	1.7	2.4
125	-4.8	3.2	1.9	5.6	6.9
Average	20.6	8.4	-0.4	14.8	9.8

When doing a conformational search in Catalyst, there is a user-defined energy threshold (default 84 kJ/mol). Conformations having a conformational energy penalty above this limit are rejected. To find the influence of this limit on the conformational model generated, Best and Fast conformational search of compound **43** were done with several energy limits. The conformational ensembles were exported to MacroModel and minimised by using MMFFs. Both a full minimisation and a partial geometry optimisation with flat bottomed Cartesian constraints were done. Table 4.16 displays the average conformational energies of each conformational ensemble. When optimised with flat bottomed constraints, the average conformational energy penalty rises with increasing energy limit. However, when fully minimised, the average conformational energy does not show this trend. Decreasing the energy limit results in an insufficient coverage of conformational space.

Table 4.16: Average conformational energies of ensembles of compound **43** generated by Catalyst Best and Fast search with varying energy limits. Energies in kJ/mol.

Energy limit	Catalyst Fast search				Catalyst Best search			
	MMFFs	MMSFFs Constr	Catalyst	Number of conf.	MMFFs	MMSFFs Constr	Catalyst	Number of conf.
2.1	15.0	31.2	0.2	2	20.4	31.6	0.6	2
4.2	14.7	32.5	1.3	2	26.1	32.7	1.3	3
8.4	41.1	51.6	2.8	2	34.9	40.9	4.2	7
12.6	41.1	43.2	1.4	2	26.7	34.6	7.7	9
16.8	30.2	44.0	9.7	19	29.7	36.9	8.2	10
21	31.7	45.4	14.5	77	27.6	36	9.6	12
42	32.0	51.8	22.6	74	39.2	54.3	19.3	44
63	32.1	55.1	37.7	185	39.5	69.5	34.1	134
84	34.4	60.1	43.6	236	34.9	74.9	43.8	197

As discussed in Section 2.1, the binding constant K_i is related to the free energy of binding ΔG , and the conformational energy contribute to ΔG for the binding of the ligand to the receptor [13]. A high energy conformation therefore cannot be biologically active, and all high energy hits are false positives. Imposing a low energy limit would have been the solution, if Catalyst's force field could correctly calculate conformational energy penalties. However, this does not work for three reasons. A low energy limit gives an incomplete sampling of conformational space (Table 4.16). True low energy conformations that are high energy conformations in Catalyst's force field are missed (Table 4.17). Even with a low energy limit, most of Catalyst conformations are high in conformational energy.

When constructing a pharmacophore model it is important only to consider low energy conformations, otherwise one might construct a wrong model. When using the HipHop or HypoGen modules for automatic pharmacophore model generation, it is necessary to do a conformational search for all structures to be used for the model generation. Accelrys recommends that Catalyst Best search be used. Knowing that the quality of the conformational model generated by Catalyst is poor, it would be highly surprising if Catalyst should generate a correct pharmacophore model. With the present analysis in mind, it must be recommended to import an externally generated conformational model when using HipHop or HypoGen. However, with the present version of Catalyst, this is time consuming and not without problems. Catalyst calculates an energy of each imported conformation, and if it is higher than 84 kJ/mol, the conformation might be disregarded.

4.10.2 Diverse Sampling

Catalyst did not find the same global energy minima as MM3*, MM3*+GB/SA, MMFFs, or MMFFs+GB/SA for any of the compounds. The global energy minima of MM3*, MM3*+GB/SA, MMFFs, and MMFFs+GB/SA were imported into Catalyst to see if they were present in the conformational model generated by Catalyst Best or Fast search. A best conformation fast fit returned the Catalyst conformation closest to the imported global energy minima. The RMS values are listed in Table 4.17. In most cases, Catalyst does not find conformations close to the global energy minima found by MM3*, MM3*+GB/SA, MMFFs, and MMFFs+GB/SA. Catalyst Best search performs a little better than Fast search. Catalyst Best search only finds a conformation close to the global minima found by Catalyst Fast search for compound **31**. Catalyst Fast search also finds only a conformation close to the global minima found by Catalyst Best search for compound **31**. This demonstrates that Catalyst Best and Fast searches find different conformations, and that both algorithms miss important low energy conformations. The RMS value might not be the best measure for conformational similarity, because a small change of a torsional angle can lead to a large overall difference in RMS. However, for the most restricted compounds like **12**, **20**, and **31** (Figure 4.7), RMS is a good measure, and for those, only a conformation close to the global minima of compound **31** is found by Fast search.

Table 4.17: RMS (\AA) between global energy minima and the closest conformation in Catalyst's ensemble. The RMS is calculated between all heavy atoms and hydrogens on heteroatoms. Cpd.: Compound. Av.: Average. Colour codes: Red: RMS below 0.5 \AA . Cyan: RMS below 1.0 \AA .

Cpd.	Catalyst Best search					Catalyst Fast search				
	MM3*	MM3* GB/SA	MMFFs	MMFFs GB/SA	Catalyst Fast	MM3*	MM3* GB/SA	MMFFs	MMFFs GB/SA	Catalyst Best
43	1.440	1.657	1.323	1.694	1.700	1.203	1.633	1.358	1.633	1.977
74	1.494	1.594	1.121	1.360	1.287	1.871	1.970	0.938	1.358	1.505
116	1.945	1.935	1.820	1.985	1.060	2.477	1.231	1.697	1.773	1.346
102	1.395	0.751	0.723	1.005	1.601	1.553	1.364	1.648	1.716	1.606
12	0.767	0.754	1.306	1.307	0.987	1.289	1.295	1.260	1.237	1.361
20	0.736	0.409	0.577	0.592	0.824	1.657	1.551	1.714	1.709	1.559
31	0.547	1.065	0.482	1.201	0.197	0.759	0.877	0.597	0.666	0.483
125	1.942	1.909	1.548	1.889	1.952	1.685	1.776	1.182	1.802	2.446
Av.	1.283	1.259	1.113	1.379	1.201	1.562	1.462	1.299	1.487	1.535

Catalyst searches feature space, and that is claimed to be a more diverse sampling than other conformational search algorithms [5]. This is not always true. In compound **31**, the tricyclic ring system can be in two conformations, as shown in Figure 4.10. Table 4.18 compares the number of conformations as found by Monte

Carlo search with MMFFs or MM3* and Catalyst Fast or Best search algorithm having either of the tricyclic ring system conformations. The Monte Carlo search finds approximately equal number of conformations with either of the tricyclic ring system conformations, whereas Catalyst Best search finds almost exclusively one of the conformations. Figure 4.10 left displays a superimposition of the first 9 conformations of compound **31** found by Best conformational search. The only difference between these conformations is the tilt of the di-trifluoromethylphenyl ring. Fast search generates a more diverse ensemble since the ratio is about 1:2.

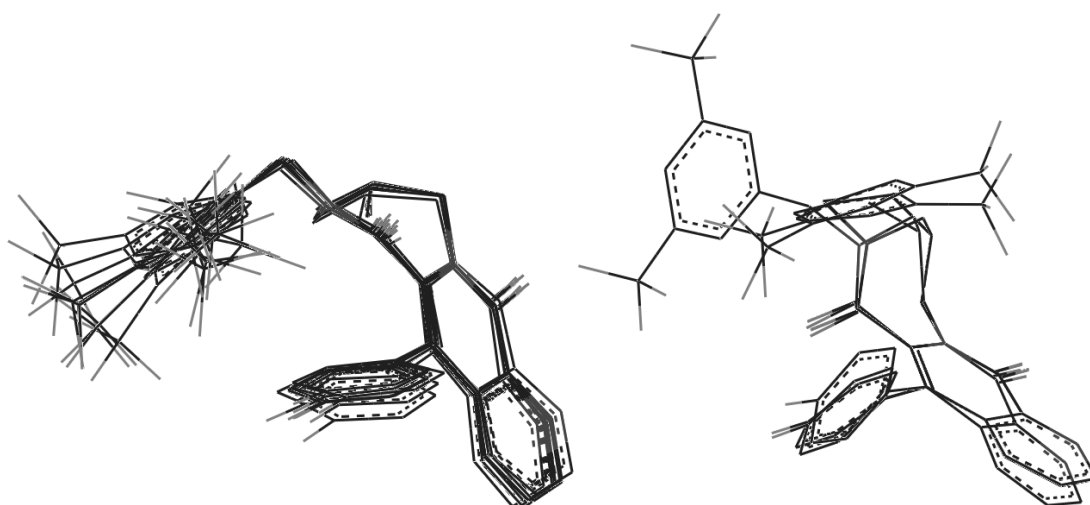


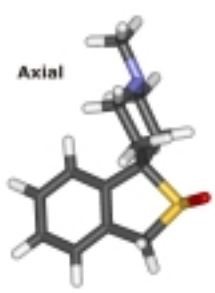
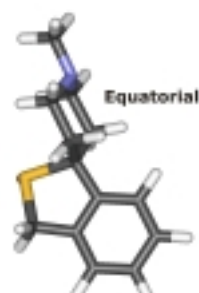
Figure 4.10: The seven membered ring of compound **31** can be in two conformations as displayed left or right. Left: A superimposition of the nine first conformations found by Catalyst best search. Right: A superimposition of the three conformations found with the tricyclic ring system in that conformation.

Table 4.18: Number of conformations of compound **31** with the tricyclic ring system having a conformation as defined in Figure 4.10 left and right.

Method	Right	Left
Catalyst Best	3	137
Catalyst Fast	24	43
MMFFs	29	24
MMFFs+GB/SA	30	47
MM3*	9	8
MM3*+GB/SA	9	7

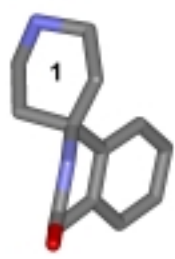
In the spiro ring system of compound **74** (Figure 4.7), the phenyl ring can be either axial or equatorial to the piperidine ring, as shown in Table 4.19. Using Monte Carlo/MMFFs or MM3* with or without GB/SA, the axial and equatorial conformations are equally represented. Catalyst Best search finds 183 conformations. Only 7 of these have the phenyl ring in the axial position, and in all 7, the piperidine ring is twisted. Catalyst Fast search finds 100 conformations. 22 of these have the phenyl ring in the axial position and the piperidine ring is in a chair conformation in all 22.

Table 4.19: In compound **74** the phenyl ring can be equatorial or axial to the piperidine ring. The representation of these conformations in ensembles generated by the various methods are shown.

		Conformation	Axial	Equatorial	Total
		Catalyst Best	7	176	183
		Catalyst Fast	22	78	100
		MMFFs			
		MMFFs+GB/S			
		A	~50%	~50%	
		MM3*			
		MM3*+GB/SA			

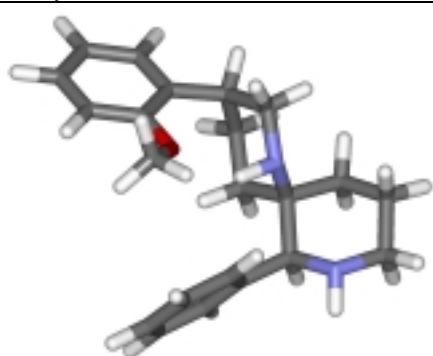
Compound **116** (Figure 4.7) also has a spiro ring system (Table 4.20). Catalyst Best search finds 107 conformations, 12 of them having the phenyl ring equatorial to the piperidine ring, which is in a chair conformation. Catalyst Fast search finds 225 conformations, 120 of them having the phenyl ring equatorial to the piperidine ring, which is always in a twisted conformation. The spiro system has three low energy conformations, as shown in Table 4.20. Catalyst Best search finds four conformations with the spiro system adopting conformation 3, and three conformations in which the lactam ring is flat, as in conformation 2. Fast search finds 34 conformations with the spiro system adopting conformation 1, the remaining conformations have a flat ring (conformation 2). A Monte Carlo search using MMFFs or MM3* finds roughly equal numbers of conformations with the spiro system adopting conformation 1 or 3, but no conformation in which the lactam ring is flat. The flat conformation is 5 kJ/mol and 10 kJ/mol higher in energy than the other conformations calculated by MMFFs and MM3*, respectively. Conformation 2 is the transition state for inversion between conformations 1 and 3.

Table 4.20: The spiro ring system of compound **116** have three low energy conformations. The representation of these conformations in ensembles generated by the various methods are shown.

		Conformation	1	2	3	
			Catalyst Best	4.7%	2.6%	3.5%
			Catalyst Fast	15%	38%	0%
		MMFFs				
		MMFFs+GB/S				
		A	~50%	0%	~50%	
		MM3*				
		MM3*+GB/SA				

Compound **20** (Figure 4.7) has two piperidine rings in a spiro system. The most stable conformations as calculated by MM3*, MMFFs, MM3*+GB/SA, and MMFFs+GB/SA have both rings in a chair conformation, as shown in Table 4.21. Catalyst Best search finds 56 conformations. Three of these have both rings in a chair conformation and four have one ring in a chair conformation and one ring in a distorted chair conformation. Catalyst Fast search finds no conformations with both piperidine rings in a chair conformation.

Table 4.21: Only conformations where the two piperidine rings of compound **20** are in chair conformations are of low energy. The representation of these conformations in ensembles generated by Catalyst are shown.



Catalyst Method	Fast	Best
Chair Chair	0 (0%)	3 (5.3%)
Unexpected	5 (100%)	53 (94.6%)
No. Conformations	5	56

Compound **125** (Figure 4.7) has two piperidine rings connected by a single bond. The extended conformation, where all bonds are equatorial and the piperidine rings are in a chair conformation (Table 4.22), are the most stable conformation as calculated by MM3*, MMFFs, MM3*+GB/SA, and MMFFs+GB/SA. Catalyst Best search finds 202 conformations. 10 of them have the piperidine rings in the extended conformation, four with both rings in a chair conformation, and six in which one of the rings is twisted. Fast search finds 216 conformations, 45 of them having the piperidine rings in the extended conformation, 36 with both rings in a chair conformation, and 9 in which one of the rings is twisted.

Table 4.22: Conformations where the two piperidine rings of compound **125** are in chair conformations and the substituents equatorial are lowest in energy. The representation of these conformations in ensembles generated by Catalyst is shown

Catalyst Method	Fast	Best
	Chair Chair Equatorial	36 (17%)
Chair Twist Equatorial	9 (4.2%)	6 (2.7%)
Non Extended conformations	171 (79.2%)	212 (95.5%)
Number of Conformations	216	222

In compound **102** (Figure 4.7), the methoxy group can be either axial or equatorial to the piperidine ring (Table 4.23), with the first mentioned lowest in energy, as calculated by MM3*, MMFFs, and MM3*+GB/SA, but not MMFFs+GB/SA. Catalyst Fast search finds 49 conformations of compound **102**, all of which have the methoxy group in the equatorial conformation. Catalyst Best search finds 230 conformations, 42 of which have the methoxy group in the equatorial conformation. Of these 42, only two have the piperidine rings in a chair conformation with the N-substituent equatorial.

Table 4.23: The methoxy group of compound **102** can be equatorial or axial to the piperidine ring. The representation of axial and equatorial conformations in the ensembles generated by Catalyst are shown.

Catalyst Method	Fast	Best
	Axial Chair	0 (0%)
Axial Twist	0 (0%)	40 (17%)
Equatorial	49 (100%)	188 (81%)
No. Conformations	49	230

Diverse sampling of feature space does not always result in a diverse conformational model. For six of eight compounds examined, important low energy conformations were missing or severely underrepresented in the conformational model generated by Catalyst. A conformation close to the global energy minima in MMFFs, MM3*, MMFFs+GB/SA, and MM3*+GB/SA was only represented in the Catalyst ensemble of the three most rigid compounds (**12**, **20** and **31**). Best conformational

search gives the most diverse model in feature space. In conformation space, it seems to depend on the structure whether Best of Fast search gives the most diverse model.

There are probably three reasons for the poor quality of the conformational models generated by Catalyst. 1; The conformational coverage is evaluated in a feature space [5] which is not directly coupled to conformational space. Feature space imposes constraints on the conformational model, but the conformation of ring fragments, torsional angles etc. is independent of feature space. 2; The use of poling distorts the conformations. 3; The quality of the force field.

A search query for database search in Catalyst can be constructed from two kinds of elements. Pharmacophore elements (functions), which in Catalyst belongs to feature space and fragment, shapes and exclusion volumes, which are generated in conformational space. Since there is a large difference between the conformational models generated by Catalyst and that of conventional methods, it is probably important to use a Catalyst conformation when defining a shape query, exclusion volumes, or using fragments in the search query.

4.10.3 Conclusions on Catalyst evaluation

The primary aims of Catalyst's conformation generation module are 1: Speed. 2: To explore compounds in terms of all the energetically accessible conformations available under physiological conditions [2]. The present work clearly demonstrates that the second goal is not achieved³. Most conformations generated by Catalyst are far from a local minima and high in energy. Furthermore, the rank ordering of the conformational model is arbitrary. These high energy conformations are just noise that results in false positives when doing a database search. This noise is dangerous when doing automatic hypothesis generation, since it leads to wrong models. Low energy conformations are often missing or seriously underrepresented in the ensembles generated by catalyst. This results in false negatives when doing a database search. Furthermore, the lack of low energy conformations makes it impossible for HipHop and HypoGen to generate a realistic model.

³ The extent to which a given conformation is populated depends on the conformational energy and the temperature. Since most of Catalysts conformations are high in conformational energy, they are only accessible at higher temperatures than physiological conditions.

Diverse sampling of feature space does not always result in a diverse conformational model. The conformational diversity is often seen in distortions of true low energy conformations. Especially for rings, high energy conformations are over represented in the conformational model. Sometimes so much that no low energy conformation is found for the ring system. In six out of eight compounds examined, Catalyst failed to generate diverse conformational models due to problems with flexible ring systems. Because Smellie et al. [5] consider feature space, they conclude: “Poling: Promoting Conformational Variation”. However, considering conformational space the conclusion must be; Poling: Preventing Conformational Variation.

Catalyst is a good tool for 3D database search, but the way conformations are generated leaves a lot to wish for. Substituting the conformational search algorithm for a Monte Carlo or Low mode search would greatly enhance the quality of the conformational models. However, this would slow down the generation of a 3D database considerably. A compromise between speed and quality would be to implement a fragmented approach without the poling algorithm.

4.11 Conclusion

The pharmacophore models (Section 2.4 and Appendix I and II) were used as search queries for database search with the program package Catalyst. The search queries were evaluated by searching MDDR, a database with known biological activities. The two automated hypothesis generating methods in Catalyst (HipHop and HypoGen) were also used to generate search queries. However, the performance of these two methods was poor. Analogues of compound **1** and **12** were used as templates for constructing hypotheses for the selective NK1R antagonists described in Section 2.2. However, problems were encountered with the accessibility of the hydrogen bond donor pharmacophore element, which hampered the search results. Compound **43** was used as template for constructing hypotheses for the NKR antagonists described in Section 3.1. Good yields could be obtained with these hypotheses, but the percentage of actives returned was moderate.

These moderate results are probably due to severe shortcomings in the conformation generation module of Catalyst. The conformational ensembles of eight NKR antagonists were investigated. Ensembles generated by Catalyst were shown not to be diverse and with a significant overpopulation of high energy conformations.

Especially flexible rings pose a problem for Catalyst. Low energy conformations were missing or significantly underrepresented in six out of eight ensembles generated by Catalyst. The lacking diversity of low energy conformations results in false negatives and the many high energy conformations are noise that results in false positives. Substituting the conformation generation module of Catalyst with one that has a better performance would greatly enhance the program.

4.12 References

1. Catalyst 4.5. Accelrys Inc., 9685 Scranton Road, San Diego, CA 92121-3752.
2. Accelrys Inc., www.accelrys.com/catalyst.
3. Sprague, P. W. and Hoffmann, R., In van de Waterbeemd, H., Testa, B. and Folkers, G., (Eds.), Computer Assisted Lead Finding and Optimization - Current Tools for Medicinal Chemistry, VHCA, Basel, **1997**: 225-240.
4. Sprague, P. W., Automated chemical hypothesis generation and database searching with Catalyst. *Perspectives in Drug Discovery and Design* **1995**, 3: 1-20.
5. Smellie, A., Teig, S. L. and Towbin, P., Poling: Promoting conformational variation. *J. Comput. Chem.* **1995**, 16: 171-187.
6. Smellie, A., Kahn, S. D. and Teig, S. L., Analysis of conformational coverage. 1. Validation and estimation of coverage. *J. Chem. Inf. Comput. Sci.* **1995**, 35: 285-294.
7. Smellie, A., Kahn, S. D. and Teig, S. L., Analysis of conformational coverage. 2. Applications of conformational models. *J. Chem. Inf. Comput. Sci.* **1995**, 35: 295-304.
8. Greene, J., Kahn, S., Savoj, H., Sprague, P. and Teig, S., Chemical function queries for 3D database search. *J. Chem. Inf. Comput. Sci.* **1994**, 34: 1297-1308.
9. MDL Drug Data Report, MDL (Molecular Design Limited). <http://www.mdli.com/products/mddr.html>.
10. Güner, O. F. and Henry, D. R. In Güner, O. F., (Ed.), Pharmacophore perception, development, and use in drug design, International University Line, La Jolla, CA, USA, **2000**: 193-212.
11. Ofner, S., Hauser, K., Schilling, W., Vassout, A. and Veenstra, S. J., SAR of 2-benzyl-4-aminopiperidines: CGP 49823, an orally and centrally active non-peptide NK1 antagonist. *Bioorg. Med. Chem. Lett.* **1996**, 6: 1623-1628.
12. Gundertofte, K., Liljefors, T., Norrby, P. O. and Pettersson, I., A comparison of conformational energies calculated by several molecular mechanics methods. *J. Comput. Chem.* **1996**, 17: 429-449.
13. Boström, J., Norrby, P.-O. and Liljefors, T., Conformational energy penalties of protein-bound ligands. *J. Comput.-Aided Mol. Des.* **1998**, 12: 383-396.

5 Neurokinin 7TM receptor models

5.1 7TM receptor models

This chapter describes the development of receptor models for the NK1R, NK2R and NK3R, as well as their use in identifying receptor-ligand interactions and residues responsible for subtype selectivity.

Neurokinin receptors do not readily crystallise, and structures of these receptors are not yet available. However, an X-ray structure of bovine rhodopsin has been published [1], and the NKRs have sufficient sequence identity to bovine rhodopsin for an alignment to be made. Rhodopsin is a photoreceptor found in the retina of the eye. It is comprised of seven transmembrane alpha helices, each approximately 25 residues long. The helices are connected by intra- and extracellular loops. The helices are arranged in a bundle with a counter clockwise orientation, as seen from the extracellular side. The residues facing the lipid membrane are mostly hydrophobic, whereas those facing the interior may be more polar. Residues in the loops are generally hydrophilic. The first intra- and extracellular loops are short, five and six residues, respectively, whereas the other loops are longer.

Several receptor modelling studies of the NK1R [2-6], the NK2R [2;7-9] and the NK3R [7] have been published and are reviewed in Section 5.2. These receptor models are based on the bacteriorhodopsin structure by Henderson et al. [10] or the rhodopsin structure by Baldwin et al. [11]. Bacteriorhodopsin is a proton pump, not a GPCR, and the sequence identity with any known GPCR are too low for sequence based alignment. (Alignment is hydrophobicity based). Furthermore, the resolution of the cryo electron microscopy structure is 3.5 Å too low to provide the atomic coordinates directly. Thus, bacteriorhodopsin is not an ideal template for modelling GPCRs. The structural rationale for employing bacteriorhodopsin as a template for a GPCR is that bacteriorhodopsin has 7TM helices in a similar counter clockwise orientation as the GPCRs. Rhodopsin is a true GPCR. Baldwin's rhodopsin model is based on a cryo microscopy electron density map of frog rhodopsin [12], but the resolution is 7.5 Å in the membrane plane and 16.5 Å normal to it, too low to provide atomic coordinates directly. An X-ray structure of bacteriorhodopsin with a resolution of 2.5 Å have been published by Pebay-Peyroula et al. [12a], but this structure have seen little use for homology modelling of GPCRs.

Bovine rhodopsin is a GPCR that shares approximately 20-25% sequence identity with most known GPCRs. Using the recently published bovine rhodopsin X-ray structure (resolution 2.8 Å) [1] as template is expected to produce better GPCR models.

Extensive site-directed mutagenesis work has been performed on the NK1R and NK2R identifying residues essential for ligand binding (see Section 5.2). Another type of mutagenesis work performed on the NK1R is the introduction of metal ion binding sites [13-15]. From this work, information about the relative orientation of helices, distance constraints and solvent accessibility can be obtained. By contrast, the only mutagenesis data available for NK3R are a few chimeric NK1/NK3 receptors [16-20].

5.2 Previously published mutagenesis and receptor model studies

5.2.1 Selective NK1R antagonists

Several mutagenesis studies on the NK1R have been published. See Table 5.1 for data and references. Only data for compounds fitting the pharmacophore models described in Section 2.4 and Appendix II are listed in the table. Some of these studies are conducted by the use of the selective NK1R antagonists compounds **1** and **12** [3-5;21]. Interactions between some residues in the NK1R and specific groups and atoms in compound **1** have been identified by the following method [21]: If a residue interacts directly with a specific pharmacophore element in the ligand, then an analogue of the ligand where that pharmacophore element has been removed should bind equally well to both the wild-type and the mutant receptor, because the proposed interaction is no longer present.

Compound **3** is a close analogue of **1** in which one of the benzhydryl phenyls is missing. Compound **3** has the same affinity for the His197Ala mutant as the wild-type receptor [21]. However, for compound **1** a decreased affinity by a factor of 6.6 is seen for the mutated receptor. This suggests that His197 interacts with the benzhydryl moiety in compound **1**. It is also suggested that Gln165 forms a hydrogen bond to the nitrogen atom of the benzylamine of compounds **1** and **12**. This is supported by the fact that compound **4**, a close analogue of **1**, has the same affinity for the Gln165Ala mutant as the wild-type receptor. For compound **1**, a decreased affinity by a factor of 16-44 is seen for the mutated receptor. Compound **4** has a methylated amino group

where the benzyl amine in compound **1** is secondary. It is hypothesised that the methyl group in **4** is positioned so the hydrogen bond to Gln165 cannot be formed [22]. His265 probably interacts with the benzyl moiety or substituents thereof. Compound **1** binding is not affected by the His265Ala mutation but compound **8**, the 3,5bis-CF₃ analogue, loses a factor of 20 in binding affinity, and compound **12** loses a factor of 4 [5]. Pro112 and Phe268 might also be important residues for binding of compounds **1** and **12** to the NK1R. Consistent with the SAR discussion in Sections 2.2 and 3.1, the mutagenesis data suggest a common binding mode for compounds **1** and **12** that is not shared by compounds **68** and **87**.

Table 5.1: Mutation data for the NK1R. Decrease is the fall in affinity for the receptor mutant compared to the wild-type.

Ligand	Mutation	Decrease	Reference	Ligand	Mutation	Decrease	Reference
68	Gln165Ala	6.8	[2]	1	Ile283Ala	4.1	[23]
68	His197Ala	7.9	[2]	1	Pro112Ala	13	[24]
68	Ile204Ala	9.0	[2]	1	Pro112Asp	4300	[24]
68	Phe264Ala	26	[2]	12	Pro112His	4600	[24]
68	Phe264Tyr	>480	[2]	12	Gln165Ala	63, 100, 44	[3;22;23]
68	His265Ala	17	[2]	12	His197Ala	9.9	[23]
68	His267Ala	NB	[2]	12	Phe264Ala	4.4	[23]
68	Tyr272Ala	1.3	[2]	12	His265Ala	4.0	[3]
1	Pro112Ala	3.5	[24]	12	Phe267Ala	NB	[23]
1	Pro112Asp	150	[24]	12	Phe268Ala	4.0, 15	[3;24]
1	Pro112His	210	[24]	12	Pro112Ala	2.0	[24]
1	Glu165Ala	16, 18, 44	[3;22;23]	12	Gln165Ala	2.0	[3]
1	Ser169Ala	5.2	[22]	87	His197Ala	2.0	[3]
1	His197Ala	13, 70, 34	[3;22;23]	87	Phe268Ala	4.0, 4.8	[3;24]
1	His197Gln	6.6	[23]	3	His197Ala	1.2	[21]
1	Phe267Ala	NB	[23]	4	Gln165Ala	3.0	[6]
1	Phe268Ala	5.0, 71	[3;24]	8	His265Ala	20	[5]
1	Tyr272Ala	4.0, 4.2	[22;23]				

5.2.2 Dual NK1R/NK2R and selective NK2R antagonists

Greenfeder et al. [2] have conducted a study on the binding sites of the dual NK1/NK2 receptor antagonist compound **68**. They conclude that the binding sites differ and that the bioactive conformations at the two receptor subtypes are different. This is a surprising conclusion considering the high sequence identity between the NK1R subtypes (see Section 1.2). They conclude that compound **68** binds to the NK1R in a conformation close to that represented by pharmacophore Model 2 (Appendix II) and to the NK2R in a conformation close to that represented by pharmacophore Model 1 (Appendix I and II). However, their modelling work is flawed because the dichlorophenyl group of their docked antagonist is connected to C2 of the pyrrolidine ring instead of C3 as in compound **68**. This might be the reason for their surprising

conclusion. But the site-directed mutagenesis data in this article are still valuable (Table 5.2).

Giolitti et al. [9] have conducted a study on the binding sites of the selective NK2R antagonist compound **43**. They conclude that compound **43** binds in a conformation close to that represented by the NK2 pharmacophore Model 2 (Appendix II). By site-directed mutagenesis they identify the same residues important for binding as Greenfeder et al. [2]. This suggests a common binding mode for compounds **43** and **68**. However, the binding mode suggested in the two papers is different.

Table 5.2: Mutation data for the NK2R. Decrease is the fall in affinity for the receptor mutant compared to the wild-type.

Ligand	Mutation	Decrease	Reference	Ligand	Mutation	Decrease	Reference
68	Trp156Ala	NB	[2]	43	His198Ala	16	[9;25]
68	Gln166Ala	7.0	[2]	43	Tyr266Ala	NB	[9]
68	His198Ala	NB	[2]	43	Tyr266Phe	4.0	[9]
68	His198Phe	0.8	[2]	43	His267Ala	NB	[9]
68	Tyr266Ala	NB	[2]	43	Phe270Ala	5.3	[9]
68	His267Ala	NB	[2]	43	Tyr289Ala	NB	[9]
68	Tyr269Ala	NB	[2]	43	Tyr289Phe	2900, 3000	[26;27]
68	Ile285Ala	NB	[2]	43	Ser27Ala	6.0	[27]
68	Tyr289Ala	NB	[2]	43	Trp31Ala	5.0	[27]
68	Tyr289Phe	300	[2]	43	Trp99Ala	NB	[27]
43	Met117Leu	4.4	[25]	102	His198Ala	100	[27]
43	Gln166Ala	5.7	[9]	102	Tyr266Phe	>250	[27]
43	Thr171Ala	6.3	[9]	102	Phe293Ala	22	[27]

5.3 The binding site for NKR antagonists

The monoaminergic receptors were among the first GPCRs to be studied. The muscarine M1 receptor is used as an example for comparison with the NKRs. Figure 5.1 shows the alignment of the NKRs to the M1 receptor. The residues identified by site directed mutagenesis as significant for binding of compounds **43** and **68** are displayed in bold in Figure 5.1 and listed in Table 5.2. The putative binding site of the NKRs is located in the same area as that proposed for the monoaminergic receptors. The important residues for M1 receptor antagonists binding [28] is located either at the same position as in the NKRs or one helix turn above or below the NKR positions. It has been proposed that this is a common binding site for small molecule antagonists, shared by many of the rhodopsin-like GPCRs [5;29]. This NKR antagonist binding site is different from the proposed binding site of the endogenous

NKR ligands. These bind to the extracellular loops with a small part of the peptide extending into the 7TM region [16;30;31].

Bovine rhodopsin, the template used for our NKR models, is crystallised with the endogenous ligand retinal [1]. Retinal is special since it is covalently bound to the receptor. The binding site of retinal partly overlaps with that of the small molecule antagonists and are located just below the extracellular loops. There is a change in receptor conformation upon activation. Ideally, the inactive receptor conformation should be used for modelling of the antagonist binding site. Fortunately, the bovine rhodopsin structure is in the inactive state.

Most of the residues in the binding site are preserved throughout the NKR subtypes. The residues identified by site-directed mutagenesis are important for the binding of compounds **43** and **68** to the NK2R are Met117, Gln166, His198, Tyr266, Phe270 and Tyr289 [2;9;27]. The residues important for the binding of compound **68** to the NK1R are Gln165, His197, Ile204, Phe264 and His265 [2]. The NK1 binding site differs from that of NK2 in residues 117, 202 and 266 (NK2 numbering). The NK3 binding site differs from that of NK2 in residues 117 and 205.

The residues identified by site-directed mutagenesis as being important for the binding of the selective NK1 antagonists compounds **1** and **12** to the NK1R are His197, Gln165, His265 and Phe268 [3]. This binding site is not identical to the binding site of compounds **43** and **68**, but they overlap. The site-directed mutagenesis data are supported by a study by Gether et al. [32], who have constructed a number of chimeric NK1/NK2 receptors. They show that TM6 and part of TM7 (amino acids 251-293 in the NK1R) are responsible for most of the subtype selectivity of compound **12** and **43**, but not that of SP and NKA.

		TM3		IL-2	
NK1R_HUMAN	105	CKFHNFPIAA V FASIYSMTAVAFDRYMAIIHPLQPRLS-			
NK2R_HUMAN	106	CYFQNLFPIT A MFVSIYSMTAIAADRYMAIVHFPQPRLS-			
NK3R_HUMAN	158	CRFQNFPPIT V FASIYSMTAIAVDRYMAIIDPLKPRLS-			
M1	114	CDLWLALDYVASNAS V MNLLLSIFDRYFSVTRPLSYRAKR			
		-			
		TM4		EXL-2	
NK1R_HUMAN	144	ATATKVVICVI-WVLALL L LAF P Q G -YYSTTETMPS--RVVCMIEWPEHPNKIYEK			
NK2R_HUMAN	145	APSTKAVIAGI-WLVAL L ASP Q C-FYSTVTMDQ G --ATKCVVAVPEDSGGKTL			
NK3R_HUMAN	197	ATATKIVIGSI-WILAF L LAF P Q C -LYSKTKVMP G --RTL C VFQWPE G P--KQHF			
M1	138	TPRRAALMIGLAWLVSFVLWAPAILFWQYLVGERTVLAGQCYIQFLS----QPII			
			*	*	
		TM5		IL-3	
NK1R_HUMAN	195	V Y H I C V T V L I Y F L P L L V I G Y A Y T V V G I T L W A S E I P G -DSSD			
NK2R_HUMAN	196	L Y H L V V I A L I Y F L P L A V M F V A S V I G L T L R R A V P G H Q A H G			
NK3R_HUMAN	246	T Y H I I V I L V Y C F P L L I M G I T Y T I V G I T L W G G E I P G -DTC			
M1	189	T F G T A M A A --F Y L P V T M C T L Y			
			**	*-	-*
		TM6		EXL-3	
NK1R_HUMAN	235	RYHEQVS A KR K V V K M M I V V V C T F A I C W L P F H I F F L L P Y I N P D L Y L K K F I			
NK2R_HUMAN	237	ANLRHLQAK K K F V K T M V L V L T F A I C W L P Y H L Y F I L G S F Q E D I Y C H K F I			
NK3R_HUMAN	286	KYHEQLKAK R K V V K M M I V V M T F A I C W L P Y H I Y F I L T A I Y Q L N R W K Y I			
M1	357	LVKEK K AARTLSA I L L A F I L T W T P Y N I M V L V S T F C K D --C V P --			
			-	*	
		TM7		C-terminal	
NK1R_HUMAN	284	QQ V Y L A I M W L A M S S T M Y N P I I Y C L N D R F R L G F K H A F R C C P F I			
NK2R_HUMAN	286	QQ V Y L A L F W L A M S S T M Y N P I I Y C L N H R F R S G F R L A F R C C P W			
NK3R_HUMAN	335	QQ V Y L A S F W L A M S S T M Y N P I I Y C L N K R F R A G F K R A F R W C P F I			
M1	397	ETLWEL G Y W L C Y V N S T I N P M C Y A L C N K A F R D T F R L L L L C			
			*		

Figure 5.1: Alignment of the M1 receptor to the NKRs. The residues in bold marks the residues in the proposed antagonist binding site. * The residues are identical in the NKRs. – The residues differ in the NKRs. Notice that the important residues for M1 binding are located at the same place or one helix turn away from the putative NK antagonist binding site.

5.4 Development of the neurokinin 7TM receptor models

Construction of the NKR models was done by the iterative distance geometry method by Lomize et al. [29]. This method involves: 1) Alignment of the NKRs to bovine rhodopsin; 2) construction of an initial crude NKR model by amino acid replacement of the X-ray structure of bovine rhodopsin; 3) refinement of the initial NKR model by the iterative distance geometry method. In the construction of the crude NK1R and

NK3R model, information about loop and side chain conformation obtained from the previously constructed NKR models was used.

5.4.1 Alignment

The sequences for bovine rhodopsin, NK1R, NK2R and NK3R, were obtained from the GPCR Data Bank (GPCRDB) [33], and they were manually aligned [34] (Figure 5.2). Each helix in the rhodopsin-like family contains a number of highly conserved residues [35]. They were used to check if the alignment is correct, and they are marked in bold in Figure 5.2. An alignment of the sequences was also obtained from Expert Protein Analysis System (ExpPASy) [36] (Figure 5.3). The sequence data was submitted using default settings. The sequence identity to bovine rhodopsin was found to be 23.1% for the NK1R in 293 residues, 23.9% for the NK2R in 289 residues, and 22.1% for the NK3R in 289 residues.

The manually alignment differs from that obtained from ExpPASy in the areas where there are insertions. These are:

- Residues 144-146 (rhodopsin numbering) in the second intracellular loop.
- Residues 174-197 in TM4 and the second extracellular loop. Here the insertion is in the extracellular loop in the manual alignment where as it is situated in TM4 in the ExpPASy alignment.
- Residues 239-245 in TM6 and the third intracellular loop. Here the insertion is in the intracellular loop in the manual alignment whereas it is situated in TM6 in the ExpPASy alignment.
- Residues 281-294 in the third extracellular loop and TM7. Here the insertion is in the extracellular loop in the manual alignment whereas it is situated in both the loop and TM7 in the ExpPASy alignment.
- For the NK3R, the manual and ExpPASy alignments also differ throughout TM5 and the third intracellular loop. By comparing this region of the three NKRs in the ExpPASy alignment, it is obvious that the NK3R is aligned differently than the NK1R and NK2R.

This was an unexpectedly poor result. It is preferred to have the insertions in the extra- and intracellular loops, since the 7TM part is generally more conserved than the loops. Therefore the manual alignment was chosen.

		N-terminal
OPSD_BOVIN	1	MNGTEGPNFYVPPFSNKTGVVRSPPFEAPQY-----YLAEP
NK1R_HUMAN	1	-MDNVLPVDSDLSPNISTNTS----EPNQ-----FVQPA
NK2R_HUMAN	1	----MGTCDIVTEANISSGPESNTTGITA-----FSMPS
NK3R_HUMAN	42	-----LQLLDQAGNLSSSPSALGLPVASPPSPQWANLTNQ-FVQPS
		-----X-x-----xx--x-
		TM1 IL-1
OPSD_BOVIN	35	WQFSMLAAYMFLLLIMLGFP IN FLTLTYVTVQHKKLRT
NK1R_HUMAN	30	WQIVLWAAAYTVIVVTSVVG NV VVMWII LAHKRMRT
NK2R_HUMAN	31	WQLALWATAYLALVAVT GN AIVIWI LAHRRMRT
NK3R_HUMAN	83	WRIALWSLAYGVVAVAVL GN LIVIWI LAHKRMRT
		X--xx--xx---x---x-xX--x-xxxxxX-xxXX
		TM2 EXL-1
OPSD_BOVIN	71	PLNYILLN LAV ADLFMVFGGF ^T TTLYTSLHG ^Y FVFGPTG
NK1R_HUMAN	66	VTNYFLVN LAF A ^E ASMAAFNTV ^N NFTYAVHNEWYGLFY
NK2R_HUMAN	67	VTNYFIVN LAL ADLCMAAFNAAFNFVYASHNIWYFGRF
NK3R_HUMAN	119	VTNYFLVN LAF S ^D ASMAAFNTLVNF ^I YALHSEWYFGANY
		xxXXx-xXXX-----Xxxxx---xx-xX--xx-X---
		TM3 IL-2
OPSD_BOVIN	110	CNLEGGFFATLGGEIALWLSLVLA IER VVVCKPMSNFRFG
NK1R_HUMAN	105	CKFHNF ^F PIAAVFASISMTAVAF DR YMAI IHPL-QPRLS
NK2R_HUMAN	106	CYFQNL ^F PITAMFVSIYSMTAIA DR YMAIVHPF-QPRLS
NK3R_HUMAN	158	CRFQNF ^F PITAVFASISMTAIA DR YMAIIDPL-KPRLS
		X-x-x-xxx-x-x-xxxXxxx-X-xXXxxx--X-x-xxXx
		TM4 EXL-2
OPSD_BOVIN	150	ENHAIMGVAFT W VMALACA AP PLVGSRYIPEGMQCSCGIDYYTPHEE--TNNE
NK1R_HUMAN	144	ATATKVVICV I WVLALLLAF P QGYST ^T ETMP ^S R-VVCMIE--WPEHPNKIYEK
NK2R_HUMAN	145	APSTKAVIAG I WLVALALAS P QCFYSTV ^T MDQGA-TKCVVA--WPEDSGGK ^T LL
NK3R_HUMAN	197	ATATKIVIGS I WILAFLLAF P QCLY ^S KTKVMPGR-TLCFVQ--WPEGP--KQHF
		x--xx-xx--xX--X--xX-Xx--xx-----X---xxxXx-----
		TM5 IL-3
OPSD_BOVIN	202	SFVIYMFVV H F I IP L IVIFFCYGQLVFTVKEAAAQQQ----
NK1R_HUMAN	195	VYHICVTVLIY F L PL LVIGYAYTVVGITLWASEIPG-DSSD
NK2R_HUMAN	196	LYHLVVIALIY F L PL AVMFVAYSVIGLTLWRRVPGHQAHG
NK3R_HUMAN	246	TYHIIVILVY C F PL LIMGIT ^T Y ^T IVGITLWGGEIPG-DTCD
		-xx--x--x-x--XX-----X---x-Xxx-----xx-----
		TM6 EXL-3
OPSD_BOVIN	239	ESATTQKAEKEVTRMVIIMVIAFLIC W LPYAGVAFYIFTHQG---SDFG
NK1R_HUMAN	235	RYHEQVSAKRKVVKMMIVVCTFAIC W LPFHIFLLPYINPDLYLKKFI
NK2R_HUMAN	237	ANLRHLQAKKKFVKTMVLVVLTFAC W LPYHLYFILGSFQEDIYCHKFI
NK3R_HUMAN	286	KYHEQLKAKRKVVKMMIIVVMTFAC W LPYHIYFILTAIYQQLNRWKYI
		-----Xx-x-xx-x--xX-xXxXXXXX-x--x-x-----x-x
		TM7 C-terminal
OPSD_BOVIN	285	PIFMTIPAFFAKTSAVY NP VIYIMMNKQFRNCMV ^T TLCCGKNP
NK1R_HUMAN	284	QQVYLAIMWLAMSSTMY NP IYCLNDRFRLGFKHAFRCCPFI
NK2R_HUMAN	286	QQVYLALFWLAMSS ^T MY NP IYCLNHRFRSGFRLAFRCCPFW
NK3R_HUMAN	335	QQVYLASF ^W LAMSSTMY NP IYCLNKRFRAGFKRAFRWCPFI
		xxxxxx--xxXxxXxxXXXxXXxxxX-xXX-xx--xxx-xx--

Figure 5.2: Manually generated alignment of h-NK1R, h-NK2R, h-NK3R and bovine rhodopsin. Residues in bold are highly conserved and used in the numbering scheme by Schwartz [35]. X marks residues conserved over all four receptors. x marks residues conserved over the three NKR.

		TM1	IL1	TM2
bovine	27	PQYYLAEFPWQFSMLAAYMFLILMLGFPINFLTLYVTVQHKKLRTPLNILLNLAVADLFM		
h-NK1R,	22	PNQFVQPAWQIVLWAAAYTVIVVTVSVGNVVMWII LAHKRMRTVTNYFLVNLAFAEASM		
h-NK2R,	31	WQLALWATAYLALVLVAVTGNAIWI I LAHRRMRVTVTNYFIVNLALADLCM		
h-NK3R,	78	FVQPSWRIALWSLAYGVVAVAVLGNLIVIWI I LAHKRMRTVTNYFLVNLAFSDASM		
		XX		
		EXL1	TM3	IL2
bovine	87	VFGGFTTFLYTSLHGYPVFGPTGCNLEGGFFATLGGEIALWSLVLAIERVYVVVCKPMSNF		
h-NK1R,	82	AAFNTVNFYAVHNEWYGLFYCKFHNFFPIAAVFASISMTAVAFDRYMAI IHPLQP-		
h-NK2R,	83	AAFNAAFNFVYASHNIWYFGRFCYFQNLFPITAMFVSIYSMTAIAADRYMAIVHPFPQ-		
h-NK3R,	135	AAFNTLVNFIYALHSEWYFGANYCRFQNFPPITAVFASISMTAIAVDRYMAIIDPLKP-		
		XX		
		TM4	EXL2	TM5
bovine	147	RFGENHAIMGVAFTWVMALACAAPPLVWGSRYIPEGMQCSCGIDYYTPHEETNNESFVIY		
h-NK1R,	141	RLSATATKVVICVIVLALLLAFPPQGY-YSTTETMPSRVVCMIEWEHPHNKIYEKVYHIC		
h-NK2R,	142	RLSAPSTKAVIAGIWLVALALASPQCF-YSTVTMDQGATKCVVAWPEDSGGKTLVLLHLV		
h-NK3R,	194	RLSATATKIVIGSIWILAFLLAFPPQCLYSKTKVMPG-RTLFCVQWPEGPKQHFTYHIIVI		
		XXXXXXXXXXXXXXXXXXXXXXXXXXXXX-----XXXXXXXXXXXXXXXXXXXXXXXXXXXX		
		IL3	TM6	
bovine	207	MFVVHFI I PLIVIFFCYGQLVFTVKEAAAQQQESATTQ---K---AEKEVTRMVIIMVI		
h-NK1R,	200	VTVLIYFLPLLIGYAYTVVGITLWASEIPGDSSDRYH---EQVSAKRKVVKMMIVVVC		
h-NK2R,	208	VIALIYFLPLAVMFVAYSVIGLTLWRRVAVPGHQAAGANLRHLQ---AKKKFVKTMVLVVL		
h-NK3R,	253	ILVYCFPLLIMGITTYTIVGITLWGGEIPGDTCDKYHEQL---K---AKRKVVKMMIIVVM		
		XX		
		EXL3	TM7	
bovine	260	AFLICWLPYAGVAFYIFTHQGSDFGPIFM--TI---PA---FF---AKTSAVYNPVIYIMM		
h-NK1R,	256	TFAICWLPFHIFFLLPYINPDLYLKKFIQ--QV---YLAIMWL---AMSSTMYNPIIYCCL		
h-NK2R,	258	TFAICWLPYH-LYFILGSFQEDIYCHKFIQVY---LA---LFWLAMSTMYNPIIYCCL		
h-NK3R,	307	TFAICWLPYHIYFILTAIYQQLNRWKYIQ--QVYLASF---WL---AMSSTMYNPIIYCCL		
		XXXXXXXXXXXXXXXXXXXXX-----XXXXXXXXXXXXXXXXXXXXXXXXXXXX		
		C-term		
bovine	310	NKQFRN		
h-NK1R,	309	NDRFR		
h-NK2R,	311	NHRFRS		
h-NK3R,	360	NKRFR		
		XXXXXX		

Figure 5.3: Alignment of h-NK1R, h-NK2R, h-NK3R and bovine rhodopsin obtained from the ExPASy server. X indicates regions where the manual alignment is identical to the ExPASy alignment. _ indicates regions where the two alignments differ. x indicates regions where only the alignment of h-NK3 to rhodopsin differs in the two alignments.

5.4.2 The program DIANA [37]

DIANA (Distance geometry Algorithm for NMR Applications) is a program that calculates a 3D protein structure from distance and torsional constraints. The algorithm employed by DIANA is based on the minimisation of a target function $T(\phi_1, \dots, \phi_n)$, where n is the number of dihedral angles around rotatable bonds. Bond lengths and bond angles are kept constant. The target function T , with $T \geq 0$, is defined so $T=0$ if no constraints are violated. The problem to be solved is to find the values (ϕ_1, \dots, ϕ_n) that yields low values of the target function. Violations of the distance constraints, torsional angle constraints, and van der Waals distances are the values that contribute to the target function. In the treatment of the non-bonded interactions, only the repulsive part of the Lennard-Jones potential is employed. A conjugate gradient algorithm is used for the minimisation of the target function. The target function is continuously differentiable over the entire conformational space and defined so that a small violation δ is given by $c\delta^2$, where c is a constant. The

minimisation is stopped when the gradient is smaller than a predefined value, or the maximum number of iterations is exceeded.

5.4.3 Construction of an initial receptor model

The X-ray structure of bovine rhodopsin (PDB file 1F88) was obtained from the Protein Data Bank (PDB) [38]. This structure and the manually generated alignment were used as input for the program Thread [39]. This program mutates the residues in the input structure into those residues it is aligned to. The program will retain the torsional angles of the side chains if possible and use a rotamer library to determine the rest. In the alignment, there are insertions in the second and third intracellular as well as the second extracellular loop of the NKRs (Figure 5.2). These cannot be handled by Thread and has to be inserted manually.

This crude model was refined by manually changing side chain torsional angles that resulted in severe clashes. Rhodopsin has a sulfur bridge between TM3 and the second extracellular loop (EXL-2) (residues C110 and C187). Since these cysteine residues are conserved in the NKR [40], they were connected to form a sulphur bridge. Loops are especially problematic since there is low or no homology to rhodopsin in these regions, and this is also where the insertions and deletions occur. If the loop regions are not involved in the binding of ligands, it is common to omit them in the receptor model. However, DIANA requires that all residues are connected in one strand. This problem could easily be solved by mutating all residues in loop regions to glycine. Unfortunately, most of the NK antagonists studied bind just below EXL-2. It was therefore decided not to use glycine mutation but model the loops with their native residues.

5.4.4 Refinement of the initial model

The initial model served as a starting point for the distance geometry iteration procedure. This is described in the diagram in Figure 5.4. The initial model was imported into Quanta where torsional angles and hydrogen bonds were exported to a file. The initial model also served as input for C-Beta [41]. This is a program that creates a file containing all C^β to C^β distances within a cut-off distance. The torsional angles, the hydrogen bonds and the C^β - C^β distances were used as constraints in the distance geometry calculations by DIANA. Together with the sequence this is the

only input to DIANA. The torsional angle constraint is an interval that was set to the actual torsional value $\pm 15^\circ$. The distance constraint is an upper limit. The C^β - C^β constraints were set to the C^β - C^β distances $+1\text{\AA}$, and all values below 4\AA were removed in order to avoid van der Waals clashes. The hydrogen bond constraints were set to 2.9\AA for constraints between heavy atoms and 1.9\AA for constraints between hydrogen and heavy atom.

The iterations consisted of a cycle with three steps: 1) Examination of the structures that is the output from the previous DIANA calculation. Constraint violations and van der Waals clashes are detected; 2) modifications of angle and distance constraints files; 3) DIANA calculation with the modified constraints.

Since the constraints are intervals, the position of the transmembrane helices is allowed to change somewhat. The RMS between C^α atoms in the 7TM region of the initial and final structure was 1.38\AA for the NK1R, 1.32\AA for the NK2R, and 1.35\AA for the NK3R.

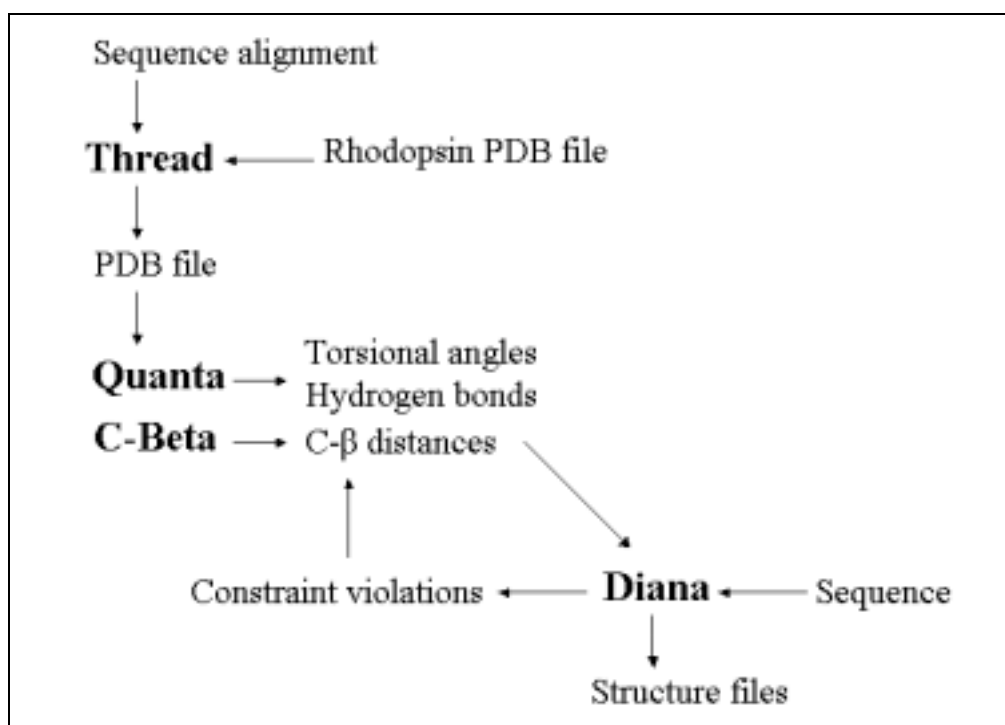


Figure 5.4: Overview of the iterative distance geometry method used for the construction of the NKR models. Names in bold are programs, the rest is input and output files.

5.4.5 Evaluation of the models

In the Asp79Asn NK2R mutant, a decrease in current amplitude and agonist-induced desensitisation is observed. However, in the double NK2R mutant Asp79Asn +

Asn303Asp these effects are reversed. Based on these observations, Donnelly et al. [26] conclude that there is a direct interaction between the side chains of the two residues. That places TM2 and TM7 in contact, and the relative orientation of the two helices can be deduced. A C^β - C^β distance constraint can be obtained from this information, but it was included in the list of constraints generated by C-Beta. It was verified that in the models Asp79 and Asn303 are oriented so that a hydrogen bond can be formed between their side chains.

Another way of obtaining experimental distance constraints is from engineering metal ion binding sites. Elling et al. [13;14] have performed extensive mutagenesis work to identify zinc ion binding sites in the NK1R. In the Glu193His + Tyr272His mutant, they observed an increase in Zn(II) affinity by a factor of 620. In the NK1R model, these two residues are sufficiently close to His197 for the three residues together to form a zinc-binding site. Again, this information was included in the list of constraints generated by C-Beta. In the two mutants Tyr92His and Tyr92His + His95Ala, an increase in Zn(II) affinity by a factor of 12 was observed. In the NK1R model, residue 92 is sufficiently close to His108 for the two residues (but not residue 95) to form a zinc-binding site.

In a protein structure, only some torsional angles are “allowed”, i.e. of low conformational energy. The main chain torsional angles can be visualised by the Ramachandran plot, a plot of the torsional angles C^α - C' versus C' -N. Except for glycine, the side chain restricts the torsional values of the main chain that are low in energy. The list of allowed torsional angles is called a rotamer library. The number of residues in each receptor model with torsional angles not found in Quanta’s rotamer library is listed in Table 5.3. This number is comparable to that of the rhodopsin structure.

A buried polar atom results in a destabilisation of the protein conformation. If the buried polar atom can form a hydrogen bond to another buried polar atom, the hydrogen bond will help stabilise the protein conformation. Burying an unpaired hydrogen bond donor or acceptor is around 5.7 kJ/mol more unfavourable than burying a hydrogen bond [42]. The number of solvent inaccessible polar atoms not participating in a hydrogen bond is shown in Table 5.3. Again, this number is comparable to that of the rhodopsin structure.

The receptor models were also analysed for van der Waals clashes. However, no clashes were found. This was also expected since they contribute to the target function and should be removed during the minimisation of that.

Table 5.3: Number of rotamers not in the Quanta rotamer library and number of buried polar water inaccessible residues in the NKR models compared to the rhodopsin structure.

Receptor	Rotamer not in Quanta library			Buried polar residues ^a		
	Main chain	Side chain	All	Helix	Loop	All
Rhodopsin	22	41	63	4	8	12
NK1	14	48	62	6	7	13
NK2	26	57	73	2	2	4
NK3	18	47	65	3	4	7

^a Defined as water inaccessible polar residues not participating in at least one hydrogen bond.

5.5 Predictions made from the NKR models

5.5.1 Selective NK1R antagonists

Figure 5.5 shows compound **1** docked in the NK1R model. This binding mode is consistent with the published site-directed mutagenesis data, and the NK1 pharmacophore model described in Section 2.4, except that the direction of the hydrogen bond acceptor interaction differs by 120°. The interactions discussed in Section 5.2 between compound **1** and His265, Gln165 and His197 are present. The benzyl group of compound **1** makes an aromatic edge to ring face interaction with Phe268 and a hydrophobic interaction with Ile113. However, no direct interaction with Pro112 could be identified, but this residue is in proximity of the binding site. The mutation of Pro112 might induce a local conformational change in the receptor and thereby alter the affinity of the antagonists. Hydrophobic interactions are observed between the quinuclidine ring and Val200, Ile204 and Leu161. The polar residues Thr201 and Asn109 and the hydrophobic residue Leu269 are also found in the binding site. However, no direct interactions with these residues could be identified.

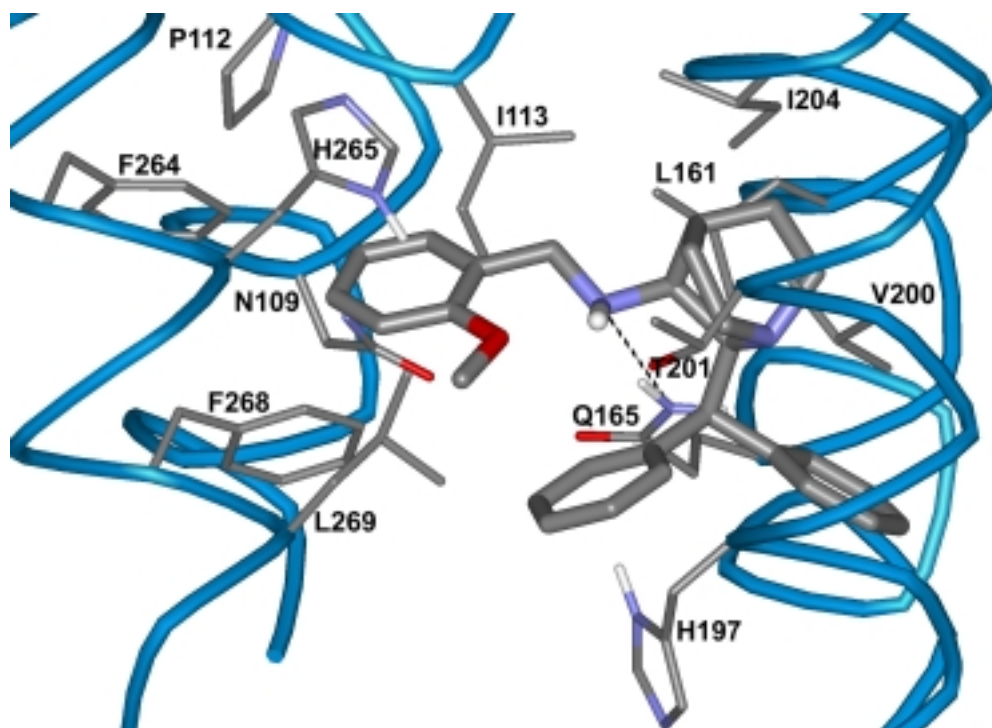


Figure 5.5: Compound **1** docked into the NK1R model. Loops have been removed for clarity. Only side chains lining the binding site are shown. The extracellular site is at the bottom.

5.5.2 Selective NK2R and non selective NK1R/NK2R antagonists

Figure 5.6 shows compound **68** docked in the NK1R and NK2R model. In the NK1R model, compound **68** makes a direct interaction with the residues identified by site-directed mutagenesis. In the NK1R model, pharmacophore element A (Figure 1 in Appendix II) and the methoxy substituents interact with His197, Leu161 and Thr201. Pharmacophore element B interacts with Ile204. Pharmacophore element C makes an aromatic edge to ring face interaction with Tyr287. This residue also makes a hydrogen bond to pharmacophore element G. Pharmacophore element E forms a hydrogen bond to Gln165. In the NK2R model, compound **68** interacts with the equivalent residues. Furthermore, a hydrogen bond between pharmacophore element D and Tyr266 are found and a hydrophobic interaction between pharmacophore element B and Met117. It is evident that the location of the binding site in the NK1R and NK2R models are the same, and that the conformations of the antagonists docked into the NK1R and NK2R models are almost identical. This conclusion is the opposite to that of Greenfeder et al. [2]. However, our binding mode is similar to that suggested by Giolitti et al. [9]. The hydrogen bond between pharmacophore element D and the receptor is only found in the NK2R model, where it is formed to Tyr266. The equivalent residue in the NK1R is Phe264. If the antagonists are protonated as

suggested by the pharmacophore models, then an ion-aromatic interaction can be formed between the ammonium nitrogen and Phe264. This explains the decreased affinity for the Phe264Ala mutant but not the decreased affinity for the Phe264Tyr mutant. In the NK1R model, Thr201 is located in the binding pocket for the trimethoxyphenyl group of compound **68**. The equivalent residues in the NK2R and NK3R are Ile202 and Ile252, respectively. Since threonine is polar as opposed to isoleucine, this can explain the difference in the observed SAR around pharmacophore element A. For high NK2 affinity, an unsubstituted phenyl ring is preferable, while the polar substituents 3,5-di-CF₃ and 3,4,5-tri-OMe are preferred for high NK1 affinity.

5.5.3 NK3R antagonists

While the binding site of the NK1R and NK2R has been extensively explored by site-directed mutagenesis, this is not the case for the NK3R. In Figure 5.7, the weak NK3 antagonist compound **43** is docked in to the NK3R model. Interactions with the equivalent residues as in the NK2R model are observed except for V116 (the equivalent of Met117). The selective NK3 antagonists compound **80** have a reversed amide group compared to NK1 and NK2 antagonists. The carbonyl of compound **43** interacts with Gln218 in the NK3R. When superimposed on compound **43**, the carbonyl of compound **80** points in another direction than that of compound **43**. Therefore, it must have another binding mode, or the carbonyl must interact with another residue. When fitted to pharmacophore Model 2 and then docked in the NK3R model, the carbonyl of compound **80** can form a hydrogen bond to Tyr256. The equivalent residue in the NK1R and NK2R is also a tyrosine (Tyr205 and Tyr206, respectively). Since the residues are the same in the three receptor subtypes, this cannot explain why compound **80** is a selective NK3 antagonist.

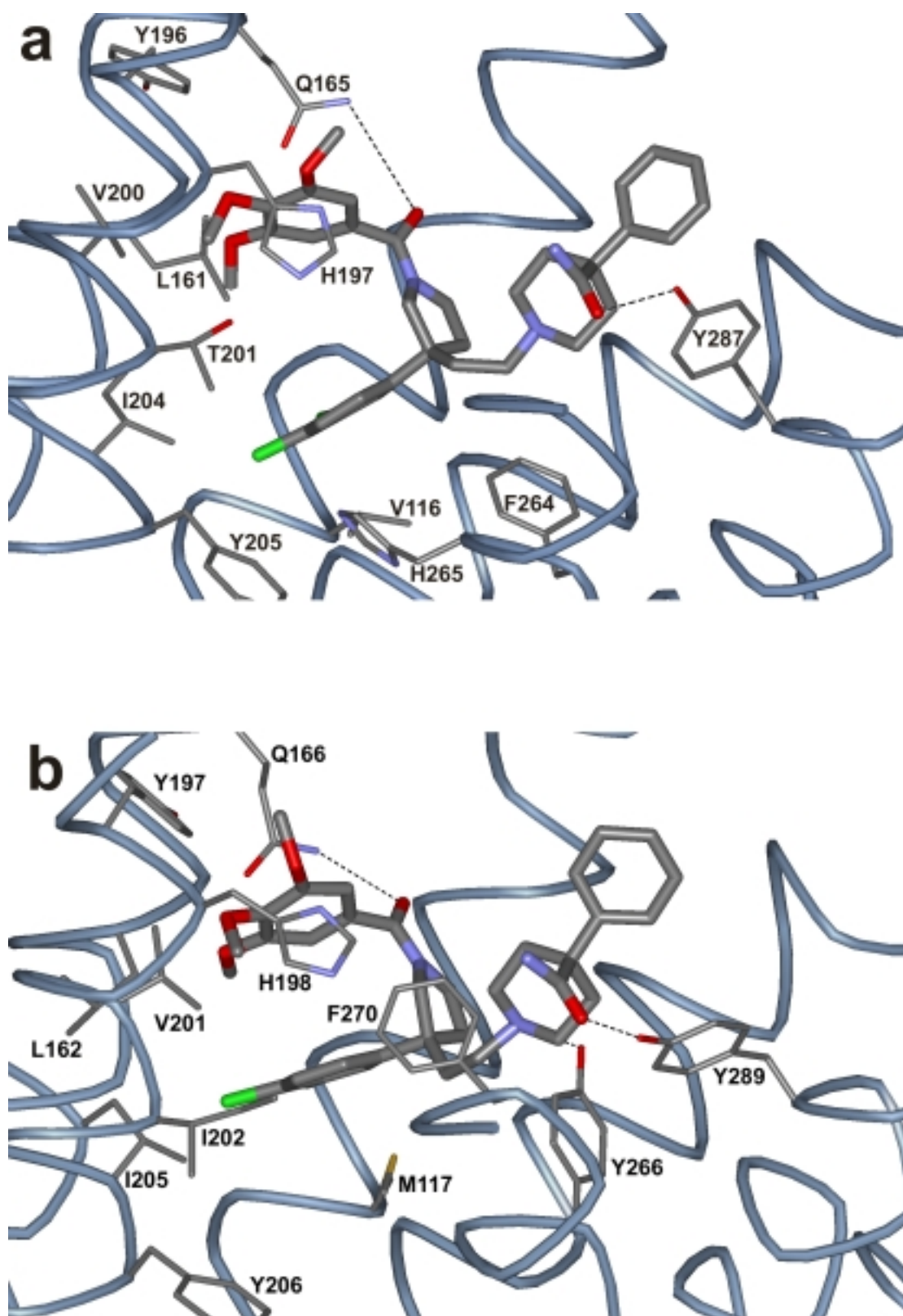


Figure 5.6. a: Compound **68** docked into the NK1R model. b: Compound **68** docked into the NK2R model. Loops and the last three residues of helix 6 have been removed for clarity. Only side chains lining the binding site are shown. The extracellular site is at the top.

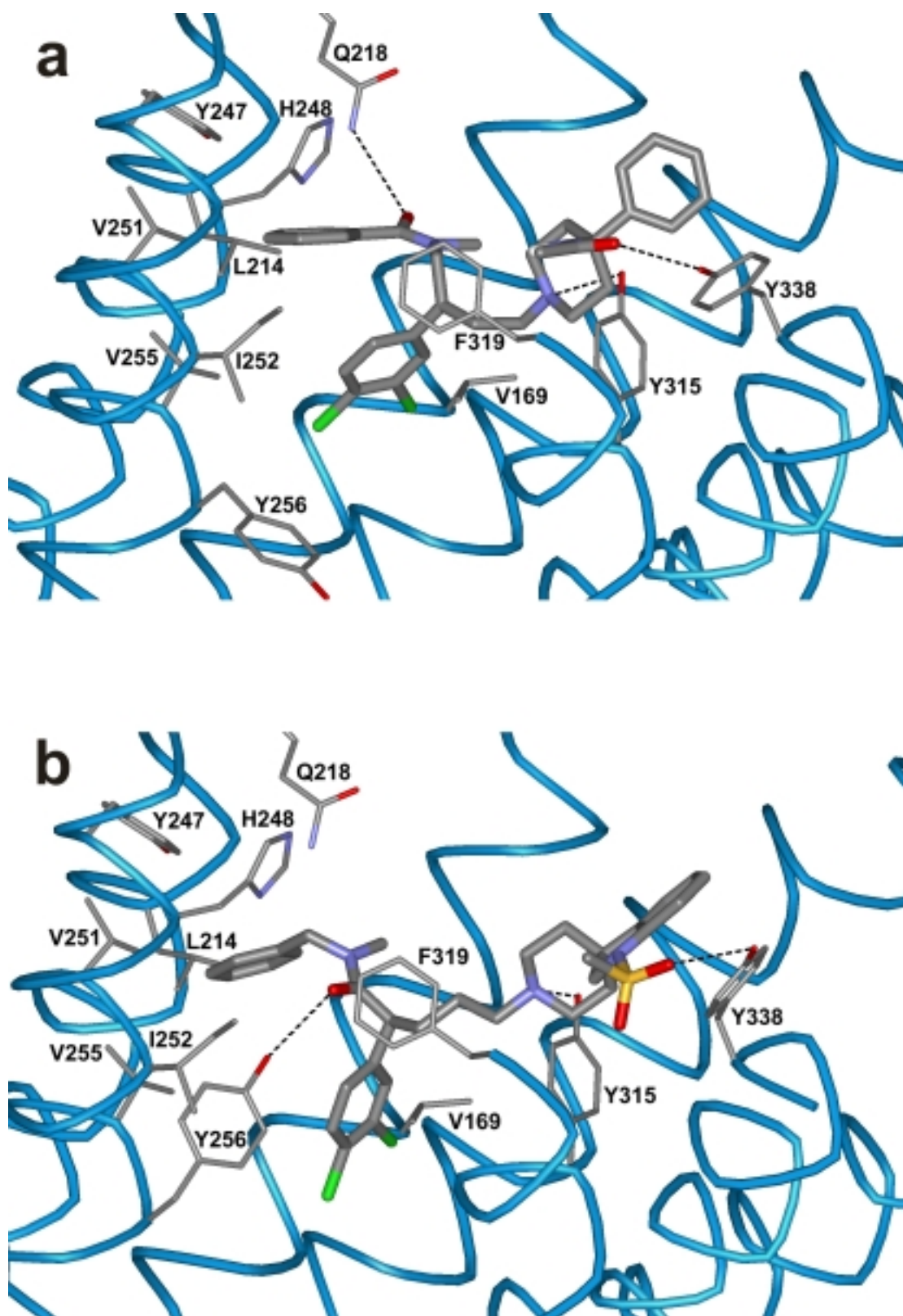


Figure 5.7. a: Compound **43** docked into the NK3R model. b: Compound **80** docked into the NK3R model (bottom). Loops and the last three residues of helix 6 have been removed for clarity. Only side chains lining the binding site are shown. The extracellular site is at the top.

5.6 Conclusion

Three receptor models, one of each NKR subtype, have been constructed by the iterative distance geometry approach of Lomize et al. [29]. The X-ray structure of bovine rhodopsin was used as a template. The models are consistent with experimental data. The binding site for several NK1 and NK2 antagonists have been outlined in a number of site-directed mutagenesis studies. The selective NK1 antagonists compounds **1** and **12** have been manually docked into the NK1R model. They were found to bind to the NK1R in a conformation represented by the NK1 pharmacophore model (Section 2.4) in consistency with published mutagenesis data.

NKR antagonists with a binding mode similar to compound **43** were docked into the three NKR models. Direct interactions with the NK2R were identified for all pharmacophore elements in compound **43** and **68** except pharmacophore element F (Figure 1 in Appendix II). However, no hydrogen bond could be found between the basic nitrogen of compound **68** and the NK1R. The dual NK1 and NK2 antagonist compound **68** was found to have analogous binding sites in the two NKR subtypes, and it binds to both receptor subtypes in the same conformation. This conformation is approximately the same as that represented by NK2 pharmacophore Model 2 (Appendix II). The results are also consistent with published mutagenesis data and the receptor model study of Giolitti et al. [9], but contrary to that of Greenfeder et al. [2]. Thr201 is located in the NK1 binding site of compound **68**. The equivalent residues in the NK2R and NK3R are Ile202 and Ile252, respectively. This can explain the difference in the observed SAR of pharmacophore element A. For high NK2 and NK3 affinity, an unsubstituted phenyl ring is preferable, while the polar substituents 3,5-di-CF₃ and 3,4,5-tri-OMe are preferred for high NK1 affinity. The selective NK3 antagonist compound **80** has a reversed amide group compared to that of compound **43**. Therefore, it must have another bioactive conformation, or the amide must interact with another residue. While the carbonyl of compound **43** interacts with Gln218 in the NK3R, a hydrogen bond can be formed between the carbonyl of compound **80** and Tyr256. Since the equivalent residues in the NK1R and NK2R are also tyrosines, this cannot explain why compound **80** is a selective NK3 antagonist.

5.7 References

1. Palczewski, K., Kumasaka, T., Hori, T., Behnke, C. A., Motoshima, H., Fox, B. A., Le, T., I, Teller, D. C., Okada, T., Stenkamp, R. E., Yamamoto, M. and Miyano, M., Crystal structure of rhodopsin: A G protein-coupled receptor. *Science* **2000**, 289: 739-745.
2. Greenfeder, S., Cheewatrakoolpong, B., Billah, M., Egan, R. W., Keene, E., Murgolo, N. J. and Anthes, J. C., The neurokinin-1 and neurokinin-2 receptor binding sites of MDL103,392 differ. *Bioorg. Med. Chem.* **1999**, 7: 2867-2876.
3. Lundstrom, K., Hawcock, A. B., Vargas, A., Ward, P., Thomas, P. and Naylor, A., Effect of single point mutations of the human tachykinin NK1 receptor on antagonist affinity. *Eur. J. Pharmacol.* **1997**, 337: 73-81.
4. Cascieri, M. A., MacLeod, A. M., Underwood, D., Shiao, L. L., Ber, E., Sadowski, S., Yu, H., Merchant, K. J., Swain, C. J. and Strader, C. D., Characterization of the interaction of N-acyl-L-tryptophan benzyl ester neurokinin antagonists with the human neurokinin-1 receptor. *J. Biol. Chem.* **1994**, 269: 6587-6591.
5. Fong, T. M., Yu, H., Cascieri, M. A., Underwood, D., Swain, C. J. and Strader, C. D., The role of histidine 265 in antagonist binding to the neurokinin-1 receptor. *J. Biol. Chem.* **1994**, 269: 2728-2732.
6. Fong, T. M., Yu, H., Cascieri, M. A., Underwood, D., Swain, C. J. and Strader, C. D., Interaction of glutamine 165 in the fourth transmembrane segment of the human neurokinin-1 receptor with quinuclidine antagonists. *J. Biol. Chem.* **1994**, 269: 14957-14961.
7. Blaney, F. E., Raveglia, L. F., Artico, M., Cavagnera, S., Dartois, C., Farina, C., Grugni, M., Gagliardi, S., Luttmann, M. A., Martinelli, M., Nadler, G. M., Parini, C., Petrillo, P., Sarau, H. M., Scheideler, M. A., Hay, D. W. and Giardina, G. A., Stepwise modulation of neurokinin-3 and neurokinin-2 receptor affinity and selectivity in quinoline tachykinin receptor antagonists. *J. Med. Chem.* **2001**, 44: 1675-1689.
8. Ali, M. A., Bhogal, N., Fishwick, C. W. and Findlay, J. B., Spatial requirements of the antagonist binding site of the NK2 receptor. *Bioorg. Med. Chem. Lett.* **2001**, 11: 819-822.
9. Giolitti, A., Cucchi, P., Renzetti, A. R., Rotondaro, L., Zappitelli, S. and Maggi, C. A., Molecular determinants of peptide and nonpeptide NK-2 receptor antagonist binding sites of the human tachykinin NK-2 receptor by site-directed mutagenesis. *Neuropharmacology* **2000**, 39: 1422-1429.
10. Henderson, R., Baldwin, J. M., Ceska, T. A., Zemlin, F., Beckmann, E. and Downing, K. H., Model for the structure of bacteriorhodopsin based on high-resolution electron cryo-microscopy. *J. Mol. Biol.* **1990**, 213: 899-929.
11. Baldwin, J. M., Schertler, G. F. and Unger, V. M., An alpha-carbon template for the transmembrane helices in the rhodopsin family of G-protein-coupled receptors. *J. Mol. Biol.* **1997**, 272: 144-164.
12. Unger, V. M., Hargrave, P. A., Baldwin, J. M. and Schertler, G. F., Arrangement of rhodopsin transmembrane alpha-helices. *Nature.* **1997**, 389: 203-206.
- 12a. Pebay-Peyroula, E., Rummel, G., Rosenbusch, J.P. and Landau, E.M., X-ray structure of bacteriorhodopsin at 2.5 angstroms from microcrystals grown in lipidic cubic phases. *Science.* **1997**, 277: 1676-1681.
13. Elling, C. E., Thirstrup, K., Nielsen, S. M., Hjorth, S. A. and Schwartz, T. W., Engineering of metal-ion sites as distance constraints in structural and functional analysis of 7TM receptors. *Fold. Des.* **1997**, 2: S76-S80.

14. Elling, C. E. and Schwartz, T. W., Connectivity and orientation of the seven helical bundle in the tachykinin NK-1 receptor probed by zinc site engineering. *EMBO J.* **1996**, 15: 6213-6219.
15. Elling, C. E., Nielsen, S. M., and Schwartz, T. W., Conversion of antagonist-binding site to metal-ion site in the tachykinin NK-1 receptor. *Nature* **1995**, 374: 74-77.
16. Gether, U., Johansen, T. E., Snider, R. M., Lowe, J. A., Emonds-Alt, X., Yokota, Y., Nakanishi, S. and Schwartz, T. W., Binding epitopes for peptide and non-peptide ligands on the NK1 (substance P) receptor. *Regul. Pept.* **1993**, 46: 49-58.
17. Tian, Y., Wu, L. H., Oxender, D. L. and Chung, F. Z., The unpredicted high affinities of a large number of naturally occurring tachykinins for chimeric NK1/NK3 receptors suggest a role for an inhibitory domain in determining receptor specificity. *J. Biol. Chem.* **1996**, 271: 20250-20257.
18. Gether, U., Johansen, T. E. and Schwartz, T. W., Chimeric NK1 (substance P)/NK3 (neurokinin B) receptors. Identification of domains determining the binding specificity of tachykinin agonists. *J. Biol. Chem.* **1993**, 268: 7893-7898.
19. Yokota, Y., Akazawa, C., Ohkubo, H. and Nakanishi, S., Delineation of structural domains involved in the subtype specificity of tachykinin receptors through chimeric formation of substance P/substance K receptors. *EMBO J.* **1992**, 11: 3585-3591.
20. Wu, L. H., Vartanian, M. A., Oxender, D. L. and Chung, F. Z., Identification of methionine134 and alanine146 in the second transmembrane segment of the human tachykinin NK3 receptor as reduces involved in species-selective binding to SR 48968. *Biochem. Biophys. Res. Commun.* **1994**, 198: 961-966.
21. Fong, T. M., Cascieri, M. A., Yu, H., Bansal, A., Swain, C. and Strader, C. D., Amino-aromatic interaction between histidine 197 of the neurokinin-1 receptor and CP 96345. *Nature* **1993**, 362: 350-353.
22. Fong, T. M., Huang, R. C., Yu, H., Swain, C. J., Underwood, D., Cascieri, M. A. and Strader, C. D., Mutational analysis of neurokinin receptor function. *Can. J. Physiol. Pharmacol.* **1995**, 73: 860-865.
23. Greenfeder, S., Cheewatrakoolpong, B., Anthes, J., Billah, M., Egan, R. W., Brown, J. E. and Murgolo, N. J., Two related neurokinin-1 receptor antagonists have overlapping but different binding sites. *Bioorg. Med. Chem.* **1998**, 6: 189-194.
24. Holst, B., Zoffmann, S., Elling, C. E., Hjorth, S. A. and Schwartz, T. W., Steric hindrance mutagenesis versus alanine scan in mapping of ligand binding sites in the tachykinin NK1 receptor. *Mol. Pharmacol.* **1998**, 53: 166-175.
25. Bhogal, N., Donnelly, D. and Findlay, J. B., The ligand binding site of the neurokinin 2 receptor. Site-directed mutagenesis and identification of neurokinin A binding residues in the human neurokinin 2 receptor. *J. Biol. Chem.* **1994**, 269: 27269-27274.
26. Donnelly, D., Maudsley, S., Gent, J. P., Moser, R. N., Hurrell, C. R. and Findlay, J. B., Conserved polar residues in the transmembrane domain of the human tachykinin NK2 receptor: functional roles and structural implications. *Biochem. J.* **1999**, 339 (Pt 1): 55-61.
27. Huang, R. R., Vicario, P. P., Strader, C. D. and Fong, T. M., Identification of residues involved in ligand binding to the neurokinin-2 receptor. *Biochemistry* **1995**, 34: 10048-10055.
28. Moltzen, E. K. and Bjornholm, B., Medicinal chemistry of muscarinic agonists: Developments since 1990. *Drugs of the Future* **1995**, 20: 37-54.
29. Lomize, A. L., Pogozheva, I. D. and Mosberg, H. I., Structural organization of G-protein-coupled receptors. *J. Comput.-Aided Mol. Des.* **1999**, 13: 325-353.

30. Huang, R. R., Vicario, P. P., Strader, C. D. and Fong, T. M., Identification of residues involved in ligand binding to the neurokinin-2 receptor. *Biochemistry* **1995**, 34: 10048-10055.
31. Li, Y.-M., Marnerakis, M., Stimson, E. R. and Maggio, J. E., Mapping peptide-binding domains of the substance P (NK-1) receptor from P388D1 cells with photolabile agonists. *J. Biol. Chem.* **1995**, 270: 1213-1220.
32. Gether, U., Yokota, Y., Emonds-Alt, X., Breliere, J. C., Lowe, J. A., Snider, R. M., Nakanishi, S. and Schwartz, T. W., Two nonpeptide tachykinin antagonists act through epitopes on corresponding segments of the NK1 and NK2 receptors. *Proc. Natl. Acad. Sci. USA* **1993**, 90: 6194-6198.
33. GPCR Data Bank, <http://www.gpcr.org/7tm/>.
34. Irina Pogozeva, College of Pharmacy, University of Michigan, Ann Arbor, MI 48109, USA.
35. Schwartz, T. W., Locating ligand-binding sites in 7TM receptors by protein engineering. *Curr. Opin. Biotechnol.* **1994**, 5: 434-444.
36. ExpASy (Expert Protein Analysis System), the Swiss Institute of Bioinformatics (SIB), <http://us.expasy.org>.
37. Guntert, P., Braun, W. and Wuthrich, K., Efficient computation of three-dimensional protein structures in solution from nuclear magnetic resonance data using the program DIANA and the supporting programs CALIBA, HABAS and GLOMSA. *J. Mol. Biol.* **1991**, 217: 517-530.
38. Protein Data Bank (PDB), <http://www.rcsb.org/pdb/>.
39. Thread, Andrei L. Lomize, College of Pharmacy, University of Michigan, Ann Arbor, MI 48109, USA.
40. Elling, C. E., Raffetseder, U., Nielsen, S. M. and Schwartz, T. W., Disulfide bridge engineering in the tachykinin NK1 receptor. *Biochemistry*. **2000**, 39: 667-675.
41. C-Beta, Andrei L. Lomize, College of Pharmacy, University of Michigan, Ann Arbor, MI 48109, USA.
42. Andrews, P. and Dooley, M., In Krogsgaard-Larsen, P., Liljefors, T. and Madsen, U., (Eds.), Textbook of drug design and discovery, Taylor & Francis, London and New York, **2002**: 35-53.

List of abbreviations

3D	three-dimensional
5-HT	serotonin
7TM	seven transmembrane
ADMET	absorption, distribution, metabolism, excretion and toxicity
AM1	Austin model 1
AMBER	assisted model building with energy refinement
B3LYP	Becke 3 Lee Yang Parr
CNS	central nervous system
DA	dopamine
DFT	density functional theory
DIANA	distance geometry algorithm for NMR applications
E	enrichment
EXL	extra cellular
ExPASy	Expert Protein Analysis System
GB/SA	generalised Born/solvent accessible surface
GH	goodness of hit list
GPCR	G-protein coupled receptor
GPCRDB	GPCR Data Bank
IL	intra cellular
HF	Hartree-Fock
M1	muscarine 1 receptor
MAO	monoamine oxidase
MAOI	monoamine oxidase inhibitor
MCMM	Monte Carlo multiple minimum
MDDR	MDLs Drug Data Report
MDL	Molecular Design Limited
MM	molecular mechanics
MMFF	Merck molecular force field
MMFFS	Merck molecular force field static
NE	norepinephrine
NK	neurokinin
NKA	neurokinin A
NKB	neurokinin B
NKR	neurokinin receptor
NMR	nuclear magnetic resonance
PDB	protein data bank
QM	quantum mechanics
QSAR	quantitative structure-activity relationship
QXP	quick explore
RMS	root mean square
RMSD	root mean square deviation
SAR	structure activity relationship
SP	substance P
SSRI	selective serotonin reuptake inhibitor
TM	transmembrane
TNCG	truncated Newton conjugate gradient algorithm

Standard one and three letter abbreviations for amino acids are applied.

Appendix I

Poulsen, A., Liljefors, T., Gundertofte, K. and Bjørnholm, B.

A pharmacophore model for NK2 antagonist comprising compounds from several structurally diverse classes, *J. Computer-Aided Mol. Design*, 16 (2002) 273.

Reprint with kind permission from Kluwer Academic Publishers.



A pharmacophore model for NK2 antagonist comprising compounds from several structurally diverse classes

Anders Poulsen^{a,b}, Tommy Liljefors^{a*}, Klaus Gundertofte^b and Berith Bjørnholm^b

^aDepartment of Medicinal Chemistry, The Royal Danish School of Pharmacy, 2 Universitetsparken, DK-2100 Copenhagen, Denmark

^bH. Lundbeck A/S, 9 Ottiliavej, DK-2500 Copenhagen-Valby, Denmark

Received 16 October 2001; accepted in revised form 28 June 2002

Key words: Bioactive conformation, conformational analysis, enantioselectivity, MMFF force field, neurokinin A, NK1 receptor, NK2 receptor, pharmacophore model, substance P, tachykinin.

Summary

A neurokinin 2 (NK2) antagonist pharmacophore model has been developed on the basis of five non-peptide antagonists from several structurally diverse classes. To evaluate the pharmacophore model, another 20 antagonists were fitted to the model. By use of exhaustive conformational analysis (MMFF's force field and the GB/SA hydration model) and least-squares molecular superimposition studies, 23 of the 25 antagonists were fitted to the model in a low energy conformation with a low RMS value. The pharmacophore model is described by four pharmacophore elements: Three hydrophobic groups and a hydrogen bond donor represented as a vector. The hydrophobic groups are generally aromatic rings, but this is not a requirement. The antagonists bind in an extended conformation with two aromatic rings in a parallel displaced and tilted conformation. The model was able to explain the enantioselectivity of SR48968 and GR159897.

Introduction

The tachykinins or neurokinins (NKs) Substance P (SP), neurokinin A (NKA), and neurokinin B (NKB) are regulatory peptides that play an important role in immune responses and as neurotransmitters and neuromodulators. The three peptides, SP, NKA and NKB bind to the neurokinin (NK) receptors NK1, NK2 and NK3 with affinities in the respective order [1]. NK receptors are distributed in the central nervous system (CNS), as well as in peripheral tissues, and belong to the superfamily of G-protein coupled receptors (GPCRs). As is the case for all GPCRs, except rhodopsin, NK receptors have not yet been crystallised, therefore no experimental structures are available.

Corresponding author: Prof. Tommy Liljefors, Department of Medicinal Chemistry, The Royal Danish School of Pharmacy, 2 Universitetsparken, DK-2100 Copenhagen, Denmark; Tel.: +45 35 30 65 05; Fax: +45 35 30 60 40; e-mail: tl@dfh.dk

NKs are involved in a number of pathological conditions, including psychiatric diseases like anxiety [2], depression [3], schizophrenia [4], neurodegradation [4], airways diseases like asthma [5] as well as numerous other diseases including pain [6], emesis [7], arthritis [8], etc. For that reason, NK receptors are of great interest as targets for the treatment of these diseases.

Since the discovery of the first non-peptide NK1 antagonist CP96345 [9], numerous NK1, NK2 and NK3 antagonists belonging to different structural classes have been published [10, 11]. Most of these compounds contain at least two aromatic ring systems connected by a linker holding a hydrogen bond acceptor. We define the part of the NK antagonists containing the two aromatic rings as the head of the molecules, and the rest is defined as the tail (Figure 1). The major difference between the NK1 and NK2 antagonists is that only the head fragment is required to obtain high NK1 (nM range) affinity while also the tail is required for NK2 affinity. However, addition

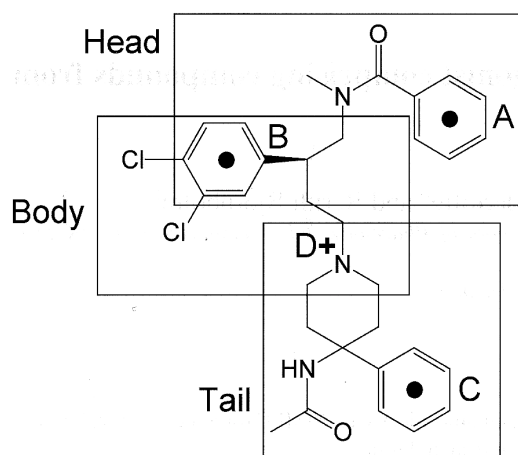


Figure 1. Definition of fragments with compound **2** as an example. Centroids and '+' marks the selected pharmacophore elements A–D.

of a tail also enhances affinity of most NK1 antagonists. Figure 2 shows the structure of the selective NK1 antagonist CP99994 [12].

A number of NK1 pharmacophore models have been published [13–18], and there is a fair agreement on the definition of the pharmacophore elements. Apart from a few studies [13, 14], there is consensus about an arrangement with the two aromatic ring systems in a tilted arrangement (Figure 2) [19]. We present an NK2 pharmacophore model that contains the same aromatic ring systems as the published NK1 pharmacophore models, but in a different arrangement. In this model, the aromatic groups are parallel displaced and tilted [20]. These results agree with previously published NK1, NK2, and μ -opioid receptor model studies. Thus, in a study of the dual NK1 and NK2 antagonist MDL103,392 (a close analogue of compound **4** in Figure 3) by 7-TM receptor modelling, Greenfeder et al. [21] proposed the compound to bind to the NK1 receptor in a conformation represented by the NK1 pharmacophore model in Figure 2. The ligand is predicted to bind to the NK2 receptor in an extended conformation with the two aromatic rings in a parallel displaced and tilted orientation. (Note, that the docked structure displayed in the paper is not MDL103,392). Blaney et al. [22] docked dual NK2 and NK3 antagonists of the 2-phenylquinoline class (analogues of compound **18** in Figure 3) into 7-TM models of the NK2, NK3 and μ -opioid receptors. These compounds are predicted to bind to the NK2 receptor in an extended conformation with two aromatic

ring systems in an arrangement similar to a parallel displaced and tilted orientation.

Computational methods

Conformational search and force fields

The molecules were built using MacroModel 7.0 [23]. The basic amines were protonated as in an aqueous solution at physiological pH. The conformational space was then searched using the Monte Carlo (MCM) method [24]. All heavy atoms and hydrogens on heteroatoms were superimposed in the test for duplicate conformations. All rotatable single bonds were included in the conformational search. All flexible rings were ring-opened and quaternary carbon and nitrogen atoms were allowed to invert. The search was continued until the lowest energy conformations were found at least five times. The energy minimisations were carried out with the truncated Newton conjugate gradient (TNCG) algorithm and the MMFF94s [25, 26] force field as implemented in MacroModel. Default parameters was used. For compounds for which no low energy conformation that fitted the model could be found, further conformational searches by this standard procedure using the AMBER*, MM3* and MM2* force fields as implemented in MacroModel were performed.

Solvation model

The conformational searches were done for aqueous solution with the Generalised Born/Solvent Accessible surface (GB/SA) continuum solvation model [27, 28] as implemented in MacroModel. Default parameters were applied, except that van der Waals and electrostatic cut-offs were set to 100 Å. This means effectively no cut-offs on van der Waals and electrostatic forces.

Calculation of the conformational energy penalty

The conformational energy penalty for the putative bioactive conformation of each ligand was calculated by subtracting the internal (steric) energy of the preferred conformation in aqueous solution (i.e. the energy of the global minimum in solution excluding the hydration energy) from the calculated energy of the putative bioactive conformation [29]. Since the conformational ensemble was represented by only the global minimum, entropy effects have not been taken into account. For flexible molecules this leads to an

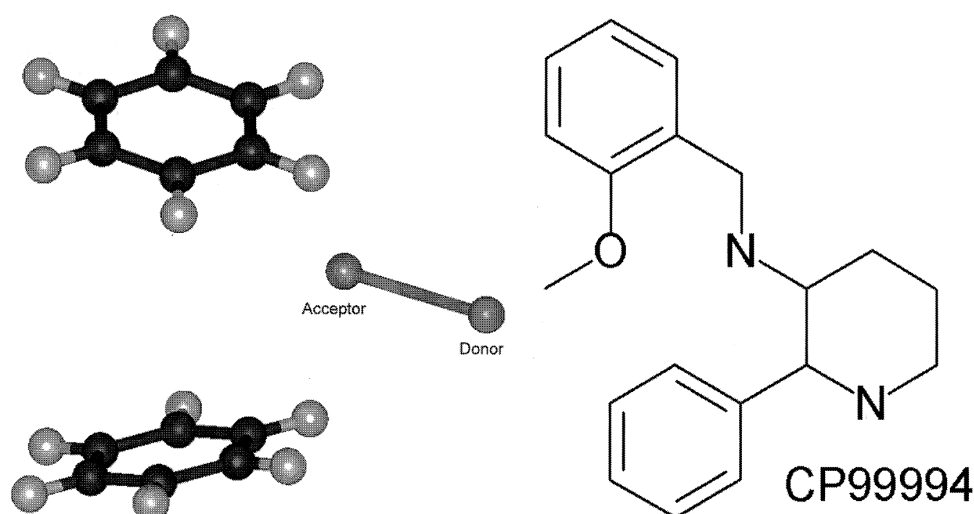


Figure 2. Left: The generally accepted NK1 pharmacophore model. Two aromatic rings in a tilted arrangement with a hydrogen bond acceptor (represented as a vector) in the arm connecting the two rings. To the right is shown the selective NK1 antagonist CP99994 [12].

underestimation of the energy penalty. A limit of 3 kcal/mol (12.6 kJ/mol) for acceptable energy penalties was imposed as recommended by Boström et al. [29].

Superimposition studies

Three aromatic rings and a hydrogen bond donor (in most cases the protonated nitrogen atom of an amine) were chosen as pharmacophore elements. For each of the aromatic rings, centroids were constructed. A putative hydrogen bonding site point was represented by a dummy atom 2.8 Å from the nitrogen in the direction of the nitrogen-hydrogen bond. The dummy atom was not used as a fitting point, but used to evaluate the direction of the hydrogen bond donor-acceptor interaction. The centroids and the nitrogen atom of the hydrogen bond donor were used for superimposing the ligands. Least-squares rigid body molecular superimpositions were performed using MacroModel. The superimposition was evaluated in terms of RMS values of the fitting points. An RMS value of 0.6 Å has been used as a soft indicator to determine whether a fit is acceptable or not. The aromatic pharmacophore elements were fitted in a coplanar orientation if energetically possible. The RMS values do not give any measure of this coplanarity since only the centroids are superimposed.

Flo99 flexible superimposition search

The automatic fitting program Flo99 [30, 31] was used to check if all possible fits had been taken into account during the manual fitting. Structures were built and imported from MacroModel into program Flo99. Only two structures were fitted at a time. Either one structure was used as a template or both structures were kept flexible. The output from Flo99 was exported back into MacroModel where each structure was relaxed by using flat bottom cartesian constraints with a half width of 0.2 Å and the default restraining force constant of 500 kJ/mol*Å². The conformational energy was calculated using the MMFF94s force field [29].

pK_a calculations

In order to identify the most basic nitrogen for compounds containing more than one basic nitrogen, pK_a were calculated for the most basic nitrogen by use of the program MolSurf 99/1 [32]. MolSurf requires a Spartan [33] archive file as input. Each of the unprotonated putative bioactive conformations was imported into Spartan for a full AM1 geometry optimisation followed by a single point HF calculation with the 3-21G* basis set. Default settings were used.

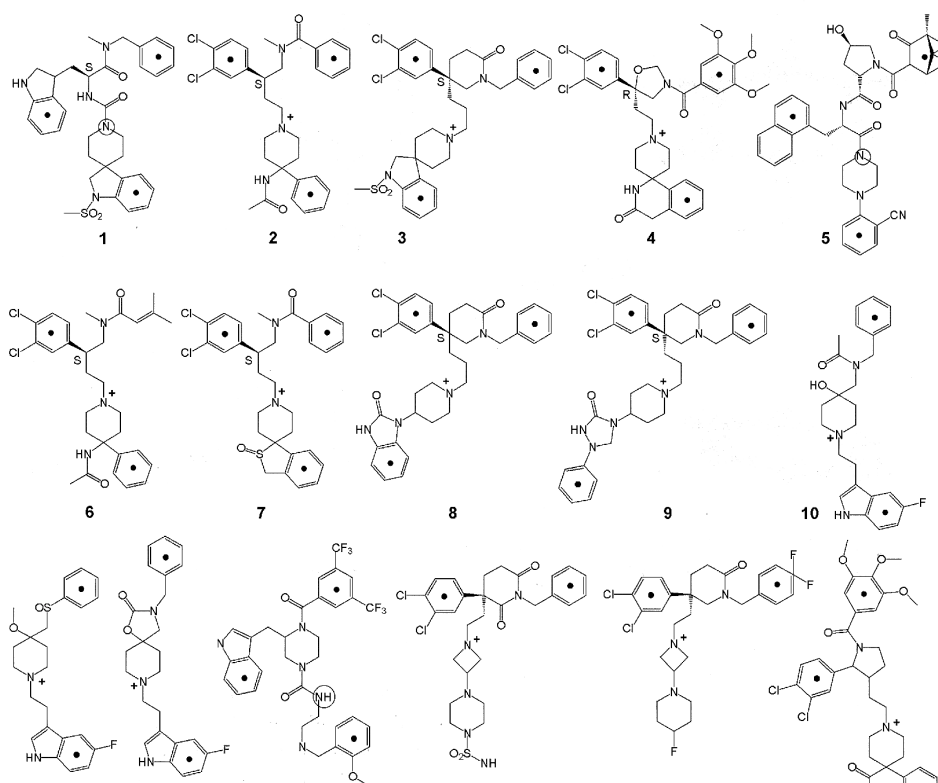


Table 1. Data of compounds fitted to the pharmacophore model. Calculated conformational energy penalties for putative bioactive conformations. pK_a values of the amine pharmacophore element.

Compound	NK2 Activity nM		Energy kJ/mol		RMS Å		pK _a
	IC ₅₀	K _i	Equatorial	Axial	Equatorial	Axial	
1 [35]	24		1.4	10.4	0.61	0.69	–
(S)- 2 (S-SR48968) [36]		0.5	–2.3	3.6	Template	Template	9.1
(R)- 2 (R-SR48968) [36]		945	17.0	21.1	0.37	0.30	9.1
3 [37]	2.2		2.9	2.7	0.85	0.88	8.9
4 [38]	3.0		–7.6	–3.5	0.19	0.31	8.9
5 (DE4445939a1) [39]	19		2.6	8.1	0.27	0.41	–
6 [40]	11		–63.4	–75.2	0.25	0.42	9.1
7 (YM38336) [41]	8.9		6.4	39.4	0.11	0.36	9.1
8 [37]	6.4		35.2	10.2	0.78	1.44	9.0
9 [37]	2.5		4.0	16.3	0.42	0.67	8.9
10 [42]		1.6	5.4	2.9	0.31	0.53	9.2
(R)- 11 (R-GR159897)[43]		0.1	–0.2	–10.6	0.42	0.61	9.1
(S)- 11 (S-GR159897) [43]	N.A.	N.A.	6.2	12.1	0.39	0.58	9.1
12 [42]		1.3	1.2	–0.5	0.40	0.43	9.1
13 (EP899270a1) [44]	60		118.9	28.4	0.67	0.51	10.1
14 (EP791592a2) [45]	0.5		31.8	73.0	0.27	0.38	7.6
15 (WO9727185a1) [46]		0.6	6.5	6.5	0.40	0.57	8.3
16 (US5824690a) [47]	7.93		–8.5	4.4	0.41	0.52	9.0
17 (WO9827086a1) [48]	16.3		12.4	29.9	0.47	0.47	9.0
18 (WO9852942a1) [49]	0.9	0.9	10.0	15.2	0.90	0.60	6.3
19 (EP739891a2) [50]		23	9.8	21.6	0.63	0.70	9.0
20 (WO9857972a1) [51]	4		–0.9	0.5	0.46	0.85	–
21 [52]		33	7.1	1.8	0.18	0.50	10.1
22 (US5688960a) [53]		4.5	3.5	6.5	0.90	0.77	9.2
23 [54]		23	–4.9	1.1	0.31	0.32	–
24 (ZD7944) [55]	8.9		–3.6	–0.5	0.77		9.0
(R)- 25 [43]		0.3	10.3	16.9	0.56	0.63	9.1
(S)- 25 [43]		7.9	–37.0	–31.9	0.43	0.50	9.1

N.A. = Not available

Results and discussion

Construction of the pharmacophore model

The NK2 antagonists used to derive and evaluate the pharmacophore model are shown in Figure 3. The set was chosen on the basis of high NK2 receptor affinity and structural diversity. Selective NK2 as well as dual NK1 and NK2 antagonists are included in the set. Affinity data and references for the compounds are given in Table 1. Most of the compounds are highly flexible and, in order to derive the model, the molecules were cut into three fragments as defined in Figure 1. The fragments overlap partly, which means that the fragments can finally be assembled in an

unambiguous way. Three to four pharmacophore elements were defined for each compound. The aromatic pharmacophore elements are marked in Figure 3 with a centroid and the basic nitrogens with a '+'. Compounds **1–5** were used to derive the pharmacophore model. For these compounds, each of the defined fragments contains two pharmacophore elements (Figures 1 and 3). The fragments were used to derive three sub-pharmacophores, which were assembled into the final NK2 pharmacophore model.

An exhaustive conformational analysis of the head fragments of compounds **3** and **4** were performed (Figure 4) in order to find the 3D arrangement of the pharmacophore elements A and B (Figure 1). These structures were selected because of their relative rigid-

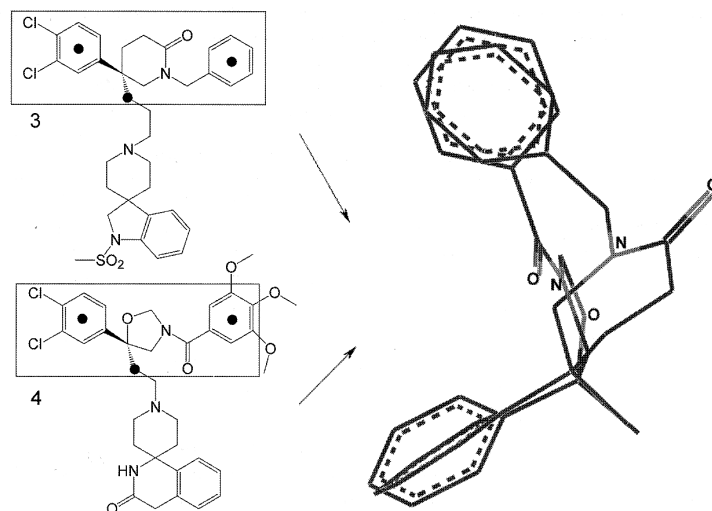


Figure 4. Superimposition of the head fragments of compounds **3** and **4**. The two fragments could only be superimposed well in the conformations shown. Solid dots mark the fitting points. RMS = 0.32 Å.

ity. Four conformations of the fragment of compound **4** were found within 50 kJ/mol of the global energy minimum, and 16 conformations of the fragment of compound **3**. When removing the tail fragments a methyl group is formed on the quaternary atoms of the aliphatic rings. Since the spiro-piperidine tails of compounds **3** and **4** should occupy the same area, the carbon atoms of the methyl groups were used as fitting points together with the centroids of the aromatic rings (Figure 4). Only one reasonable superimposition of the two fragments could be obtained. Flexible fitting of the fragments using the semi-automatic program Flo99 gave the same result as that obtained by rigid body least squares superimposition.

To derive the tail sub-pharmacophore, conformational searches of the tail fragments of compounds **3** and **4** were performed (Figure 5). Four conformations of the fragment from compound **4** and 21 conformations of the fragment from compound **3** were found within 50 kJ/mol of the global energy minimum. The fragments could be superimposed in two different ways as shown in Figure 5, one in which the aromatic ring is in an equatorial position on the piperidine ring and one in which it is axial. The two different conformations have similar conformational energies. The aromatic rings and the piperidine rings superimpose very well in both conformations with RMS values below 0.1 Å. Note that the protonated amino groups have their hydrogens pointing in the same direction. By use

Table 2. Cartesian coordinates (Å) for the pharmacophore elements A–D.

Pharmacophore element	x	y	z
A	-1.906	8.804	-1.256
B	-4.474	2.919	0.919
C equatorial	3.219	-4.749	0.374
C axial	-1.468	-4.573	-0.340
D donor	0.000	0.000	0.000
D acceptor	2.462	1.317	0.214

of Flo99, the same superimpositions were obtained, and the axial and the equatorial conformations were found to have similar energies (data not shown).

Compounds **1** and **5** contain the most rigid 'body' fragments. These fragments were fitted by the use of Flo99. Two reasonable superimpositions were found as shown in Figure 6. Both of these superimpositions overlay very well with the linker part of the global energy minimum conformation of the (*S*)-enantiomer of compound **2**. An identical linker fragment is found in several of the molecules. This conformation of the body fragment is also found in the global energy minima conformations of compounds **4**, **6**, **19–21** and **24** and was chosen as the body sub-pharmacophore.

Finally, the three sub-pharmacophores were connected. This produced two pharmacophore models,

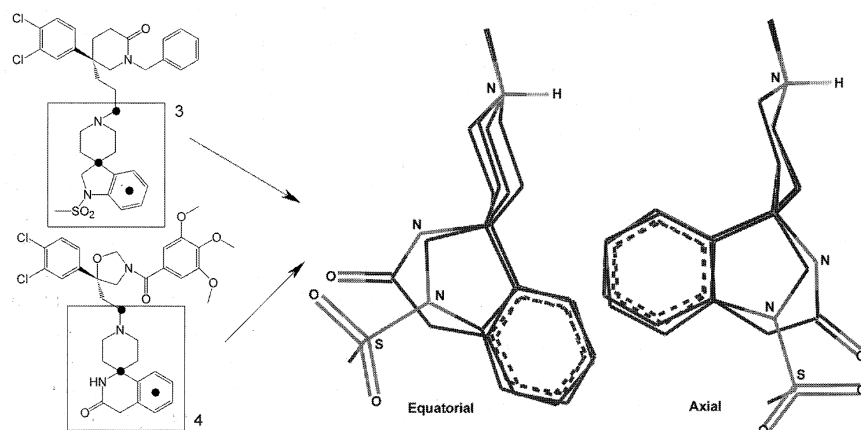


Figure 5. Superimposition of the tail fragments of structures 3 and 4. Both an equatorial (left) and an axial conformation (right) were found. Energetically, there was no difference between the two conformations. Solid dots mark the fitting points. RMS = 0.08 (Equatorial), RMS = 0.07 (Axial).

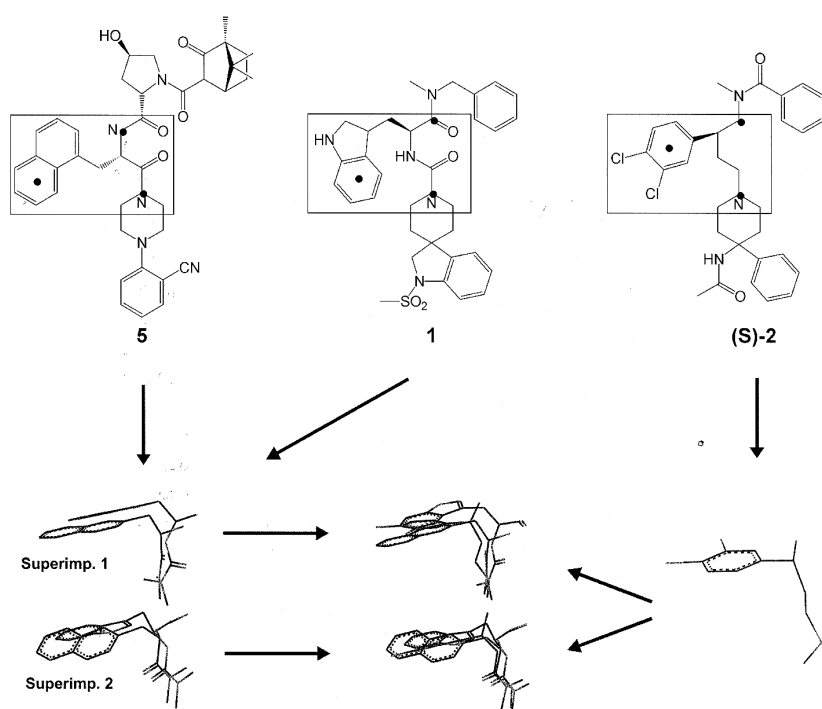


Figure 6. Left: Superimposition of the body fragments of structures 1 and 5. Center: Superimposition of the body fragment from the global minimum of (S)-2 onto 1 and 5. Right: The body fragment of (S)-2 was chosen as template. Solid dots mark the fitting points.

one in which the pharmacophore element C is in an equatorial position on the piperidine ring and one in which it is axial (Figure 7). It was found that two low energy minima of compound (S)-**2** superimpose very well onto all pharmacophore elements in each of the two pharmacophore models. Consequently, these conformations of compound (S)-**2** were used as templates on which all other compounds were superimposed (Figure 7). Cartesian coordinates for the derived pharmacophore elements A–D are given in Table 2.

Pharmacophore elements

Two or three hydrophobic groups are found in all NK2 antagonists (pharmacophore elements A, B and C, Figure 7). A basic amino group is also present in most structures (pharmacophore element D, Figure 7). The hydrophobic groups are marked in Figure 3 by centroids, and the basic nitrogen is marked with a positive charge. The pharmacophore element labelled B (Figure 7) is found to be an aromatic ring in all structures except compounds **10** – **12** and **25**. These compounds have electronegative groups in this area. Compounds **10** and **25** have a hydroxy group, compound **11** a methoxy group and compound **12** a carbonyl group. The pharmacophore element A need not be aromatic rings but can be aliphatic hydrophobes as is the case for compounds **5** and **6**. In compounds **14** and **15**, the aromatic pharmacophore element C is lacking. The basic amino group should be protonated at physiological pH as confirmed by pK_a calculations using MolSurf (Table 1). In all compounds having pharmacophore element D, this nitrogen always had the highest pK_a value. If protonated, the amine can only act as a hydrogen bond donor, and the donor receptor interaction is represented as a vector of length 2.8 Å pointing in the direction of the nitrogen-hydrogen bond. The basic nitrogen is exchanged for a urea NH group in compounds **1** and **13**, an amide nitrogen in compound **5** and a quarternary nitrogen in compound **20**. It is known that a quarternary nitrogen can replace a basic amine as a pharmacophore element as previously described for e.g. muscarinic agonists [34].

Solvation energies

All the compounds, except **1**, **5** and **22**, were found to have a solvation energy between –253 to –377 kJ/mol as calculated by using the GB/SA hydration model. Compounds **1** and **5** have a solvation energy of –163 kJ/mol and –187 kJ/mol respectively. These

compounds do not contain a protonated nitrogen in the piperidine or piperazine ring. Since compounds **1** and **5** are lacking this hydrogen bond donor pharmacophore element, one would expect the compounds to have a low binding affinity for the NK2 receptor. This is, however, not the case (Table 1). Since the energy penalty for desolvation is much lower for these compounds, we suggest that the favourable desolvation energy make up for the loss of the pharmacophore element. Compound **13** has a protonated nitrogen, but according to our model, it is the urea group that holds the hydrogen bond donor pharmacophore element. The solvation energy is highly negative (–346.5 kJ/mol) but the interaction energy of the urea group with the receptor is lower than for a basic nitrogen. Therefore, one would expect the ligand to have a lower affinity for the receptor than ligands with a basic amine hydrogen bond donor. This can explain that compound **13** have an IC₅₀ of 60 nM, whereas most of the other ligands studied have an affinity below 10 nM.

Evaluation of the model

It was possible to fit most compounds onto the ‘axial’ as well as ‘equatorial’ pharmacophore model (Figure 7) in a low energy conformation and with low RMS values. In contrast to the compounds used to derive the tail part of the pharmacophore model (compounds **3** and **4**), the conformations of the evaluation set fitted to the ‘equatorial’ model are energetically favoured over the conformations fitted to the ‘axial’ model (Table 1). This was expected since bulky substituents on cyclohexane prefer an equatorial conformation. There are no conclusive facts that can determine whether the ‘equatorial’ or ‘axial’ pharmacophore model represents the conformation that binds to the receptor. However, a number of observations lead us to conclude that it is the conformations fitted to the equatorial model that bind to the receptor. The average conformational energy penalty is higher for the conformations fitted to the ‘axial’ model. The hydrogen bonding groups of the tail fragment of some compounds only fall into the same area in the conformations fitted to the ‘equatorial’ model (e.g. **2**, **7** and **17**). The aromatic pharmacophore element C of the spiro compounds **1**, **3**, **4** and **7** could be fitted to the ‘equatorial’ model in a coplanar orientation but not to the ‘axial’ model.

Some of the ligands have RMS values above 0.6 Å (Table 1). In compound **1**, pharmacophore element B (an indole ring) superimposes onto the template in

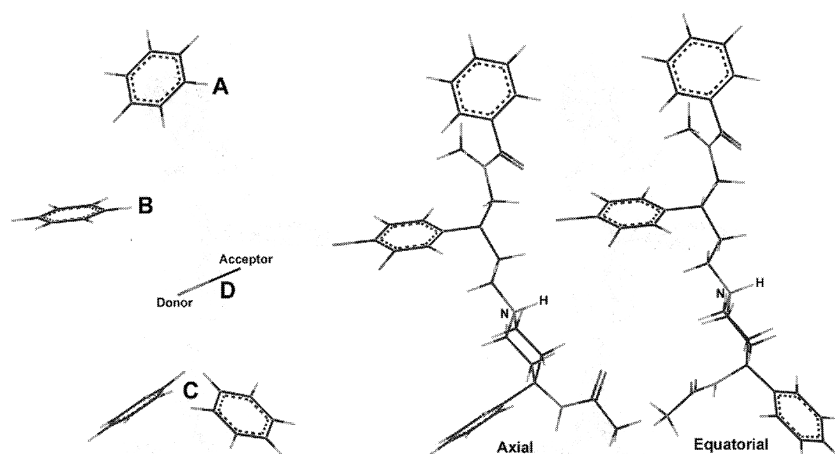


Figure 7. The final pharmacophore model. Left: Arrangement of pharmacophore elements. Element C can be in an axial or equatorial conformation. We propose that the equatorial conformation is most likely to be the bioactive conformation. Center and right: The putative bioactive conformations of (S)-2 with pharmacophore element C axial (center) and equatorial (right). These two conformations were chosen as templates for fitting of the validation set.

a coplanar orientation, but the centroids do not superimpose well. The same is true for pharmacophore element A in compound **24**. If these elements are not used as fitting points, the RMS is 0.07 Å for both compounds **1** and **24**. In compounds **3**, **8** and **9**, the linkers in the body fragments are three carbon atoms long whereas it is two carbon atoms long in the template. The rings superimpose onto the template in a coplanar orientation, but the centroids do not superimpose well. Compound **18** is different from the rest of the compounds, as there is no flexibility in the scaffold holding elements A and B. Elements B and D superimpose well onto the template whereas elements A and C overlay partly. In summary, the compounds described in this section fit the model, but RMS may not be the best parameter to apply in the evaluation of all the fits [29].

Figure 8 shows a superimposition of nine structurally diverse compounds (listed in the Figure text) with pharmacophore element C in the equatorial position relative to the template. Even though the dummy atoms of the interaction point vectors were not used as fitting points, they all fall into the same area.

Using the MMFFs force field, it was not possible to find a low energy conformation of compounds **8**, **13** and **14** that fitted the pharmacophore model with pharmacophore element C in the 'equatorial' position (Figure 7, Table 1). Furthermore, compound **6** was found to have an unrealistically large negative

conformational energy (Table 1). To investigate this, conformational analysis of compounds **6**, **8** and **13** was repeated with the AMBER* and MM3* force fields. As no MM3* parameters are available for the sulfonamide of compound **14**, the AMBER* and MM2* force fields was used for this structure. Compounds **6**, **8**, **13** and **14** fitted to the 'equatorial' pharmacophore model were again partially optimised using flat bottom cartesian constrains and AMBER* or MM3* (MM2*) force fields, and their conformational energies were calculated (Table 3). To determine the AMBER* and MM3* (MM2*) global energy minima, conformational searches using the above mentioned force fields were also performed. Compound **8** was found to have a reasonable conformational energy using AMBER* and MM3*. MMFFs seems to overestimate the electrostatic interaction of the 1,3-dihydro-benzimidazol-2-one oxygen and the protonated amine, whereas AMBER* and MM3* calculates a more reasonable interaction energy. Compound **6** was found to have a high conformational energy penalty using AMBER*, but a negative energy penalty using MM3*. The reason for this force field dependence probably lies in the implementation of the GB/SA solvation model. The solvation energy of **6** is found to be -232 kJ/mol, -323 kJ/mol and -345 kJ/mol by AMBER*, MM3* and MMFFs, respectively.

The conformational energy penalties of compounds **13** and **14** are found to be high by all

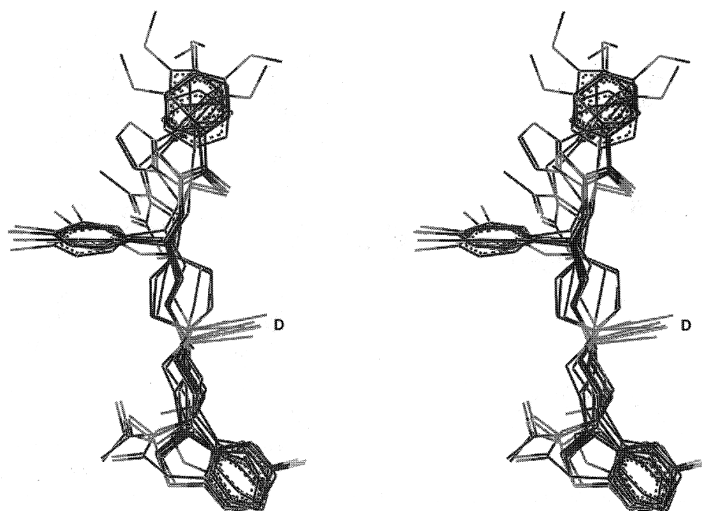


Figure 8. Stereo image. A superimposition of (S)-**2**, **3**, **4**, **6**, **10**, (R)-**11**, **12**, **19** and **21**. Hydrogens are removed for clarity. Notice how well the interaction point vectors (D) superimpose although they are not used as fitting points.

Table 3. Conformational energy penalties (E_{Conf} /kJ/mol) calculated by various force fields.

Compound	$E_{\text{Conf}}/\text{AMBER}^*$	$E_{\text{Conf}}/\text{MM3}^*$	$E_{\text{Conf}}/\text{MMFFs}$
6	75.3	-25.4	-63.4
8	-3.4	1.3	35.2
13	103.7	44.3	118.9
14 ^a	78.0	87.7	31.8

^aMM2* data (MM3* parameters of sulfonamide not available).

force fields, but they vary considerably (Table 3). Figure 9 shows the global energy minima of compound **13** found by the use of MMFFs, MM3* and AMBER* compared to the putative bioactive conformation. There is a large difference between these conformations. In the global energy minimum conformation found by AMBER*, all three aromatic rings are stacked, whereas with MMFFs and MM3*, the global energy minima conformations only display stacking of the di-meta-trifluoromethylphenyl and the indole rings. The AMBER* global energy minimum conformation have the di-meta-trifluoromethylphenyl ring sandwiched between the other two rings, whereas in the MMFFs and MM3* global energy minima conformations, the indole lies between the other rings. The MM3* global energy minimum conformation have a hydrogen bond between the protonated amine and the oxygen of the urea group. In the MMFFs global energy minimum conformation and the putative

bioactive conformation, a hydrogen bond between the protonated amine and the oxygen of methoxy group is found. The AMBER* global energy minimum conformation has no hydrogen bonds. The stacking of the aromatic rings is probably due to the force fields' inability to correctly calculate the electrostatic attraction between aromatic systems with electron withdrawing and donating substituents. Furthermore, the solvation model might force the compound to adopt a conformation with a small surface area. We suggest that the inability to find a low energy conformation of compound **13** that fit the pharmacophore model is due to these factors.

Figure 10 shows the global energy minima of compound **14** found by MMFFs, MM2* and AMBER* compared to the putative bioactive conformation. In all three global energy minima, there is a hydrogen bond between the protonated nitrogen and the carbonyl in the 2-position of the piperidine-2,6-dione. This hy-

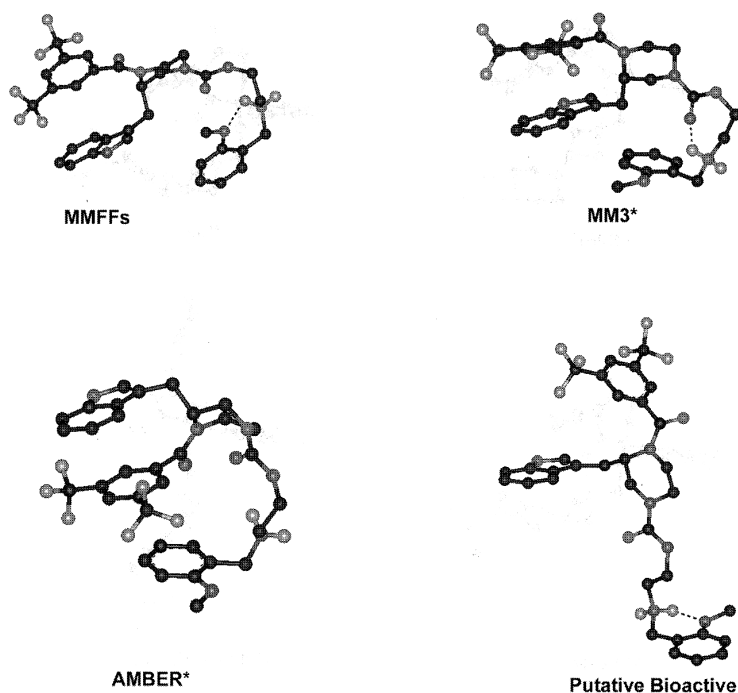


Figure 9. The global energy minima of **13** found by MMFFs, MM3* and AMBER* compared to the putative bioactive conformation. Internal hydrogen bonds are marked with dashed lines.

drogen bond is not present in the putative bioactive conformation. Compound **15** is a close analogue of **14** with similar affinity towards the NK2 receptor (Table 1). In compound **15**, the carbonyl corresponding to the one in the 2-position of compound **14** is lacking. The global energy minimum conformation of compound **15** does not display an internal hydrogen bond, and **15** could be fitted to the pharmacophore model with a low energy penalty (Table 1). The inability to correctly calculate the conformational energies of compounds **14** and **15** is probably an artefact of the forcefields. The combination of the GB/SA solvation model and the force fields overestimates the strength of internal hydrogen bonds leading to the 'collapsed' conformations displayed in Figure 10.

Enantioselectivity

The R enantiomer of compound **2**, ((R)-**2**) was fitted to the model using Flo99. For both the 'axial' and 'equatorial' models, a conformation that superimposed very

well with the template was found (Figure 11). These conformations were imported into MacroModel and relaxed using flat bottom cartesian constraints and the conformational energy calculated to be 19.3 kJ/mol (equatorial) and 18.1 kJ/mol (axial) above compound (S)-**2** (Table 1).

ΔG , the change in free energy can be described by Equation 1 where R is the gas constant, T the temperature and K the equilibrium binding constant.

$$\Delta G = -RT \ln K \quad (1)$$

This means that each 5.9 kJ/mol of energy penalty will decrease K_i by a factor of 10. For the equatorial and axial conformation, the calculated energy difference between the (S)- and the (R)-enantiomers in the putative bioactive conformations corresponds to a drop in affinity by a factor of 2100 and 1170, respectively. This agrees well with the factor of 1900 found experimentally.

Compound **25** has a chiral centre at the sulphur atom. The (R)-sulfoxide is found to be about 30 times

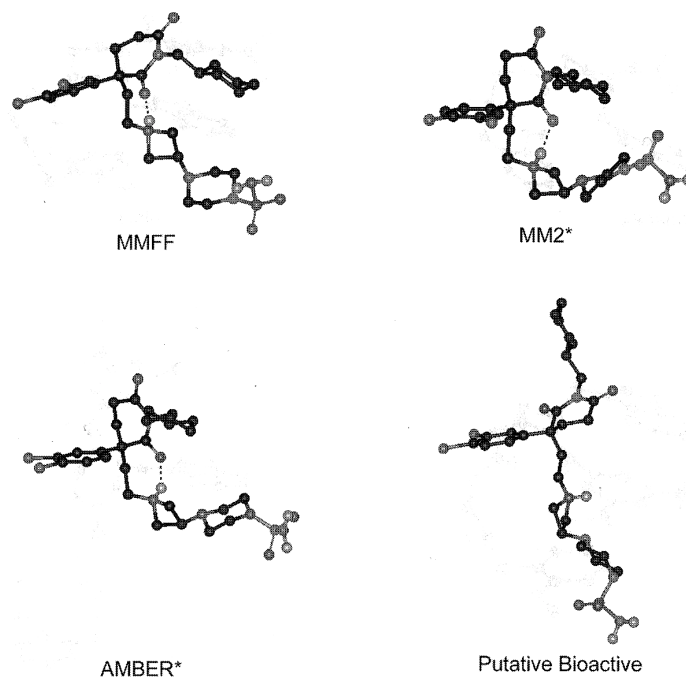


Figure 10. The global energy minima of **14** found by MMFFs, MM2* and AMBER* compared to the putative bioactive conformation. Internal hydrogen bonds are marked with dashed lines.

more active than the corresponding (S)-enantiomer. The formation of an intramolecular hydrogen bond between the hydroxy and sulfoxide groups makes the analysis of the compound difficult. This is not the case for compound **11** where the hydroxy group has been substituted for a methoxy group. Both enantiomers of compound **11** could be fitted to the model. The (R) enantiomer in its bioactive conformation has a conformational energy 6.4 kJ/mol below the (S) enantiomer. If one assumes the same enantioselectivity for compounds **11** and **25**, the conformational energy difference accounts for most of the observed enantioselectivity (a factor of 11). From Figure 12, it is evident that the carbonyl oxygen of (S)-**2** superimposes with the sulfoxide oxygen of (R)-**11** but not that of (S)-**11**. It can also be seen in Figure 8 that several compounds have a carbonyl oxygen that falls within this area. Although a bit speculative, it is tempting to conclude that these oxygen atoms participate in an interaction with the receptor. In that case, another site-point could be defined as a fifth pharmacophore element.

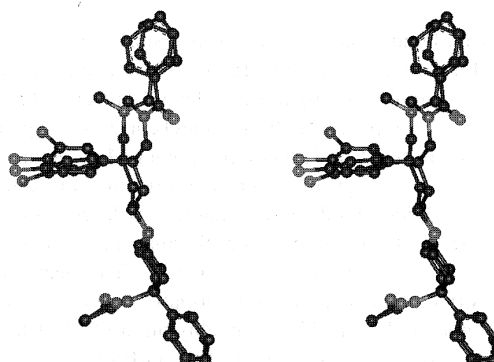


Figure 11. The putative bioactive conformation of (R)-**2** fitted to (S)-**2** (RMS 0.37 Å). Hydrogens are removed for clarity. Both (R)-**2** and (S)-**2** are shown with pharmacophore element C equatorial on the piperidine ring.

Conclusions

A pharmacophore model for NK2 antagonists has been derived. The model consists of three hydropho-

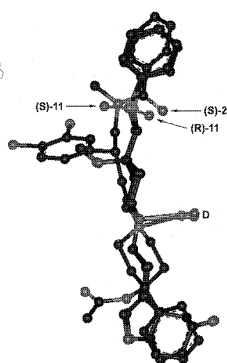


Figure 12. Superimposition of (R)-11, (S)-11 and (S)-2. Hydrogens are removed for clarity. Notice how well the dummy atoms superimpose (D), and the carbonyl oxygen of (S)-2 and the sulfoxide oxygen of (R)-11 fall within the same area. This is not true for (S)-11.

bic pharmacophore elements (A, B and C) and one hydrogen bond donor/acceptor interaction represented as a vector (D). The antagonists bind in an extended conformation with pharmacophore elements A and B in a parallel displaced and tilted arrangement. Relative to the template ((S)-2), the pharmacophore element C can be in either an equatorial or an axial conformation, with the former as the most probable. The model was evaluated against 20 structurally diverse, high affinity NK2 and dual NK1 and NK2 antagonists. For all compounds except two, a low energy conformation was found that fitted the model. In these, the hydrogen bond donor was pointing in the same direction. The structures for which no low energy conformation was found had a collapsed global energy minimum. The model was successfully able to explain the stereoselectivities of compounds 2 and 11.

Acknowledgements

This work was financially supported by the Academy of the Technical Sciences, the Lundbeck Foundation and the NeuroScience PharmaBiotech Centre, which is gratefully acknowledged.

References

1. Regioli, D., Boudon, A. and Fauchère, J.-L., *Pharmacol. Rev.*, 46 (1994) 551.
2. File, S.E., *Pharmacol., Biochem. Behav.*, 58 (1997) 747.
3. Nutt, D., *Lancet*, 352 (1998) 1644.
4. Raffa, R.B., *Neurosci. Behav. Rev.*, 22 (1998) 789.
5. Schoor, J.V., Joos, G.F., Chasson, B.L., Brouard, R.J. and Pauwels, R.A., *Eur. Respir. J.*, 12 (1998).
6. Sakurada, T., Sakurada, C., Tan-No, K. and Kisara, K., *CNS Drugs*, 28 (1999) 1997.
7. Bountra, C., Bunce, K., Dale, T., Gardner, C., Jordan, C., Twissell, D. and Ward, P., *Eur. J. Pharmacol.*, 249 (1993) R3.
8. Sprecher, A.v., Gerspacher, M. and Anderson, G.P., *Current Research in Rheumatoid Arthritis*, 2 (1998) 49.
9. Lowe, J.A., Drozda, S.E., Snider, R.M., Longo, K.P., Zorn, S.H., Morrone, J., Jackson, E.R., McLean, S., Bryce, D.K., Bordner, J., Nagahisa, A., Kanai, Y., Suga, O. and Megumi, T., *J. Med. Chem.*, 35 (1992) 2591.
10. Gao, Z. and Peet, N.P., *Curr. Med. Chem.*, 6 (1999) 375.
11. Gerspacher, M. and Sprecher, A.v., *Drugs of the Future*, 24(8) (1999) 883.
12. Desai, M.C., Lefkowitz, S.L., Thadeio, P.F., Longo, K.P. and Snider, R.M., *J. Med. Chem.*, 35 (1992) 4911.
13. Elliott, J.M., Broughton, H., Cascieri, M.A., Chicchi, G., Huscroft, I.T., Kurtz, M., MacLeod, A.M., Sadowski, S. and Stevenson, G.I., *Bioorg. Med. Chem. Lett.*, 8 (1998) 1851.
14. Takeuchi, Y., Shands, E.F.B., Beusen, D.D. and Marshall, G.R., *J. Med. Chem.*, 41 (1998) 3609.
15. Swain, C.J., Seward, E.M., Cascieri, M.A., Fong, T.M., Herbert, R., MacIntyre, D.E., Merchant, K.J., Owen, S.N., Owens, A.P., Sabin, V., Teall, M., VanNiel, M.B., Williams, B.J., Sadowski, S., Strader, C., Ball, R.G. and Baker, R., *J. Med. Chem.*, 38 (1995) 4793.
16. Goldstein, S., Neuwels, M., Moureau, F., Berckmans, D., Lassoie, M.-A., Differding, E., Houssin, R. and Hénichart, J.-P., *Lett. Pept. Sci.*, 2 (1995) 125.
17. Jacoby, E., Boudon, A., Kucharczyk, N., Michel, A. and Fauchère, J.-L., *J. Recept. Signal Transduction Res.*, 17 (1997) 855.
18. Vedani, A., Briem, H., Dobler, M., Dollinger, H. and McMasters, D. R., *J. Med. Chem.*, 43 (2000) 4416.
19. Singh, J. and Thornton, J.M., *FEBS*, 191 (1985) 2989.
20. Williams, D.E., *Acta Crystallographica*, A36 (1980) 715.
21. Greenfeder, S., Cheewatrakoolpong, B., Billah, M., Egan, R.W., Keene, E., Murgolo, N.J. and Anthes, J.C., *Bioorg. Med. Chem.*, 7 (1999) 2867.
22. Blaney, F.E., Raveglia, L.F., Artico, M., Cavagnera, S., Dartois, C., Farina, C., Grugni, M., Gagliardi, S., Luttmann, M.A., Martinelli, M., Nadler, G.M.M.G., Parini, C., Petrillo, P., Sarau, H.M., Scheideler, M.A., Hay, D.W.P. and Giardina, G.A.M., *J. Med. Chem.*, 44 (2001) 1675.
23. Macromodel V6.5: Mohamadi, F., Richards, N.G.J., Guida, W.C., Liskamp, R., Lipton, M., Caufield, C., Chang, G., Hendrickson, T. and Still, W.C., *J. Comput. Chem.*, 11 (1990) 440.
24. Chang, G., Guida, W.C. and Still, W.C., *J. Am. Chem. Soc.*, 111 (1989) 4379.
25. Halgren, T.A., *J. Comput. Chem.*, 20 (1999) 720.
26. Halgren, T.A., *J. Comput. Chem.*, 20 (1999) 730.
27. Hasel, T.F., Hendrickson, T.F. and Still, W.C., *Tetrahedron Comput. Method.*, 1 (1988) 103.
28. Still, W.C., Tempczyk, A., Hawley, R.C. and Hendrickson, T., *J. Am. Chem. Soc.*, 112 (1990) 6127.
29. Boström, J., Norrby, P.-O. and Liljefors, T., *J. Comput.-Aided Mol. Des.*, 12 (1998) 383.
30. McMartin, C. and Bohacek, R.S., *J. Comput.-Aided Mol. Des.*, 9 (1995) 237.
31. McMartin, C. and Bohacek, R.S., *J. Comput.-Aided Mol. Des.*, 11 (1997) 333.

32. Sjöberg, P., in Waterbeemd, H.v.d., Testa, B. and Folkers, G. (Eds.): *Computer-Assisted Lead Finding and Optimization*, Verlag Helvetica Chimica Acta, Basel 1997, p 83.
33. Spartan 5.0, Wavefunction, Inc., 18401 Von Karman Ave., Suite 370, Irvine, CA 92612, 1997.
34. Wu, E.S.C., Kover, A. and Semus, S.F., *J. Med. Chem.*, 41 (1998) 4181.
35. Qi, H., Shah, S.K., Cascieri, M.A., Sadowski, S. and Mac-Coss, M., *Bioorg. Med. Chem. Lett.*, 8 (1998) 2259.
36. Edmonds-Alt, X., Proietto, V., Broeck, D.V., Vilain, P., Advénier, C., Neliat, G., Fur, G.L. and Brelière, J.-C., *Bioorg. Med. Chem. Lett.*, 3 (1993) 925.
37. Harrison, Korsgaard, M.P.G., Swain, C.J., Cascieri, M.A., Sadowski, S. and Seabrook, G.R., *Bioorg. Med. Chem. Lett.*, 8 (1998) 1343.
38. Nishi, T., Fukazawa, T., Ishibashi, K., Nakajima, K., Sugioka, Y., Iio, Y., Kurata, H., Iyoh, K., Mukaiyama, O., Satoh, Y. and Yamaguchi, T., *Bioorg. Med. Chem. Lett.*, 9 (1999) 875.
39. Schnorrenberg, G., Esser, F., Dollinger, H., Jung, B., Speck, G. and Buerger, E., DE4445939-A1.
40. Selway, C.N. and Terrett, N.K., *Bioorg. Med. Chem.*, 4 (1996) 645.
41. Kubota, H., Kakefuda, A., Nagaoka, H., Yamamoto, O., Ikeda, K., Takeuchi, M., Shibamura, T. and Isomura, Y., *Chem. Pharm. Bull.*, 46 (1998) 242.
42. Smith, P.W., Cooper, A.W.J., Bell, R., Beresford, I.J.M., Gore, P.M., McElroy, A.B., Pritchard, J.M., Saez, V., Taylor, N.R., Sheldrick, R.L.G. and Ward, P., *J. Med. Chem.*, 38 (1995) 3772.
43. Cooper, A.W.J., Adams, H.S., Bell, R., Gore, P.M., McElroy, A.B., Pritchard, J.M., Smith, P.W. and Ward, P., *Bioorg. Med. Chem. Lett.*, 4 (1994) 1951.
44. Jasseand, D., David, S., Antel, J., Brueckner, R., Eeckhout, C. and Bielenberg, G.-W., EP-899270-A1.
45. MacKenzie, A.R., Marchington, A.P., Meadows, S.D. and Middleton, D.S., EP-791592-A2.
46. Mackenzie, R.R., Marchington, A.P., Middleton, D.S. and Meadows, S.D., WO9727185-A1.
47. Burkholder, T.P., Kudlacz, E.M., Le, T.-B. and Maynard, G.D., US5824690-A.
48. Burkholder, T.P., Maynard, G.D. and Kudlacz, E.M., WO9827086-A1.
49. Giardina, G.A.M., Grugni, M., Graziani, D. and Raveglia, L.F., WO-09852942.
50. Miller, S.C., Jacobs, R.T. and Shenvi, A.B., EP-739891-A2.
51. Monaghan, S.M., Alker, D. and Burns, C.J., WO9857972-A1.
52. McCormick, K.D. and Lupo, A.T., WO-09639383.
53. Shankar, B.B., US5688960-A.
54. Shanker, B.B., WO-09818785.
55. Shenvi, A.B., Jacobs, R.T., Miller, S.C., Macht, C.J. and Veale, C.A., WO-09516682.

Appendix II

Anders Poulsen, Berith Bjørnholm, Klaus Gundertofte, Irina D. Pogozeva, and Tommy Liljefors: Pharmacophore and receptor models for neurokinin receptors.

Submitted to Journal of Computer-Aided Molecular Design

Pharmacophore and receptor models for neurokinin receptors

Anders Poulsen^{a,b}, Berith Bjørnholm^b, Klaus Gundertoft^b, Irina D. Pogozheva^c, and Tommy Liljefors^{a*}

^a*Department of Medicinal Chemistry, The Royal Danish School of Pharmacy,*

2 Universitetsparken, DK-2100 Copenhagen, Denmark

^b*H. Lundbeck A/S, 9 Ottiliavej, DK-2500 Copenhagen-Valby, Denmark*

^c*College of Pharmacy, University of Michigan, Ann Arbor, MI 48109, USA*

Corresponding author: Prof. Tommy Liljefors, Department of Medicinal Chemistry,
The Royal Danish School of Pharmacy, 2 Universitetsparken, DK-2100 Copenhagen,
Denmark.

Tel.: +45 35 30 65 05, Fax: +45 35 30 60 40, e-mail: tl@dfh.dk

Abstract

Three neurokinin 2 (NK2) antagonist pharmacophore models (Models 1-3) have been developed on the basis of a previously published NK2 pharmacophore model [Poulsen et. al., *J. Comput.-Aided Mol. Design*, 16 (2002) 273]. By use of a new procedure for superimposition it was possible to add one hydrogen bond acceptor to our previous model. By altering the position of a hydrophobic pharmacophore element two more pharmacophore elements, both connected to the same carbonyl, could be incorporated resulting in Models 2 and 3. Both Model 2 and Model 3 are described by seven pharmacophore elements: Three hydrophobic groups, three hydrogen bond acceptors and a hydrogen bond donor. Model 1 contains the same hydrophobic groups and hydrogen bond donor as Model 2 and 3, but only one hydrogen bond acceptor. The hydrogen bond acceptors and donor are represented as vectors. Two of the hydrophobic groups are always aromatic rings whereas the other hydrophobic group can be either aromatic or aliphatic. In Model 1 the antagonists bind in an extended conformation with two aromatic rings in a parallel displaced and tilted conformation. Model 2 has the same two aromatic rings in a parallel displaced conformation whereas Model 3 has the rings in an edge to face conformation. The pharmacophore models were evaluated using 21 non-peptide antagonists from several structurally diverse classes. By use of exhaustive conformational analysis (MMFFs force field and the GB/SA hydration model) and least-squares molecular superimposition studies, 16 of 21 antagonists could be fitted to Model 2 and Model 3 with a low RMS value and a low conformational energy penalty. Two of the remaining five compounds could be fitted to Model 2 with a low conformational energy, but not to Model 3. We believe the remaining three compounds that could not be fitted to either model have another

binding mode. The pharmacophore Model 2 was successfully able to explain the NK1, NK2 and NK3 subtype selectivity of the compounds fitted to the model. Three NK 7TM receptor models were constructed, one for each receptor subtype. The location of the antagonist binding site in the three NK receptor models is identical. Compounds fitted to pharmacophore Model 2 could be docked into the NK1, NK2 and NK3 receptor models when the conformation of the flexible linker connecting the head and tail fragments were altered.

Keywords: Bioactive conformation, conformational analysis, MMFF force field, neurokinin, neurokinin A, neurokinin B, NK1 receptor, NK2 receptor, NK3 receptor, pharmacophore model, 7TM receptor model, substance P, subtype selectivity, tachykinin.

Introduction

The neurokinin receptors (NKRs) are peptides composed of 350 to 500 amino acids. They belong to the superfamily of G-protein coupled receptors (GPCRs) [1]. Three NKR subtypes, NK1, NK2 and NK3, have been identified by molecular cloning and sequence analysis. They are characterised by their endogenous ligands. NK1 has highest affinity for substance P, NK2 has highest affinity for NKA and NK3 has highest affinity for NKB [1]. Most of the published NK2 antagonists contain at least two ring systems connected by a linker holding a hydrogen bond acceptor. We define this part of the NK antagonists as the head fragment, and the rest is defined as the tail (Figure 1). The tail of the majority of NK2 antagonists contains a basic nitrogen, a hydrophobic group and a hydrogen bond acceptor. Figure 2 shows our previously published NK2 pharmacophore model [2]. In this model the antagonists binds in an extended conformation with two aromatic groups in a parallel displaced and tilted conformation [3] (A and B in Figure 2). The model consists of an additional hydrophobic group and a hydrogen bond donor represented as a vector (C and D in Figure 2 respectively). Most of the studied NK2 antagonists have a piperidine ring in the tail. The most probable orientation of pharmacophore element C is equatorial relative to the piperidine ring. This model agrees with NK1/NK2 and NK2/NK3 receptor model studies [4, 5]. However, this model does not account for the importance of hydrogen bond accepting groups in the head and tail of NK2 antagonists (compare compounds **2** and **34**). By using a new procedure for superimposition we can now present three new pharmacophore models that incorporate these hydrogen bond acceptors.

As is the case for most GPCRs, NKRs have not yet been crystallised, so no experimental structures are available. However, the X-ray structure of the GPCR bovine rhodopsin has recently been published [6] and the NKRs have sufficient sequence homology to bovine rhodopsin that an alignment can be made. The GPCRs contain seven transmembrane α -helices (7TM) of approximately 25 residues length. The helices are connected by intra- and extracellular loops. The *N*-terminal is located on the extracellular side whereas the *C*-terminal extends into the cytoplasm. The loop regions and the *N*- and *C*-terminal are surrounded by an aqueous environment and consists primary of hydrophilic amino acids. The 7TM region are in a lipid environment and consists mainly of hydrophobic amino acids. Some experimental work have been published from which structural information of the NKR have been obtained. Elling et al. [7, 8] have performed extensive mutagenesis work to identify zink ion binding sites in the NK1R. Donnelly et al. [9] have made a Asp79Asn + Asn303Asp NK2R double mutant and they conclude that there is a direct interaction between the side chains of the two residues. That places TM2 and TM7 in contact, and the relative orientation of the two helices can be deduced.

Several receptor modelling studies of the NK1R have been published [4, 10-13], the NK2R [4, 5, 14, 15] and the NK3R [5]. These models are based on the bacteriorhodopsin cryo electron microscopy structure by Henderson et al. [16] or the rhodopsin structure by Baldwin et al. [17]. Bacteriorhodopsin is a proton pump, not a GPCR, and the sequence identity with any known GPCR are too low for sequence based alignment. Furthermore, the resolution of these structures is too low to provide the atomic coordinates directly. Thus, bacteriorhodopsin is not an ideal template for modelling GPCRs. Rhodopsin is a true GPCR. Baldwin's rhodopsin model is based on a cryo microscopy electron density map of frog rhodopsin [18], but the resolution

is too low to provide atomic coordinates directly. Using the recently published bovine rhodopsin X-ray structure [6] as a template is expected to produce better GPCR models. Our NKR models were used to evaluate the pharmacophore models. The conformations of compounds manually docked into the receptor models were compared to the pharmacophore models and the pharmacophore elements were compared to specific interactions observed in the receptor-ligands complex.

Computational methods

Force fields, conformational analysis and calculation of conformational energies

Conformational space was searched by using the Monte Carlo Multiple Minimum (MCMM) method as implemented in MacroModel 7.1 [19]. Force field calculations were carried out using the MMFF94s force field, the GB/SA hydration model [20, 21] and the truncated Newton conjugate gradient algorithm (TNCG) as implemented in MacroModel. The conformational energy penalties were calculated as the difference in internal energy between the putative bioactive conformation and the global energy conformation obtained for aqueous solution [22]. The solvation energy was calculated by using the GB/SA hydration model [20, 21]. No compound had a solvation energy that differed markedly from the other compounds. A more detailed description of conformational search, force fields and calculation of the conformational energy penalty is given in [2].

Superimposition studies

Three hydrophobic rings, one hydrogen bond donor (in most cases the protonated nitrogen atom of an amine) and three hydrogen bond acceptors (two of which are connected to the same carbonyl oxygen) were chosen as pharmacophore elements. For each of the hydrophobic rings, centroids were constructed. The structures were fitted to the pharmacophore model using the centroids as fitting points. Dummy atoms were placed 2.8 Å from the donor/acceptor atoms in the direction of the putative hydrogen bond interaction vectors defined by the pharmacophore model. The compounds were again fitted to the pharmacophore models now using both the centroids and the dummy atoms as fitting points. The RMS values in Tables 1 and 3 were obtained from this second fit. The hydrogen bond donor and acceptor atoms in the molecules were not used in the superimposition. A second putative hydrogen bonding site point was represented by a dummy atom 2.8 Å from the donor/acceptor atom in the direction of the nitrogen-hydrogen bond (for pharmacophore element D) or the lone pair (for pharmacophore elements E, F and G). The second dummy atom was not used as a fitting point, but used to evaluate the direction of the hydrogen bond donor-acceptor interaction. The angle of deviation from the ideal hydrogen bond geometry, ϕ , is defined in Figure 3 where pharmacophore element F in the head fragment of compound 4 is used as an example.

Least-squares rigid body molecular superimpositions were performed using the MacroModel program. The superimpositions were evaluated in terms of RMS values of the fitting points. An RMS value of 0.6 Å has been used as a soft indicator to determine whether a fit is acceptable or not. The aromatic pharmacophore elements were fitted in a coplanar orientation if energetically possible. The RMS values do not give any measure of this coplanarity since only the centroids are superimposed.

DFT calculations

The program Jaguar 4.1 [23] was used for B3LYP DFT energy minimisation. The basis set was 6-31G** and accuracy level was set to "accurate". Otherwise default parameters were used.

Receptor modelling

The sequence alignment were produced for the NKRs was similar to the one obtained from the GPCRDB [24] but slightly modified in the loop regions [25]. NK1R, NK2R and NK3R models were constructed by the iterative distance geometry method of Pogozheva et al. [26]. This approach utilises the program DIANA [27] to construct a protein structure from torsional and distance constraints. The bovine rhodopsin X-ray structure (PDB file 1F88) [6] was used as a template to derive the constraints. The iterations consisted of a cycle with three steps. 1) Examination of the protein structures and the output files from the previous DIANA calculation. Constraint violations and van der Waals clashes are detected. 2) Modifications of the input files with angle and distance constraints. 3) DIANA calculation with the modified constraints. The NK antagonists were manually docked into the receptor models guided by published mutational data [4, 15, 28]. The receptor-ligand complex was minimised with all hydrogens using the CHARMM force field [29] with the adopted-basis Newton Raphson method, a dielectric constant of 10 and 50-70 minimisation steps.

Results and discussion

Construction of the pharmacophore models

The previously published model [2] does not explain the importance of hydrogen bond acceptors in the head and tail fragments of NK2 antagonists. Attempts to add a hydrogen bond acceptor pharmacophore element to the head part proved futile with the orientation of the pharmacophore elements as in the previous model. Therefore we searched for new orientations of the pharmacophore elements A and B (Figure 2) for which a hydrogen bond acceptor could be added to the model. Two new orientations were found leading to pharmacophore Models 2 and 3. The conformation of the flexible linker connecting the head and tail fragments was retained as in the previous model. This conformation of the linker is the same as in the global energy minimum of compound **2**. In all three models, pharmacophore elements B, C and D are in the same positions as in our previous model (Figure 2).

Compounds **1-3** (Figure 4) were used to derive pharmacophore Models 2 and 3, whereas compounds **4-21** were used to evaluate the models. Compounds **1-3** were chosen due to their structurally diverse head fragments. In compound **1** the pharmacophore elements A, B, E and F (Figure 1) are connected to a six-membered ring containing an amide functionality, in compound **2** the pharmacophore elements are connected by an open chain and in compound **3** an imidazole holds the pharmacophore elements. Compound **3** is lacking pharmacophore element F.

Three conformations of each of compounds **1-3** were found for which pharmacophore elements A-D could be superimposed. For the hydrogen bond acceptors in the head fragments, a dummy atom was placed 2.8 Å from the acceptor atom in the direction of the lone pairs thereby creating a vector (pharmacophore elements E and F). One mode of superimposition led to the previously published model. The hydrogen bond acceptor-donor vectors (pharmacophore element E and F)

did not superimpose in these conformations. However, for the other two modes of superimposition (Model 2 and 3) the hydrogen bond acceptor-donor vector did superimpose. In Models 2 and 3 the positions of the pharmacophore elements are defined as the average coordinate of the pharmacophore elements in the superimposition of compounds **1-3**. The position of pharmacophore elements B, C and D are identical in all three models.

Construction of pharmacophore element G

As evident from Figure 5 and Table 1, the heteroatoms of the tail part of NK2 antagonists are important for the affinity of the compounds. For instance, by comparing compounds **2** and **34** it is obvious that a hydrogen-bonding group in the tail is needed in order to obtain high NK2 affinity. Since a number of the high affinity NK2 antagonists do only have hydrogen bond acceptors in the tail (e.g. compounds **7**, **22**, **27**, **28**, **30** and **31**), the simplest would be to assume that the interaction is one in which the receptor is the donor. However, with our previous method for superimposition [2] attempts to add a hydrogen bond acceptor vector to the pharmacophore model failed because we did not allow the vector to deviate from the ideal lone pair direction. Therefore a new method as described in the Computational methods section was adopted.

The tail fragments have the same conformation in all three pharmacophore models, therefore the hydrogen bond interaction vector also has the same position in the three models. Compounds **2**, **7**, **16**, and **22-32** (Figure 5) were superimposed on the previous model using pharmacophore elements A-D as fitting points. A dummy atom was placed 2.8 Å from the hydrogen bond acceptor in the direction of the lone pair. The coordinates of the hydrogen bond interaction vector (pharmacophore

element G) was defined as the average position of the acceptor and dummy atoms respectively in the superimposition of compounds **2**, **7**, **16**, and **22-32**.

Pharmacophore Models 1-3 and the coordinates of the pharmacophore elements are shown in Figures 6-8. Figure 9 shows a superimposition of the three pharmacophore models. The position of pharmacophore element B, C and D are identical in all three models. In Model 1, pharmacophore elements A and B are in a parallel displaced and tilted conformation. In Model 2, pharmacophore elements A and B are in a parallel displaced conformation, whereas they are in an edge to ring face conformation in Model 3 [3].

Compounds and pharmacophore elements

The set of compounds **1-21** were chosen for its structural diversity and it contains high affinity selective NK2, dual NK1/NK2 and triple NK1/NK2/NK3 antagonists. Compounds **2-17** and **19-21** were also used to derive or evaluate our previous model [2]. Two or three hydrophobic groups are found in all NK2 antagonists (pharmacophore elements A, B and C, Figure 1). A basic amino group is also present in all structures (pharmacophore element D, represented as a vector in Figure 2) except for compound **20** [2]. Pharmacophore elements A and B are connected by a linker holding a hydrogen bond acceptor (pharmacophore elements E and F). In most cases this is a carbonyl or ether oxygen. Furthermore, a hydrogen bond acceptor is found in the tail part of most NK2 antagonists (pharmacophore element G). The hydrophobic groups are marked in Figure 4 by centroids, the basic nitrogen is marked with a "+" sign and the hydrogen bond acceptors are marked by bold type atom labels.

The pharmacophore element labelled B (Figure 1) is found to be an aromatic ring in all structures except compounds **10-12**. These compounds have electronegative

groups in this area. Compound **10** has a hydroxy group, compound **11** a methoxy group and compound **12** a carbonyl group. The pharmacophore element A does not need to be an aromatic ring but can be aliphatic or olefinic hydrophobes as is the case for compounds **1**, **6**, **14**, and **15**. In compounds **1**, **14**, and **15**, the aromatic pharmacophore element C is lacking.

The hydrogen bond acceptor in the head fragment (pharmacophore elements E and F) is present in all compounds. Compounds **3** and **20** have only been fitted to pharmacophore element E, where as compounds **5** and **13** have only been fitted to pharmacophore element F. The rest of the compounds could be fitted to both pharmacophore elements E and F. However, in the ligand-receptor complex, both interactions represented by the pharmacophore element E and F may not be present (See The receptor models section below).

The hydrogen bond acceptor in the tail (pharmacophore element G) is lacking in compounds **8**, **10-12**, **15**, and **20**. The basic amino group is protonated at physiological pH. pK_a calculations using MolSurf 99/1 [30] (Table 2) show that in all compounds having pharmacophore element D, this nitrogen always has the highest pK_a value.

Evaluation of the pharmacophore models

Compounds **2**, **7**, **16** and **22-32** (Figure 5) were fitted to Model 1 by the procedure described under Computational methods. The angle (ϕ defined in Figure 3) between the lone pair of the hydrogen bond acceptor atom, and pharmacophore element G are shown in Table 1 as well as the RMS values. It has been shown that hydrogen bonds involving an ether oxygen do not have a lone pair preference [31]. The strength of the hydrogen bond in the plane between the lone pairs do not vary significantly with the

angle ϕ . Hydrogen bonds involving a ketone oxygen have a lone pair preference. However this preference is small in the plane between the lone pairs. A ϕ angle of 60° is calculated to reduce the strength of the hydrogen bond to approximately 80% compared to that of a hydrogen bond in the lone pair direction [31]. Only compound **24** exceeds this deviation. A superimposition of the tail fragments of compounds **2**, **7**, **16** and **22-32** are shown in Figure 10.

Compounds **1-21** were fitted to both pharmacophore Models 2 and 3 as described in the Computational methods section. RMS values and the deviations of the hydrogen bond interaction vectors from the ideal geometry are shown in Table 3. Figure 11 shows a superimposition of compounds **1-9** and **13-21** fitted to pharmacophore Model 2 (compounds **10-12** are believed to have another binding mode as described below). Figure 12 shows a superimposition of the same compounds fitted to pharmacophore Model 3.

Compounds **1-3**, **6-8**, **13**, and **15**, **16**, **18** and **19** could be fitted to both Model 2 and 3 with low conformational energies and low RMS values (Tables 2 and 3). Compounds **4**, **5**, **9**, **17**, **20** and **21** have high RMS values when calculated over all pharmacophore elements. However, if pharmacophore element A is excluded from the RMS calculation, these compounds all have an acceptably low RMS value. Some compounds have large substituents in the aromatic ring that maps to pharmacophore element A (e.g. compounds **16** and **17**) and some have a bulky aliphatic ring (e.g. compounds **14** and **15**). It is therefore reasonable to assume that the centroid of pharmacophore element A is not located exactly in the same place within the receptor for all the compounds examined, but rather falls within the same area.

We have previously shown that the force fields MMFFs, MM2 and AMBER are unable to correctly calculate the conformational energy penalty of compound **14**

due to an "electrostatic collapse" [2]. Since the structurally related compound **15** could be fitted to both models with a low conformational energy, we assume that compound **14** can also be fitted to both models with a low conformational energy and that the high calculated energy is a computational artefact.

In compound **20**, the imidazole nitrogen is assumed to be involved in hydrogen bonding to the receptor. The nitrogen can be a hydrogen acceptor (unprotonated imidazole as for compound **20**) or donor (protonated imidazole as in compound **20a** in Table 2). Whether the nitrogen acts as a donor or acceptor has a large impact on the torsional energy of the bond connecting the carbonyl carbon to the imidazole ring. A torsional drive of this angle of the model system shown in Figure 13 was performed by using MMFFs and B3LYP/6-31G**. The energy profile calculated by MMFFs compares well with that of the DFT method for both the neutral and protonated systems. The torsional barrier of the protonated system is lower than that of the neutral system, and the profiles as calculated by both methods are different for the two model systems. When compound **20** is fitted to Models 2 and 3 this angle (defined in Figure 13 for the model system) is 144.3° and 131.2°, respectively. By assuming that the imidazole acts as a hydrogen bond donor, **20a** could be fitted to both models with a low conformational energy penalty. It is not unreasonable to assume that pharmacophore element E is a hydrogen bond donor as well as an acceptor if the hydrogen bond is formed to a water molecule or to a residue with a side chain that can act as both hydrogen bond donor and acceptor.

Compound **9** could be fitted to Models 2 and 3, but only to Model 2 with a low conformational energy. Compound **21** could be fitted to Models 1 and 2 but not to Model 3. When fitted to Model 3 the ethyl substituent in the 2-position of the 2,3-dihydro-isoindol-1-one group would fall in the area of pharmacophore element A. The

aromatic part of the 2,3-dihydro-isoindol-1-one group could only map the pharmacophore model when the stereochemistry was inverted at the 3-position, and the ring could not be fitted in a coplanar orientation. Compounds **10–12** were fitted to Model 1 with a low conformational energy and a low RMS value [2]. However they could only be fitted to Models 2 and 3 with a high conformational energy and high RMS. Structurally these compounds differ from the rest as previously described.

The angle (ϕ defined in Figure 3) between the lone pair of the hydrogen bond acceptor atom, and pharmacophore elements E, F and G is shown in Table 3. Only compounds **9-12** have a large angle for pharmacophore element E while the angle ϕ for pharmacophore element G is large for compounds **4** and **18**. The angle ϕ for pharmacophore element D is also shown in Table 3. Except for compounds **11-12** this angle is small for all compounds.

If the amide in the head of compound **2** is de-methylated, the affinity for the NK2R drops by more than a factor of 200 [32]. There are three possible explanations for this. 1) There could be a favourable interaction between the methyl group and the receptor. 2) The de- methylated compound has a more negative solvation energy that is not counteracted by a favourable interaction with the receptor. 3) For compound **2** low energy conformations exist where the amide adopts either a cis or a trans conformation. When compound **2** is de-methylated only the trans conformation is found in low energy conformations. Therefore the methyl group serves to make the cis conformation energetically accessible. If the third explanation is correct Model 1 can not represent the actual binding mode.

On the basis of these observations we suggest that Model 2 represents the best pharmacophore model for the examined NK2 antagonists. Model 2 includes all the pharmacophore elements necessary for high affinity and only compounds **10-12** could

not be fitted to this model with a low RMS and a low conformational energy penalty. We believe that the compounds **10-12** bind to the receptor in a different mode.

The receptor models

It was verified that the NK1R 7TM receptor models were compatible with the zinc ion binding sites found by Elling et al. [7, 8] and the Asp79Asn + Asn303Asp double mutant by Donnelly et al. [9]. The compounds were fitted to pharmacophore Model 2 before being docked into the receptor model followed by minimisation of the ligand-receptor complex. The conformation of the flexible linker connecting the head and tail part of the antagonists was changed upon docking. However, the conformational change of the head and tail fragments were minor. Conformations fitted to pharmacophore Models 1 and 3 were found to be incompatible with the receptor models. Pharmacophore element A were found to clash with the receptors in conformations fitted to either Models 1 or 3.

The proposed antagonist binding sites of the NK1R and NK2R models binding compound **16** are shown in Figure 14. The residues identified by site directed mutagenesis as important for the binding of compound **2** and **16** to the NK2R are M117, Q166, H198, Y266, F270 and Y289 [4, 15, 28]. The residues important for the binding of compound **16** to the NK1R are Q165, H197, I204, F264 and H265 [4]. Compound **16** is docked in the NK2R model so that it makes a direct interaction with the above mentioned residues. In the NK1R model, compound **16** also has direct interactions with the residues identified by site directed mutagenesis. Furthermore, an interaction with Y287 is found. It is evident that the location of the binding site in our NK1R and NK2R models are the same and that the conformations of the antagonists docked into the NK1R and NK2R models are almost identical. This conclusion is the

opposite to that of Greenfeder et al. [4] who conclude that the binding sites of the NK1R and NK2R differ, and that the conformations of compound **16** bound to the NK1R and the NK2R are different.

Predictions made from the NKR models

When docked into the NK2R model the compounds in this study (except **10-12**) were found to bind in a conformation represented by pharmacophore Model 2. However, the linker connecting the head and the tail part of the antagonists has a different conformation when docked in the NKRs as compared to the conformations fitted to Model 2. Therefore the head and tail fragments have the same conformation but different relative orientations in the docked conformations as compared to pharmacophore Model 2. For each pharmacophore element except F a favourable interaction with the receptor was identified. These are shown in Figure 14. This suggests that pharmacophore Model 2 excluding pharmacophore element F represents the actual binding mode.

The NK2R model and mutational data [28] indicates that compounds **10-12** bind in the same area as the rest of the compounds in this study, but in a different orientation. Manual docking of compound **20a** into our NK2R model suggests that two hydrogen bonds can be formed from Gln166 to the protonated nitrogen and the benzyl oxygen.

The NK2R model indicates that pharmacophore element E interacts with a proton in the amide group of the sidechain of Gln166 (Figure 14). Glutamine is a flexible residue so the angle ϕ between the lone pair of the ligand and the proton on Gln166 may be significantly smaller than the value in Table 3. Pharmacophore element G interacts with Tyr289 in the NK2R (Figure 14). Since tyrosine can act as

both a hydrogen bond donor and acceptor it is possible that Tyr289 interacts with a hydrogen on the amide group in the tail of compounds **4** and **18**. This would result in a lower ϕ value than given in Table 3. Pharmacophore element D also interacts with a tyrosine (Tyr266 in the NK2R). Therefore we are unable to conclude whether the basic nitrogen is protonated or not when the ligands bind to the receptor.

In the conformation of compound **2** docked into the receptor models, the amide in the head fragment is in a cis conformation. No specific interactions are observed between the methyl group on the amide, and the NK2R model. In the demethylated analogue of compound **2** specific interactions between the amide and the NK2R model were also absent. Therefore the role of the methyl group is either conformational (to make the cis conformation energetically available) or to lower the solvation energy.

Selectivity for the NK1, NK2 and NK3 receptors

The most important information provided by a pharmacophore model is the putative bioactive conformation of each ligand and the alignment of these conformations. A correct molecular alignment makes it possible to identify the structural relationships between different types of ligands. Receptor subtype selectivity may arise either from differences in the bioactive conformations at the receptor subtypes, or from different substitution patterns. We believe the latter is true for NK1/NK2 subtype selectivity. Table 4 shows the NK subtype selectivity for two head fragments. Selective NK1, selective NK2 dual NK1/NK2 and triple NK1/NK2/NK3 antagonists can be obtained from the same scaffold. The subtype selectivity is determined by the substitution pattern of the pharmacophore elements A, B and C. An unsubstituted phenyl ring and a 3,4-di-chlorophenyl as pharmacophore elements A and B, respectively, is optimal

for NK2 activity [33, 34]. 3,5-Di-methylphenyl, 3,5-di-trifluoromethylphenyl and 3,4,5-tri-methoxyphenyl as pharmacophore element A is optimal for NK1 activity where as substituents in pharmacophore element B are of minor importance for NK1 activity [33, 35, 36]. Subtle changes around pharmacophore elements C and G also seems to be important for subtype selectivity. Of the different compounds examined only compounds **10-12** and **21** have a scaffold that is not claimed to have both NK1 and NK2 activities. We concluded earlier that compounds **10-12** have another binding mode than the rest of the compounds. The head fragment of compound **21** is for NK1 antagonists to our knowledge unique for this compound. Therefore all the scaffolds (except one) from which we have built the NK2 pharmacophore models can also have NK1 activity. It is likely that the bioactive conformations of the NK1R and NK2R subtypes are very similar and that our pharmacophore models are dual NK1/NK2 pharmacophore models. This is supported by the receptor model (Figure 14). In the NK1R model, Thr201 is located in the binding pocket for the trimethoxyphenyl group of compound **16**. The equivalent residues in the NK2R and NK3R are Ile202 and Ile252, respectively. Since threonine is polar as opposed to isoleucine this could explain the subtype difference in the observed SAR around pharmacophore element A.

Reversing the amide group in the tail of compound **2** increases NK3 activity [37]. However, potent and selective NK3 antagonists have a reversed amide group in the linker holding pharmacophore element A, B, E and F (cf. compounds **2** with **37** and compound **19** with **36** in Figure 4 and Table 4) [37, 38]. Changing the position of the carbonyl from that in compound **2** to that in **37** changes the conformational properties of the head fragment considerably, but the change of the carbonyl position from that in compound **19** to that in **36** has only a minor effect on the conformations.

The selective NK3 antagonists also differ from the NK2 antagonists in the length of the linker connecting the head and the tail fragments. In the examined NK2 antagonists (except compound **19**) the linker is a C2 chain whereas it is a C3 chain in the selective NK3 antagonists. Compound **36** could be fitted to all pharmacophore models while compound **37** could not be fitted to any of the models. However, if pharmacophore elements E and F are ignored compound **37** can be fitted to Model 2. These observations suggest that the bioactive conformations of NK antagonists at the NK2R and NK3R subtypes could be different or that the carbonyl in compound **37** is interacting with another residue. Pharmacophore element E is forming a hydrogen bond to Glu166 in the NK2R. The equivalent residue in the NK3R is Glu218. When compound **2** is docked into the NK3R model a hydrogen bond between pharmacophore element E and Glu218 is observed. This interaction is not found for compound **37**. Instead pharmacophore element E of **37** can form a hydrogen bond to Tyr256. However while the binding site of the NK1R and NK2R have been extensively explored by site directed mutagenesis this is not the case for the NK3R.

Conclusions

Three pharmacophore models (Models 1-3) for NK2 antagonists have been derived on the basis of a previously published model [2]. Model 1 is identical to our previous model except that a hydrogen bond acceptor pharmacophore element has been added to the tail. Both Models 2 and 3 consist of three hydrophobic pharmacophore elements (A, B and C), a hydrogen bond donor element (D), and three hydrogen bond acceptor elements (E, F and G). The hydrogen bond donor-acceptor interactions are represented as vectors. In Model 2, the antagonists bind in an extended conformation

with pharmacophore elements A and B in a parallel displaced conformation. In Model 3, pharmacophore elements B, C, D and G are in the same arrangement as in Model 1 and 2, but pharmacophore elements A and B are in an edge to ring face conformation.

Pharmacophore Model 2 and 3 models were evaluated against 21 structurally diverse, high affinity selective NK2, dual NK1/NK2 and triple NK1/NK2/NK3 antagonists. All compounds except five could be fitted to both models with a low conformational energy penalty and low RMS value. We believe that three of the remaining five compounds have another binding mode. The last two compounds could be fitted to Model 2 but not Model 3. Therefore we suggest that Model 2 represent the actual binding mode for the examined NK2 antagonists. This conclusion is supported by our receptor model study. Compounds fitted to pharmacophore Model 2 but not to Models 1 and 3 could be docked in the receptor models with only minor changes to the conformation of the head and tail fragments. The flexible linker connecting the fragments has another conformation in the docked conformations compared with pharmacophore Model 2. For each pharmacophore element except F, a specific interaction with the NK2R model was observed. This binding mode is compatible with published site directed mutagenesis data.

The NK1/NK2 subtype selectivity is determined by the substitution pattern of the pharmacophore elements A, B, C and G and not by differences in the bioactive conformations at the receptor subtypes. Therefore our pharmacophore models can be used for the design of both potent and selective NK1 and NK2 antagonists. However, we believe that NK2/NK3 subtype selectivity is determined by differences in the bioactive conformations at the receptor subtypes or that pharmacophore element E is interacting with different residues in the two receptor subtypes. These findings are also supported by our NK1R, NK2R and NK3R model study.

Acknowledgements

This work was financially supported by the Danish Academy of Technical Sciences, the Lundbeck Foundation and the NeuroScience PharmaBiotech Centre, which is gratefully acknowledged.

References

1. Regoli, D., Boudon, A. and Fauchere, J. L. *Pharmacol. Rev.*, (1994) 551.
2. Poulsen, A., Liljefors, T., Gundertofte, K. and Bjørnholm, B., *J Comput.-Aided Mol. Des.*, 16 (2002) 273.
3. Williams, D. E., *Acta Crystallographica*, A36 (1980) 715.
4. Greenfeder, S., Cheewatrakoolpong, B., Billah, M., Egan, R. W., Keene, E., Murgolo, N. J. and Anthes, J. C., *Bioorg. Med. Chem.*, 7 (1999) 2867.
5. Blaney, F. E., Raveglia, L. F., Artico, M., Cavagnera, S., Dartois, C., Farina, C., Grugni, M., Gagliardi, S., Luttmann, M. A., Martinelli, M., Nadler, G. M., Parini, C., Petrillo, P., Sarau, H. M., Scheideler, M. A., Hay, D. W. and Giardina, G. A., *J. Med. Chem.*, 44 (2001) 1675.
6. Palczewski, K., Kumasaka, T., Hori, T., Behnke, C. A., Motoshima, H., Fox, B. A., Le, T., Teller, D. C., Okada, T., Stenkamp, R. E., Yamamoto, M. and Miyano, M., *Science*, 289 (2000) 739.
7. Elling, C. E., Thirstrup, K., Nielsen, S. M., Hjorth, S. A. and Schwartz, T. W., *Fold. Des.*, 2 (1997) S76.
8. Elling, C. E. and Schwartz, T. W., *EMBO J.*, 15 (1996) 6213.
9. Donnelly, D., Maudsley, S., Gent, J. P., Moser, R. N., Hurrell, C. R. and Findlay, J. B., *Biochem. J.*, 339 (Pt 1) (1999) 55.
10. Lundstrom, K., Hawcock, A. B., Vargas, A., Ward, P., Thomas, P. and Naylor, A., *Eur. J. Pharmacol.*, 337 (1997) 73.
11. Cascieri, M. A., MacLeod, A. M., Underwood, D., Shiao, L. L., Ber, E., Sadowski, S., Yu, H., Merchant, K. J., Swain, C. J. and Strader, C. D., *J. Biol. Chem.*, 269 (1994) 6587.
12. Fong, T. M., Yu, H., Cascieri, M. A., Underwood, D., Swain, C. J. and Strader, C. D., *J. Biol. Chem.*, 269 (1994) 2728.
13. Fong, T. M., Yu, H., Cascieri, M. A., Underwood, D., Swain, C. J. and Strader, C. D., *J. Biol. Chem.*, 269 (1994) 14957.

14. Ali, M. A., Bhogal, N., Fishwick, C. W. and Findlay, J. B., *Bioorg. Med. Chem. Lett.*, 11 (2001) 819.
15. Giolitti, A., Cucchi, P., Renzetti, A. R., Rotondaro, L., Zappitelli, S. and Maggi, C. A., *Neuropharmacology*, 39 (2000) 1422.
16. Henderson, R., Baldwin, J. M., Ceska, T. A., Zemlin, F., Beckmann, E. and Downing, K. H., *J. Mol. Biol.*, 213 (1990) 899.
17. Baldwin, J. M., Schertler, G. F. and Unger, V. M., *J. Mol. Biol.*, 272 (1997) 144.
18. Unger, V. M., Hargrave, P. A., Baldwin, J. M. and Schertler, G. F., *Nature*, 389 (1997) 203.
19. Macromodel 7.1. Schrödinger Inc., 1500 SW First Avenue, Suite 1180, Portland, Oregon 97201.
20. Hasel, T. F., Hendrickson, T. F. and Still, W. C., *Tetrahedron Comput. Methods*, 1 (1988) 103.
21. Still, W. C., Tempczyk, A., Hawley, R. C. and Hendrickson, T., *J. Am. Chem. Soc.*, 112 (1990) 6127.
22. Boström, J., Norrby, P.-O. and Liljefors, T., *J. Comput.-Aided Mol. Des.*, 12 (1998) 383.
23. Jaguar 4.1. Schrödinger Inc., 1500 SW First Avenue, Suite 1180, Portland, Oregon 97201.
24. Horn, F., Weare, J., Beukers, M. W., Hörsch, S., Bairoch, A., Chen, W., Edvardsen, Ø., Campagne, F. and Vriend, G., *Nucleic Acids Res.*, 26 (1998) 275.
25. Pogozeva, I. D., College of Pharmacy, University of Michigan, Ann Arbor, MI 48109, USA. 2002.
26. Pogozeva, I. D., Lomize, A. L. and Mosberg, H. I., *Biophys. J.*, 72 (1997) 1963.
27. Guntert, P., Braun, W. and Wuthrich, K., *J. Mol. Biol.*, 217 (1991) 517.
28. Huang, R. R., Vicario, P. P., Strader, C. D. and Fong, T. M., *Biochemistry*, 34 (1995) 10048.
29. CHARMM. Accelrys Inc., 9685 Scranton Road, San Diego, CA 92121-3752.
30. Sjöberg, P. In Waterbeemd, H. Van de., Testa, B. and Folkers, G., (Eds.), *Computer-Assisted Lead Finding and Optimization*, Verlag Helvetica Chimica Acta, Basel, 1997, 83.
31. Lommerse, J. P. M., Price, S. L. and Taylor, R., *J. Comput. Chem.*, 18 (1997) 757.
32. Edmonds-Alt, X., Proietto, V., Broeck, D. V., Vilain, P., Advenier, C., Neliat, G., Fur, G. L. and Brelière, J.-C., *Bioorg. Med. Chem. Lett.*, 3 (1993) 925.
33. Kubota, H., Kakefuda, A., Okamoto, Y., Fujii, M., Yamamoto, O., Yamagiwa, Y., Orita, M., Ikeda, K., Takeuchi, M., Shibamura, T. and Isomura, Y., *Chem. Pharm. Bull. (Tokyo)*, 46 (1998) 1538.
34. Burkholder, T. P., Kudlacz, E. M., Maynard, G. D., Liu, X. G., Le, T.-B., Webster, M. E., Horgan, S. W., Wenstrup, D. L., Freund, D. W., Boyer, F., Bratton, L., Gross, R. S., Knippenberg, R. W., Logan, D. E., Jones, B. K. and Chen, T.-M., *Bioorg. Med. Chem. Lett.*, 7 (1997) 2531.

35. Shih, N. Y., Albanese, M., Anthes, J. C., Carruthers, N. I., Grice, C. A., Lin, L., Mangiaracina, P., Reichard, G. A., Schwerdt, J., Seidl, V., Wong, S. C. and Piwinski, J. J., *Bioorg. Med. Chem. Lett.*, 12 (2002) 141.
36. Burkholder, T. P., Kudlacz, E. M., Le, T.-B., Knippenberg, R. W., Shatzer, S. A., Maynard, G. D., Webster, M. E. and Horgan, S. W., *Bioorg. Med. Chem. Lett.*, 6 (1996) 951.
37. Giardina, G. A. M., Raveglia, L. F. and Grugni, M., *Drugs of the Future*, 22 (1997) 1235.
38. Shah, S. K., US5434158, 1995.
39. Kubota, H., Kakefuda, A., Nagaoka, H., Yamamoto, O., Ikeda, K., Takeuchi, M., Shibamura, T. and Isomura, Y., *Chem. Pharm. Bull. (Tokyo)*, 46 (1998) 242.
40. Burkholder, T. P., Kudlacz, E. M., Le, T.-B. and Maynard, G. D., US5824690, 1998.
41. Giardina, G. A. M., Grugni, M., Graziani, D. and Raveglia, L. F., WO-09852942, 1998.
42. Kubota, H., Fujii, M., Ikeda, K., Takeuchi, M., Shibamura, T. and Isomura, Y., *Chem. Pharm. Bull. (Tokyo)*, 46 (1998) 351.
43. Mackenzie, A. R., Marchington, A. P., Middleton, D. S. and Meadows, S. D., WO9719942, 1997.
44. Miller, S. C., Jacobs, R. T. and Shenvi, A. B., EP-739891, 1996.
45. Nishi, T., Fukazawa, T., Ishibashi, K., Nakajima, K., Sugioka, Y., Iio, Y., Kurata, H., Itoh, K., Mukaiyama, O., Satoh, Y. and Yamaguchi, T., *Bioorg. Med. Chem. Lett.*, 9 (1999) 875.
46. Shankar, B. B., WO-09818785, 1998.
47. Selway, C. N. and Terrett, N. K., *Bioorg. Med. Chem.*, 4 (1996) 645.
48. McCormick, K. D. and Lupo, A. T., WO-09639383, 1996.
49. Shankar, B. B., US5688960, 1997.
50. Smith, P. W., Cooper, A. W., Bell, R., Beresford, I. J., Gore, P. M., McElroy, A. B., Pritchard, J. M., Saez, V., Taylor, N. R. and Sheldrick, R. L., *J. Med. Chem.*, 38 (1995) 3772.
51. Cooper, A. W. J., Adams, H. S., Bell, R., Gore, P. M., McElroy, A. B., Pritchard, J. M., Smith, P. W. and Ward, P., *Bioorg. Med. Chem. Lett.*, 4 (1994) 1951.
52. Reichard, G., Aslain, R., Alaimo, C., Kirkup, M. and Lupo, A., US5696267, 1997.
53. Mackenzie, A. R., Marchington, A. P., Meadows, S. D. and Middleton, D. S., EP-791592, 1997.
54. Mackenzie, A. R., Marchington, A. P., Middleton, D. S. and Meadows, S. D., WP9727185, 1997.
55. Burkholder, T. P., Maynard, G. D. and Kudlacz, E. M., WO9827086, 1998.
56. Oka, H., Lida, M., Sato, Y. and Honda, M., WO9900388, 1999.
57. Harrison, T., Korsgaard, M. P., Swain, C. J., Cascieri, M. A., Sadowski, S. and Seabrook, G. R., *Bioorg. Med. Chem. Lett.*, 8 (1998) 1343.
58. Monaghan, S. M., Alker, D. and Burns, C. J., WO9857972, 1998.

59. Shenvi, A. B., Jacobs, R. T., Miller, S. C., Macht, C. J. and Veale, C. A., WO-09516682, 1995.
60. Gerspacher, M. and von Sprecher, A., *Drugs of the Future*, 24 (1999) 883.
61. Burkholder, T. P., *Bioorg. Med. Chem. Lett.*, 7 (1997) 2531.

Table 1: Data of compounds fitted to pharmacophore Model 1. HB acceptor angle is the deviation from the ideal hydrogen bond geometry (Angle =0°). IC₅₀ is the NK2 affinity of the racemate. K_i is the NK2 affinity of the highest affinity enantiomer.

Compound	Reference	HB acceptor Angle / °	RMS ^a / Å	IC ₅₀ / nM	K _i / nM
2	[32, 39]	32.7	0.29	4.1	0.5
7	[39]	9.3	0.11	8.9	
16	[40]	25.6	0.02	7.93	
22	[39]	0	0.14	12	
23	[39]	29.7	0.17	13	
24	[39]	98.0	0.29	4.0	
25	[39]	41.3	0.40	9.1	
26	[41]	26.0	0.25		1.0
27	[39]	22.6	0.20	84	
28	[39]	24.6	0.18	30	
29	[41]	47.1	0.24		50
30	[41]	42.3	0.36		0.9
31	[41]	37.2	0.39		0.3
32	[41]	22.8	0.35		23
33	[39]			250	
34	[42]			>1000	
35	[42]			180	

^a The fitting points are pharmacophore element A-D and G.

Table 2: Data of compounds fitted to pharmacophore Models 2 and 3. Energy is the calculated conformational energy penalty for the putative bioactive conformation. pK_a values are for the amine pharmacophore element D.

Cpd.	Ref. ^a	NK2 Affinity		Energy in kJ/mol		pK _a
		IC ₅₀ /nM	K _i /nM	Model 2	Model 3	
1	[43]	N.A.	N.A.	11.8	11.9	8.9
2	[32]		0.5	13.9	14.7	9.1
3	[44]		23	-5.3	8.4	9.0
4	[45]	3.0		9.5	7.6	8.9
5	[46]		23	-2.2	7.6	
6	[47]	11		0.0	0.2	9.1
7	[39]	8.9		0.0	1.8	9.1
8	[48]		33	-0.8	9.6	10.1
9	[49]		4.5	14.2	40.4	9.2
10	[50]		1.6	43.3	86.7	9.2
11	[51]		0.1	27.8	31.2	9.1
12	[50]		1.3	33.1	52.6	9.1
13	[52]	N. A.	N.A.	-4.5	9.6	9.0
14	[53]	0.5		67.5	102.0	7.6
15	[54]		0.6	8.3	0.0	8.3
16	[40]	7.93		5.2	-7.9	9.0
17	[55]	16.3		7.9	0.2	9.0
18	[56]	N.A.	N.A.	3.9	2.7	6.3
19	[57]	2.2		1.7	15.1	8.9
20	[58]	4		51.7	38.0	-
20a	[58]	4		-8.1	-1.3	
21	[59]	8.9		6.2	0.5	9.0

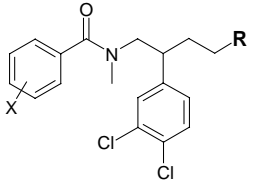
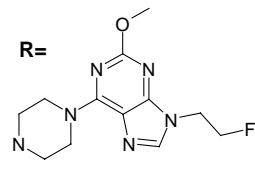
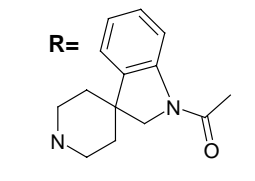
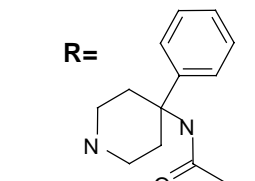
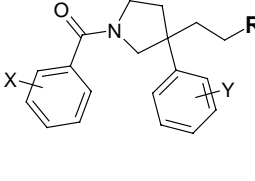
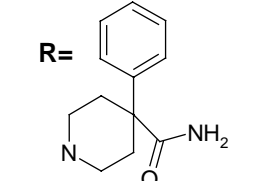
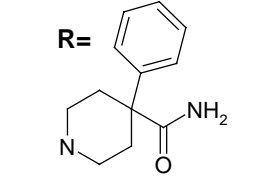
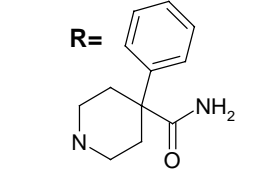
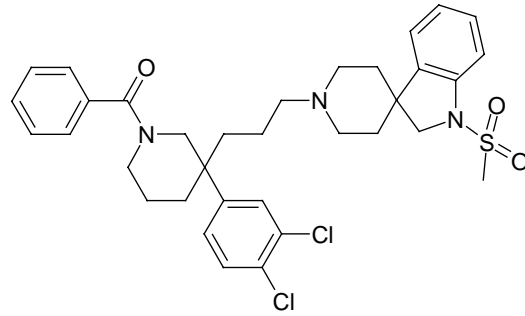
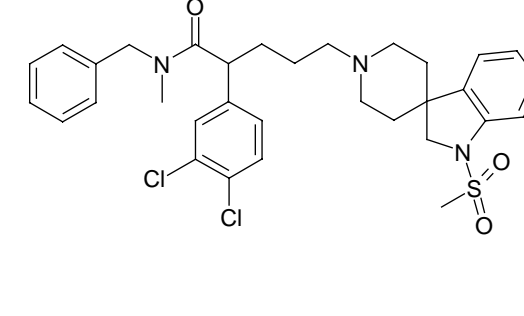
^a Ref.: Reference.

Table 3: Data of compounds fitted to pharmacophore Models 2 and 3. Angle is the deviation from ideal hydrogen bond geometry.

Cpd.	Model 2					Model 3				
	Angle /°				RMS	Angle /°				RMS
	D	E	F	G	/ Å ^a	D	E	F	G	/ Å ^a
1	23.3	37.2	9.5	49.9	0.44	15.2	28.9	18.0	36.0	0.25
2	12.0	28.8	11.8	49.0	0.43	0.0	27.2	10.0	43.2	0.47
3	0.0	27.5	-	13.9	0.19	0.0	13.7	-	15.6	0.24
4	14.6	27.9	25.7	101.3	(0.60) 0.84	14.5	25.9	25.4	103.5	(0.41) 0.92
5	15.4	-	36.5	41.8	(0.47) 0.74	0.0	-	13.9	14.2	0.35
6	11.8	7.7	7.4	59.0	0.44	0.0	25.4	12.7	64.1	0.41
7	0.0	0.0	0.0	0.0	0.46	8.3	25.4	4.8	34.8	0.31
8	0.0	0.0	0.0	-	0.46	5.0	26.2	5.1	-	0.29
9	14.2	74.9	68.4	17.2	(0.52) 0.69	52.4	18.2	80.7	55.4	0.44
10	76.6	84.4	81.8	-	0.92	27.3	74.5	72.8	-	0.66
11	42.6	67.1	57.6	-	0.62	24.4	29.2	44.4	-	(0.66) 1.52
12	40.1	8.9	80.0	-	1.08	66.6	57.5	37.2	-	0.56
13	13.9	-	39.2	37.0	(0.35) 0.63	0.0	-	16.5	22.2	0.29
14	11.8	32.6	23.0	27.6	(0.39) 0.63	30.8	49.2	14.1	51.3	0.40
15	13.2	33.5	20.6	39.3	0.48	52.9	54.9	0.0	6.8	0.35
16	20.3	35.2	51.8	39.9	0.46	20.0	31.8	13.7	14.5	(0.51) 0.86
17	17.0	21.0	14.6	31.3	(0.60) 0.89	17.3	29.6	14.8	13.6	(0.45) 0.76
18	26.2	35.7	23.3	77.0	0.27	20.4	18.2	3.3	82.2	0.45
19	18.7	25.9	99.6	55.5	(0.47) 0.56	5.8	9.8	55.4	30.2	0.71
20	-	40.5	-	-	(0.31) 0.92	-	49.4	-	-	0.42
20a	-	5.1	-	-	(0.27) 0.74	-	17.8	-	-	(0.26) 0.82
21	14.0	37.4	25.9	-	(0.61) 0.97	10.4	33.4	46.9	-	(0.18)

^a The fitting points are pharmacophore elements A-G. Number in parenthesis are RMS without pharmacophore element A as fitting point.

Table 4: SAR of two NK antagonist head fragments and two selective NK3 antagonists.

			
X	3,5 di-Me	3,4,5 tri-OMe	H
NK1 IC ₅₀ (nM)	0.45	0.2	593
NK2 IC ₅₀ (nM)	9	1.5	0.44
NK3 IC ₅₀ (nM)	25	N.A.	208
Reference	[60]	[60]	[37]
			
X	3,4,5 tri-OMe	H	3,4,5 tri-OMe
Y	3-Cl	3,4-Cl	3,4-Cl
NK1 IC ₅₀ (nM)	10.7	161	3.11
NK2 IC ₅₀ (nM)	190	2.25	8.40
NK3 IC ₅₀ (nM)	N.A.	N.A.	21.0
Reference	[61]	[37]	[37]
			
36	37		
NK1 IC ₅₀ 497nM	NK1 IC ₅₀ 100-500nM		
NK2 IC ₅₀ 177nM	NK2 IC ₅₀ 30nM		
NK3 IC ₅₀ 1.2nM	NK3 IC ₅₀ 0.6nM		
Reference [37]	Reference [38]		

N.A.: Not available.

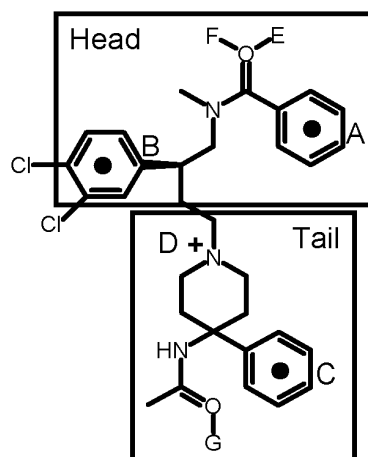


Figure 1: Definition of fragments with compound **2** as an example. Centroids, lonepairs and "+" marks the selected pharmacophore elements A-G.

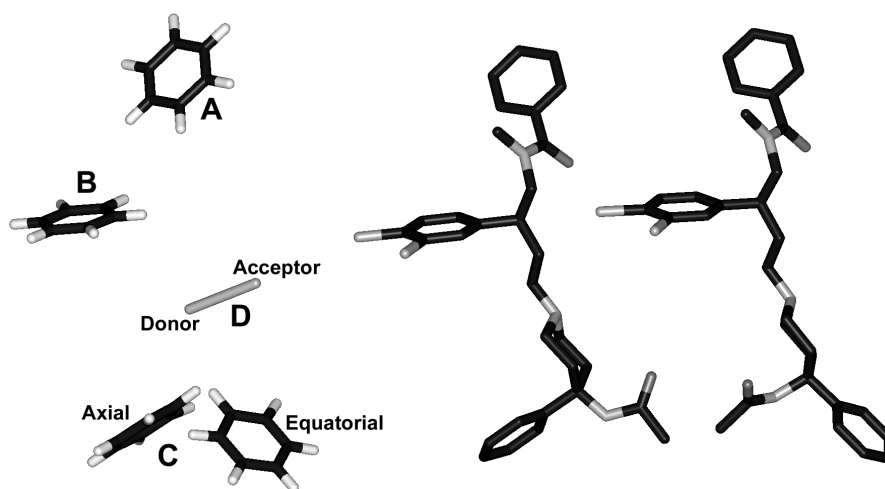


Figure 2: The previously published pharmacophore model. Left: Arrangement of pharmacophore elements. Element C can be in an axial or equatorial conformation. We propose that the equatorial conformation is most likely to be the bioactive conformation {Poulsen, Liljefors, et al. 2002 ID: 19}. Center and right: The putative bioactive conformations of (S)-**2** with pharmacophore element C axial (center) and equatorial (right).

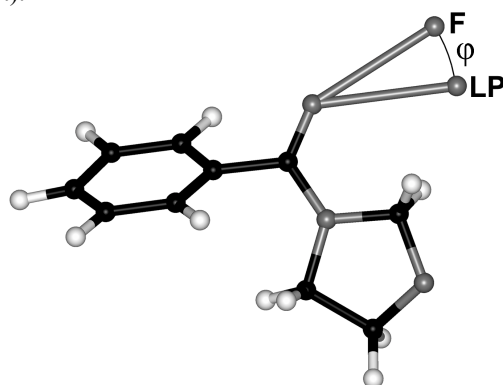


Figure 3: Definition of the angle ϕ (the deviation from ideal hydrogen bond geometry). The head fragment of compound **2** is used as an example. LP is the vector in direction of the lonepair. F is pharmacophore element F.

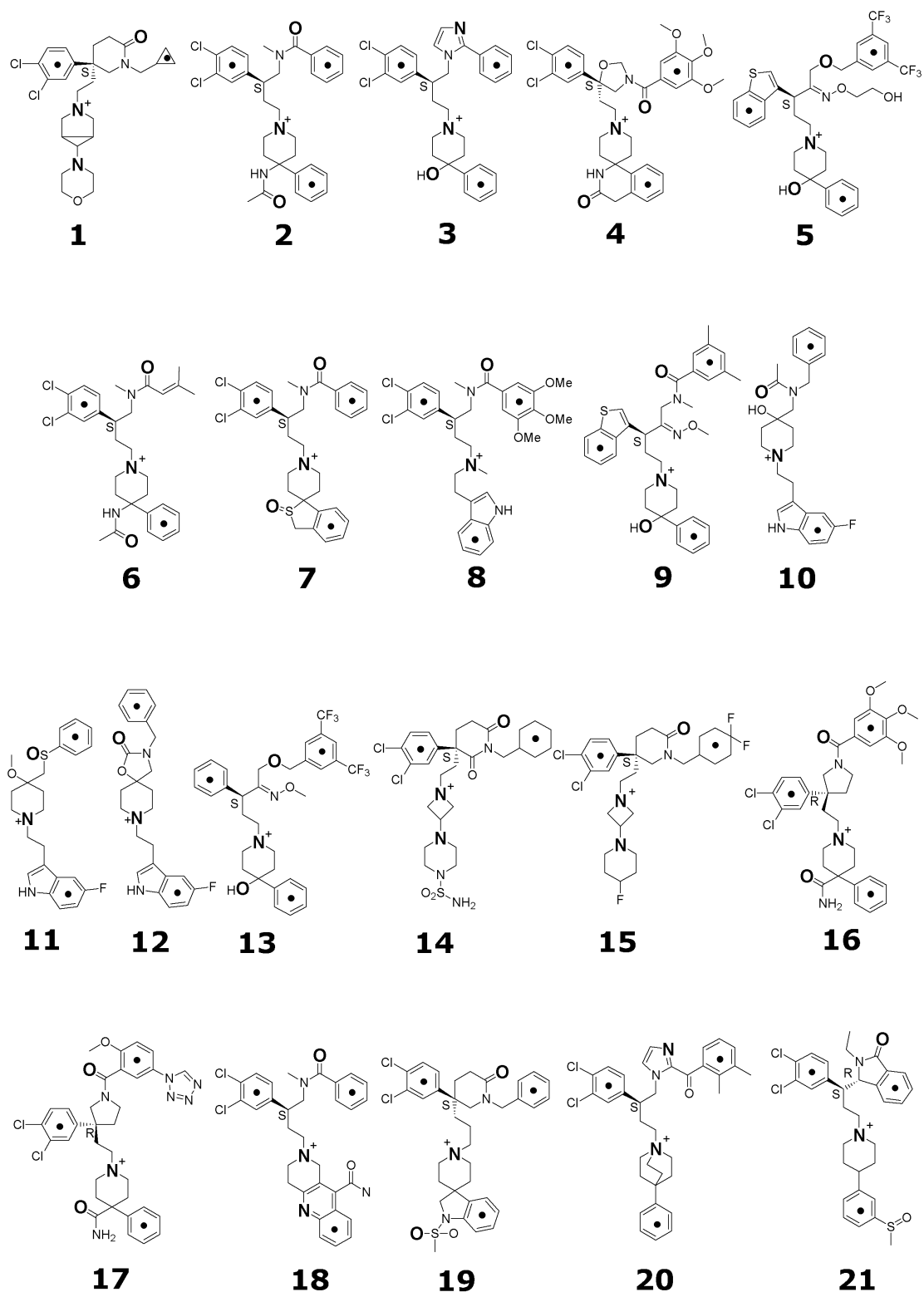


Figure 4: Compounds 1-21 were fitted to the pharmacophore models. Centroids, "+" and atoms in bold mark the selected pharmacophore elements. The atoms in bold are hydrogen bond acceptors. Data and references are given in Table 2.

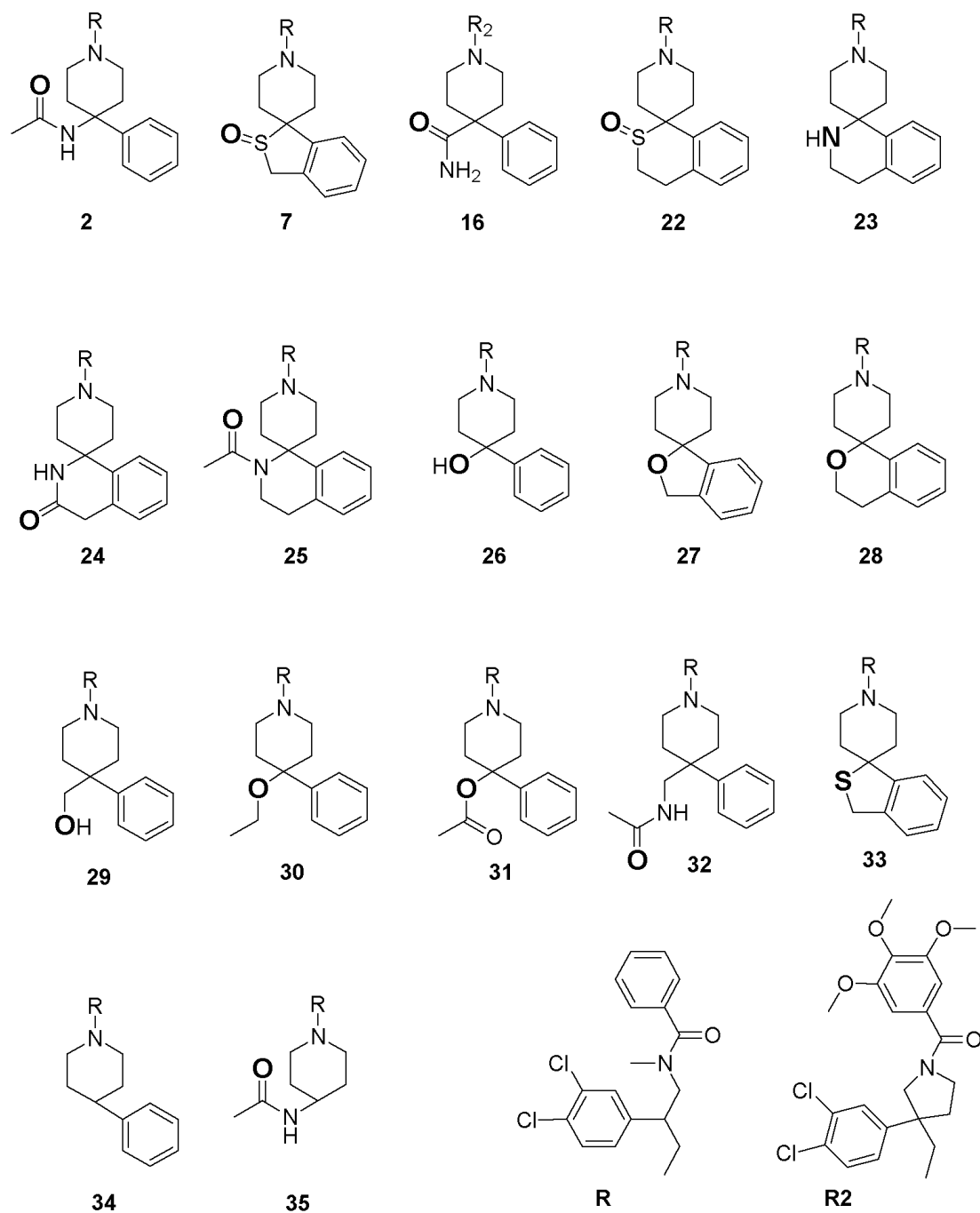


Figure 5: Compounds 2, 7, 16, 22-32 were used to derive the position of pharmacophore element G. Atoms in bold mark the selected hydrogen bond acceptors pharmacophore elements. Data and references are given in Table 1.

Element	X	Y	Z
A	-1.69	6.58	6.06
B	-3.46	0.38	4.13
C	2.72	-2.70	-4.19
D	2.43	1.38	0.07
D'	0.00	0.00	0.00
G	0.92	-4.46	0.17
G'	-1.34	-3.83	-1.25

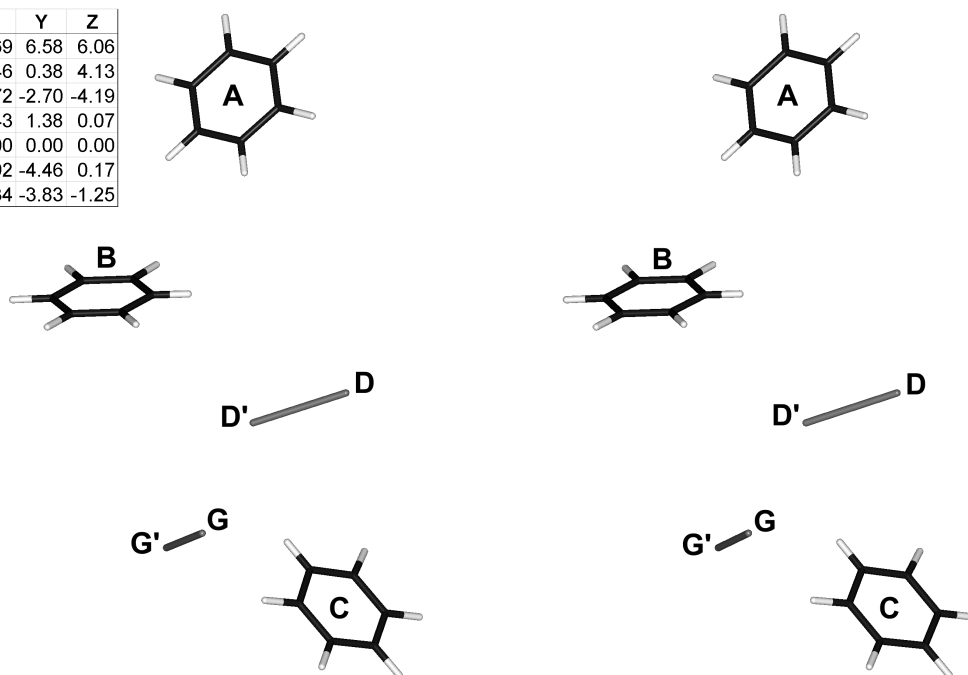
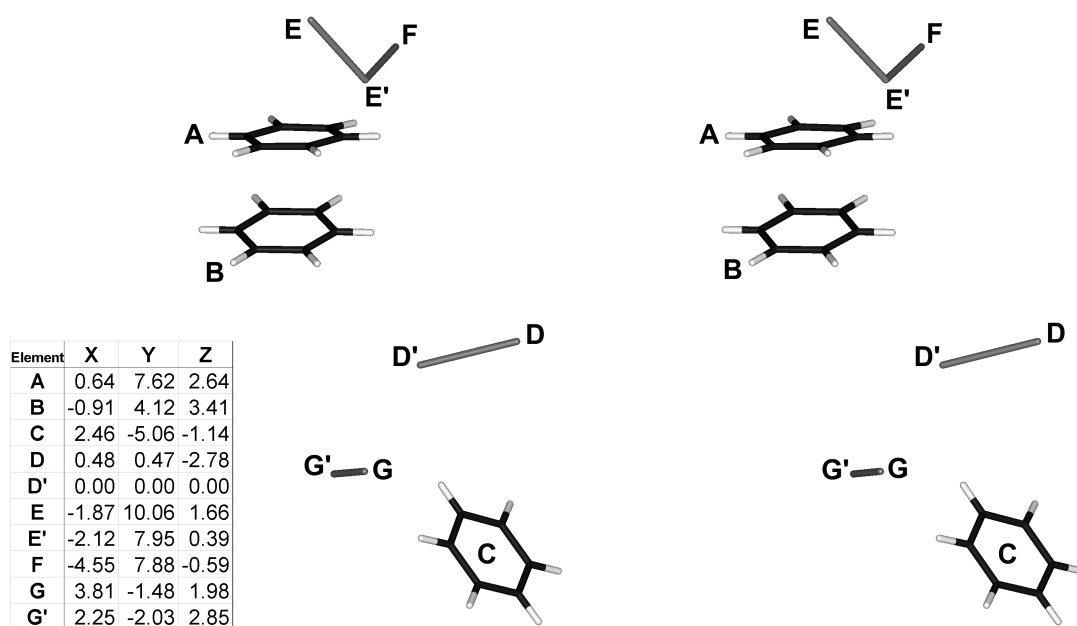


Figure 6: Pharmacophore Model 1. Stereo image. The coordinates for the pharmacophore elements are shown in the box. G' is the acceptor atom of the hydrogen bond acceptor pharmacophore element. D' is the hydrogen bond donor atom of the hydrogen bond donor pharmacophore element.



Element	X	Y	Z
A	0.64	7.62	2.64
B	-0.91	4.12	3.41
C	2.46	-5.06	-1.14
D	0.48	0.47	-2.78
D'	0.00	0.00	0.00
E	-1.87	10.06	1.66
E'	-2.12	7.95	0.39
F	-4.55	7.88	-0.59
G	3.81	-1.48	1.98
G'	2.25	-2.03	2.85

Figure 7: Pharmacophore Model 2. Stereo image. The coordinates for the pharmacophore elements are shown in the box. E' and G' are the acceptor atoms of the hydrogen bond acceptor pharmacophore elements. D' is the hydrogen bond donor atom of the hydrogen bond donor pharmacophore element.

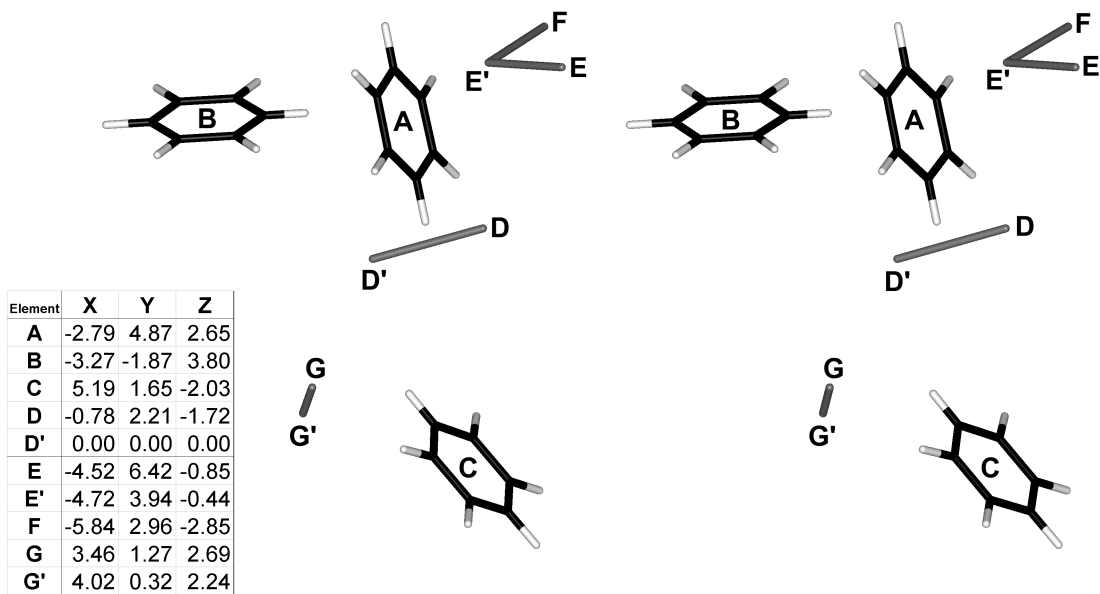


Figure 8: Pharmacophore Model 3. Stereo image. The coordinates for the pharmacophore elements are shown in the box. E' and G' are the acceptor atoms of the hydrogen bond acceptor pharmacophore elements. D' is the hydrogen bond donor atom of the hydrogen bond donor pharmacophore element.

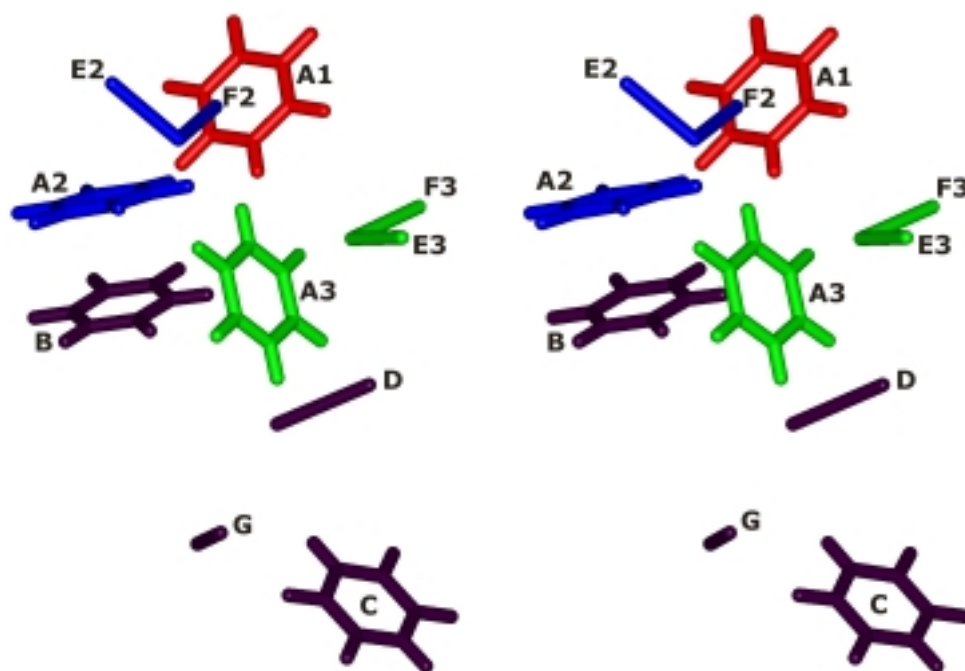


Figure 9: Stereo image. A superimposition of pharmacophore Models 1-3. Black: The pharmacophore elements B, C, D and G have the same position in the three models. Red: Model 1. Blue: Model 2. Green: Model 3.

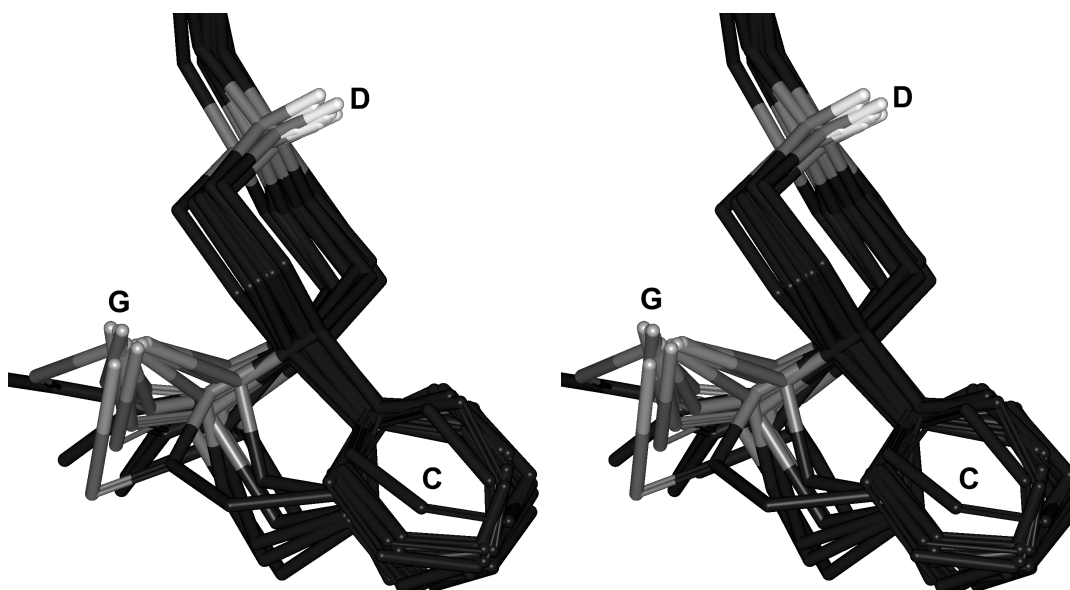


Figure 10: Superimposition of compounds **2**, **7**, **16** and **22-32**. Stereo image, hydrogens are removed for clarity. The hydrogen bond acceptor pharmacophore element **G** is shown as vectors.

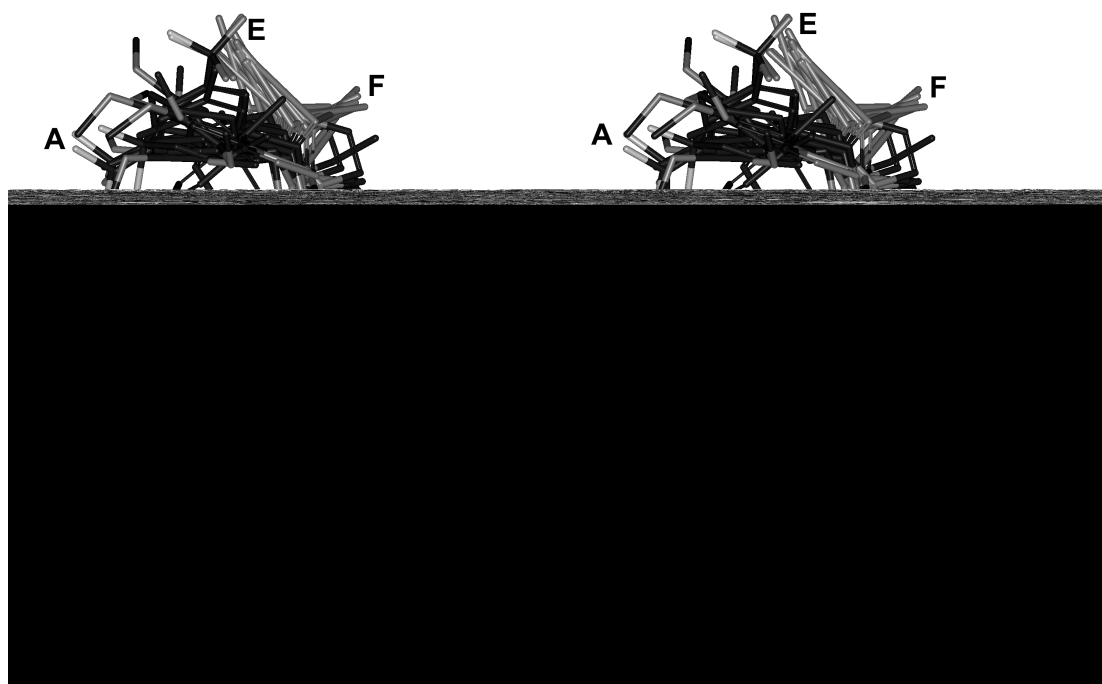


Figure 11: Superimposition of compounds **1-9** and **13-21** fitted to Model 2. Stereo image, hydrogens are removed for clarity. The hydrogen bond donor and acceptor pharmacophore elements **D**, **E**, **F** and **G** are shown as vectors.

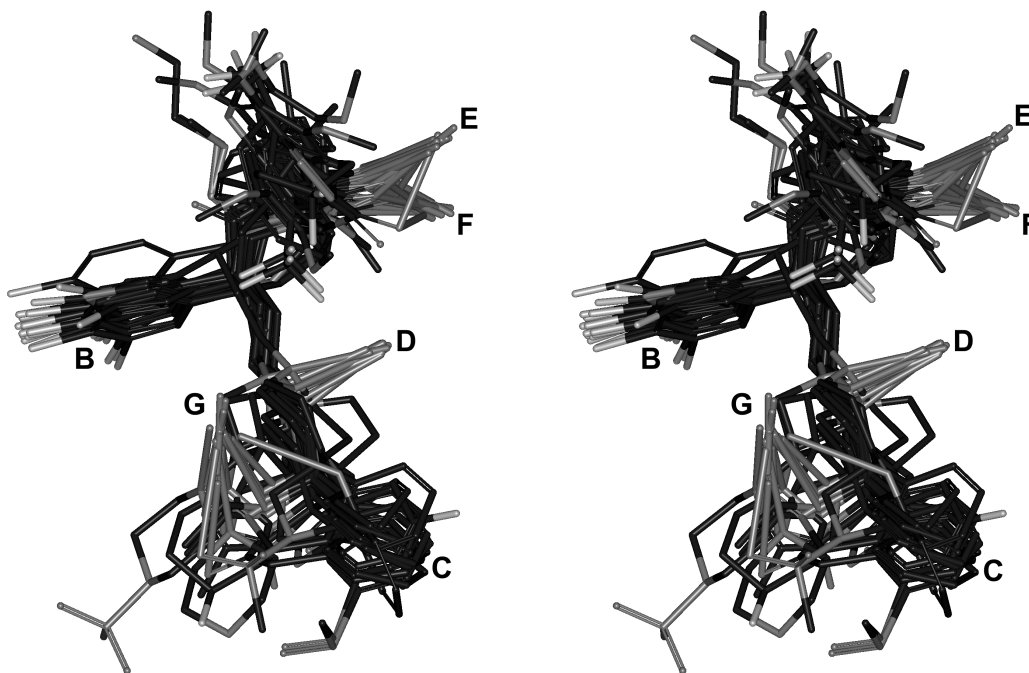


Figure 12: Superimposition of compounds 1-9 and 13-21 fitted to Model 3. Stereo image, hydrogens are removed for clarity. The hydrogen bond donor and acceptor pharmacophore elements D, E, F and G are shown as vectors.

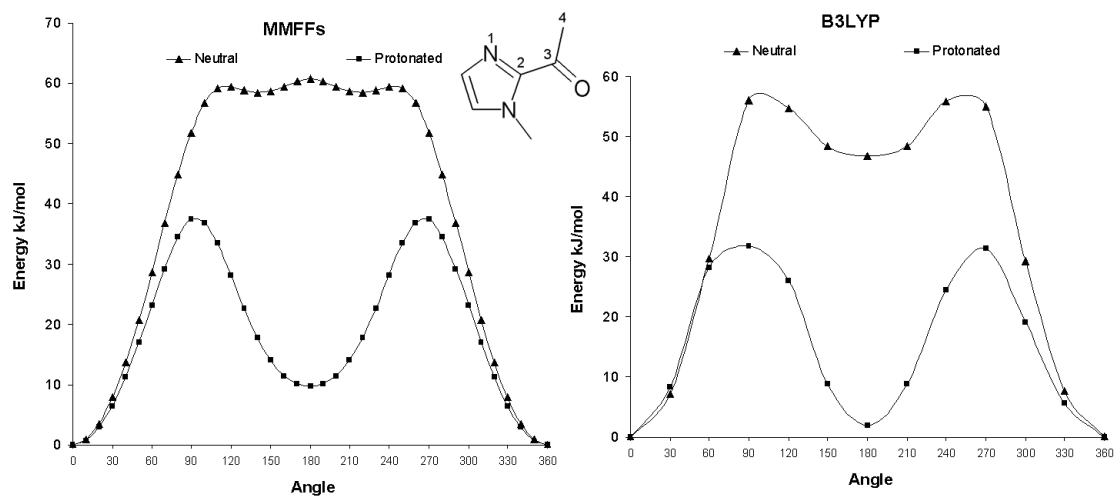


Figure 13: Torsional drive of the angle 1-2-3-4 in model system for the head fragment of compound 20.

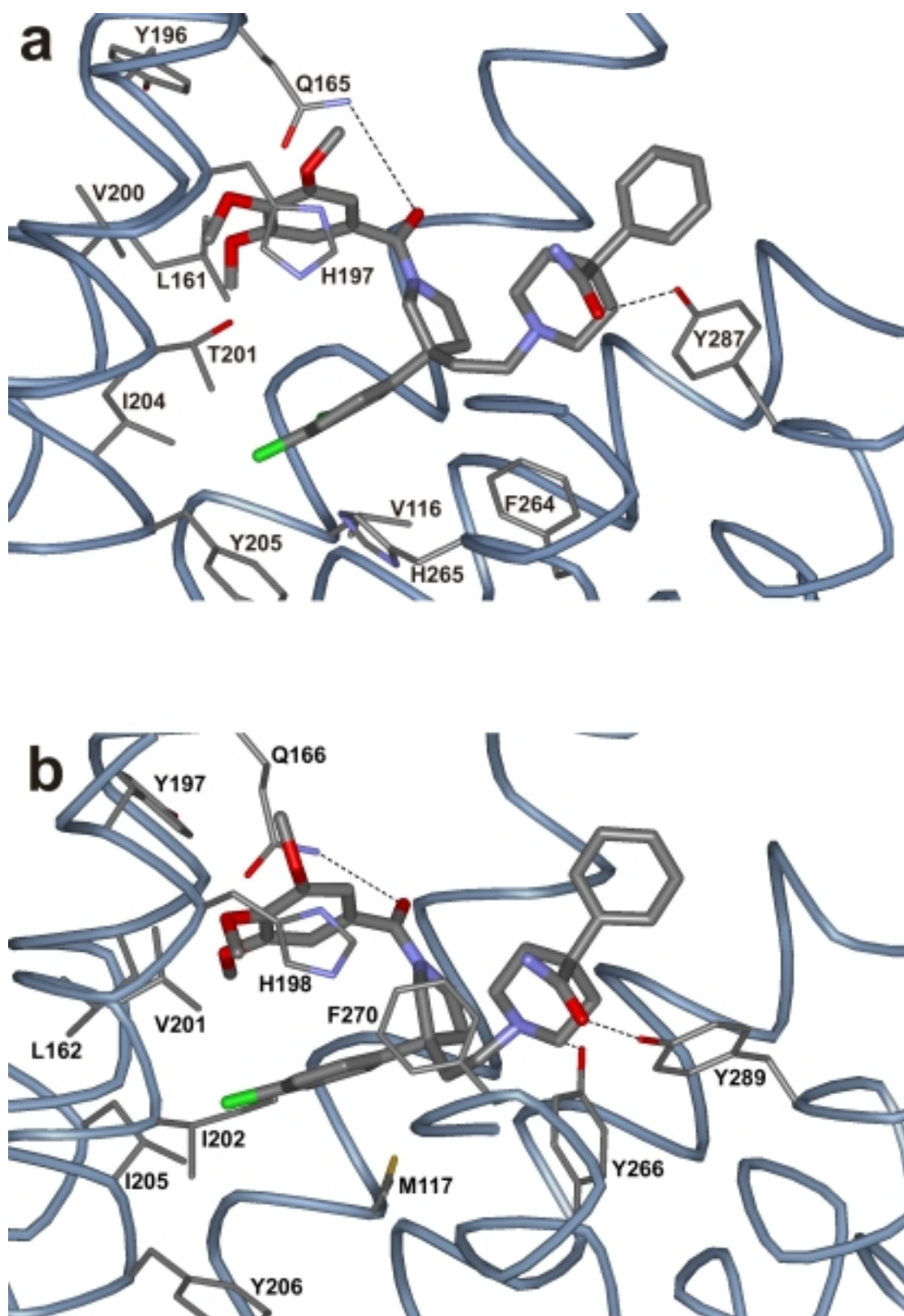


Figure 14. a: Compound **16** docked into the NK1 receptor model. b: Compound **16** docked into the NK2 receptor model. Loops and the last three residues of helix 6 have been removed for clarity. Only sidechains identified by site-directed mutagenesis to be important for antagonist binding as well as residues in the binding site are displayed.